ISSN : 2349-6495(P) | 2456-1908 (O)

# International Journal of Advanced Engineering Research and Science

(IJAERS)

An Open Access Peer Reviewed International Journal

Journal DOI: 10.22161/ijaers

Issue DOI: 10.22161/ijaers.5.1

AI PUBLICATIONS

Vol.- 5 | Issue - 1 | Jan, 2018

editor@ijaers.com | http://www.ijaers.com/

# FOREWORD

I am pleased to put into the hands of readers Volume-5; Issue-1: 2018 (Jan, 2018) of **"International Journal of Advanced Engineering Research and Science (IJAERS) (ISSN: 2349-6495(P) | 2456-1908(O)" ,** an international journal which publishes peer reviewed quality research papers on a wide variety of topics related to Science, Technology, Management and Humanities. Looking to the keen interest shown by the authors and readers, the editorial board has decided to release print issue also, but this decision the journal issue will be available in various library also in print and online version. This will motivate authors for quick publication of their research papers. Even with these changes our objective remains the same, that is, to encourage young researchers and academicians to think innovatively and share their research findings with others for the betterment of mankind. This journal has DOI (Digital Object Identifier) also, this will improve citation of research papers.

I thank all the authors of the research papers for contributing their scholarly articles. Despite many challenges, the entire editorial board has worked tirelessly and helped me to bring out this issue of the journal well in time. They all deserve my heartfelt thanks.

Finally, I hope the readers will make good use of this valuable research material and continue to contribute their research finding for publication in this journal. Constructive comments and suggestions from our readers are welcome for further improvement of the quality and usefulness of the journal.

With warm regards.

**Dr. Swapnesh Taterh**
Editor-in-Chief
Date: Jan, 2018

# ***Editorial/ Reviewer Board***

# Vol-5, Issue-1, January 2018

*https://dx.doi.org/10.22161/ijaers.5.1.1* *ISSN: 2349-6495(P) | 2456-1908(O)*

# Introduction to the Method of Finite Elements by a balance Sheet Problem: A Simplification for an Initial understanding of the Method

Júlio Paulo Cabral dos Reis, Pedro Américo Almeida Magalhães Júnior

Graduate Program in Mechanical Engineering, Pontifical Catholic University of Minas Gerais, Belo Horizonte - MG

***Abstract*****—** *The Finite Element method is one of the most widely used methods by Engineers in the various areas of activity, especially Mechanical Engineering, to design or solve problems. However, the understanding of the method is not always easy to perform, since in the literature, when explaining the method, the examples are generic or presented quickly. Thus, this paper presents the solution of a problem involving a rocking beam (set), which is solved analytically and later by the finite element method. The comparison of the solutions found is established as reflection analysis. Elasticity theory, Ordinary Differential Equations and Finite Element Method are used to approximate the reader of the Finite Element Method, in a concise and objective, easy-to-understand reading performed with a reduced explanation. Comparing the method by means of a problem.*

***Keywords*****— Finite Element Method, Beams, Differential Equations.**

## I. INTRODUCTION

Mathematical models are increasingly present in the area of Engineering. In Elasticity Theory, for example, there are several models that work with tensions, deformations and displacements of structures. Be applied to one-dimensional, two-dimensional or three-dimensional problems. In the search for these models, [1] says that several problems fall into the Differential Equations, whether these are ordinary, when the treated model is one-dimensional or partial where the model can be two-dimensional or three-dimensional. Therefore, a problem of obtaining a model for the understanding of a certain phenomenon can become a problem of solving the model found, that is, the problem of physical phenomenon can be modeled by a Differential Equation, and however, it needs a method resolution.

In [2], the resolution methods can be analytical and / or numerical. Where, among the various numerical methods, for the described situation, the Finite Element Method (MEF) stands out. This method was developed by the need to solve complex problems of Engineer, and can advance, nowadays, with the advent of Technology. Today it is widely used for the resolution and reflection of various problems in the Engineering area. The purpose of this method is to approach the searched solution in a discrete way.

Due to its potentialities, for the Engineer interested, it becomes interesting to understand such a method.

## II. OBJECTIVE

To present succinctly, by the resolution of a problem of balance beam (set), the Finite Element method;

.

## III. METHODOLOGY

A problem is presented, on beam, to deduce the solution via analytical mode and via numerical mode. Being the second resolution based on the MEF, in order to lead the reader, to a first contact with the method. The problem proposed is:

A set beam of homogeneous steel, whose length is 2 meters, has a cross section in I format and W250x17,9 specification. Such a beam will be subjected to a Q (concentrated) charge of intensity 10 kN at its free end.

The sketch of the problem, using the presented conditions, with reference axes adopted, can be worked in a one-dimensional way.

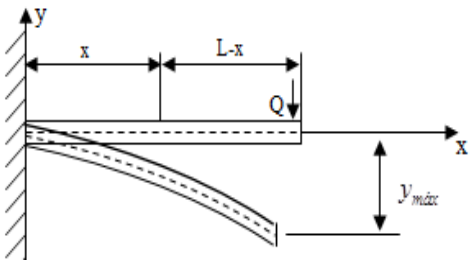


*Fig. 1: Diagram elaborated for Resolution*

To determine the bending moment, using the right side, it is established:

$$M(x) = -Q(L - x) \qquad (1)$$

Using the differential equation whose solution is the deflection curve, we have

*https://dx.doi.org/10.22161/ijaers.5.1.1* *ISSN: 2349-6495(P) | 2456-1908(O)*

$$\int \frac{d^2y}{dx^2}dx = \int \frac{-Q(L-x)}{EI}dx \Rightarrow \frac{dy}{dx} = \frac{1}{EI}\left(\frac{Qx^2}{2} - QLx\right) + C \quad (2)$$

From the proposed problem statement, initial conditions can be extracted.

At the point where the beam is embedded, that is, in the adopted frame, y (0) = 0 and y '(0) = 0. Thus, by replacing in (2), the value of C = 0 is found. Then, as the analytic resolution continues:

$$\int \frac{dy}{dx} = \int \frac{1}{EI}\left(\frac{Qx^2}{2} - QLx\right)dx \Rightarrow y(x) = \frac{Qx}{2EI}\left(\frac{x^3}{3} - Lx^2\right) + C \quad (3)$$

Soon

$$y(x) = \frac{Qx}{2EI}\left(\frac{x^3}{3} - Lx^2\right) \quad (4)$$

The function (4) provides the generalized elastic line for all problems of homogeneous beams (with spheres) with concentrated load at the free end, worked in a one-dimensional manner, that is, the extension with respect to one axis is relatively larger than when compared to others. For the problem in question we have: L = 2 m, Q = 10 kN = 10000 N, E = Pa and I =, the values of E and I, for the steel used can be obtained in the table of NBR-8800 2008, obtained from the [3] website. Thus, the elastic curve is:

$$y(x) = \frac{10000x}{2.200.10^9.2291.10^{-8}}\left(\frac{x^3}{3} - 2x^2\right) \Rightarrow y(x) = \frac{5x}{4582}\left(\frac{x^3}{3} - 2x^2\right) \quad (5)$$

Making a table and analyzing values of the deflections in the points: x = 0, x = 1 and x = 2, we obtain:

*Table.1: Analysis by the analytical method of some deflections*

| X | Deflexão (y) - mm |
|---|---|
| 0 | 0 |
| 1 | -1,8187108977157 |
| 2 | -11,6397497453805 |

It is found that the largest deformation occurs at x = 2 m, as was expected at the free end of the beam, where the load Q is acting, making this point move approximately m or 11.64 mm.

To prepare the numerical response via MEF, we use [4] and [5]. Initially, the Elasticity Theory equations and the discretization of the worked object. Discretization can be thought of here as dividing the beam into other "pieces". For the problem in question, the beam was divided into two elements of the same length (T and R), that is, L = 1 m for each element, with such discretization we obtain three nodes (1, 2, 3), according to the figure, which also contains the adopted framework.

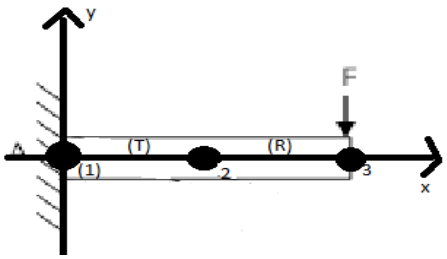


*Fig. 2: Beam being discretized by elements*

With this discretization configuration, at the end of the process, the method will provide the displacements relative to the established nodes (1, 2, and 3), that is, relative displacements ax = 0, x = 1 ex = 2, according to the established initial constructions and the adopted reference.

Once the discretization is established, a stiffness matrix is assembled for each of the elements. This rigidity matrix is established by the theorems of the Variational Calculus, Elasticity Theory and Physics, worked in a discrete way. For the configuration adopted, each element (T and R) will have its stiffness matrix.

For the problem in question each element will have a stiffness matrix in the format presented:

$$\begin{bmatrix} \frac{EA}{L} & 0 & 0 & -\frac{EA}{L} & 0 & 0 \\ 0 & \frac{12EI}{L^3} & \frac{6EI}{L^2} & 0 & -\frac{12EI}{L^3} & \frac{6EI}{L^2} \\ 0 & \frac{6EI}{L^2} & \frac{4EI}{L} & 0 & -\frac{6EI}{L^2} & \frac{2EI}{L} \\ -\frac{EA}{L} & 0 & 0 & \frac{EA}{L} & 0 & 0 \\ 0 & -\frac{12EI}{L^3} & -\frac{6EI}{L^2} & 0 & \frac{12EI}{L^3} & -\frac{6EI}{L^2} \\ 0 & \frac{6EI}{L^2} & \frac{2EI}{L} & 0 & -\frac{6EI}{L^2} & \frac{4EI}{L} \end{bmatrix} \quad (6)$$

Where L is the length of the element and A is the area of the profile adopted (in this case, it is the steel beam W250x17,9), to obtain the value of A, a query to Gerdau's website, and then we have that A =. Then, replacing the values of A, E, I and L in (6) and overlapping the matrices we have

$$\begin{bmatrix} 4.6210^8 & 0 & 0 & -4.6210^8 & 0 & 0 & 0 & 0 & 0 \\ 0 & 5.498410^7 & 2.749210^7 & 0 & -5.498410^7 & 2.749210^7 & 0 & 0 & 0 \\ 0 & 2.749210^7 & 1.832810^7 & 0 & -2.749210^7 & 9164000.0 & 0 & 0 & 0 \\ -4.6210^8 & 0 & 0 & 9.2410^8 & 0 & 0 & -4.6210^8 & 0 & 0 \\ 0 & -5.498410^7 & -2.749210^7 & 0 & 1.0996810^8 & 0.0 & 0 & -5.498410^7 & 2.749210^7 \\ 0 & 2.749210^7 & 9164000.0 & 0 & 0.0 & 3.665610^7 & 0 & -2.749210^7 & 9164000.0 \\ 0 & 0 & 0 & -4.6210^8 & 0 & 0 & 4.6210^8 & 0 & 0 \\ 0 & 0 & 0 & 0 & -5.498410^7 & -2.749210^7 & 0 & 5.498410^7 & -2.749210^7 \\ 0 & 0 & 0 & 0 & 2.749210^7 & 9164000.0 & 0 & -2.749210^7 & 1.832810^7 \end{bmatrix}$$

(7)

*https://dx.doi.org/10.22161/ijaers.5.1.1* *ISSN: 2349-6495(P) | 2456-1908(O)*

From the theory of elasticity it is known that: [K] [D] = [F], the product of the global stiffness matrix [K], by the displacement matrix [D], is equal to the force matrix acting on the system [ F].

The force matrix and the displacement matrix are assembled from the forces acting on the problem and from the degrees of freedom of each node of the problem, respectively.

$$D = \begin{pmatrix} u_1 \\ v_1 \\ r_1 \\ u_2 \\ v_2 \\ r_2 \\ u_3 \\ v_3 \\ r_3 \end{pmatrix} = \begin{pmatrix} O \\ O \\ O \\ O \\ v_2 \\ r_2 \\ O \\ v_3 \\ r_3 \end{pmatrix} \quad F = \begin{pmatrix} 0 \\ 0 \\ 0 \\ 0 \\ 0 \\ 0 \\ 0 \\ -10000.0 \\ 0 \end{pmatrix} \quad (8)$$

Note that the force matrix [F], there is only one force acting in the opposite direction to the established reference frame, with respect to the y-axis, thus occupying the indicated position with the negative signal and the displacement matrix [D], was established from the following (2) and (3) will have two degrees of freedom - displacement with respect to the axis and rotation with respect to the xy-plane - so we will have no degree of freedom for the problem in question. in the displayed mode, ie, where there are no displacements, it is assumed to be zero.

To solve this linear system you can use mathematical software such as Visual Calculus Numerical (VCN), Maxima, Scilab and / or Maple or even Microsoft Excel. When solving the linear system, we find the mentioned displacements.

$$D = \begin{pmatrix} u_1 \\ v_1 \\ r_1 \\ u_2 \\ v_2 \\ r_2 \\ u_3 \\ v_3 \\ r_3 \end{pmatrix} = (9) \quad \begin{pmatrix} 0.0 \\ 0.0 \\ 0.0 \\ 0.0 \\ -0.001818710897715699 \\ -0.003273679615888258 \\ 0.0 \\ -0.005819874872690237 \\ -0.004364906154517678 \end{pmatrix}$$

It is interesting here to compare the displacements suffered by nodes (1), (2) and (3), in relation to the y axis, that is, those obtained in matrix D. Interestingly, in node (1), as already was expected, there is no displacement, either horizontal, vertical or rotation, $u_1 = v_1 = r_1 = 0$ this is due to the fact that node (1) has no degree of freedom in the proposed problem. Thus, by comparing the analytical method with the numerical method and presenting it in a table, we have:

*Table 2: Numerical method comparison and analytical method*

| X | Deflexão (Em relação a y) – Método Numérico - mm | Deflexão (Em relação a y) – Método Analítico - mm |
|---|---|---|
| 0 | 0 | 0 |
| 1 | -1,8187108977 | -1,818710897157 |
| 2 | -5,8198748726 | -11,639749453805 |

When comparing the methods, it is possible to verify that the first two approximations are satisfactory, that is, referring to node (1), which occurs at x = 0 and to node (2), which occurs at x = 1. However, 3, which occurs at x = 2, a very large error can be verified by comparing the analytical method with the numerical method.

An attempt to control this error is to work with more elements in the discretization, but the global linear system will have more unknowns to consider and the stiffness matrix will be larger. What is not configured at the present time as a major problem, since the technology supports linear systems such as those mentioned.

Therefore, with this small demonstration of the method, it is possible to verify that the approximations found for the solution of the proposed problem are satisfactory to present the MEF as a numerical method for solving structural problems. If the approximations in another problem are not enough or to the liking of the engineer it is possible to refine the solution found, as much as one wants.

## IV. CONCLUSION

In order to employ a reductionist character, the Theory, by MEF, which is rigorous and elegant, was aimed here, to offer a reader interested north to the understanding of this numerical method and its theory. In short, the solutions of the same problem, by the analytical method and by the numerical method, succinctly, the general objective of the article is reached, together with the specific ones: an introduction by the resolution of a problem on MEF beams

*https://dx.doi.org/10.22161/ijaers.5.1.1* *ISSN: 2349-6495(P) | 2456-1908(O)*

Thus, it is possible to analyze the complement of analytical and numerical solutions, expressing a problem that offers the intersection of these solutions. However, it is necessary for the future engineer, the engineer and the interested reader to verify that there are problems that the analytical solution is not suitable, so to resort to the numerical solution becomes a complement, and this occurs with the MEF.

Allowing those interested in using the method, a first contact or even glimpsing an application of the method is a way of contributing to the academic milieu. This leaves the possibility for the reader to broaden his knowledge about the MEF, understanding its full potential and theory.

## REFERENCES

[1] LAUDARES, João Bosco; MIRANDA, Dimas F.; REIS, Júlio Paulo Cabral; FURLETTI, Saulo. **Equações Diferenciais Ordinárias e Transformadas de Laplace**. Belo Horizonte: Artesã. 2017

[2] SOUZA, Remo Magalhães de. **O método dos Elementos Finitos Aplicado ao Problema de Condução de Calor**. UFPA. Belém. PA. 2003Myers, D. G. (2007). Psychology(1stCanadian ed.). New York, NY: Worth.

[3] GERDAU. **Tabela de Bitolas**. Perfis Gerdau Açominas. São Paulo. SP. 2017. Disponível in:< http://www.soufer.com.br/arquivos/laminados/2.pdf> . Acesso: 29/09/2017.

[4] ASSAN, Alosio Enersto. **Método dos elementos finitos – primeiros passos**. Ed. Unicamp. 2ª ed. São Paulo. SP. 2003.

[5] DEPARTAMENTO DE ENGENHARIA MECÂNICA. DEMEC. **Apostila de introdução ao método de elementos finitos.** UFPR. 2016. Disponível in: <http://ftp.demec.ufpr.br/disciplinas/TM266/Apostila/Introdu%C3%A7%C3%A3o%20ao%20MEF.pdf> Acesso in: 25 de Setembro de 2017.

*https://dx.doi.org/10.22161/ijaers.5.1.2* *ISSN: 2349-6495(P) | 2456-1908(O)*

# Vibration Analysis of Silencer Based on FEM and FFT Analyser

Sonali D. Alone[1], M.A.Mohite[2]

P.G.Student, Department of Mechanical Engineering,Sinhgad Institute of Technology, Lonavala, Maharashtra, India
Associate Professor,Department of Mechanical Engineering,Sinhgad Institute of Technology, Lonavala, Maharashtra, India

***Abstract*—***Silencer was considered with and without modifying in order to reduce the vibration. Design and modelinghave been done with specifying different material properties. Finite Element Method was used for the modeling and simulations. The harmonic analysis has been performed by using ANSYS 18.0. The natural frequency and working frequency are the very important parameters to study the resonance. It is mandatory to avoid this resonating condition. These frequencies are distinguished with the help of ANSYS 18.0.*

***Keywords—ANSYS, CFD, Frequency, Silencer, Vibration.***

## I. INTRODUCTION

Silencer looks like a cantilever structures which is one of the important parts of the exhaust system. At running condition of vehicle Silencers and Mufflers are subjected to various structural, thermal and vibration loads. The Silencer may get afailure or damaged because of many reasons, vibration from engine and road excitations are amongst them. The vibration failure happens mainly because of the resonant frequencies occurring in the defined frequency range. If we consider the road excitation, vertical accelerations are dominant in Mufflers [7]. The selection ofexhaust silencer is depends on the level of reduction in the engine exhaust noise. In order to select the exhaust silencer, we have to compromise between the mechanical, aerodynamic, structural and acoustical performance in conjunction with the cost of the resulting system. Hence, it is more important study the vibrations in deep which would further help to improve the efficiency of Silencer, improving life, minimize cracks and life of a silencer [1].The main objective to achieve Vibration optimization of Silencer using FEA (ANSYS).Silencers and Mufflers are used to control the engine exhaust noise. Mufflers and Silencers work in a similar way. The technical functionality between these two is very similar. A silencer is a traditional name given to a device which attenuates noise, Muffler is a device, designed to minimize the engine exhaust noise [3]. The basic function of the silencer is to reduce noise and pass exhaust generated in the engine.

## II. NEED FOR ANALYSIS

In India, the Automobile silencer under study belongs to a popular 2-Wheeler manufacturer with the rated HP of the engine up to @7.69HP. at very high speed and temperature exhaust gases coming out from the engine. Silencer has to reduce noise, vibrations. While doing so it is subjected to thermal, vibration and fatigue failures which cause cracks. So it is necessary to analyze the vibrations which would further help to pursue future projects to minimize cracks, improving life and efficiency of the silencer.[1]

## III. LITERATURE REVIEW

The first stage of design and analysis of exhaust system had done [1]. For the modeling of the exhaust system, he used conventional FEM package. The material property was the main parameter to study. To avoid the resonating condition, FFT analysis was carried out to distinguished natural frequency and working frequency. From his study it is cleared that to increase the dynamic performance, the thickness of the different parts plays an important role [1]. The advantages of different designs of Mufflers had listed [7]. He took into consideration different functional requirements of muffler like style, shape, size, cost, desired sound, durability, backpressure and adequate insertion loss [7].

The experimental and numerical study had performed for the tailpipe noise of a muffler for a wide range of throttle acceleration [6]. Thevalidation was done for the transient acoustic characteristics of a muffler in theanechoic chamber according to the Japanese Standard (JIS D 1616). At the 2nd order of engine rotational frequency, the simulation results are in good agreement with the experimental data CFD simulations had performed to calculate transfer matrix of an engine exhaust muffler [5]. The study considers the effect of with an without mean flow on the acoustic performance of a silencer. The developed CFD model has theability to predict the acoustic performance of a complex muffler. It also has theeffecton heat transfer to produce reasonable results of the exhaust noise [5].

Next study considers weak shock wave propagation inside silencer of exhaust pipe [4]. To solve Euler, unsteady,

*https://dx.doi.org/10.22161/ijaers.5.1.2* *ISSN: 2349-6495(P) | 2456-1908(O)*

compressible, two-dimensional equations, 2nd order total variation diminishing (TVD) scheme was used. To study the effect of silencer configuration on weak shock wave propagation eight different models of the silencer used. At the inlet incident plane shock was assumed and its Mach no. was varied from 1.01 to 1.30. The pressure distribution and velocity field of flow system wereanalyzed on designed silencer [4].

## IV. MODAL ANALYSIS OF EXISTING MODEL

Silencer model has been taken for the modal analysis. Table 1 shows the some of the properties which have been exclusively used in the simulation. Figure 1 shows the geometry file which has been drawn and model by using Ansys package. Figure 2 shows the meshing of existing silencer model. For the meshing Tetrahedral elements were used. The existing silencer model is somewhat complex, and because of this complexity, a simple tetrahedral mesh element was selected while meshing in Ansys. In the numerical simulations, geometry and meshing are the very crucial steps. So, special attention was given towards the modeling of thesilencer. After these two main steps, understanding of the physics is mandatory. For solving this complex system, initial and boundary condition plays an important role. Figure 3. shows the boundary condition used in the simulations. After meshing,simulations have been performed to obtain the model analysis for first five natural frequencies. These frequencies are shown in Table 2. The contours of natural frequencies of theexisting model have been shown in Figure. (4-8). On comparing all these natural frequencies, maximum bending was observed in mode 4.

*Table 1.Material Properties.*

| | |
|---|---|
| Element type | Tetrahedral |
| Material | Steel |
| Mesh type | Solid Mesh |
| Density | 7.85e-6 Kg/Mm3 |
| Poisons ratio | 0.3 |
| Yield Strength | 520Mpa |

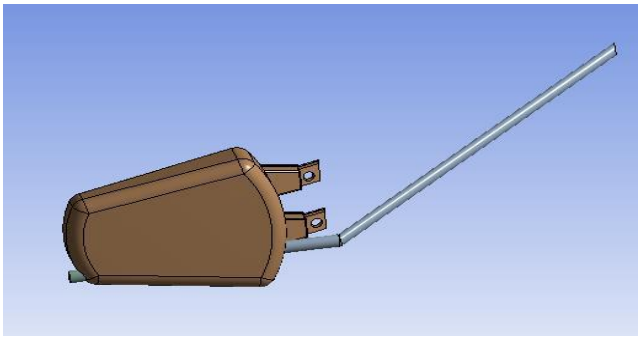

*Fig. 1.Silencer existing model.*

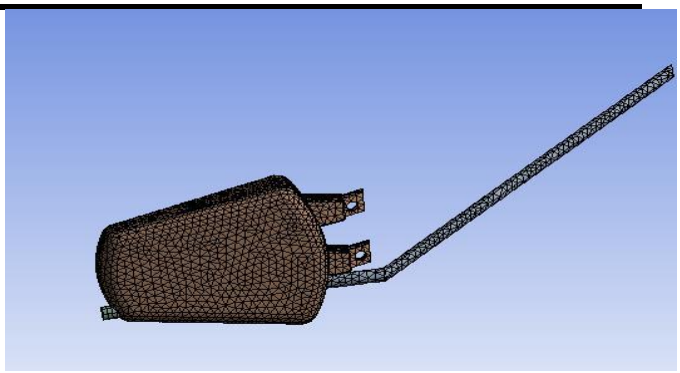

*Fig. 2.Meshing of silencer mode*

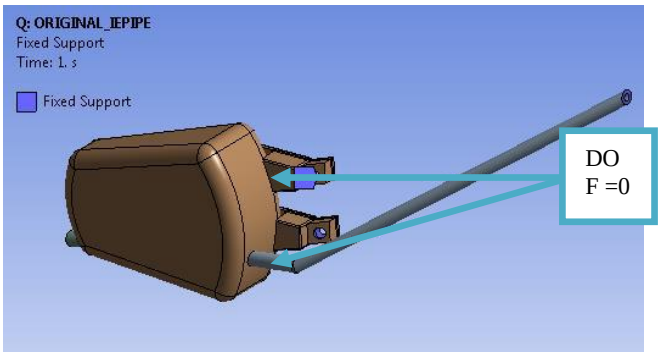


*Fig. 3.Boundary conditions for existing silencer model*

Geometry and meshing were done using ANSYS 18.0. After meshing simulations has been performed to obtain the model analysis for first five natural frequencies. These frequencies are shown inTable 2.

*Table 2.Natural Frequency at first 5 modes for anExisting silencer.*

| Mode | 1st | 2nd | 3rd | 4th | 5th |
|---|---|---|---|---|---|
| Frequency (Hz) | 146.58 | 287.71 | 294.96 | 435.74 | 574.54 |

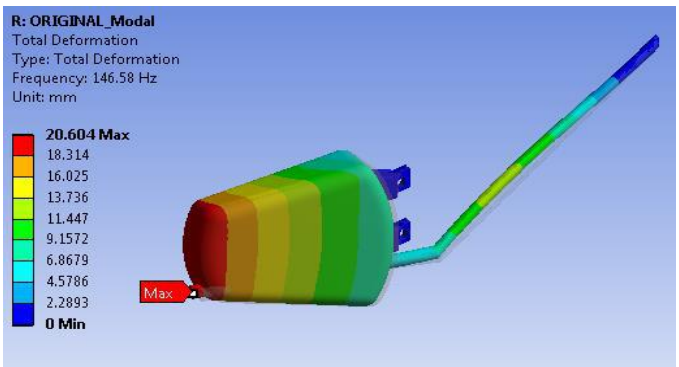


*Fig. 4.mode frequency for 146.58Hz*

*https://dx.doi.org/10.22161/ijaers.5.1.2* *ISSN: 2349-6495(P) | 2456-1908(O)*

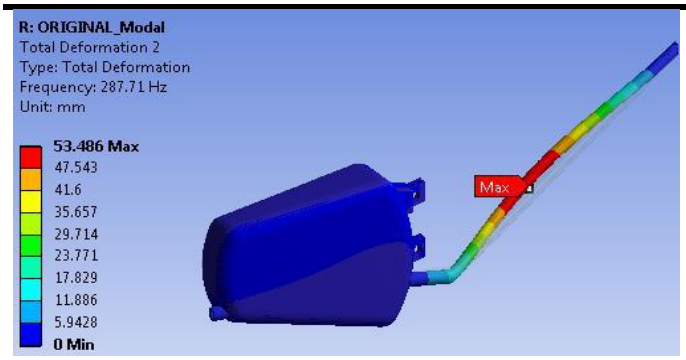


*Fig.5.mode frequency for 287.71Hz.*

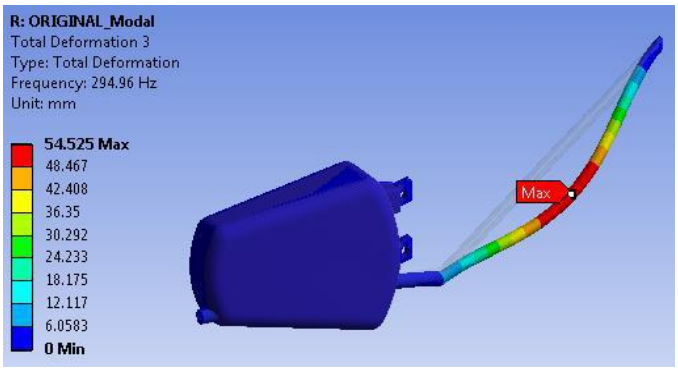


*Fig.6.3rd mode frequency for 294.96Hz.*

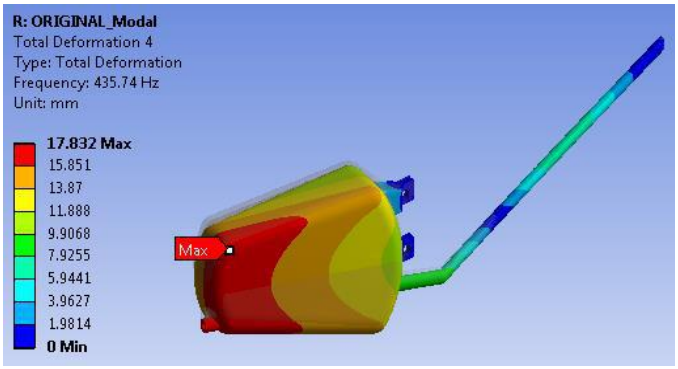


*Fig.7.4th mode frequency for 435.74Hz*

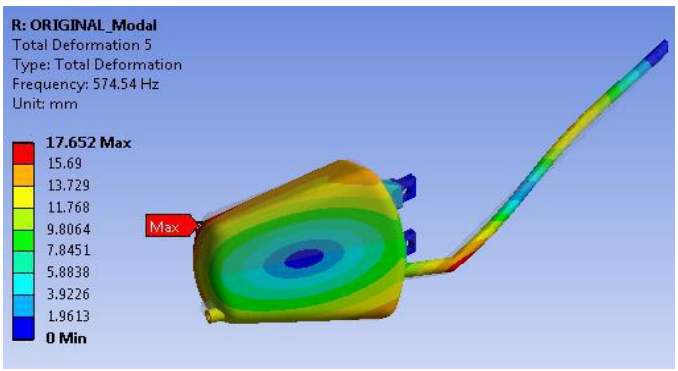


*Fig.8.5th mode frequency for 574.54Hz.*

## V. HARMONIC ANALYSIS OF EXISTING MODEL

The harmonic analysis has been performed on the existing model. The mode 4 was selected for the harmonic analysis because it shows maximum bending. The excitation of 5G has been applied to the model. The boundary condition used in the simulation is shown in figure 9. In Table 3, boundary conditions are specified.

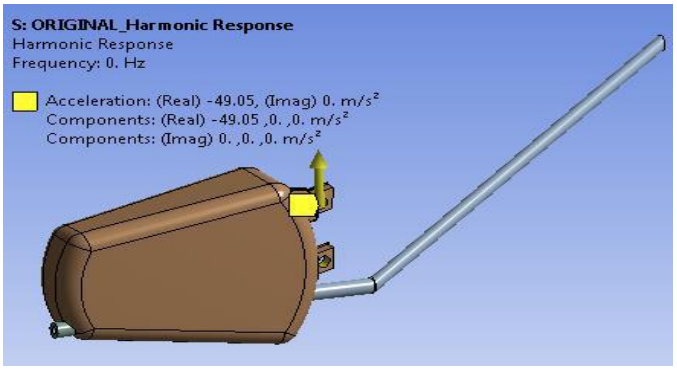


*Fig.9.Boundary condition of existing model*

*Table 3.Boundary condition of existing model.*

| | |
|---|---|
| Frequency spacing | Linear |
| Range Minimum | 0 Hz |
| Range Maximum | 1000 Hz |
| Solution Interval | 10 |
| User Defined Frequencies | Off |
| Solution method | Mode Superposition |
| Include Residual Vector | No |
| Cluster Result | No |

Figure 10. gives the clear idea regarding the amplitude in Mega-Pascal (MPa) and natural frequencies of different modes. The maximum frequency was observed in mode four, Hence it corresponds to the maximum amplitude of 13.981 MPa. For the same mode, the equivalent stress is found 2.143 MPa (See Figure 11).

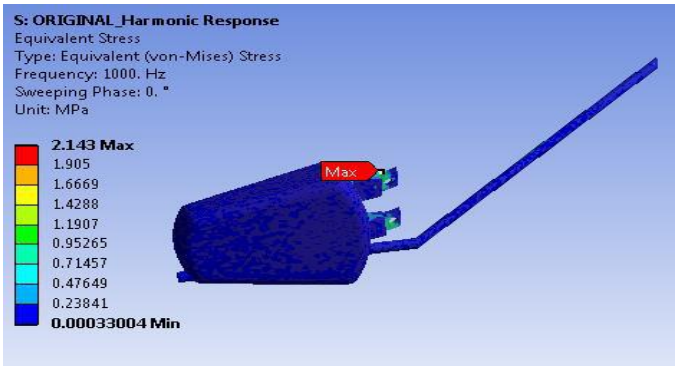


*Fig.10.Equivalent Stress of existing model*

*https://dx.doi.org/10.22161/ijaers.5.1.2* *ISSN: 2349-6495(P) | 2456-1908(O)*

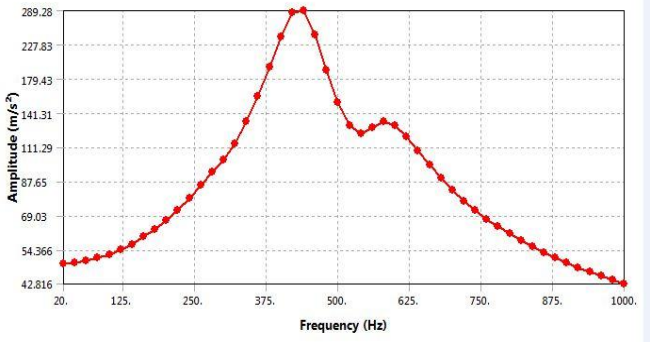


*Fig.11.Acceleration frequency response of theexisting model.*

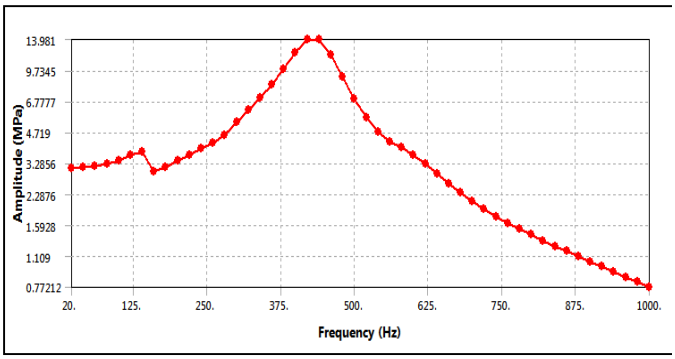


*Fig.12.Maximum principal stress response of existing model*

## VI. NEED OF MODIFICATION OF SILENCER

According to Jis D 1601 (JapaneseStandard), 33 Hz to 67 Hz is the damageable frequencies of vibration testing for automobile silencer. Vibration frequencies are necessary to be reduced, these causes more vibration hence noise in the exhaust system. Mode 4 shows more bending, so we took mode 4,an optimized modal for reducing the vibration. For reducing the failure in the existing model we add single stiffener in the existing model.

## VII. ADDITION OF SINGLE STIFFENER IN OPTIMIZED MODEL

Single Stiffener is added to shift the frequency of the optimized model. First, we add a single stiffener and analysis results. The analysis was done and first five natural frequencies are determined and tabulated in Table 4. Figure13. Shows the modified geometry in which a stiffener is added. After modifying the geometry, thenew mesh was generated with the Ansys package. Fig.14shows the meshing of the modified geometry. The boundary condition for the modified model is shown in Fig. 15.

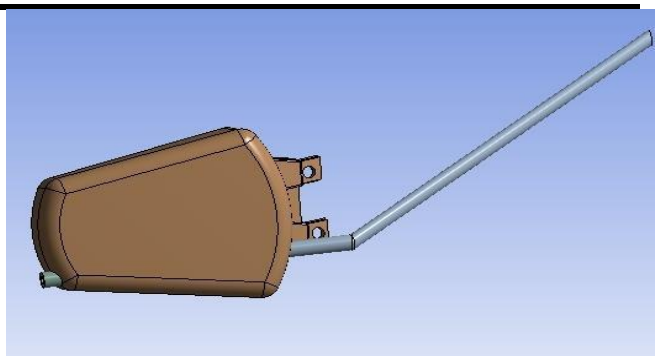

*Fig.13.Modified Model by adding a single stiffener plate*

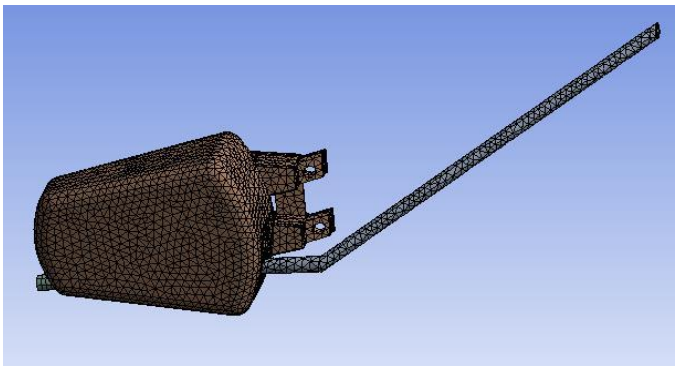

*Fig.14. Discretized Modified Model by adding a single stiffener plate*

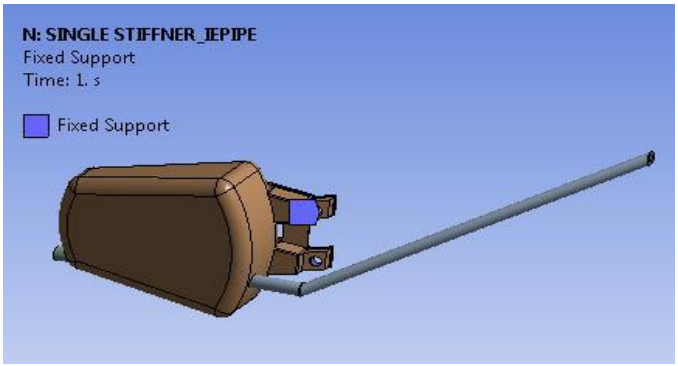


*Fig. 15. Boundary conditions for modified model by adding a single stiffener plate*

## VIII. MODAL ANALYSIS OF OPTIMIZED MODEL

The modification was done in the existing silencer model with adding a stiffener plate. After this modification, modal analysis has been performed and itsresults in ten natural frequencies. The contour of total deformation is shown for different natural frequencies in Figure. (16-25). The first ten natural frequencies after the modification is tabulated in Table 4.

*https://dx.doi.org/10.22161/ijaers.5.1.2* *ISSN: 2349-6495(P) | 2456-1908(O)*

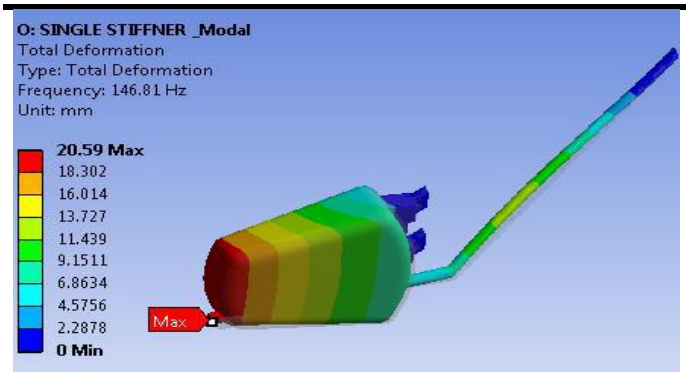


*Fig.16.1st mode of modified silencer*

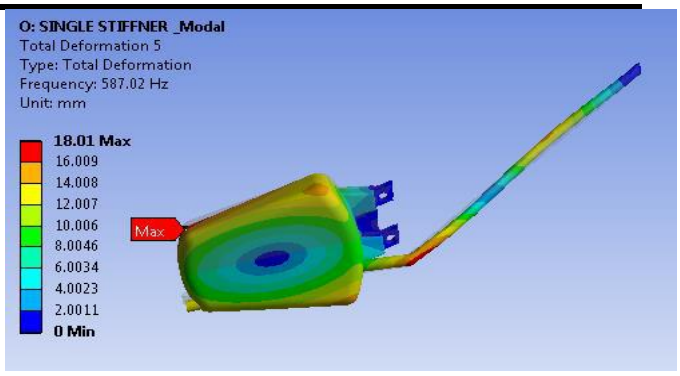


*Fig.20.5th mode of themodified silencer.*

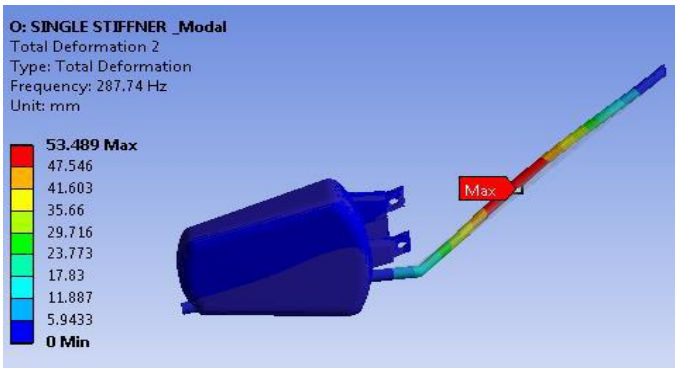


*Fig.17.2ndmode of themodified silencer.*

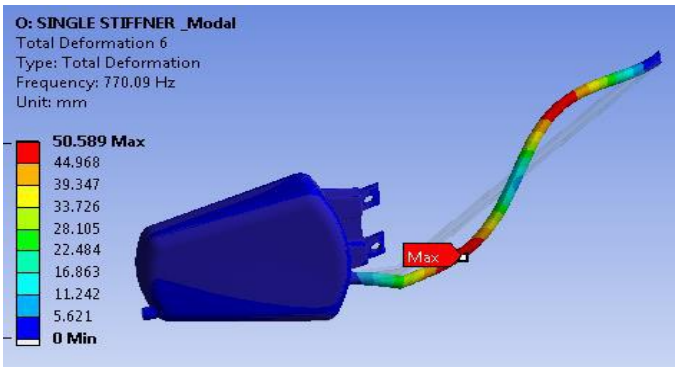


*Fig.21.6thmode of modified silencer by adding single stiffener.*

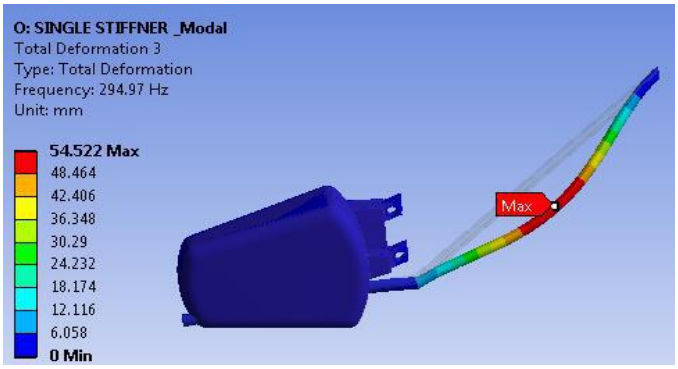


*Fig.18.3rd mode of themodified silencer.*

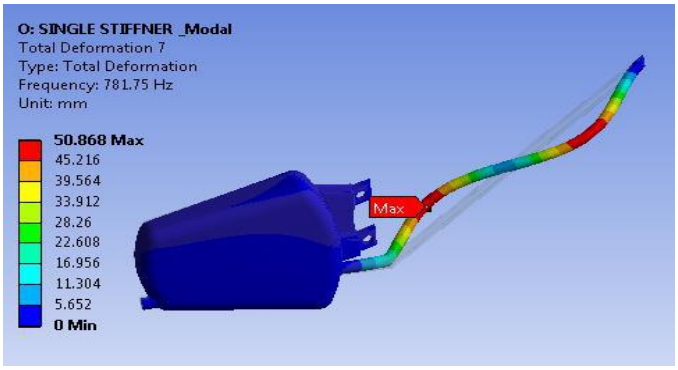


*Fig.22. 7thmode of modified silencer by adding asingle stiffener*

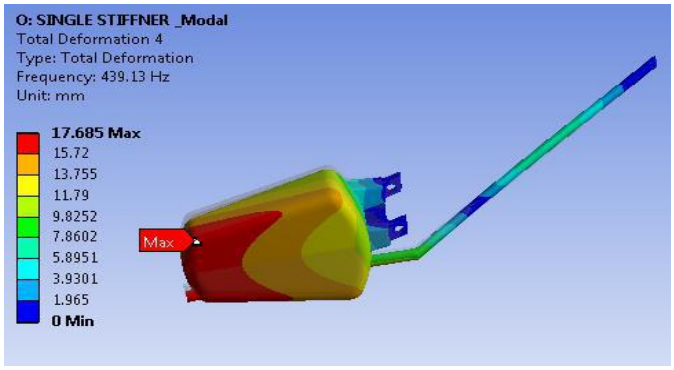


*Fig.19.4th mode of themodified silencer.*

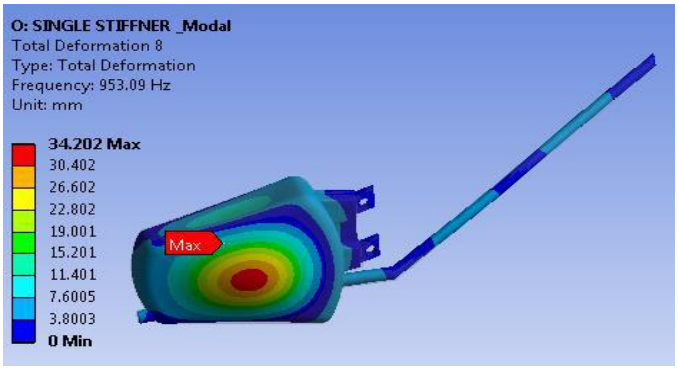


*Fig.23. 8thmode of modified silencer by adding single stiffener*

*https://dx.doi.org/10.22161/ijaers.5.1.2* *ISSN: 2349-6495(P) | 2456-1908(O)*

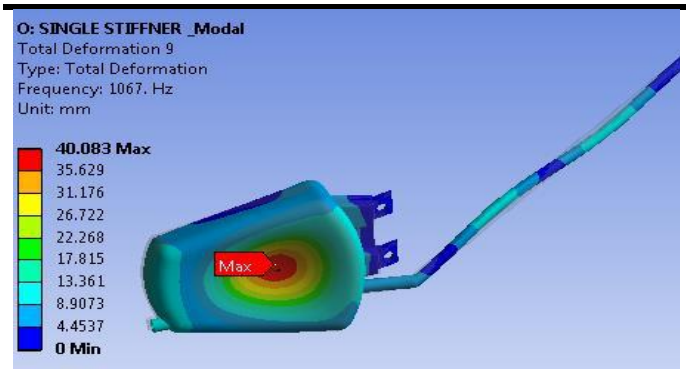


*Fig.24. 9th mode of modified silencer by adding asingle stiffener*

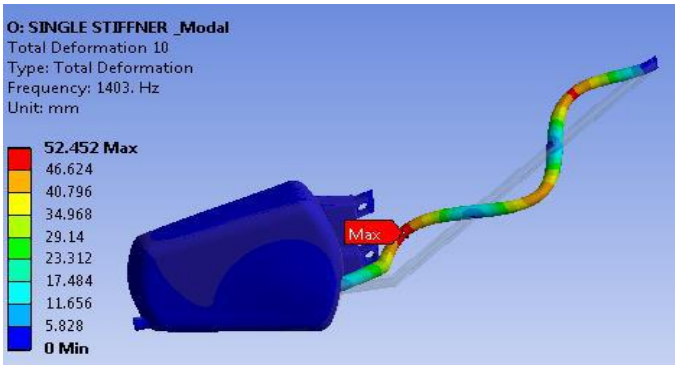


*Fig.25. 10th mode of modified silencer by adding single stiffener.*

*Table 4.Natural Frequency at first 10 modes for anoptimized silencer.*

| Mode | 1st | 2nd | 3rd | 4t | 5t | 6t | 7t | 8t | 9th | 10th |
|---|---|---|---|---|---|---|---|---|---|---|
| Frequency | 146. | 287. | 294. | 43 | 58 | 77 | 78 | 95 | 1067 | 1403 |

## IX. HARMONIC ANALYSIS OF OPTIMIZED MODEL

After the adding a single stiffener plate again the harmonic analysis has been done in thesame manner as previously done for the existing model. Table 5 shows the boundary condition used in the modified model. The same procedure has been performed for the harmonic analysis. The excitation of 5g had applied to the modified model. Figure 26 shows the boundary condition used in the modified model.

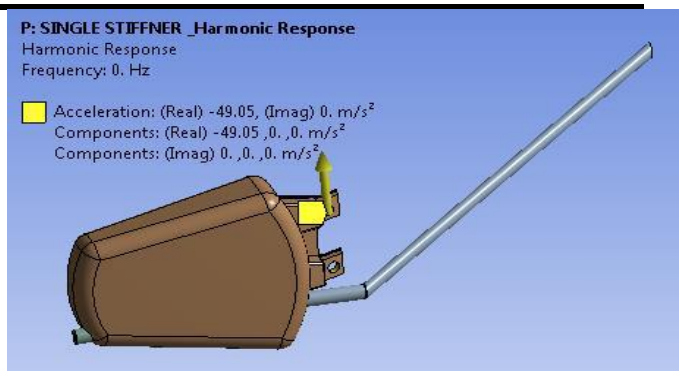


*Fig.26.Boundary Conditions of optimized model.*

Amplitude vs. frequency plot for the modified model after the addition of single stiffener plate is shown in Figure 29. The maximum amplitude of the stress is found 7.0695 MPa at 435 frequency. The corresponding equivalent stress is 1.9199 MPa (see Figure 29). The acceleration and frequency response is also plotted in Figure 27. The maximum acceleration of 156.85 m/s$^2$ is obtained at the natural frequency of 435 Hz.

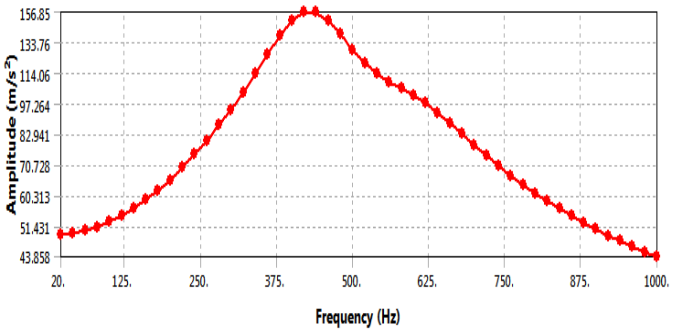


*Fig.27.Acceleration frequency response of theoptimized model.*

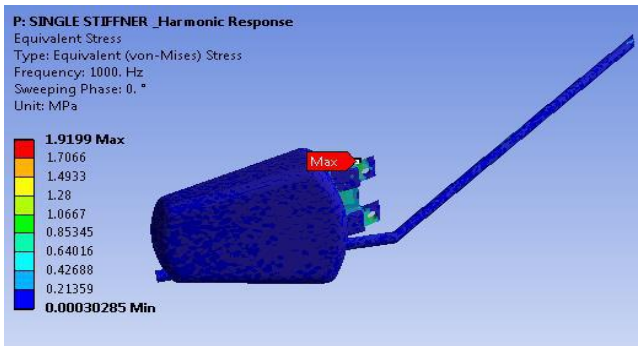


*Fig.28.Maximum principal stress response of optimized model*

*https://dx.doi.org/10.22161/ijaers.5.1.2* *ISSN: 2349-6495(P) | 2456-1908(O)*

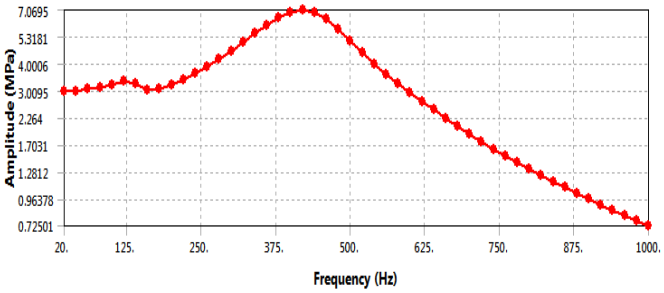


*Fig.29.Maximum principal stress response of optimized model*

## X. EXPERIMENTAL VALIDATION

The silencer model has been taken for the experiment. The experiment includes the testing of vibration by theaccelerometer.Fig.30 shows the experimental setup for amodified model having single stiffener. The sensor was mounted at the top of the modified silencer as shown in Fig.30. To impose the vibration to the model a hammer has been applied to the silencer. Because of the hammering action, the vibrations get induced in the model. These vibrations are then sensed with the sensor and corresponding readings are shown by theaccelerometer.

*Fig.30.Experimentation System*

The experimental validation is done by using FFT (Fast Fourier Transform) analyzer. The FFT spectrum analyzer samples the input signal computes the magnitude of its sine and cosine components and displays the spectrum of these measured frequency components. The advantage of this technique is its speed. Because FFT spectrum analyzers measure all frequency components at the same time, the technique offers the possibility of being hundreds of times faster than traditional analog spectrum analyzers.
The result obtained by FFT analyzer for first six natural frequencies are determined and tabulated as follow.

*Table 5.First six modal frequency of vibration by FFT analyzer*

| Mode | 1 | 2 | 3 | 4 | 5 | 6 |
|---|---|---|---|---|---|---|
| (Frequency in Hz) | 97 | 391 | 614 | 775 | 958 | 1066 |

Frequency response function of the exhaust system is shown in Fig.31for different modes.

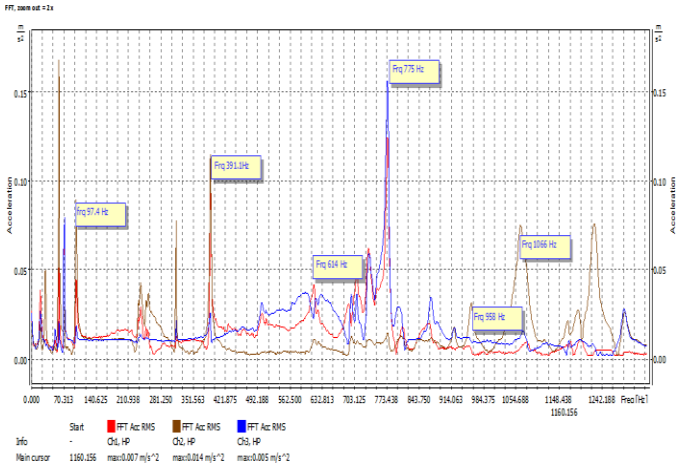


*Fig.31.Frequency response function of the exhaust system for different modes.*

## XI. RESULT

Table 17 shows the comparison of the natural frequencies of vibration silencer by FEM package and FFT analyzer. The comparison shows that the natural frequency by both methods is nearly same (see Fig.32).

*Table 6.Six modal frequency of vibration.*

| Mode | FEM (Frequency in Hz) | FFT(Frequency in Hz) |
|---|---|---|
| 1 | 146 | 97 |
| 2 | 439 | 391 |
| 3 | 587 | 614 |
| 4 | 770 | 775 |
| 5 | 953 | 958 |
| 6 | 1067 | 1066 |

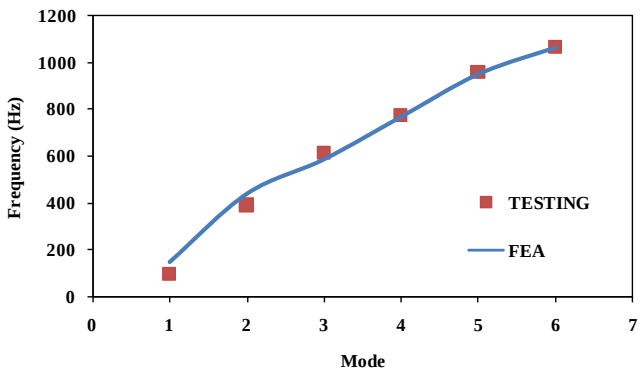


*Fig.32.Comparison of FEA and testing*

*https://dx.doi.org/10.22161/ijaers.5.1.2* *ISSN: 2349-6495(P) | 2456-1908(O)*

## XII. CONCLUSION

The silencer natural frequencies have been calculated by using the ANSYS package and by FFT analyzer. By both the method the natural frequencies are nearly same and that are useful while the design of silencer to avoid the resonance.The natural frequency silencer has been calculated by using the Ansys 18.0. The modification in the design has enhanced the dynamic performance of a silencer. Particular modification in design incorporates the addition of stiffener in the modified silencer. The amplitude of acceleration is reduced from 289.28 $m/s^2$ to 156.85 $m/s^2$ due to theaddition of stiffeners. Maximum Principal Stress value reducedto alower value than existing design.from 13.981Mpa to 7.0695Mpa. Vibration modes of silencer haven't been drastically altered, but stiffener method can be used to reduce excitations and helptoincrease fatigue life and efficiency of the silencer.

## REFERENCES

[1] V.P. Patekar and R.B. Patil " Vibrational Analysis of Automotive Exhaust Silencer Based on FEMand FFT Analyzer" International Journal on Emerging Technologies 3(2): 1-3(2012)

[2] Amit Mahadeo Asabe1, Prof.Pravin P Hujare "Performance Enhancement ofAutomotive Silencer Using Finite Element Analysis" International Journal of Engineering Science Invention ISSN (Online): 2319 – 6734, ISSN (Print): 2319 – 6726 www.ijesi.org Volume 3 Issue 8, August 2014, PP.14-22

[3] Silex Exhaust Slincer

[4] H. D. Kima, Y.-H. Kweona, T. Setoguchib "A study of the weak shock wave propagating through" Journal of Sound and Vibration 275, 2004 PP.893–915engine exhaust silencer system.

[5] Lian-yun LIU, Zhi-yong HAO, Chi LIU "CFD analysis of a transfer matrix of exhaust muffler with mean flow and prediction of exhaust noise" Appl Phys & Eng. 2012 13(9), PP. 709-716

[6] Takashi Yasuda, Chaoqun Wua, Noritoshi Nakagawa, Kazuteru Nagamura "Predictions and experimental studies of the tail pipe noise of an automotive muffler using a one dimensional CFD model" Applied Acoustics 71 2010, PP. 701–707

[7] Potente Daniel "General design principles for an automotive muffler" November 2005, PP. 9-11

*https://dx.doi.org/10.22161/ijaers.5.1.3* *ISSN: 2349-6495(P) | 2456-1908(O)*

# Optimization of the Parameters of a Hydraulic Excavator Swinging Mechanism

Rosen Mitrev

Mechanical Engineering Faculty, Technical University-Sofia, Sofia, Bulgaria

***Abstract—*** *The presented paper is focused to the optimization of the parameters of a hydraulic excavator swinging mechanism. A trapezoidal velocity profile is considered for rotation of the excavator platform to the predefined angle. Equations for the torque and power, needed to rotate the platform according to the prescribed trapezoidal trajectory are derived. The maximum values of the driving torque and power are optimized.*

***Keywords— hydraulic excavator, swinging mechanism, optimization.***

## I. INTRODUCTION

The hydraulic excavator is a multifunctional earth moving machine, widely used in the construction and mining industry. Its swinging mechanism is intended to rotate the excavator platform together with the front digging manipulator about a vertical axis. It does not participate directly in the earthmoving operations and has auxiliary functions, mainly by performing the transport operations of the excavated soil, as well as the positioning of the digging manipulator in the required position [1]. Typically [2], the motion of the prime mover is transferred to the platform by a powertrain, which consists of a hydraulic pump, of an axial-piston hydraulic motor (Fig.1, pos.1) coupled to a vertical two-stage planetary gearbox (Fig.1, pos.2), whose output shaft with the coupled small sprocket is engaged with the slewing bearing toothed ring (Fig.1,pos.3).

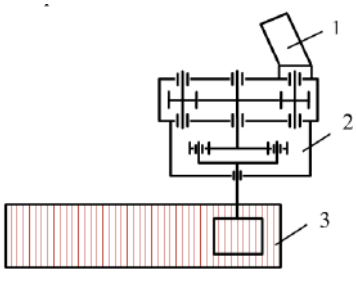


*Fig.1: Kinematic scheme of the excavator swinging mechanism*

The motion trajectory of the rotational platform $\varphi_{pl}(t)$ (Fig.2) determines the kinematic and dynamic properties of the swinging mechanism components, including the prime mover, as well as the ergonomic characteristics of the operator.

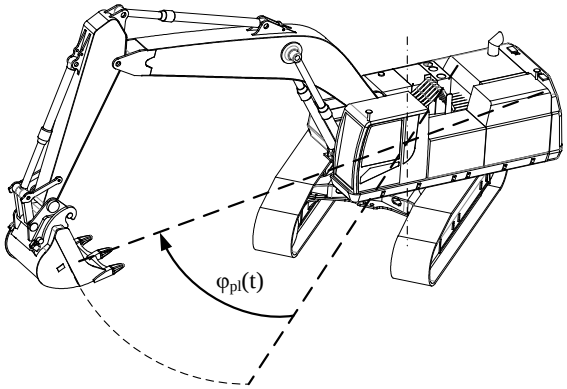


*Fig.2: Angle of rotation of the platform*

Different trajectories $\varphi_{pl}(t)$ are possible to use [3] including widely used linear segment joined with parabolic blends. For the linear segment the velocity is constant, while for the parabolic blends the velocity is a linear function of the time, that is why the velocity profile is called trapezoidal velocity profile. The rotation of the platform is divided into three phases: 1) acceleration phase, characterized by a linear increase of the velocity, a positive acceleration and a parabolic increase of the rotation angle; 2) phase of the constant velocity, characterized by a zero acceleration and linear increase of the rotation angle; 3) deceleration phase, characterized by a linear decrease of the velocity, a negative acceleration and a parabolic increase of the rotation angle. In the most cases, the acceleration and the deceleration phases have the same duration. Although the acceleration is discontinuous and contributes to the producing of vibrational effects in the mechanical systems with structural elasticity, this type of motion law is widely used [4] due to its simplicity and wide use in the real applications.

## II. KINEMATIC MODEL

Fig. 3 depicts the trapezoidal velocity profile, where by $\dot{\varphi}_{pl}^{\max}$ is denoted the constant angular velocity of the platform, by $\Delta t$ is denoted the duration of the acceleration/deceleration phase, and by $t_f$ is denoted the total duration of the rotation.

*https://dx.doi.org/10.22161/ijaers.5.1.3* *ISSN: 2349-6495(P) | 2456-1908(O)*

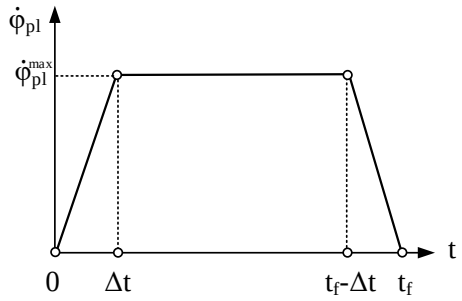


*Fig.3: Trapezoidal velocity profile*

If by $\varphi_{pl}^{f}$ is denoted the value of the needed angle of rotation and by $\ddot{\varphi}_{pl}^{tr}$ - the angular acceleration during the acceleration and deceleration phases then the considered motion law is represented by the following piecewise defined function:

$$\varphi_{pl}=\begin{cases}\dfrac{\ddot{\varphi}_{pl}^{tr}}{2}t^2, & 0\le t\le \Delta t\\ \dfrac{1}{2}\left(\varphi_{pl}^{f}+\dot{\varphi}_{pl}^{\max}\left(2t-t_f\right)\right), & \Delta t<t\le t_f-\Delta t\\ \varphi_{pl}^{f}-\dfrac{\ddot{\varphi}_{pl}^{tr}}{2}\left(t-t_f\right)^2, & t_f-\Delta t<t\le t_f\end{cases} \quad (1)$$

and therefore, the angular velocity and acceleration are:

$$\dot{\varphi}_{pl}=\omega_{pl}=\begin{cases}\ddot{\varphi}_{pl}^{tr}t, & 0\le t\le \Delta t\\ \dot{\varphi}_{pl}^{\max}, & \Delta t<t\le t_f-\Delta t\\ \ddot{\varphi}_{pl}^{tr}\left(t_f-t\right), & t_f-\Delta t<t\le t_f\end{cases} \quad (2)$$

$$\ddot{\varphi}_{pl}=\varepsilon_{pl}=\begin{cases}\ddot{\varphi}_{pl}^{tr}, & 0\le t\le \Delta t\\ 0, & \Delta t<t\le t_f-\Delta t\\ -\ddot{\varphi}_{pl}^{tr}, & t_f-\Delta t<t\le t_f\end{cases} \quad (3)$$

where

$$\Delta t=\frac{\dot{\varphi}_{pl}^{\max}}{\left|\ddot{\varphi}_{pl}^{tr}\right|} \quad (4)$$

The duration of the platform rotation is presented by the following equation:

$$t_f=\frac{\varphi_{pl}^{f}}{\dot{\varphi}_{pl}^{\max}}+\frac{\dot{\varphi}_{pl}^{\max}}{\left|\ddot{\varphi}_{pl}^{tr}\right|} \quad (5)$$

Equation (5) can be represented as a quadratic equation in relation to $\dot{\varphi}_{pl}^{\max}$:

$$\left(\dot{\varphi}_{pl}^{\max}\right)^2-t_f\left|\ddot{\varphi}_{pl}^{tr}\right|\dot{\varphi}_{pl}^{\max}+\varphi_{pl}^{f}\left|\ddot{\varphi}_{pl}^{tr}\right|=0 \quad (6)$$

and then by using (4), eq. (6) takes the following form:

$$\ddot{\varphi}_{pl}^{tr}\Delta t^2-t_f\ddot{\varphi}_{pl}^{tr}\Delta t+\varphi_{pl}^{f}=0 \quad (7)$$

The equation (7) can be represented as:

$$\ddot{\varphi}_{pl}^{tr}=\frac{\varphi_{pl}^{f}}{\Delta t\left(t_f-\Delta t\right)} \quad (8)$$

Also, the following equation is valid:

$$\Delta t=\frac{\dot{\varphi}_{pl}^{\max}t_f-\varphi_{pl}^{f}}{\dot{\varphi}_{pl}^{\max}} \quad (9)$$

## III. TORQUE AND POWER MODEL

The reduced to the platform axis of rotation driving torque $M_{pl}$ is represented as a sum of the following torques [5, 6]:

$$M_{pl}=M_{pl}^{st}+M_{pl}^{dyn} \quad (10)$$

where $M_{pl}^{st}$ is a static torque, exerted mainly by the slewing bearing resistive forces and wind forces; $M_{pl}^{dyn}$ - dynamic torque, exerted by the inertial forces of the platform and powertrain elements.

The dynamic torque is calculated as:

$$M_{pl}^{dyn}=J\ddot{\varphi}_{pl} \quad (11)$$

where $J$ is the total mass moment of inertia of the rotational platform together with the front digging manipulator and the powertrain elements, reduced to the axis of rotation of the platform.

Using (3), the torque equation (10) obtains the following form:

$$M_{pl}=M_{pl}^{st}+J\begin{cases}\ddot{\varphi}_{pl}^{tr}, & 0\le t\le \Delta t\\ 0, & \Delta t<t\le t_f-\Delta t\\ -\ddot{\varphi}_{pl}^{tr}, & t_f-\Delta t<t\le t_f\end{cases} \quad (12)$$

and its maximum value is during the acceleration phase:

$$M_{pl}^{\max}=M_{pl}^{st}+J\ddot{\varphi}_{pl}^{tr} \quad (13)$$

By the use of (8), $M_{pl}^{\max}$ is represented as a function of $\Delta t$ and $t_f$:

$$M_{pl}^{\max}=M_{pl}^{st}+J\frac{\varphi_{pl}^{f}}{\Delta t\left(t_f-\Delta t\right)} \quad (14)$$

The power, needed to drive the platform $P_{pl}$ is:

$$P_{pl}=M_{pl}\dot{\varphi}_{pl} \quad (15)$$

Taking into account (10), the power is computed as:

$$P_{pl}=\left(M_{pl}^{st}+J\ddot{\varphi}_{pl}\right)\dot{\varphi}_{pl} \quad (16)$$

By the use of (2) and (3), (16) is represented as:

*https://dx.doi.org/10.22161/ijaers.5.1.3* *ISSN: 2349-6495(P) | 2456-1908(O)*

$$P_{pl}=\begin{cases} M_{pl}^{st}\ddot{\varphi}_{pl}^{tr}t+J\left(\ddot{\varphi}_{pl}^{tr}\right)^2 t, \\ if\ \ 0\le t\le \Delta t \\ M_{pl}^{st}\dot{\varphi}_{pl}^{\max}, \\ if\ \ \Delta t<t\le t_f-\Delta t \\ M_{pl}^{st}\ddot{\varphi}_{pl}^{tr}\left(t_f-t\right)-J\left(\ddot{\varphi}_{pl}^{tr}\right)^2\left(t_f-t\right), \\ if\ \ t_f-\Delta t<t\le t_f \end{cases} \quad (17)$$

As can be seen, the maximum of the needed power is at the end of the acceleration phase and its value is:

$$P_{pl}^{\max}=M_{pl}^{st}\ddot{\varphi}_{pl}^{tr}\Delta t+J\left(\ddot{\varphi}_{pl}^{tr}\right)^2\Delta t \quad (18)$$

By using (4), the equation for the maximum value of the power is represented as:

$$P_{pl}^{\max}=M_{pl}^{st}\dot{\varphi}_{pl}^{\max}+J\frac{\left(\dot{\varphi}_{pl}^{\max}\right)^2}{\Delta t} \quad (19)$$

From (9) it follows that:

$$\dot{\varphi}_{pl}^{\max}=\frac{\varphi_{pl}^{f}}{t_f-\Delta t} \quad (20)$$

By inserting (20) in (19), for the maximum value of the power one obtains:

$$P_{pl}^{\max}=\frac{\varphi_{pl}^{f}\left(M_{pl}^{st}t_f\Delta t-M_{pl}^{st}\left(\Delta t\right)^2+\varphi_{pl}^{f}J\right)}{\Delta t\left(t_f-\Delta t\right)^2} \quad (21)$$

As one can see, for known values of $\varphi_{pl}^{f}$, $M_{pl}^{st}$ and $J$, the equations for the maximum torque (14) and the maximum power (21) are functions of the duration of the rotation $t_f$ and the duration $\Delta t$ of the acceleration/ deceleration periods, so their optimal values could found.

## IV. OPTIMIZATION OF THE MAXIMUM DRIVING TORQUE VALUE

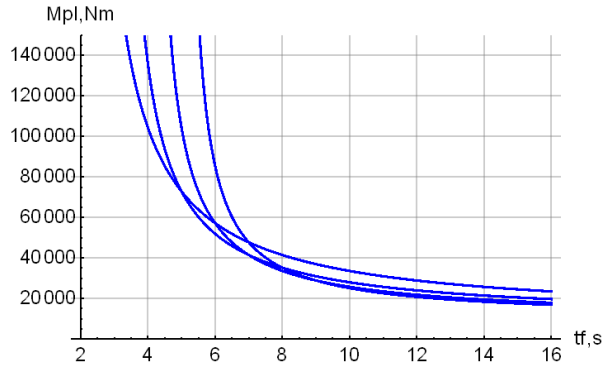


*Fig.4: Driving torque as a function of the duration of the rotation*

Fig.4 depicts the driving torque, computed according to (14) as a function of the duration of the rotation $t_f$ for the values of $\Delta t=2,3,4$ and 5 s. and: $M_{pl}^{st}=10kNm$, $\varphi_{pl}^{f}=\pi$, $J=120.10^3 kgm^2$. In Fig.5 is shown the driving torque as a function of the acceleration phase duration for $t_f$=12s and $M_{pl}^{st}=10kNm$, $\varphi_{pl}^{f}=\pi$, $J=120.10^3 kgm^2$.

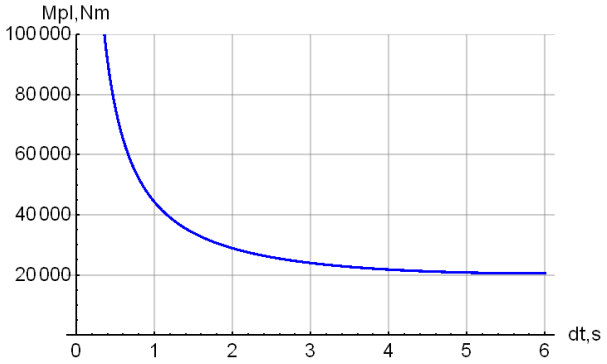


*Fig.5: Driving torque as a function of the acceleration phase duration*

As one can see from Fig.4 and Fig.5, the increase of the duration of the rotation $t_f$ and the duration $\Delta t$ of the acceleration/deceleration periods unambiguously decreases the value $M_{pl}^{\max}$ of the maximum torque.

If the value of the maximum driving torque is limited to the value $\left[M_{pl}^{\max}\right]$ and (14) is solved for $t_f$, then the following function $t_f\left(\Delta t\right)$ is obtained:

$$t_f=\Delta t+\frac{J\varphi_{pl}^{f}}{\left(\left[M_{pl}^{\max}\right]-M_{pl}^{st}\right)\Delta t} \quad (22)$$

The structure of this equation suggests that optimization by numerical or analytical methods [7] of the duration $t_f$ is possible. In Fig.6 is shown the graph of the function $t_f\left(\Delta t\right)$ for $\left[M_{pl}^{\max}\right]=30$, 60, 90, 120 and 150 kNm.

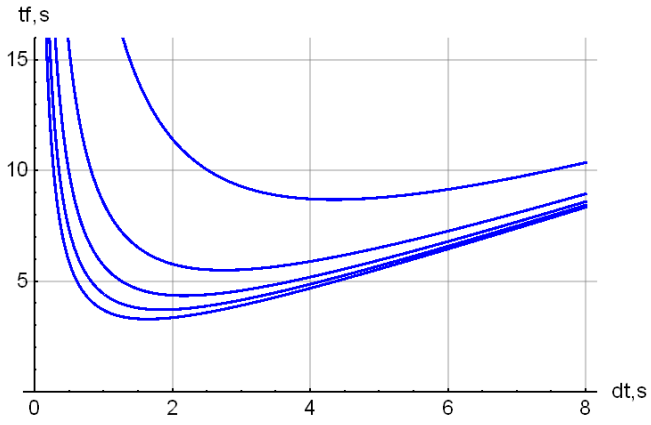


*Fig.6: The function $t_f\left(\Delta t\right)$*

The objective function is:

$$t_f\left(\Delta t\right)\rightarrow \min \quad (23)$$

and the following constraint must be satisfied:

*https://dx.doi.org/10.22161/ijaers.5.1.3* *ISSN: 2349-6495(P) | 2456-1908(O)*

$$0 < \Delta t \le \frac{t_f}{2} \tag{24}$$

The minimum of the function (22) is determined analytically by the solution of the following equation:

$$\frac{dt_f}{d(\Delta t)} = 0 \tag{25}$$

which leads to:

$$1 - \frac{J\varphi_{pl}^f}{\left(\left[M_{pl}^{\max}\right] - M_{pl}^{st}\right)\Delta t^2} = 0 \tag{26}$$

From (26) it can be found that the optimal value of $\Delta t$ is:

$$\Delta t^* = \sqrt{\frac{J\varphi_{pl}^f}{\left(\left[M_{pl}^{\max}\right] - M_{pl}^{st}\right)}} \tag{27}$$

## V. OPTIMIZATION OF THE MAXIMUM POWER VALUE

Fig.7 depicts the driving power, computed according to (21) as a function of the duration of the rotation $t_f$ for the value of $\Delta t = 2$ s., $M_{pl}^{st} = 10kNm$, $\varphi_{pl}^f = \pi$, $J = 120.10^3 kgm^2$. As one can conclude, the increase of the duration of the rotation $t_f$ unambiguously decreases the value $P_{pl}^{\max}$.

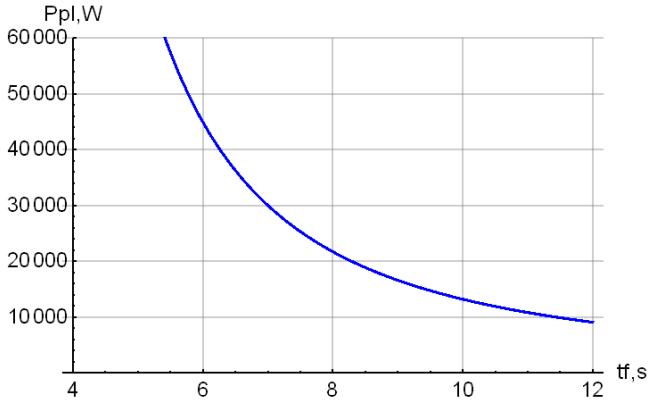


*Fig.7: The driving power, as a function of the duration of the rotation*

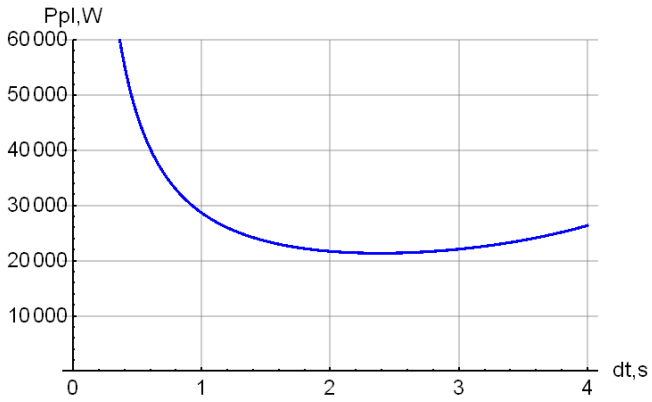


*Fig.8: The driving power as a function of $\Delta t$*

Fig.8 depicts the change of the driving power as a function of $\Delta t$ for the value of $t_f$=8 s., $M_{pl}^{st} = 10kNm$, $\varphi_{pl}^f = \pi$, $J = 120.10^3 kgm^2$. As one can see there is a well-marked minimum of the power for a certain value of $\Delta t$.

It is possible to determine $\Delta t$ for which $P_{pl}^{\max}$ is minimized. The objective function is:

$$P_{pl}^{\max}(\Delta t) \to \min \tag{28}$$

Subjected to the constraint (24).

By computing

$$\frac{dP_{pl}^{\max}}{d(\Delta t)} = 0 \tag{29}$$

one obtains the following cubic equation:

$$M_{pl}^{st}\Delta t^3 - M_{plc}^{st} t_f \Delta t^2 - 3\varphi_{pl}^f J\Delta t + \varphi_{pl}^f J t_f = 0 \tag{30}$$

Two approaches are possible to solve eq. (30) in relation to $\Delta t$:

- If the static power is much smaller then the dynamic one, then in (30) $M_{pl}^{st}$ is neglected and only the dynamic power is minimized. In this case the solution leads to the following value for the optimal duration of the acceleration phase:

$$\Delta t^* = \frac{t_f}{3} \tag{31}$$

- If the static power cannot be neglected, then the cubic eq. (30) is solved by analytical or numerical methods [8]. The value of $\Delta t^*$ is chosen satisfying constraint (24).

## VI. CONCLUSIONS

This paper presents an approach for optimization of the parameters of a hydraulic excavator swinging mechanism. A trapezoidal velocity profile is considered for rotation of the excavator platform to the predefined angle. Equations for the driving torque and power, needed to rotate the platform according to the prescribed trapezoidal trajectory are derived. The maximum values of the needed driving torque and power are optimized.

## REFERENCES

[1] Dantchev, D, Hristov, D. Basics of the road and construction machines. Technica, Sofia, 1990.

[2] Jovanović, V., Janošević, D., Djokić, R., Pavlović, J. Software development for optimal synthesis of slewing platform drive mechanism of mobile machine. 5th International conference "Transport and Logistics", Nish Serbia, 2014.

[3] Biagiotti L., Melchiorri, C. Trajectory Planning for Automatic Machines and Robots. Springer, 2008.

*https://dx.doi.org/10.22161/ijaers.5.1.3* *ISSN: 2349-6495(P) | 2456-1908(O)*

[4] Z. Yu, C. Han and M. Haihua, A novel approach of tuning trapezoidal velocity profile for energy saving in servomotor systems, 2015 34th Chinese Control Conference (CCC), Hangzhou, 2015, pp. 4412-4417. doi: 10.1109/ChiCC.2015.7260323.

[5] Danchev, D. Hydromechanical synthesis of hydraulic excavator driving mechanisms. D.Sc dissertation, TU-Sofia 1999.

[6] Ivanov V. Measurement of moments with balance torquemeter. CAx technologies, Issue 3, December 2015, pp.141-144.

[7] Georgieva B. Theoretical aspects of the Engineering design. TU-Sofia Publishing house, 2014. ISBN: 978-619-167-124-3.

[8] Chapra, S., Canale, R. Numerical Methods for Engineers. New York: McGraw Hill, 1998

*https://dx.doi.org/10.22161/ijaers.5.1.4* *ISSN: 2349-6495(P) | 2456-1908(O)*

# Thermal Analysis of a Finned Thermosyphon for Heat Exchanger Applications

V.M. Aguiar[1], G.A. Bartmeyer[1], L. Krambeck[1], P.H.D. Santos[2], T. Antonini Alves[1]

[1]Federal University of Technology - Paraná, 84.016-210, PONTA GROSSA, Brazil
Email: *viniciusmarrone@hotmail.com, gabartmeyer@hotmail.com, larikrambeck@hotmail.com, thiagoaalves@utfpr.edu.br*
[2]Federal University of Technology - Paraná, 80.230-901, CURITIBA, Brazil
Email: *psantos@utfpr.edu.br*

***Abstract*****—** *A thermosyphon is a gravity-assisted heat pipe used to improve the heat transfer in several applications. In this paper, a thermal analysis of a finned thermosyphon for heat exchanger applications was experimentally researched. The thermosyphon was manufactured from a copper tube the external diameter of 9.45 mm, the inner diameter of 7.75 mm, and a total length of 200 mm. The working fluid used was water with a filling ratio of 40% of the evaporator volume. The condenser was cooled by air forced convection, the adiabatic section was insulated with fiberglass and the evaporator was heated by an electrical resistor. Experimental tests were performed to a heat load from 5 up to 50W at vertical position (evaporator above condenser). As a result of the research, the thermosyphon operated satisfactorily to the tested position. Also, the finned thermosyphon obtained better thermal performance than the un-finned condenser, proving the effectiveness of the fin application.*

***Keywords*****— fins, thermal analysis, thermosyphon.**

## I. INTRODUCTION

A thermosyphon is a gravity-assisted heat pipe used to improve the heat transfer in several applications [1]. The main feature of a thermosyphon is the use of vaporization latent heat to transmit heat at high rates over considerable distances with small temperature decrease. Its advantages are flexibility, simple construction, and easy control with no external pumping power [2].

Thermosyphons have three regions with distinct roles in their operation. These regions are evaporator, adiabatic section, and condenser. The evaporator, the lower region of the tube, is heated by a hot source and the working fluid undergoes an evaporation process. This steam, because of the pressure difference, moves to the colder region (condenser). In this region, the steam generated in the evaporator loses energy as heat and is condensed. The working fluid in liquid state flows back to the evaporator by gravity, closing the cycle. The adiabatic section is located between the evaporator and the condenser. In this section, there is no heat transfer between the thermosyphon and the environment. In some cases, the adiabatic section is absent [3]. A schematic diagram of the thermosyphon operating principle is shown in Fig. 1. More details of the thermosyphons can be found in [2]-[6].

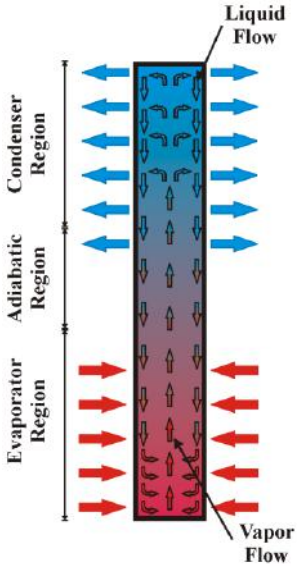


*Fig. 1: Sketch of the operating principle of a thermosyphon.*

Thermosyphons can be widely applied in the industrial environment. An application example is the heat recovery in a hot exhaust gas system by preheating air in heat exchangers of boilers. Furthermore, the heat transfer in heat exchangers can be improved by the use of fins, which can be coupled to the evaporator and/or the condenser of the thermosyphons [7].

In this context, a thermal analysis of a finned thermosyphon was experimentally researched. Due to it geometric characteristics, the thermosyphon can be applied in the preheating air of heat exchangers.

## II. METHODOLOGY

The methodology for manufacture (cleaning, assembly, the tightness test, the evacuation process, and the filling with the working fluid), experimental tests, and thermal

*https://dx.doi.org/10.22161/ijaers.5.1.4* *ISSN: 2349-6495(P) | 2456-1908(O)*

analysis of the finned thermosyphon was based taking into the consideration the instructions of [8]-[10].

**2.1 Characteristics of Developed Thermosyphon**

A copper tube ASTM B-75 Alloy 122 with an outer diameter of 9.45 mm, an inner diameter of 7.75 mm, and a length of 200 mm was used to manufacture the thermosyphon. The thermosyphon has an evaporator of 80 mm in length, an adiabatic region of 20 mm in length and, a condenser of 100 mm in length. Aluminum fins were installed in the condenser region. Figure 2 presents the manufactured thermosyphon. The working fluid used was water with a filling ratio of 40% of the evaporator volume. Table 1 shows the main features of the finned thermosyphon.

*Fig. 2: Finned thermosyphon*

*Table.1: Main characteristics of the finned thermosyphon*

| Characteristics | Thermosyphon |
|---|---|
| Inner diameter [mm] | 7.75 |
| Outer diameter [mm] | 9.45 |
| Evaporator [mm] | 80 |
| Adiabatic section [mm] | 20 |
| Condenser [mm] | 100 |
| Working fluid | Water |
| Filling ratio [%] | 40 |
| Volume of working fluid [mL] | 1.60 |

**2.2 Experimental Apparatus**

The experimental apparatus used for the experimental tests, shown in Fig. 3, is composed of a power supply unit (*Agilent*™ U8002A), a data logger (*Agilent*™ 34970A with 20 channels), a laptop (*Dell*™), an uninterruptible power supply (*NHS*™), a universal support, and a fan (*Ultrar*™).

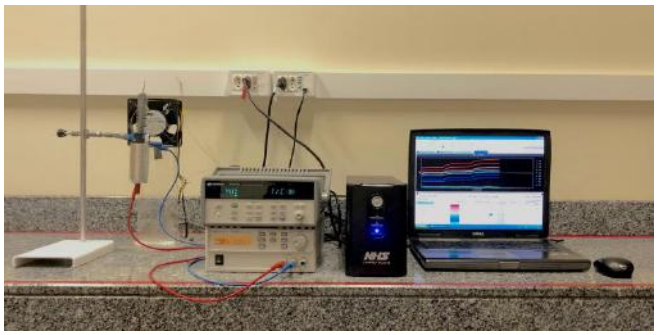

*Fig. 3: Experimental Apparatus*

For the evaluation of the thermal performance of the finned thermosyphon, K-type thermocouples *Omega Engineering*™ were used. They were fixed on the outer surface of the tube by a thermosensitive adhesive strip *Kapton*™. As shown in Fig. 4, there were three thermocouples in the evaporator ($T_{evap,1}$, $T_{evap,2}$, and $T_{evap,3}$), one thermocouple in the adiabatic section ($T_{adiab}$) e four thermocouples in the condenser ($T_{cond,1}$, $T_{cond,2}$, $T_{cond,3}$, and $T_{cond,4}$) in finned thermosyphon.

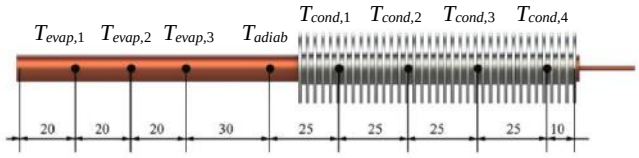


*Fig. 4: Thermocouple positions* [mm]

The heating system of the evaporator was conducted by power dissipation in a power strip resistor *Omega Engineering*™. To ensure that the generated heat by Joule effect was transmitted to the evaporator, an aeronautic thermal insulation and a layer of polyethylene were installed in this region. A fiberglass tape was used in adiabatic section as heat insulation between the support and the thermosyphon. The cooling system using air forced convection consisted of a fan in the condenser region. As mentioned above, to intensify the cooling, aluminum fins were installed in the condenser region.

**2.3 Experimental Procedure**

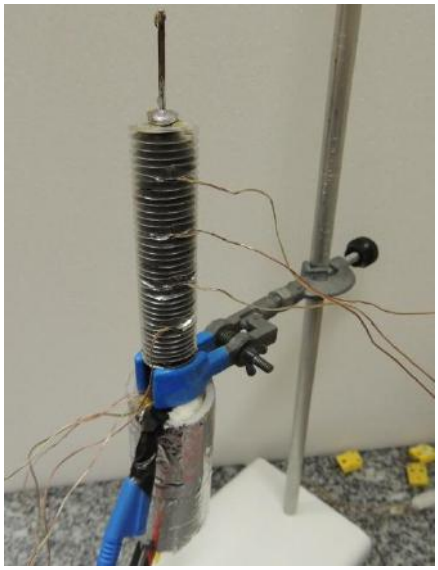

*Fig. 5: Finned thermosyphon at the vertical position.*

To ensure the best results and the repeatability of experimental tests, the ambient temperature was maintained at 19.0°C ± 1.0°C by the thermal conditioning system *Carrier*™. The finned thermosyphon was tested at the vertical position (evaporator above the condenser).

*https://dx.doi.org/10.22161/ijaers.5.1.4* *ISSN: 2349-6495(P) | 2456-1908(O)*

Figure 5 shows the finned thermosyphon test. The fan was turned on, positioned correctly in the condenser region and set at a speed of 5.0 m/s with a combined error of ± 0.2 m/s. The data acquisition system was turned on, and the temperatures measured by the thermocouples.

The power supply unit was turned on and adjusted to the dissipation power desired. The initial load was 5W and, after approximately 15 minutes, the thermocouples showed stationary values. The load increment of 5W was made up to 50W or until the maximum average temperature of the thermosyphon reached the critical temperature (150 ºC), where the melting of the materials could happen. Data were acquired every ten seconds, recorded on the laptop by the software *Agilent*™ Benchlink Data Logger 3.

The experimental uncertainties are associated to the K-type thermocouples, the data logger, and the power supply unit. The experimental temperature uncertainty is estimated to be approximately ± 1.27 °C and a thermal load was ± 1%. For the uncertainties determination, the Error Propagation Method described by [11] was used.

## III. DATA REDUCTION

The thermal performance of the finned thermosyphon was analyzed according to the operating temperature and the thermal resistance. The operating temperature analyzed was the temperature of the adiabatic region. The total thermal resistance, $R_{th}$, of a thermosyphon can be defined as the difficulty of the device to carry heat. The higher the thermal resistance, the greater the difficulty is in transporting heat from the system [12]. The total thermal resistance can be calculated by

$$R_{th} = \frac{\Delta T}{q} = \frac{\left(T_{evap} - T_{cond}\right)}{q}\ , \qquad (1)$$

where, $q$ is the heat transfer capability of the finned thermosyphon, $T_{evap}$ and $T_{cond}$ are the average wall temperature of the evaporator and the condenser, respectively.

## IV. RESULTS AND DISCUSSION

The experimental results regarding the thermal performance of the finned thermosyphon are presented considering the vertical position. The experimental tests were repeated three times and the errors were compared taking into account the difference between the mean values were less than 0.5 °C. Tests were performed to a heat load varying from 5 to 50 W. Figure 6 shows the temperature distribution as a function of time for the finned thermosyphon.

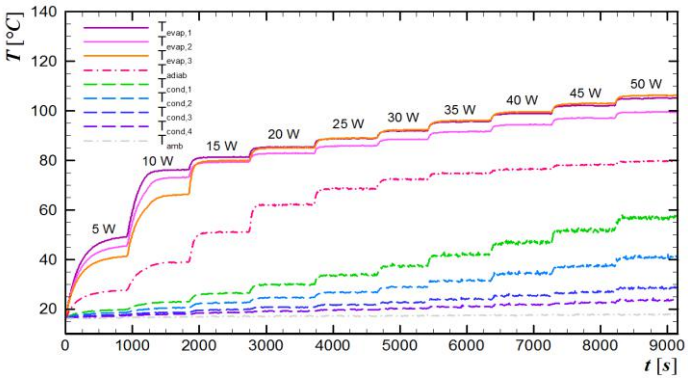


*Fig. 6: Temperature distribution versus time*

The temperature distribution in function of the finned thermosyphon length for the heat loads is presented in Fig. 7. The evaporator temperatures remain close to each other for the heat loads. The condenser temperatures reduce gradually.

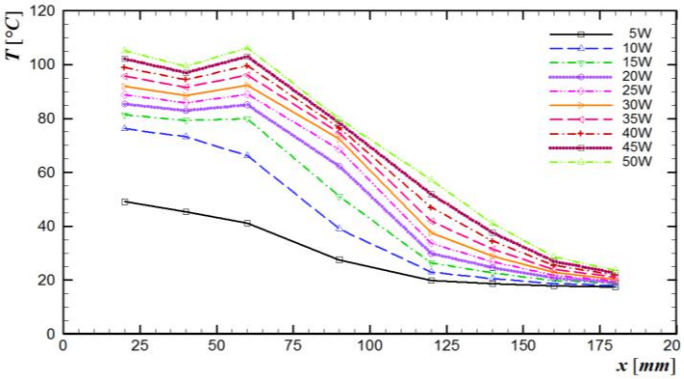


*Fig. 7: Temperature distribution versus finned thermosyphon length*

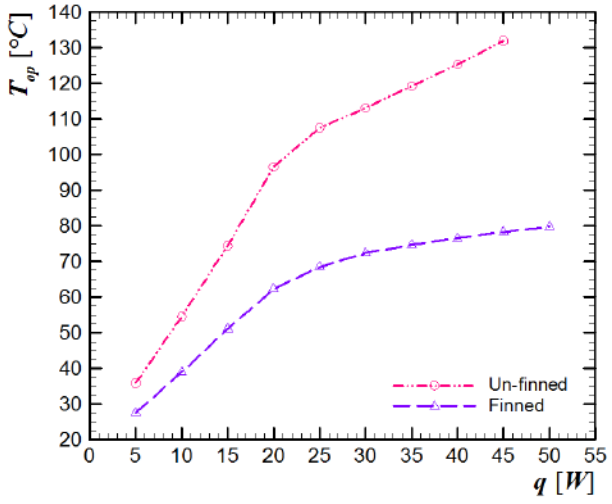


*Fig. 8: Operation temperature versus heat load*

The operating temperature of the finned thermosyphon in function of the heat load is shown in Fig. 8. Figure 9 illustrates the behavior of the thermal resistance as a function of heat load. Also in these graphs, the results of

*https://dx.doi.org/10.22161/ijaers.5.1.4* *ISSN: 2349-6495(P) | 2456-1908(O)*

un-finned thermosyphon with the same characteristics are presented [13], in order to analyze the effectiveness of the extended surfaces.

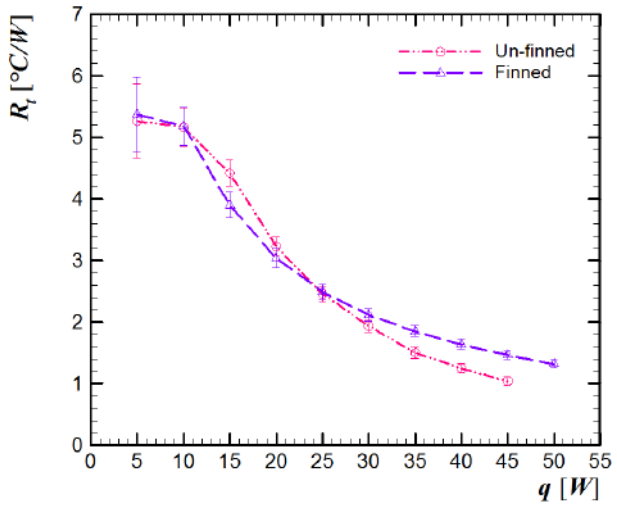


*Fig. 9: Thermal resistance versus heat load*

For both thermosyphons, the operating temperature increases with the rise of the heat load. Furthermore, the thermal resistances decrease with the increasing heat dissipation in the evaporator. According to the experimental results, the thermal resistance remains similar for the finned and un-finned condenser. Nonetheless, the operating temperature significantly drops, which proves the fins effectiveness. As a result, the finned thermosyphon can operate at higher heat load with a lower operating temperature.

## V. CONCLUSION

This paper presented a thermal analysis of a finned thermosyphon for heat exchanger applications. Experimental tests were performed to a heat load from 5 up to 50W at the vertical position. The working fluid was water. As a result of the research, the thermosyphon operated satisfactorily for the tested position. Also, the finned thermosyphon obtained better thermal performance than the un-finned condenser, proving the effectiveness of the fin application.

## ACKNOWLEDGEMENTS

Acknowledgments are provided to the Capes, the CNPq, the PROPPG/UTFPR, the DIRPPG/UTFPR, the PPGEM/ UTFPR/PG, and the DAMEC/UTFPR/PG.

## REFERENCES

[1] A. Akbasrzadeh, T. Wadowski, Heat Pipe-based cooling systems for photovoltaic cells under concentrated solar radiation, Applied Thermal Engineering, Vol. 16, pp. 81-87, 1996.

[2] D.A. Reay, P.A. Kew, RJ McGlen, Heat Pipe: Theory, Design and Applications, Butterworth-Heinemann, Amsterdam, NED, 2014.

[3] M.B.H. Mantelli, Thermosyphon technology for industrial applications, Chapter 11, In: Vasiliev L.L. and Kakaç S. (Eds.), Heat pipes and solid sorption transformations: fundamentals and practical applications. CRC Press, Boca Raton, USA, 2013.

[4] S.W. Chi, Heat Pipe Theory and Practice: A Sourcebook, Hemisphere Publishing Corporation, Washington, 1976.

[5] G.P. Peterson, An Introduction to Heat Pipes: Modeling, Testing and Applications, (Thermal Management of Microelectronic and Electronic System Series). Wiley-Interscience, New York, 1994.

[6] A. Faghri, "Heat Pipes: Review, Opportunities and Challenges", Frontiers in Heat Pipes, Vol. 5, pp 01-48, 2014.

[7] V.M. Aguiar, Influence of filling ratio and inclination angle on thermal performance of thermosyphons, Graduation work, Federal University of Technology – Paraná, Ponta Grossa, Brazil (in Portuguese).

[8] L. Krambeck, F.B. Nishida, P.HD. Santos, T. Antonini Alves, Configurations of phosphor bronze meshes in heat pipes: an experimental analysis of thermal performance, International Journal of Advanced Engineering Research and Science, Vol. 2, pp 11-14, 2015.

[9] G.M. Russo, L. Krambeck, F.B. Nishida, P.H.D Santos, T. Antonini Alves, Thermal performance of thermosyphon for different working fluids, Engenharia Térmica, Vol. 15, pp 3-8, 2016.

[10] P.H.D Santos, K.A.T. Vicente, L.S. Reis, L.S. Marquardt, T. Antonini Alves, Modeling and experimental tests of a copper thermosyphon, Acta Scientiarum. Technology (online), Vol. 39, pp 59-68, 2017.

[11] J.P. Holman, Experimental Methods for Engineers. McGraw-Hill, New York, USA, 2011.

[12] T.L Bergman, A.S. Lavine, F.P. Incropera, D.P. DeWitt, Fundamentals of Heat and Mass Transfer, John Wiley & Sons., New York, USA, 2011.

[13] L. Krambeck, F.B. Nishida, V.M. Aguiar, P.H.D. Santos, T. Antonini Alves, Thermal performance evaluation of different passive devices for electronics cooling, Thermal Science, in press, 2018.

*https://dx.doi.org/10.22161/ijaers.5.1.5* *ISSN: 2349-6495(P) | 2456-1908(O)*

# Facies Modelling of Mishrif Formation in Selected Wells of Tuba Oil Field, Southern Iraq

T.A. Mahdi, Mustafa J.

Department of Geology, University of Baghdad, collage of science, Iraq

***Abstract—*** *The current study includes building a 3D geological facies model of the Mishrif Formation (Cenomanian-Early Turonian) in Tuba oilfield, southern Iraq. Microfacies study and core samples examination reveals the occurrence of six facies associations within Mishrif succession represented by; Basin, deep marine, rudist biostrome, shoal, back- shoal, and lagoon. Each reservoir unit is characterized by distinct facies distribution that controls their quality. High reservoir quality is predominantly developed in rudistid facies that are productive from units MB1 and MB2. The 3D facies model shows that these units have greater continuity and thickness along Tuba anticline and control the structural and stratigraphic trapping. Units MA and Mishrif have lower reservoir quality due to the dominance of mud-dominated facies. The unit CR2 consists of non-reservoir facies, and can be captured along the oilfield structure.*

***Keywords—Carbonate, Mishrif, facies, Modelling, Petrophysics, reservoir***

## I. INTRODUCTION

The Tuba oil field consists of different reservoir zones and the zones considered for this study includes Mishrif Formation. The Mishrif Formation is one of the most important carbonate reservoirs in central and southern Iraq. During Cenominian-early Turonian, the carbonate succession of Mishrif Formation within the Mesopotamian basin is a part of the Wasia Group and has widespread distribution throughout Arabian plate. Currently, twelve wells producing from Mishrif Formation in Tuba oil field. An understanding of rudisitid facies distribution has been instrumental in the development of similar oil fields in the Mesopotamian Basin [1]. The reservoir model presented in this study shows the importance of these facies as a formation for future field development.

## II. THE STUDY AREA

The Tuba oil field is located nearly 35 Km southwest Basrah city between Zubair from the East (5km distance) and South Rumaila from West (2km distance (Figure1). The Tuba anticline trends approximately N-S and is 29 km long and the width reaches about 9 km (Figure 2)

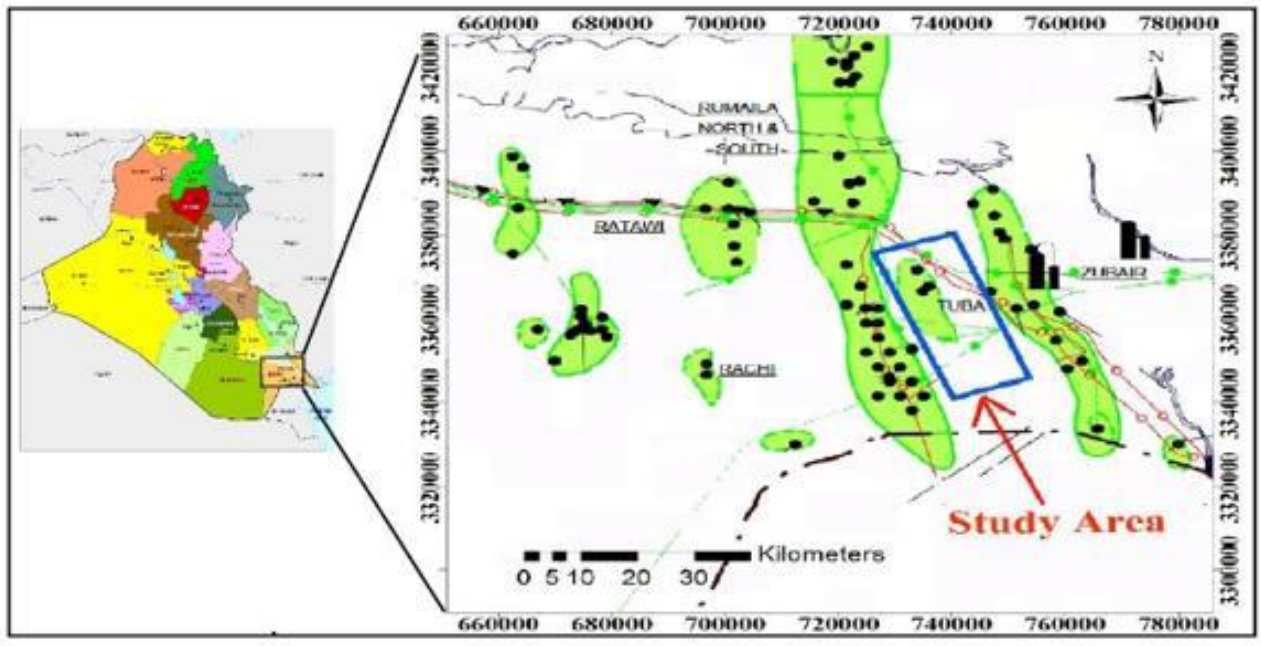


*Fig.1: Location Map of Tuba oilfield (global exploration & production service-gis-2010).*

*https://dx.doi.org/10.22161/ijaers.5.1.5* *ISSN: 2349-6495(P) | 2456-1908(O)*

## III. AIMS OF STUDY

1-Identifaction of facies associations in each reservoir unit of Mishrif formation in Tuba oil field

2-Building the 3D Facies model by using Petrel software to assess the vertical and horizontal changes in facies associations, and their distribution within Tuba oil field.

## IV. METHODOLOGY

1-The petrographic study and microfacies analysis were based on the study of more than 300 thin sections of cores from the selected wells (TU-3, TU-4, TU-5, TU-15, TU-19, TU-22).

2- Using interactive petrophysical software IP (V3.5) for the environment correction, lithology and mineralogy identification and log interpretation.

3-Using of Petrel software for construction 3D Facies model.

## V. STRATIGRAPHY

The Mishrif Formation (Cenomanian-Early Turonian) represents a heterogeneous carbonate succession originally described as organic detrital limestones, capped by limonitic freshwater limestone [3], [5]. It is considered to be an overall progradational marine shelf sequence, with the development of rudist shoal and biostromes[1].The Mishrif Formation is composed of two major sedimentary cycles abruptly terminated by the unconformity, which separates the Mishrif from the overlying Khasib Formation [5].. The lower contact of the formation is conformable with the underlying Rumaila Formation,whereas the upper contact is unconformable with Khasib Formation [4].

## VI. TECTONIC AND STRUCTURAL SETTING OF THE STUDY AREA

The study area is located in Zubair Subzone , which is the southern part of the Mesopotamian Foredeep. Mesopotamian Zone is the easternmost tectonic unit of the Stable Shelf and includes the largest and richest petroleum province in Iraq and is dominated by Cretaceous plays [5].This zone was probably uplifted during the Hercynian deformation but it subsided from Late Permian time onwards. The thickness of Cretaceous stratigraphic succession increases towards east. It comprises 700-1400m of the Upper Cretaceous. The Mesopotamian Zone contains buried faulted anticlines below the Quaternary cover, separated by broad synclines. Such structures include Tuba oil field (Figure 2), which represents an asymmetrical anticline, where the western limb dips 0.9 degree. It is worthy to be mentioned that the depression, which separate the Zubair and Tuba field is deeper approximately 40 - 60 m than the depression separate Tuba and Rumaila.

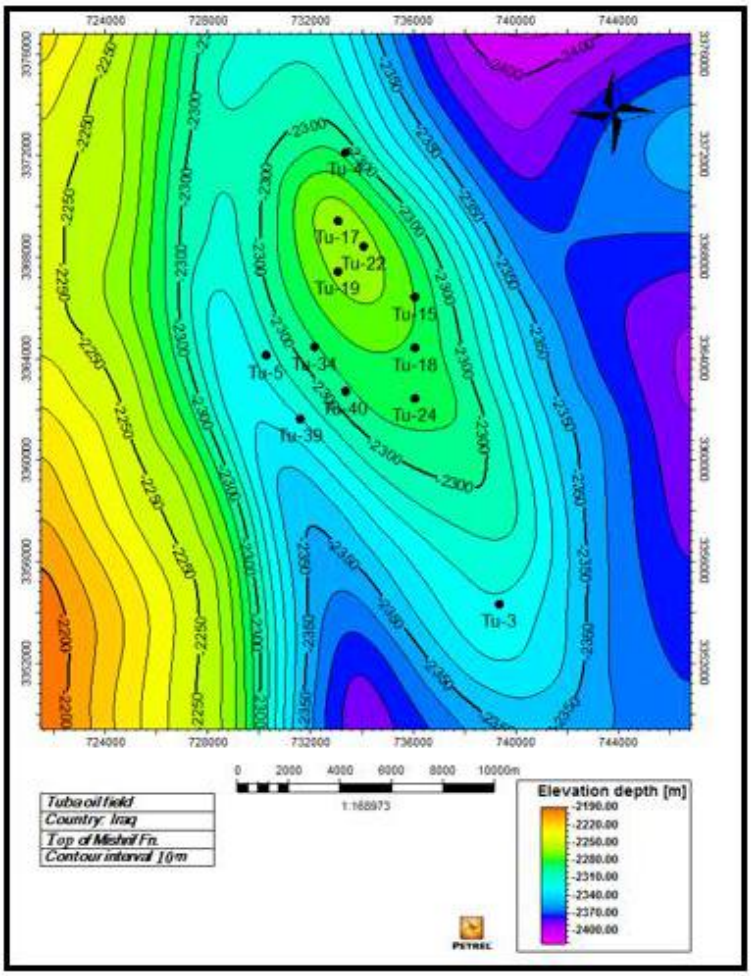


*Fig.2: Structural contour map of Top of Mishrif Formation.*

## VII. MICROFACIES ANALYSIS AND DEPOSITIONAL ENVIRONMENT OF RESERVOIRS UNITS

The Mishrif Formation can be subdivided into several reservoir units in Tuba oilfield based on petrophiscal properties. These include Top of Mishrif, MA, CR2, MB1, MB2). The depostional facies of reservoir units control their reservoir quality, and are important in reservoir characterization and geologic modeling. This is related to different texture and diagenetic overprint of carbonate facies[1].Generally mud-dominated facies show low reservoir quality and grain-dominated facies have better quality due to high porosity and permeability. A collection of thin section has been prepared from more than 300 core samples obtained from selected wells. The results of petrographic study of thin sections show that the reservoir units consist of different facies associations, which can be interpreted in terms of depositional

*https://dx.doi.org/10.22161/ijaers.5.1.5* *ISSN: 2349-6495(P) | 2456-1908(O)*

environments (Figures 3-10). Major characteristics of facies associations are summarized as follow:

**1-BasinFacies association**

This facies association consists of shale units that are found in all studied wells except well Tu-4, where it replaced by deep marine facies (Figures 3-10).The basin facies association occurs only in CR2 unit, which represent non-reservoir unit. It is characterized by highest gamma ray log values.

**2- Deep marine Facies association**

The deep marine facies association forms thick succession of Planktonic mudstone-wackestone microfacies. Stratigraphic position of this association remarkably occurs above and below CR2 unit (Figures 3-10). It has poor reservoir properties and forms part of some reservoir units including MA, MB1, and Top of Mishrif unit.

**3- Shallow open marine Facies association**

This facies association includes mainly of bioclatic packstone or packstone or wackestone. It occurs at lower and middle parts of Mishrif Formation within Mb1 and Mb2 units, in addition to MA unit (Figures. 3-10). According to [1], shallow open marine facies association is comparable with slope facies described in equivalent formations.

**4- Rudist Biostrome Facies association**

Most reservoir rocks of Mishrif Formation consist of rudist-bearing facies, which were deposited in rudist biostrome and shoal environments. In Tuba oilfiled, the rudistid packstone, and rudistid packstone-floatstone occur in reservoir units Mb1and Mb2, and characterized by high sonic log values and low gamma ray log response (Figures 2-5).The high reservoir quality of this facies association is attributed to the abundance of rudist shells and fragments that are largely affected by dissolution forming potential vuggy porosity[1],[2].

**5- Shoal Facies association**

This facies association consists of grain-dominated microfacies such as rudistid packstone-grainstone. They were deposited in shallow, high energy and current swept environment[1].They form the most important reservoir units in Tuba oilfield including MB2(Figures 3-10).

**6-Back-shoal Facies association**

The back-shoal facies association has limited occurrence in the study area. It consists of Foraminiferal-bioclastic wackestone-packstone and rudistid floatstone microfacies. This facies association has lower reservoir quality than shoal and rudist biostrome facies. It occurs mainly in MB1and MB2 units (Figures 3-10).

**7- Lagoon Facies association**

This facies association consists of mud-dominated microfacies such as fossiliferous lime-mudstone and benthonic foraminiferal wackestone. They form thick succession at uppermost part of Mishrif Formation within Top of Mishrif and MA units (Figures 3-10).The low reservoir quality of lagoon facies association is indicated by the low values of sonic log (Figures.2-5).

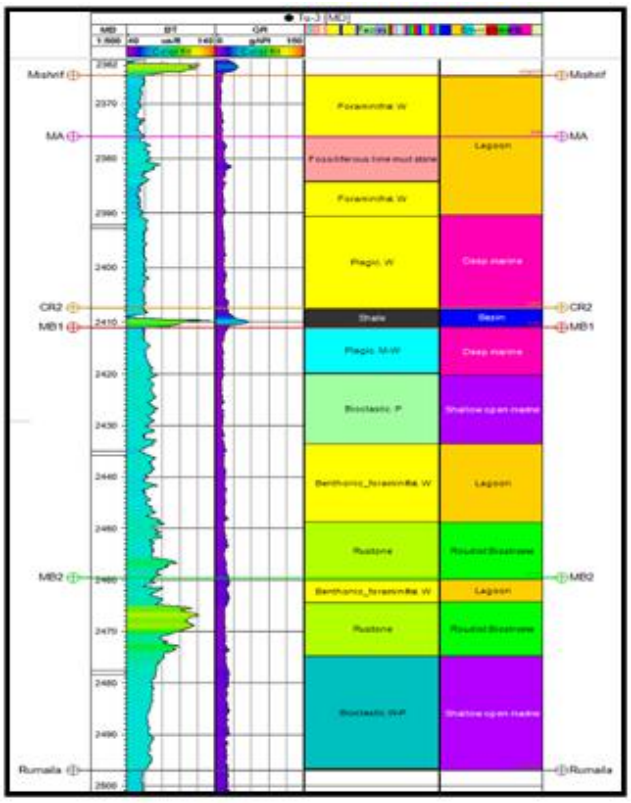


*Fig.3: Facies associations and logs response of Mishrif Formation at well Tu3.*

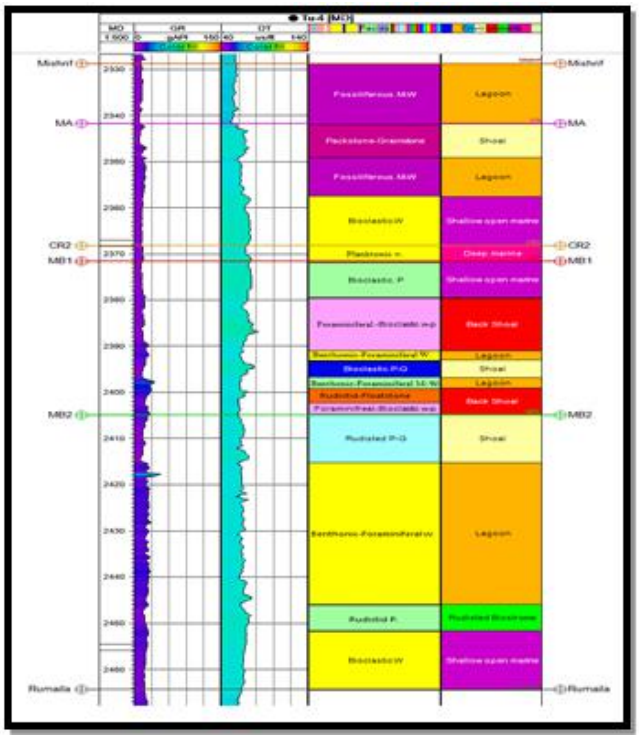


*Fig.4: Facies associations and logs response of Mishrif Formation at well Tu4.*

*https://dx.doi.org/10.22161/ijaers.5.1.5* *ISSN: 2349-6495(P) | 2456-1908(O)*

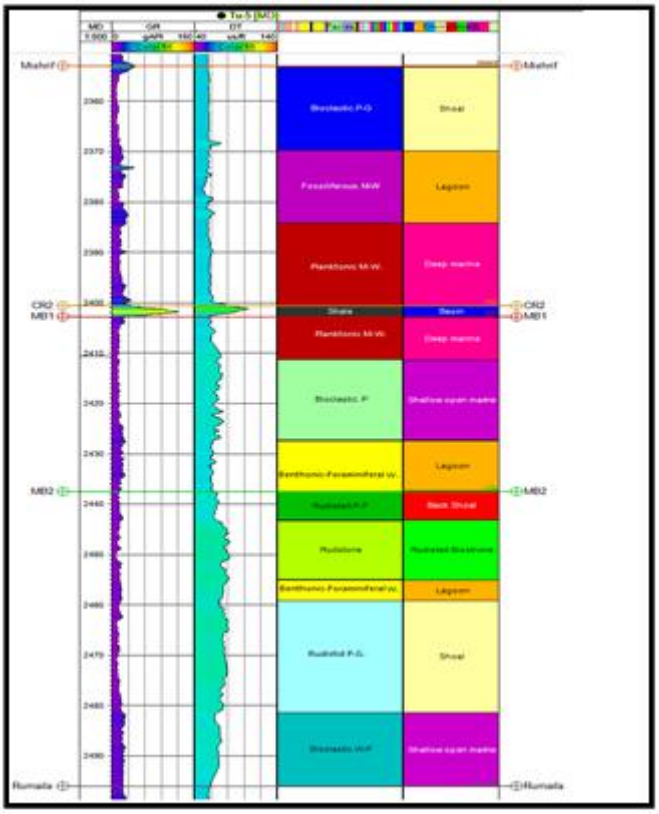

*Fig.5: Facies associations and logs response of Mishrif Formation at well Tu15.*

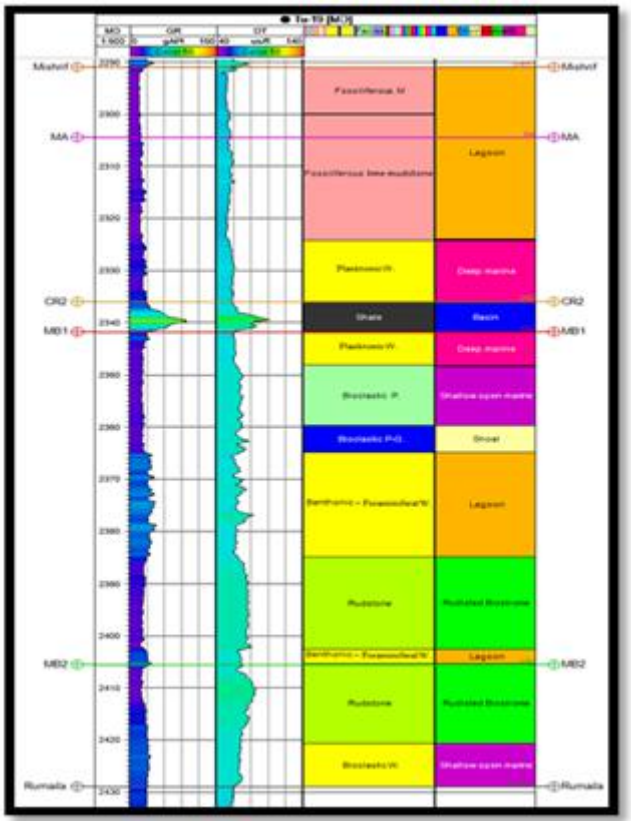

*Fig.7: Facies associations and logs response of Mishrif Formation at well Tu19*

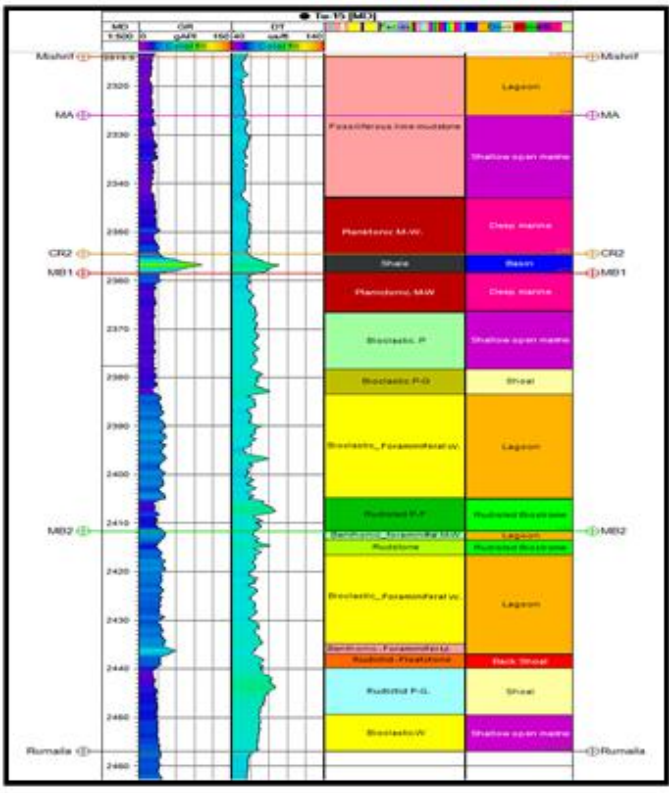

*Fig.6: Facies associations and logs response of Mishrif Formation at well Tu5.*

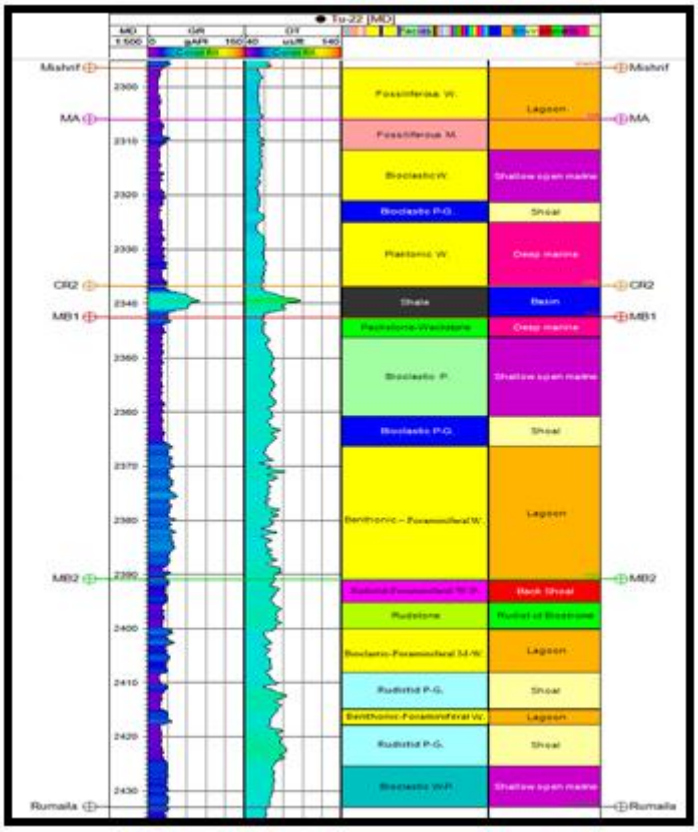

*Fig.8: Facies associations and logs response of Mishrif Formation at well Tu22.*

*https://dx.doi.org/10.22161/ijaers.5.1.5* *ISSN: 2349-6495(P) | 2456-1908(O)*

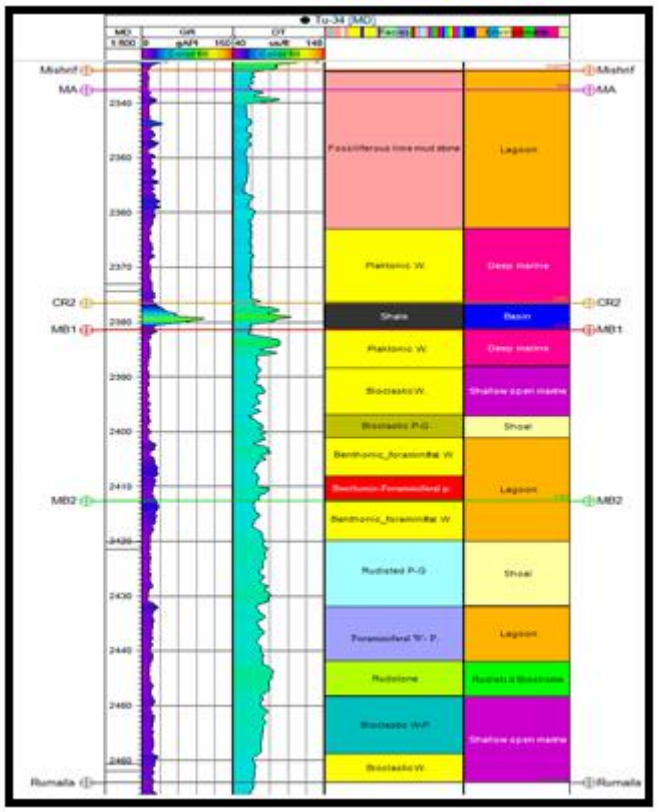


*Fig.9: Facies associations and logs response of Mishrif Formation at well Tu34.*

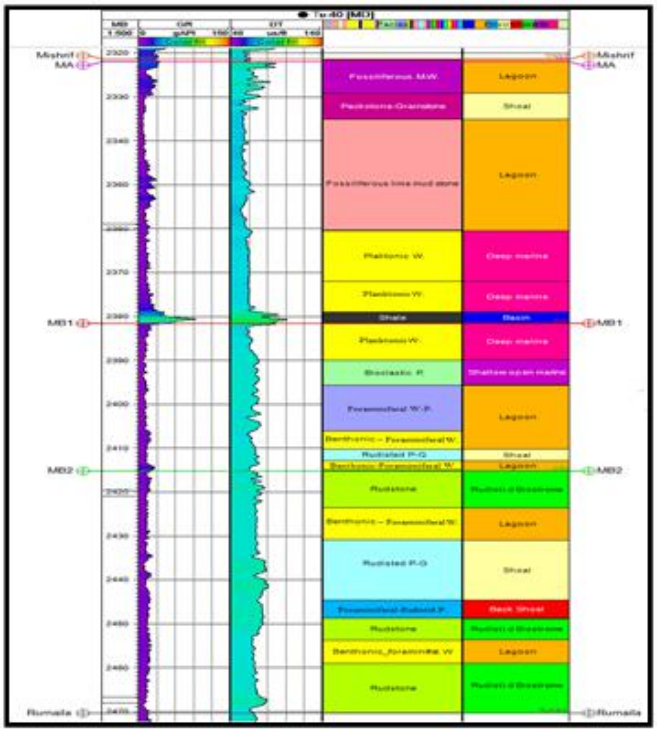


*Fig.10: Facies associations and logs response of Mishrif Formation at wellTu40.*

## VIII. FACIES MODEL OF RESERVOIR UNITS

The 3D facies Model of Mishrif Formation in Tuba oilfield is shown in Figure (11). It was constructed by petrel software through importing facies association data. The model shows a nearly uniform distribution facies association along Tuba oilfield anticline. Most reservoir Facies (Shoal and Rudist biostrome) are staked in the lower part of Mishrif Formation. They are capped by a thick succession of shallow open marine and deep marine facies (Figure 11).Each reservoir unit exhibits distinct lateral facies variations. Such variation among lagoonl, shoal and rudist biostrome facies along the limbs of Tuba anticline forming stratigraphic traps (Figures 12 and 13).The units Top of Mishrif and MA is dominated by non-reservoir facies including lagoon, shallow open marine, and deep marine (Figures 14-16). In addition, isolated occurrence of shoal facies is clear at the flank and crest of Tuba anticline (Figures 16 and 17).

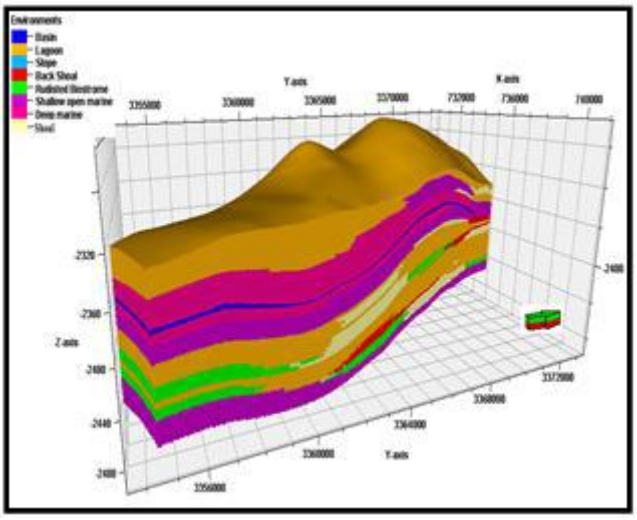


*Fig.11: Facies and Environmental model for Mishrif Formation of Tuba oilfield.*

Most homogeneous distributions of facies accrue in unit CR2, which consists mostly of basin facies with limited distribution of deep marine facies (Figure 18).Both facies associations form a cap unit with remarkable thickness at the top of unit MB1. This unit is characterized by intercalation of reservoir(Shoal, rudist biostrome)and non-reservoir facies (lagoon, back-shoal) at the lower part (Figures 15,18,21),forming stratigraphic trap as in unit MA. The vertical facies change is MB2 unit shows shallowing upwared trend, which is observed at the lower part of Mishrif Formation in several oil field [1]. As with unit MB1, the unit MB2 includes potential reservoir facies that interbeds with lagoon and back shoal facies.
However, the cap unit consists mainly of lagoon facies (Figures 22, 23, 24)

*https://dx.doi.org/10.22161/ijaers.5.1.5* *ISSN: 2349-6495(P) | 2456-1908(O)*

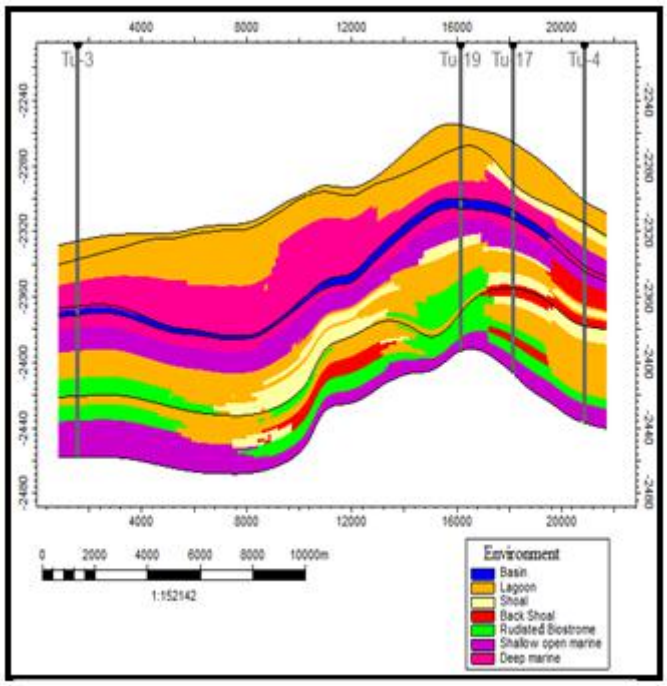


*Fig.12: Cross section in direction NW-SE shows distribution of main depositional environments for Mishrif Formation in Tuba oil*

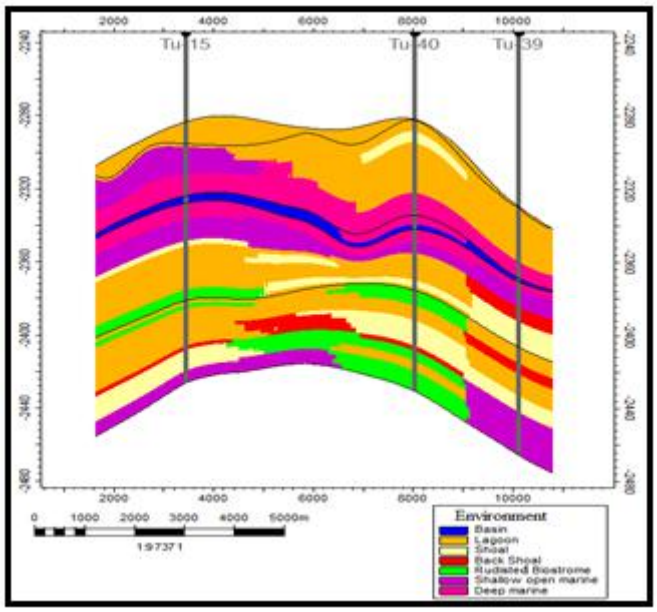


*Fig.13: Cross section in direction WNW-ESE shows distribution of main depositional environments for Mishrif Formation in Tuba oil field*

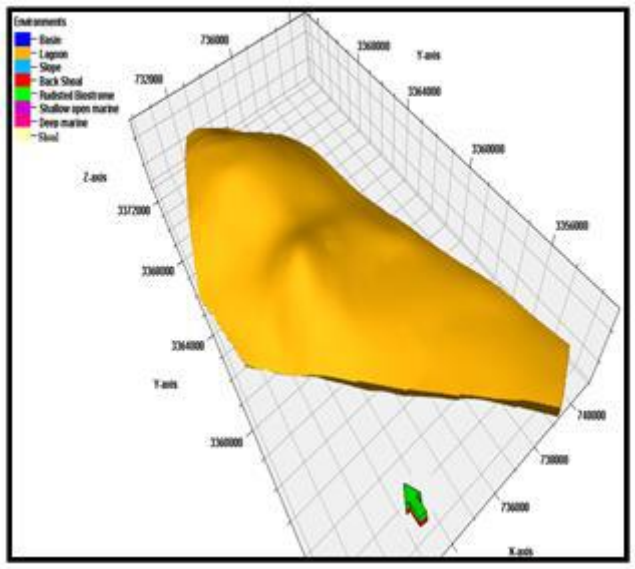


*Fig.14: The facies model of Top of Mishrif unit for Mishrif Formation in Tuba oil field.*

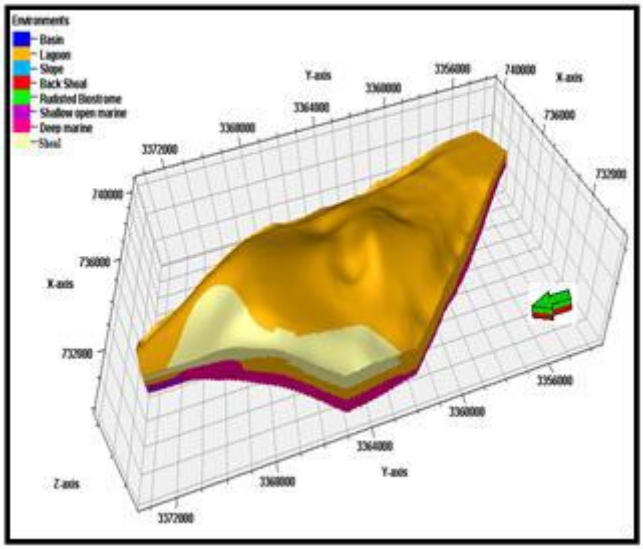


*Fig.15: The facies model of MA unit for Mishrif Formation in Tuba oil field.*

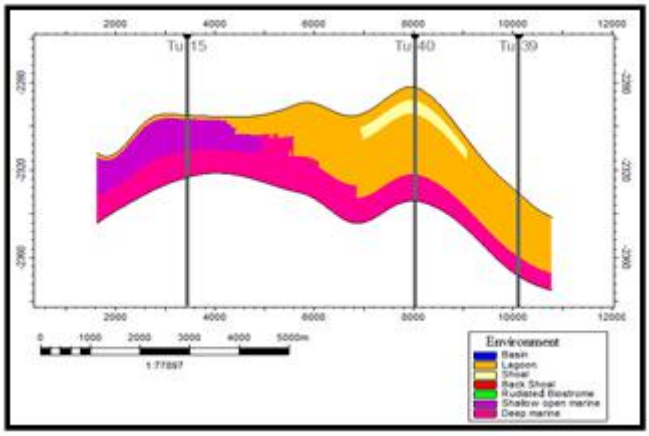


*Fig.16: Cross section in direction WNW-ESE with facies of MA reservoir unit in Tuba oil field.*

*https://dx.doi.org/10.22161/ijaers.5.1.5* *ISSN: 2349-6495(P) | 2456-1908(O)*

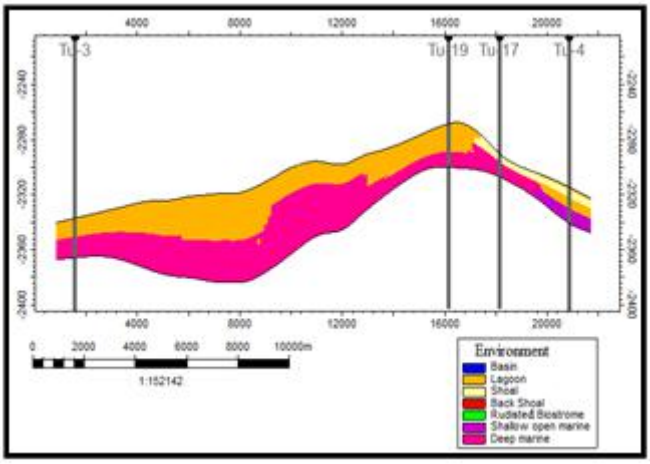


*Fig.17: Cross section in direction NW-SE with facies of MA reservoir unit in Tuba oil field.*

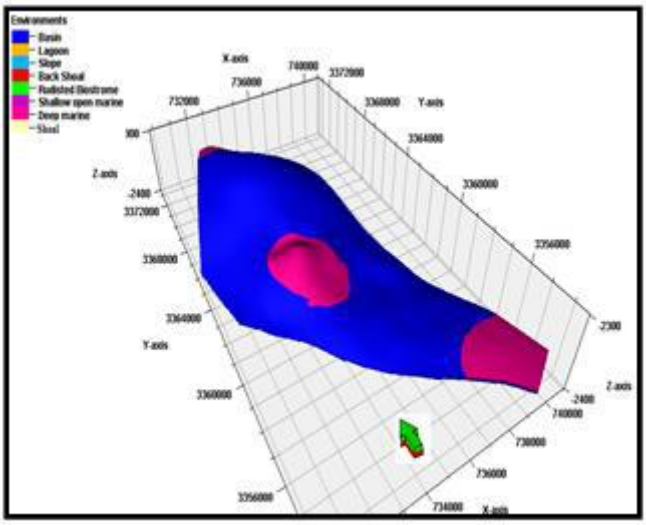


*Fig.18: The facies model of CR2 unit for Mishrif Formation in Tuba oil field.*

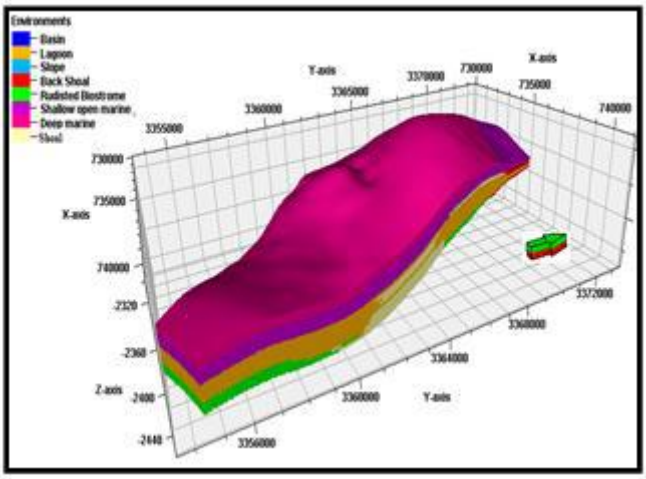


*Fig.19: The facies model of MB1 unit for Mishrif Formation in Tuba oil field.*

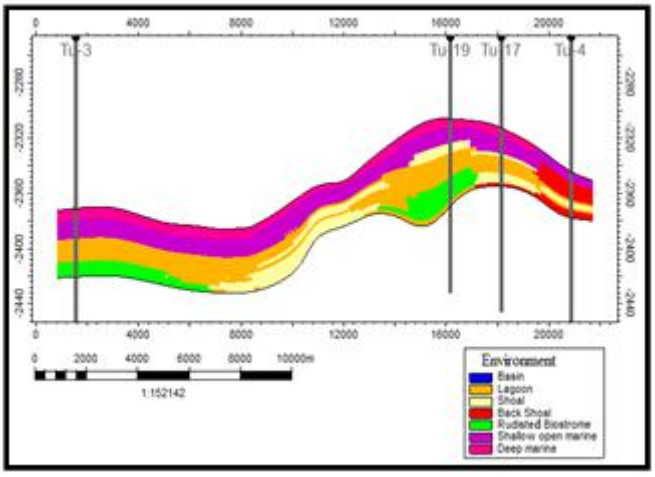


*Fig.20: Cross section in direction NW-SE with facies of MB1reservoir unit in Tuba oil field.*

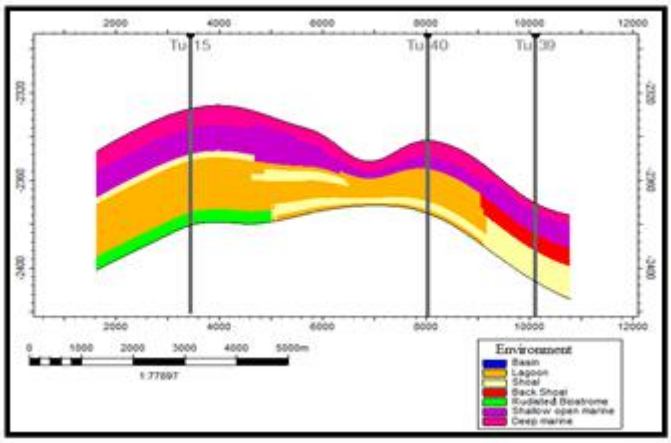


*Fig.21: Cross section in direction WNW-ESE with facies of MB1reservoir unit in Tuba oil field.*

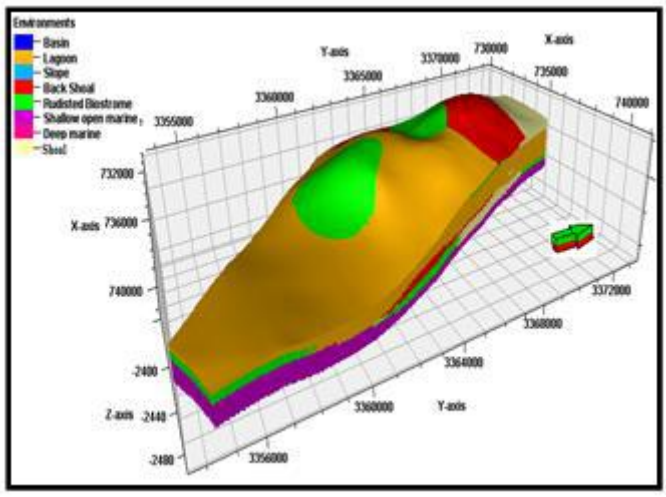


*Fig.22: The facies model of MB2 unit for Mishrif Formation in Tuba oil field.*

*https://dx.doi.org/10.22161/ijaers.5.1.5* *ISSN: 2349-6495(P) | 2456-1908(O)*

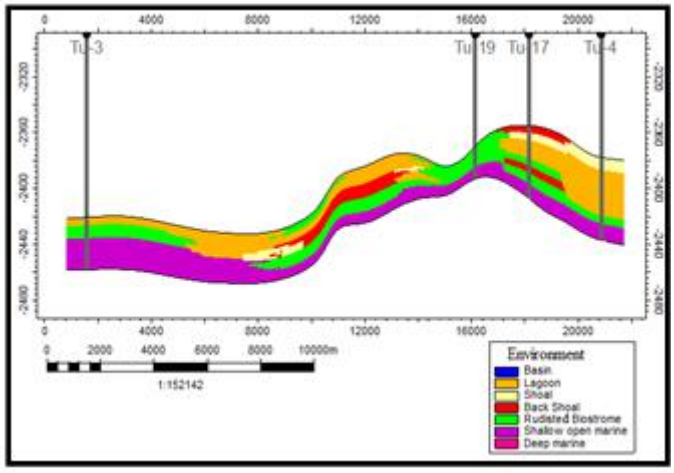


*Fig.23: Cross section in direction NW-SE with facies of MB2reservoir unit in Tuba oil field.*

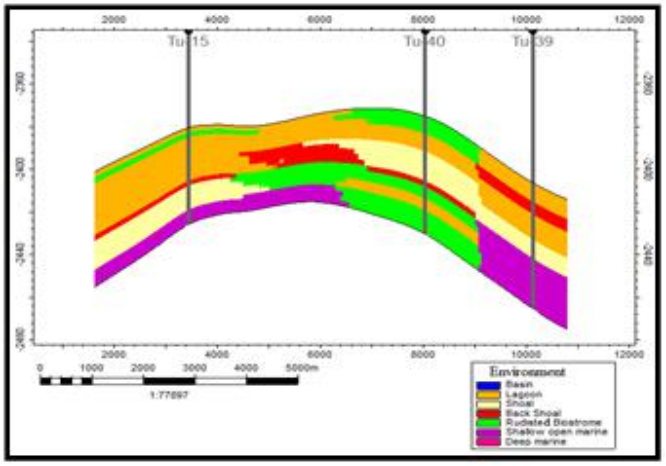


*Fig.24: Cross section in direction WNW-ESE with facies of MB2reservoir unit in Tuba oil field.*

## IX. CONCLUSION

The Mishrif Formation in Tuba oilfield is subdivided into several reservoir unit that composed of different facies associations including basin, deep marine, shallow open marine, rudist biostrome, shoal, back shoal and lagoon. Their vertical and lateral distributions control the quality of reservoir units. The 3D facies model shows that reservoir units MB1 and Mb2 are most important due to the dominance of thick rudistid facies characterized by lateral distribution along Tuba anticline. Non reservoir units consists of basin ,deep marine, lagoon and shallow open marine facies association that mainly occur in units CR2 and MA. Unit CR2 represents the cap rocks in Tuba oilfield.

## ACKNOWLEDGEMENTS

The authors thank the Department of Geology at the University of Baghdad for providing opportunities and facilities for the completion of this research. Also, the South Oil Company is acknowledged for supplying the data requirements to perform this work and for collecting rock samples.

## REFERENCES

[1] Mahdi, T.A., Aqrawi, A.A.M., Horbury, A., and Sherwani, G.H., 2013. Sedimentological characterization of the mid-Cretaceous Mishrif reservoir in southern Mesopotamian Basin, Iraq. GeoArabia, 18, 1, 139-174.

[2] Aqrawi, A.A.M., Thehni, G.A., Sherwani, G.H. and Kareem, B.M.A., 1998. Mid-Cretaceous rudist-bearing carbonates of the Mishrif Formation: An important reservoir sequence in the Mesopotamian Basin, Iraq. Journ. Petrol. Geol., v.21, p.57-82.

[3] Bellen, R.C. Van, Dunnington., H.V., Wetzel, R. and Morton, D., 1959. Lexique Stratigraphique Internal Asia. Iraq. Intern. Geol Conger. Comm. Stratigr, 3, Fasc. 10a, 333P.

[4] Buday, T., 1980. The Regional Geology of Iraq: Stratigraphy and Paleogeography. Dar Al-Kutib house, University of Mosul, Mosul, Iraq, 445p.

[5] Aqrawi, A.A.M., J.C. Goff, A.D.Horbury, and F.N. Sadooni, 2010. The Petroleum Geology of Iraq: Scientific Press, 424P.

[6] Sadooni F.N., 2005. The Nature and Origin of Upper Cretaceous Basin-Margin Rudist Buildups of the Mesopotamian Basin, Southern Iraq, with Consideration of Possible Hydrocarbon Stratigraphic Entrapment, Cretaceous Research 26, Elsevier, 213-224 p.

*https://dx.doi.org/10.22161/ijaers.5.1.6* *ISSN: 2349-6495(P) | 2456-1908(O)*

# Knowing about the Nutritional and Immunological Benefits of Breast Milk Does not Reduce Early Weaning

Nayara Nunes Pereira Silva[1], Juliana Luzia França Mesquita[2], Aline do Carmo França Botelho[2*]

[1]Graduate in Nursing, University Center of Araxá Plateau. Av Minister Olavo Drummond, 5. Zip Code: 38180-084. Araxá, Minas Gerais, Brazil.

[2]PhD Professors in University Center of Araxá Plateau.University Center of Araxá Plateau. Av Minister Olavo Drummond, 5. Zip Code: 38180-084. Araxá, Minas Gerais, Brazil.

***Abstract*** *— Breastfeeding brings great benefits to the child and the mother, however it is known that the practice requires encouragement and proper guidance. Even knowing the nutritional and immunological benefits of breastmilk, many mothers interrupt lactation and add artificial formulas in infant feeding, most often due to myths or difficulties in breastfeeding management. The aim of this study was to identify factors that influence early weaning in Ibiá, Minas Gerais, Brazil. It was an exploratory, transversal and quantitative research, conducted through questionnaires administered to mothers of children of 0-6 months. As for the most common problems related to breastfeeding experienced by respondents, the main reported was the presence of "milk weak "or"little milk" with 53.84%. When asked if their children were using pacifiers, 69.73% of respondents reported so. The family and professional support is of utmost importance to the practice of breastfeeding. Nursing should advise on lactation management as well as on the numerous benefits of breast feeding. The nursing team has na important role in this regard, promoting breastfeeding, with preventive actions that contribute to this important stage of the childrens life, thus, breast feeding can belived fully and satisfactorily.*

***Keywords — Breast milk, breast feeding, early weaning, breast feeding myths.***

## I. INTRODUCTION

The first two years of life are a critical period for the growth and development of children. Thus, for the potential physical and cognitive development is achieved, it is crucial that the nutritional status is highly satisfactory. Otherwise, ma-nutrition states are not only associated with delays in growth and worse cognitive abilities, with consequences for adult life, but also the worst health status and increased mortality and morbidity (Black et al., 2013).

Breastfeeding has been set up as the best and most efficient source of nutrition for the infant, specially when offered exclusively until six months of age, as recommended by the World Health Organization (WHO), and supplemented by the two years or more. Breastfeeding is a process that involves deep interaction between mother and child, with positive repercussions on the nutritional and immune status of the infant. Breastfeeding is important because the immaturity of the immune system of the newborn makes it vulnerable to infections (WHO, 2011).

The human milk varies as the composition on a daily basis and throughout lactation, infants and providing nutrients to specific components appropriate for each age and condition. Thus, there is no technique to artificially reproduce the complete and dynamic effects of bioactive substances present in human milk (Silva et al., 2014).

Specifically for premature babies, breastfeeding can bring some more advantages because the nutritional and immunological properties of human milk favor gastrointestinal maturation, strengthening the mother-child bond, increased psychomotor performance, antioxidant protection, lower incidence of infections, shorter hospital admissions and lower incidence of new internations (Sassa et al., 2014).

Breastfed children have lower rates of diarrhea, respiratory tract infections, otitis media and other infectious and lower mortality from these diseases compared to non-breastfed (Leon-Cava et al., 2002).

Exclusive breastfeeding, defined as the offer only milk, not even water or tea, allowing only vitamin drops or medications are recommended until the sixth month of life of children. When they receive other types other than breast milk foods before completing 180 days of life, you can assign that was the beginning of the weaning process early. According Brazil (2015), the early introduction of food can influence early weaning interfere with the absorption of nutrients from human milk increase the risk

https://dx.doi.org/10.22161/ijaers.5.1.6 ISSN: 2349-6495(P) | 2456-1908(O)

of contamination and allergic responses in the same way that the late introduction can lead to the slowing of the growth of child, increasing the risk of malnutrition and micronutrient deficiencies. The correct practice of exclusive breastfeeding until six months is as important as the proper introduction of foods from this age. The additional power is timely six months, introducing a variety of foods, slowly and gradually, in solid and pasty consistency.

There are several factors that are intertwined with the abandonment of this feeding practice, acting negatively or positively, the main ones being: socioeconomic status, level of maternal education, maternal age, maternal employment, urbanization, labor conditions, spouse of encouragement and relatives, the intention of the breastfeeding mother and previous experience (Araújo et al., 2008).

The nutritional benefits and protectors of breastfeeding are widely known and accepted, however, the management of breastfeeding is hard work, requiring broad support for breastfeeding (Santos; França-Botelho, 2010).

There are numerous factors that contribute to the increasingly early weaning, it is possible to highlight the complexity of modern lifestyles and their implications, as the division of labor by the couple and return to employment for the mother. Also noteworthy infections such as AIDS; Breast diseases (mastitis, fissures, engorgement, abscesses and other); problems with the newborn (phenylketonuria, galactosemia). External influences of family, friends and neighbors can also impact negatively on breastfeeding, as well as the culturally ingrained myths for generations (little milk, low milk and aesthetic implications, such as sagging and the fall of the breasts). These factors seem to exert greater influence on breastfeeding than the benefits and advantages of breast milk over formula and artificial milks (Barreira; Machado, 2004).

Breastfeeding brings great benefits to the child and the mother, however it is known that the practice requires encouragement and proper guidance. Many mothers interrupt lactation and add artificial formulas in infant feeding, most often due to myths or difficulties in breastfeeding management. The objective of the study was to identify factors that influence early weaning in the PSF (Health Family Program) in Ibiá, Minas Gerais, Brazil.

## II. MATERIALS AND METHODS

This is an exploratory, transversal and quantitative study. The research site was the Unit Polyclinic Jose Austernio where the same location also works PSF Santa Cruz, in the city of Ibiá, Minas Gerais, Brazil. During the period of August and September 2015 all mothers of babies from 0 to 6 months of age, who were waiting for pediatric care for their children were invited to participate.

The instrument for data collection was a semi-structured questionnaire, which aimed to identify the factors that influence early weaning and advise mothers during the interview about the importance of breastfeeding. This instrument was adapted from Araujo et al. (2013) and Santos and França-Botelho (2010) addressing socioeconomic aspects and mainly related to breastfeeding.

The procedures adopted in this study met the criteria Ethics in Human Research, according to Resolution 466/2012 of the National Health Council of Brazil, which is based regulatory rules and guidelines for research with human beings, including the submission and approval of this project to the Board of Ethics in Research of UNIARAXÁ.

## III. RESULTS

The sample consisted of 26 women, aged between 19 and 42 years, most being, 9 women (73.07%) between 19 and 29 years. As for education, 12 women (46.15%) have primary education, 10 (38.46%) have high school and only 4 (15.38%) has a background in higher level. Regarding marital status, most are married or living in a stable union, 17 (65.38%), only 9 women (34.61%) are single. The predominant family income in the sample is 1-2 minimum wages, corresponding to 20 volunteers (80.76%). Those who are working, on maternity leave and unemployed are respectively 10 (38.46%) 4 (15.38%) and 12 (46.15%) women.

Still order to know aspects that may hinder breastfeeding, mothers were asked about the type of delivery, term pregnancy and number of children. According to Table 1 the predominant type of cesarean delivery was (76.92%). As for prematurity 23.07% of babies were premature. The first pregnancy corresponded to 34.61% of the sample, most of the women interviewed have two children (61.44%).

*https://dx.doi.org/10.22161/ijaers.5.1.6* *ISSN: 2349-6495(P) | 2456-1908(O)*

***Table.1:*** *Distribution of respondents as the type of delivery, prematurity, first pregnancy and number of children.*

| Variable | Classification | N (%) |
|---|---|---|
| Type of delivery | Caesarean | 20 (76.92%) |
| | Normal | 6 (23.07%) |
| Prematurity | Yes | 6 (23.07%) |
| | No | 20 (76.92%) |
| First pregnancy | Yes | 9 (34.61%) |
| | No | 17 (65.38) |
| Number of children | 1 | 9 (34.61%) |
| | 2 | 16 (61.44%) |
| | 3 or more | 1 (3.84%) |

All mothers reported knowing benefits of breast milk, but said they had difficulties in breastfeeding. Figure 1, referring to the most common problems related to breastfeeding, there is experienced by respondents. The main was reported the presence of "weak milk" or “little milk” with 53.84% rate.

And when mothers were questioned in relation to the main reasons why stopped breastfeeding major reports were "not have milk" (33%), "the bottle is more practical" (29%), "the child does not want the breast" (28%).

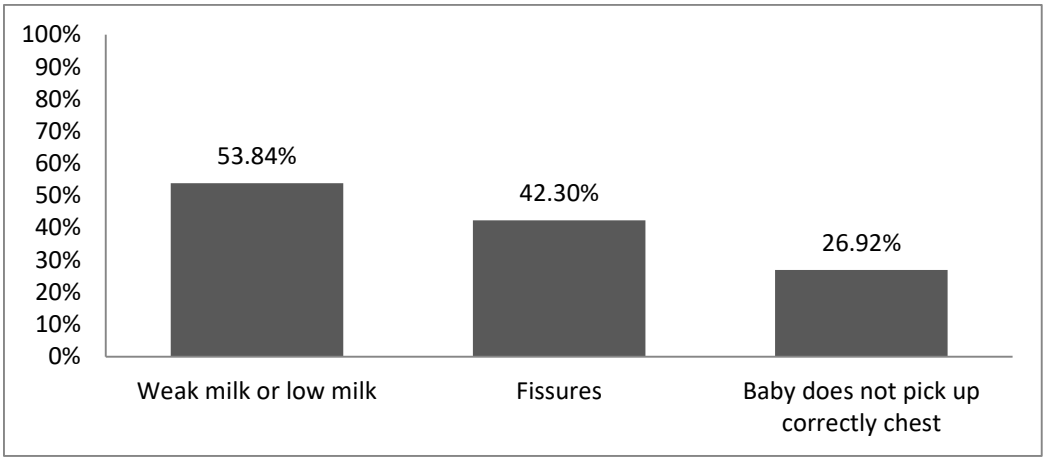


*Fig.1: Main difficulties related to the interviewees experienced breastfeeding.*

Table 2 refers to questions about the initiation of breastfeeding, pacifier use, diseases that contraindicate breastfeeding and family influence on breast feeding. Regarding the child indeed have been breastfed in the first hour 73,07% of respondentes reported so. When questioned about the diseases that contraindicate absolutely breastfeeding, the success rate was 53.84%. When asked if their children were using pacifiers, 69.73% of respondents reported so.

*Table.2: Distribution of respondents as the initiation of breastfeeding, use of pacifiers, diseases that contraindicate breastfeeding and family influence.*

| Variable | Classification | N (%) |
|---|---|---|
| First hour | Yes | 19 (73.07%) |
| | No | 7 (26.92%) |
| Use pacifiers | Yes | 18 (69.23%) |
| | No | 8 (30.76% |
| Diseases that contraindicate breastfeeding | Answer correctly | 14 (53.84%) |
| Family influences, taboos, beliefs, prohibitions on breastfeeding. | Yes, a lot | 9 (34.61%) |
| | Yes, little | 3 (11.53%) |
| | No | 14 (53.84%) |

*https://dx.doi.org/10.22161/ijaers.5.1.6* *ISSN: 2349-6495(P) | 2456-1908(O)*

Professional guidance is needed for successful breastfeeding, as is noted in Figure 2, 46.15% of respondents received guidance from doctors, 46.15% and 11.53% of nurses were not guided by any professional.

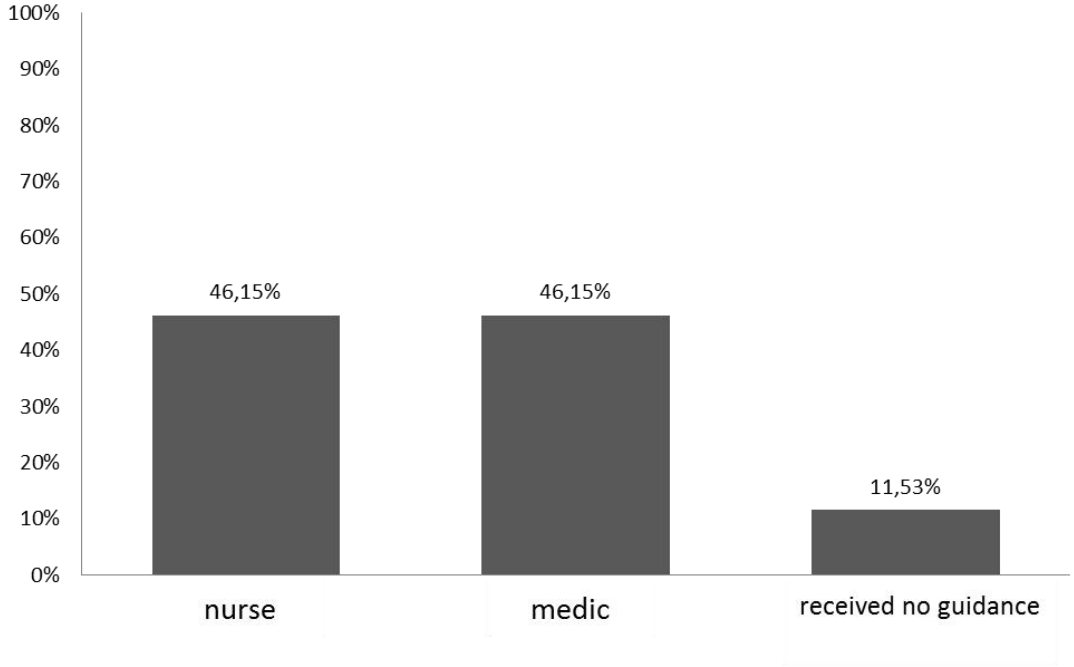


*Fig.2: Guidance on breastfeeding.*

According to figure 3 the early introduction of water was reported by 73.07%; showers by 65.38% and other milk by 61.53% of the sample.

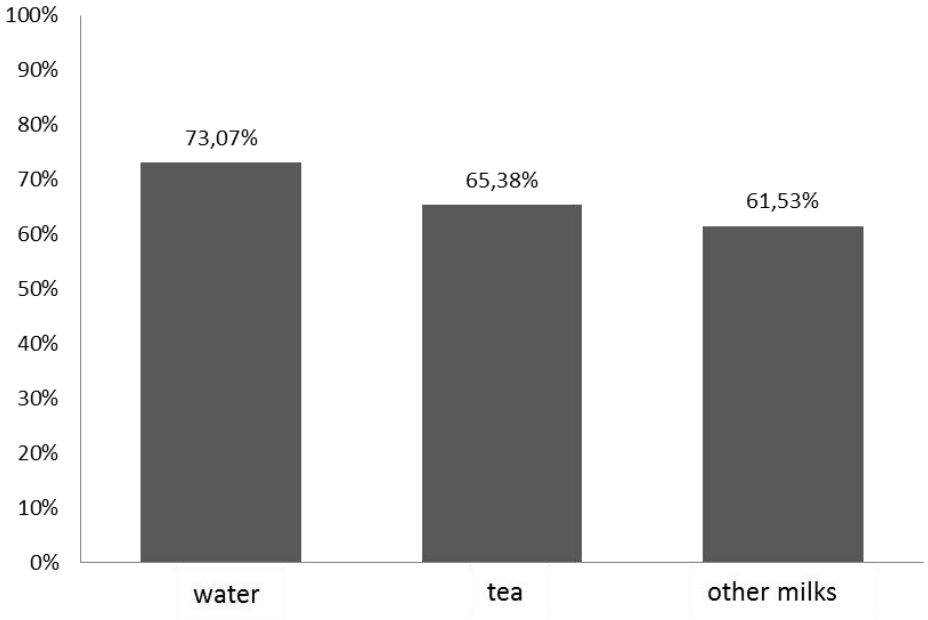


*Fig.3: Main foods introduced early to the infant.*

## IV. DISCUSSION

The return to work is aspect that may impair exclusive breastfeeding for that reason the volunteers were questioned about your current work situation. The misconception of weak milk is a major cause of the alleged early completion by mothers, and the comparison of human milk with cow served as the basis for this belief. The watery appearance of breast milk, especially colostrum, makes the mother considers her inferior milk, believing it does not serve to meet the child's demands differ from popularly known as strong milk (Souza; Almeida, 2005).

As for the volume of milk, the myth of the milk does not hold the baby for being little, may be supported in the baby crying, which is usually associated with hunger or because the milk is not being appropriate to the needs of

*https://dx.doi.org/10.22161/ijaers.5.1.6* *ISSN: 2349-6495(P) | 2456-1908(O)*

the child. However, hypogalactia is a very rare phenomenon among nursing mothers (Cury, 2003).

In the study of Santos and França-Botelho (2010) as the myths that can harm breastfeeding in Perdizes (MG - Brazil) 74.7% of women believed that there are women who have little milk and 36% said they had weak milk.

The act of breastfeeding is not always effective and peaceful way, since the cases are common in that nursing mothers give up breastfeeding their babies due to problems with lactation. Such issues may involve aspects related to postpartum, newborn or both, and, in most cases correspond to an important predisposing factor to early weaning (Brazil, 2015).

The cracks are nipple lesions by improper positioning and attachment of the newborn to breast feeding. no prolonged use nutritive sucking is also considered a predisposing factor of nipple trauma, application of the milk it self in areola complex, sun bathing is a practice for treatment of cracks and prevention of complications. It is very important on the complaint of pain related to breastfeeding technique nipples to be re-evaluated in order to fix it by avoiding the establishment of nipple trauma (Brazil, 2015).

In the study of Castro, Oliveira and França-Botelho (2009) all interviewees said that breast milk is the best food for your child. However, as the management of breastfeeding, about half of the sample claimed to have had difficulties in this regard, had problems with the breasts, especially cracking, pain, a small amount of milk and baby difficult as the act of sucking.

There are beliefs that pacifier use leaves the child calmer and quiet provide back maternal absence, whom believes to leave the appearance of the baby more beautiful, are culturally inserted in our midst. There is concern that their use might cause early weaning of breastfeeding owing to “nipple confusion” (Goldman, 2013).

Pacifier use is not recommended to have risk of contamination, affecting the health of children, promote early weaning due to the difference between breast suction technique and pacifier sucking. Moreover, their use can lead to decreased feedings reducing mammary stimulation and removal of milk produced, leading to reduced production and, consequently, the introduction of milk or other liquids for feeding infants (Lamounier, 2003).

As for the family influence in the transmission of beliefs, taboos and prohibitions on breastfeeding, about half of the sample claims to have had family influence and half of the sample answered this question negatively.

Several problems in child health as diarrhea, respiratory diseases, anemia, malnutrition, can is associated with the early introduction and inadequate supply of food before six months of life. For proper growth and development and for the physical and psychological health of the child breastfeeding plays a fundamental role.

Health care professional who provide care for women in prenatal care and childbirth, such as, medicand nurse, should know the reality, the practice related to breastfeeding and consider the culture and beliefs that influence breastfeeding. So can assist, guide and answer questions, as well as implement preventive or curative measures that contribute to breastfeeding, avoiding early weaning.

## V. CONCLUSION

With the results, we conclude that the sample needs more guidance for exclusive breast feeding, to overcome myth and effectively live successful breastfeeding. The main reasons cited by volunteers for abandoning exclusive breast feeding were "weak milk" and "low milk." In addition, it is note worthy that most participants made early introduction of water, tea and other types of milk, and the use of pacifiers as a means to "reassure" the baby, which impaired breastfeeding.

## REFERENCES

[1] Araújo O. D. Cunha A. L. Lustosa L. R. Nery I. S. Mendonça R. C. M. Campelo S. M. A. (2008). Brastfeeding: factors that cause early weaning. Revista Brasileira de Enfermagem. 61: 488-492.

[2] Araújo V. S. Medeiros A. P. D.S. Barros A. D.C. Braga L. S. Trigueiro J. V. S. Dias M. D.(2013). Early weaning: aspects of the experiences of informal workers. Revista de Enfermagem Referência. 3(10): 35-43.

[3] Barreira S. M. C. Machado M. F. A. S. (2004). Breastfeeding: understanding the family's influence. Acta Scientiarum. 26(1): 11-20.

[4] Black R. E.Victora C. G. Walker S. P.Bhutta Z. A. Christian P.Onis M.et al. (2013). Maternal and child undernutrition and overweight in low-income and middleincome countries. The Lancet. 382(9890): 427-451.

[5] Brazil. Ministério da Saúde. Secretaria de Atenção à Saúde. (2015). Departamento de Atenção Básica. Saúde da criança: aleitamento materno e alimentação complementar / Ministério da Saúde, Secretaria de Atenção à Saúde, Departamento de Atenção Básica. 2. ed. – Brasília: Ministério da Saúde, 2015. Available in: http://dab.saude.gov.br/portaldab/biblioteca.php?conteudo=publicacoes/cab23. Acess in jan 2018.

[6] Castro R. A. Oliveira E. M. França-Botelho, A.C. (2009). BreastFeeding in theare ascovered by the Family Health Program. RBPS, 22:30-35.

[7] Cury M. T. F. (2003). Aleitamento materno. In: Accioly, E. Saunders, C.Lacerda, E. M. A. (Org.).

*https://dx.doi.org/10.22161/ijaers.5.1.6* *ISSN: 2349-6495(P) | 2456-1908(O)*

Nutrição em obstetrícia e pediatria. Rio de Janeiro: Cultura Médica.

[8] Goldman RD. (2013). Pacifer use in thefrstmonth of life. Can Fam Physician. 59(5):499-500.

[9] Lamounier J. A. (2003). The influence of nipples and pacifiers on breastfeeding duration. Jornal de Pediatria.79(34): 284-286.

[10] León-Cava N. (2002). Quantifying the benefits of breastfeeding: a summary of theevidence. Washington, D.C.: PAHO.

[11] Santos K. K. França-Botelho A.C. (2010). Myths that can negativelly affect breastfeading in Perdizes, MG, Brazil. Revista Saúde e Pesquisa. 3: 139-147.

[12] Sassa A.H; Schimidt K.T; Rodrigues B. C; Ichisato S.M. T; Higarashi I.H; Marcon S.S. (2014). Preterm infants: breastfeeding and weight gain. Rev. Bras Enferm. 67(4): 594-600.

[13] Silva R. K. C. Souza N. L. Silva R. A. R. Silva J. B. Ladisláo N. B. P. R. Oliveira S. I. M. (2014). Weight gain of premature neonates related to the type of milk Rev. Eletr. Enf. 16 (3): 535-541.

[14] Souza L. M. B. M. Almeida J. A. G. (2005). História da alimentação do lactente no Brasil: do leite fraco à biologia da excepcionalidade. Rio de Janeiro: Revinter.

[15] World Health Organization - WHO. (2011). Exclusive breastfeeding for six months best for babies everywhere. Available in:http://www.who.int/ mediacentre/news/statements/2011/breastfeeding_20 110115/ en/index.html#. Acess in jan 2018.

*https://dx.doi.org/10.22161/ijaers.5.1.7* *ISSN: 2349-6495(P) | 2456-1908(O)*

# Enhancing Strength Properties of Rubberized Concrete using Waste Cement Sacks

Emmanuel Owoichoechi Momoh, Kassar Terungwa, Godwin Joel

Department of Civil Engineering, University of Agriculture Makurdi, Nigeria

***Abstract—*** *Low flexibility and brittleness of ordinary concrete limits its use as construction material for buildings prone to earthquake ground vibrations. Rubberized concrete which possesses the needed ductility on the other hand is however of low strength and durability. This study utilized waste polypropylene sacks used for packaging cement. The sacks were used in form of confinements to enhance the strength/ductility of rubberized concrete. Concrete cylinders, cubes and beams at different replacements levels of coarse aggregate with waste tire rubber chips(WTRC) (at 0, 10, 20, 30, 40, 50, 60, 70, 80, 90 and 100% by volumes) were cast and tested for fresh and hardened properties such as slump, compressive strength, flexural strength, and deformation behaviour. The result showed proportional reduction in strengths with increasing replacement of WTRC. Ductile and elasto-plastic deformations were exhibited by WTRC concretes. The use of waste cement sacks confinement as a means of overcoming the reduced strength of the rubberized concrete proved highly feasible and economic for the cylindrical specimens. Optimum performance in failure load (for confined specimens) was obtained at 80% WTRC replacement. The confined 80% WTRC failure load was 45.5 KN, approximately 300% increase in failure load of the unconfined 80% WTRC concrete. This indicates that the use of waste cement sacks to confine rubberized concrete effectively negates the decrease in strength, and retains the advantages of increased ductility and energy-dissipation that characterizes rubberized concrete.*

***Keywords— rubberized concrete, waste tyre rubber chips, strength***

## I. INTRODUCTION

Recent occurrences in nature has necessitated structures to resist wind loading, earthquake ground vibration as well as other combined axial and lateral loadings due to extreme events. It becomes imperative that structures be designed and constructed with materials that can accommodate these effects. These structures must possess good dynamic response and must be cheap enough to be afforded by citizens of especially developing countries where the government is unable to provide housing let alone supervise the quality of housing provided by citizens themselves.

In the early 1990s, recycled waste tire usage expanded into a relatively new product called rubberized concrete [1]. Rubberized concrete uses portland cement as its binder. This lead to the discovery that the use of waste tyre as aggregate replacement in concrete shows an improvement in the concrete mechanical properties such as ductility (flexibility), energy dissipation, toughness, increased damping and sound insulation among others [2], [3], [4], [5], [6], [7]. A ductile form of concrete known as rubberized concrete which was hitherto thought to be impossible to achieve has gained interests all over the world.

### 1.1 Significance of the study

In developing countries, the government is unable to provide decent shelter for her teeming population hence the abundance of many non-engineering houses having one or two storeys. These constructions usually have little to no reinforcement, and collapse at the slightest movement of the ground causing injuries or even death of their occupants [8]. Rubberised concrete provides a cheap source of construction concrete for these regions except for the low strength attributed to it. An approach to negating the drop in strength at the addition of rubber to concrete is through confinement. Several confinement methods and strengthening techniques for reinforced concrete structures have been reported [9],[10],[11],[12],[13] but all these techniques may not be within the reach of the ordinary poor citizen [12]. Aside the strengthening methods being expensive, the technical know-how of using these strengthening methods may not be available to the impoverished non-literate citizens. The use of rubberized concrete confined with waste polypropylene sacks (used for packaging cement) proves cheaper and easier to use.

It is with this in mind that the research aims to enhance the strength properties of concrete by replacement of coarse aggregate with waste tyre chips and providing confinement to the concrete.

The objectives of this investigation are as highlighted below:

- Casting 100x300mm concrete cylinders, 150x150x150mm concrete cubes and

*https://dx.doi.org/10.22161/ijaers.5.1.7* *ISSN: 2349-6495(P) | 2456-1908(O)*

100x100x450mm concrete beams at different replacement levels of coarse aggregate with waste tyre rubber chips,

- Carrying out strength tests on the cast specimens at 7, 14 and 28 days,
- Enhancing the strength properties of rubberized concrete through confinement with waste polypropylene cement sacks recovered after using cement,
- Providing recommendations for the use of polypropylene cement sacks as confinement for rubberised concrete columns.

This research evaluates the need for the use of waste polypropylene cement sacks to enhance strength properties of concrete incorporating WTRC as coarse aggregate. Section II discussed the materials and testing methods to measure the fresh and hardened concrete properties. Results of findings were presented and discussed also in section II as well as necessary graphs showing relationship between the results obtained. Section III highlighted the summary of findings, conclusions and provided recommendation for future findings and analysis. The research was limited to the laboratory investigation of fresh and hardened properties of the concrete as well as confinement to improve strength.

## II. MATERIALS AND METHODS

### 2.1 Materials

- **Cement**

The cement used for the research was ordinary Portland cement (Grade 42R satisfying BS 12:1996) produced by Dangote Cement Company, Nigeria.

- **Aggregates**

Coarse and fine aggregate used were river gravel and sand respectively and were sourced from the river Benue in Makurdi, Nigeria. The coarse aggregate was partially replaced with waste tyre rubber chips (WTRC).

- **Waste Tyre Rubber Chips (WTRC)**

The waste tyres were cut into chips using hand cutter to a size range of between 20mm and 5mm. The chips were used as partial replacement for coarse aggregate in various percentages of 0%, 10%, 20%, 30%, 40%, 50%, 60%, 70%, 80%, 90% and 100%.

- **Waste Cement Sacks**

These are polypropylene sacks used for packaging cement. They were used for the rubberized concrete cylinder confinement. The waste cement sacks were sourced from the construction site located at the College of Engineering University of Agriculture Makurdi Nigeria.

- **Water**

Fresh water (satisfying ASTM C1602) used for specimen casting was obtained from the university water works. The storage tank beside the Civil Engineering Laboratory served as access point to the water used for the research.

### 2.2 Methodology of Tests

The various tests carried out were conducted at the Department of Civil Engineering Laboratory, University of Agriculture Makurdi (UAM). The tests include:

#### 2.2.1 Specific Gravity Test

The specific gravity is the fundamental physical characteristic of the material. It is the ratio of the weight of a given material to the weight of equal volume of water. The test was conducted for both fine and coarse aggregate in accordance with BS 4550: Part 3: Section 3:1978 using the density bottle. Apparatus used include Specific gravity bottle, weighing balance, distilled water (water without impurities), trowel and dry oven.

The specific gravity bottle was weighed empty and the weight recorded as $W_1$. An amount of the sample was poured into the empty specific gravity bottle and weighed and the weight obtained gives the weight of empty bottle plus sample which was recorded as $W_2$. Distilled water was added to the sample inside the specific gravity bottle and the content was weighed. The weight obtained was recorded as $W_3$, this comprises of the weight of bottle, sample and water. The Specific gravity bottle was then emptied of its content, rinsed, and filled with distilled water which was weighed and recorded as $W_4$. The specific gravity was calculated using equation 2.1.

$$G_S = \frac{W_2 - W_1}{(W_4 - W_1) - (W_3 - W_2)} \quad \text{.....2.1}$$

For each of the materials, the test was conducted twice and the average value was taken as the specific gravity for that material. Table 2.1 shows the Specific Gravity of WTRC.

*Table.2.1: Specific Gravity of WTRC*

| Bottle Description | Bottle 1 | Bottle 2 |
|---|---|---|
| Weight of bottle ($W_1$) (g) | 25.7 | 25.7 |
| Weight of bottle + sample ($W_2$) (g) | 31.3 | 32.2 |
| Weight of bottle + sample + Water ($W_3$) (g) | 102.8 | 102.6 |
| Weight of bottle + Water ($W_4$) (g) | 102.3 | 102.3 |
| Specific Gravity (Gs) | 1.10 | 1.05 |
| Average Gs | | *1.08* |

From Table 2.1, the average specific gravity of waste tyre rubber was found to be 1.08 which falls between 1.02–1.27 as highlighted in [Rui 2013]. This is less than half of the specific gravity of the coarse aggregate. This implies that, replacement of coarse aggregates with waste tyre rubber in concrete reduces the overall weight of the concrete. Similarly, the specific gravity of both the sand

*https://dx.doi.org/10.22161/ijaers.5.1.7* *ISSN: 2349-6495(P) | 2456-1908(O)*

(fine aggregate) and river gravel (coarse aggregate) was found to be 2.62.

### 2.2.2 Sieves Analysis

The process of dividing the sample of aggregate into fractions of same particles size is known as sieve analysis. Its purpose is to determine the grading or size distribution of the aggregate (Neville 2010). This test was carried out for both fine and coarse aggregate. The apparatus used were sieve mesh**,** trowel**,** brush**,** and weighing scale. Various sieves with sizes 20 mm, 14 mm, 20 mm, 6.3 mm, 5.0 mm, 3.35 mm, 2.36 mm, 1.70 mm, 1.18 mm, 850 µm, 600 µm, 425 µm, 300 µm, 150 µm and 75 µm were used for the experiment. The sieves were arranged vertically in descending order of sizes while conducting the experiment. The 20 mm down to 3.35 mm sieve were used for the river gravel and waste tyre chips (coarse aggregates) while 3.35 mm down to 75 µm sieve were used for the river sand (fine aggregate). Fig 2.1 shows the graph of sieve analysis of WTRC.

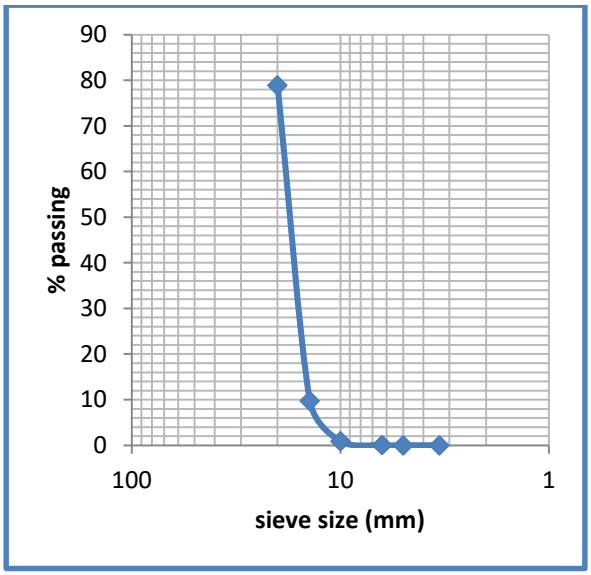


*Fig 2.1: Sieve analysis graph of waste tyre rubber chips*

The result of sieve analysis of the waste tyre rubber from Fig 2.1 indicates that the aggregates size ranges between 20 mm – 5 mm with about 69% of its whole amount predominantly of size 14 mm. The waste tyre rubber could not meet the grading requirement for coarse aggregate according to BS 882: 1992 due to its poor grading. Fig 2.2 presents the graph of sieve analysis for fine aggregate (river sand).

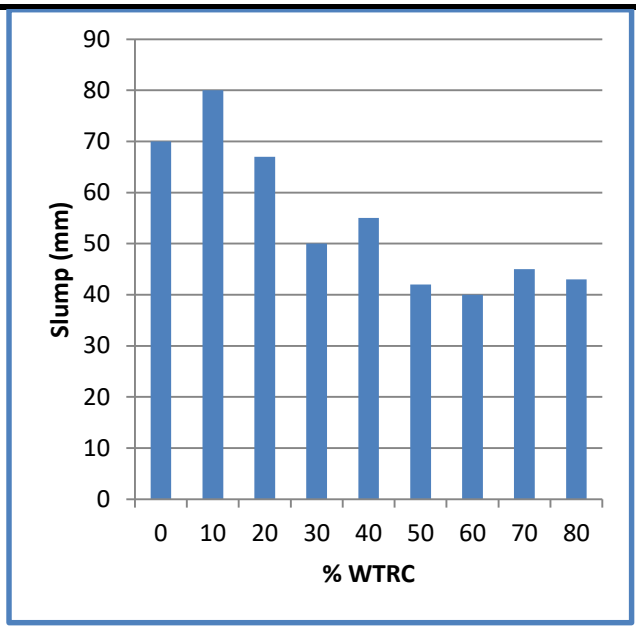


*Fig 2.2: Sieve analysis graph of river sand (fine aggregate)*

The fineness modulus of the coarse aggregate was computed and found to be 5.82. Generally, the fineness modulus of fine aggregates ranges between 2.3 and 3 [14], aggregates having higher values greater than 3 indicates coarser grading. Though, the fine aggregate meet the grading requirements for fine aggregate according to BS 882: 1992. The fineness modulus (5.82) computed may be due to the increased in the number of sieves used. Fig 2.3 presents the graph of sieve analysis for coarse aggregate (river gravel)

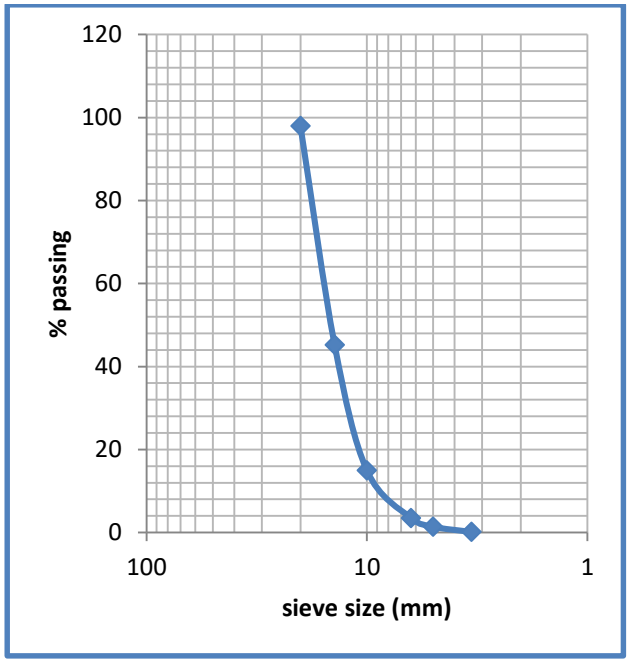


*Fig 2.3: sieve analysis graph of river gravel (coarse aggregate)*

*https://dx.doi.org/10.22161/ijaers.5.1.7* *ISSN: 2349-6495(P) | 2456-1908(O)*

From Fig 2.3, coarse aggregate sieve analysis, the result shows that majority of the aggregates are of 14 mm size with 1.4% of its weight below 5 mm size. The result of the fineness modulus clearly indicates coarser grading (since it is above 3.0). The coarse aggregate also meet the grading requirement according to BS 882: 1992.

### 2.2.3 Slump Test

Fig 2.4 shows the result of the slump obtained for each respective amount of WTRC replacement. The test was conducted according to ASTM C143. The slump value on a general note could be said to range between 40 – 80 mm. Concrete mix with less amount of WTR tends to have medium degree of workability, but the workability tends to decrease with increase amount of WTR. This decrease in slump with increasing amount of WTR confirms the report made by [4] and [15].

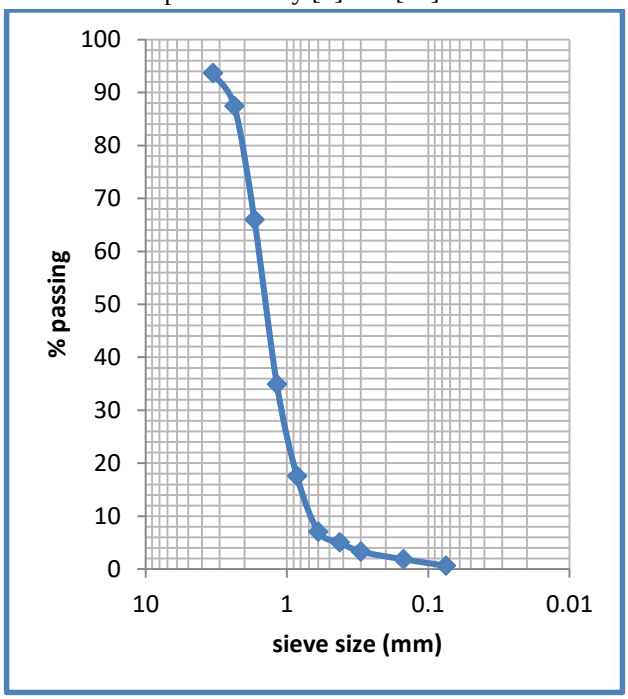


*Fig 2.4: Slump relationship with % replacement of coarse aggregate with WTRC*

From Fig 2.4, the highest and lowest value of slump was achieved at 10% WTR and 60% WTRC respectively with 50% total decrease in slump when compared between the two WTRC percentage replacements. This decrease in slump then implies that at higher percentage replacement of WTRC in concrete may not be workable for the water/cement ratio of 0.5 used.

### 2.2.4 Compressive Strength Test

The test was performed at 28 days for cubes and at 7, 14 and 28 days for the unconfined concrete cylinders in order to find out the variation of strength with the age of the concrete. The compressive strength test was conducted in accordance with IS: 516-1959. Eleven mixtures were performed for the cubes and nine mixtures for the concrete cylinders. The compressive strength computed are tabulated and plotted against the % WTRC replacement as shown in Fig 2.5. There was a general decrease in the compressive strength for the cubes and unconfined concrete cylinders. This is in agreement with the report of [5] . The reduction in strength is as a result of poor adhesion between the WTRC and binder. Since one of the objectives is to improve the structural performance of the concrete through confinement, this was done with aid of waste polypropylene sacks after using cement out of the packaging. The outcome of the results indicates a great improvement in the strength and flexibility of the WTRC concrete as seen in section 2.2.5.

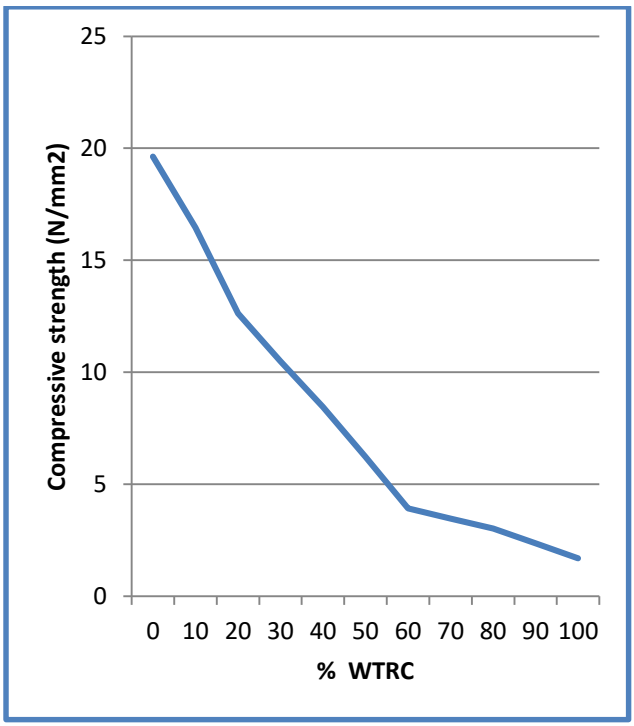


***Fig 2.5:*** *Graph of compressive strength of cubes vs % WTRC*

The compressive strength of cubes for the eleven mixes is plotted against percentage replacement of WTRC as shown in Fig 2.5. The cube strength at 28 days for the control (0% WTRC) is 19.63 N/mm$^2$. There was a proportional reduction in strength and density with increased WTRC replacement in the concrete mixtures. 10% WTRC mix tends to have the least reduction in cube strength of about 16.2 % as compared to the 100% WTRC having about 91% reduction of the control strength. This implies that the 100% WTRC mixture cannot be used for construction purposes. Concrete mix with 10% WTRC can be effectively used for the replacement with coarse aggregate since reduction in strength is minimal at this point.

*https://dx.doi.org/10.22161/ijaers.5.1.7* *ISSN: 2349-6495(P) | 2456-1908(O)*

The desirable ductile effect of including WTRC in the concrete is seen in the failure mode of the concrete as observed during crushing. Plate 2.1(a) and (b) shows the failure mode of the control concrete and WTRC concrete respectively. The mixture with WTRC underwent elasto-plastic deformation during and after failure while the control (0% WTRC) disintegrated in a brittle manner under the failure load. Though the failure load of WTRC concrete was small, elasto-plastic deformation observed at constant loading showed that the cubes tend to absorb more energy with ductile cracks developing.

### 2.2.5 Confinement

The reduction in the strength of concrete incorporating WTRC can effectively be negated by the use of lateral confinement in various forms. However for the purpose of this research, a very low cost approach is desired. Confinement of the cylindrical concrete specimens was therefore done using waste polypropylene cement sacks. The sacks are the bags used to package Portland cement in Nigeria. At construction sites, these sacks are thrown away after the cement has been used out of them. The confinement test was carried out with these waste cement sacks, wrapped and bonded using modified acrylic adhesive (4-minutes epoxy steel gum). The specimens were wrapped in three layers with aid of the adhesive. See Plate 2.1(E) and (F). The failure loads of the confined concrete cylinders obtained were found to be much greater than the failure load of the unconfined concrete cylinders. High deformations were observed for the confined concrete cylinders; deformation up to 6% of original height of specimens was obtained for the confined concrete cylinder containing 80% WTRC. The result of the confinement is presented in Fig 2.6.

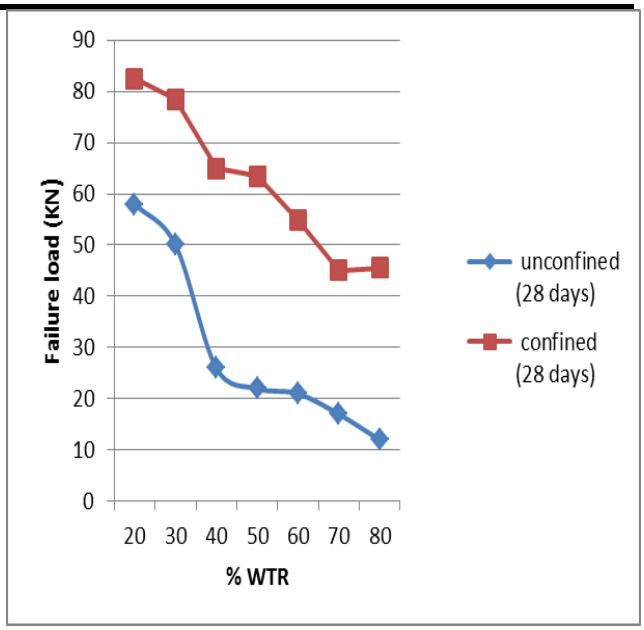


*Fig.2.6: Relationship between the failure load of unconfined and confined concrete cylinders*

The difference in failure load between the unconfined and confined cylinders is quite large. This shows the effectiveness of the confinement using waste cement sacks. Increase in failure load occurred for each of the WTRC replacement mix. The percentage increase in failure load when comparing the unconfined failure load with that of the confined for each of the WTRC replacement mixes are given as follows:

20% WTRC = 42.2%
30% WTRC = 57%
40% WTRC = 150%
50% WTRC = 188.6%
60% WTRC = 161.9%
70% WTRC = 164.7%
80% WTRC = 279.16%

https://dx.doi.org/10.22161/ijaers.5.1.7 ISSN: 2349-6495(P) | 2456-1908(O)


***Plate 2.1:*** *(A) Brittle failure of control cube (B) Brittle failure of control cylinder (C) Ductile failure of unconfined rubberized concrete cylinder (D) Ductile failure of rubberised concrete (E) Waste cement sack confinement of rubberised concrete cylinders (F) Ductile failure of confined rubberised concrete cylinders.*

Ductile mode of failure was exhibited by the confined concrete cylinders, with high ductility and compressibility. The concrete cylinders could regain their original height after application of load. Elasto-plastic deformations were also observed during loading with the concrete's ability to withstand further loading after seeming failure. The ductile mode of failure is shown Plate 2.1 (C), (D) and (F).

### 2.2.5 Flexural Strength Test

Flexural test was conducted according to BS 1881: Part 118: 1983. Six mixtures of WTRC were used. Beams of dimension 100 mm X 100 mm X 450 mm were cast and cured for 28 days. The result obtained after crushing was tabulated and plotted against the percentage of WTRC concrete. The result reveals a decrease in flexural strength with addition of WTRC. This confirms the report made by [16], [17] and [18]. The result of flexural strength of the beams for the 20% WTRC and 40% WTR replacement falls within the typical range values of ordinary Portland concrete (which is between 3 – 5.5 N/mm$^2$). This implies that WTRC replacement up to 40% can provide sufficient flexural strength. The result of flexural strength at 28 days has been presented in Fig 2.7.

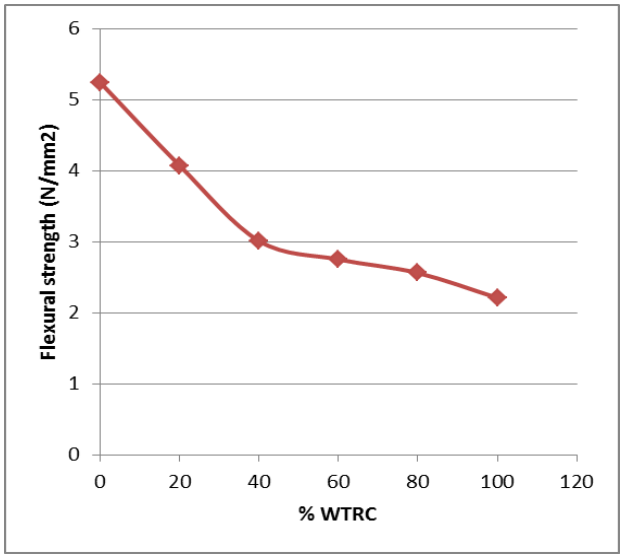


*Fig.2.7: Flexural Strength of Beams Vs % WTRC*

The graph reveals a proportional decrease in the compressive strength with increasing WTRC content. At

*https://dx.doi.org/10.22161/ijaers.5.1.7* *ISSN: 2349-6495(P) | 2456-1908(O)*

100% WTRC, there was a total reduction in flexural strength of 57.8% when compared with the control; this implies a more than half decrease in flexural strength. The percentage reduction in flexural strength of 20% and 40% WTR were 22.3% and 42.6% respectively. The percentage reductions were higher, though the value of their flexural strength fall within the range values of ordinary Portland concrete. In addition, ductile failure was observed for the concrete mixes incorporating WTRC. The failure at ultimate load was gradual not the brittle sudden failure as in the case of the control mix. This then implies that incorporation of WTRC in concrete does not only provide sufficient flexural strength but also can withstand large amount of deformations under flexure before failure.

### 2.2.6 Axial Deformation

This test was carried out for only the confined concrete cylinders. It was carried out at 7, 14 and 28 days in order to determine the variation of axial deformation with curing age as the WTRC is incorporated in concrete and increased at percentages. The initial length and final length (in the axial direction) of the specimen were measured before and after crushing. The initial and final lengths were taken before and at the point of failure respectively. The results are shown on the plot in Fig 2.8. Deformation increased with increase in WRTC replacement. This observation was also made [17]. Due to the manual hand-methods employed in wrapping the waste cement sacks over the cylindrical specimen, it may be difficult to deduce accurately the behaviour of deformation in Fig 2.8 as the 14 days deformation exceeds the rest after 20%WTRC replacement level. However, in general, it is obvious that confining the rubberized concrete cylindrical specimens results in high deformations.

This indeed is the desired behaviour needed for structural concrete employed in the construction of earthquake resistant structures. There was an increase in deformation with WTRC percentage replacement of the confined specimen. WTRC concrete can act as an elasto-plastic material under loading. After the failure load, the WTRC mixes with high amount of rubber chips could regain up to 95% of their original height after compression. It is evident that the incorporation of WTRC in the concrete influences its physical properties through enhanced flexibility, ductility and energy absorption.

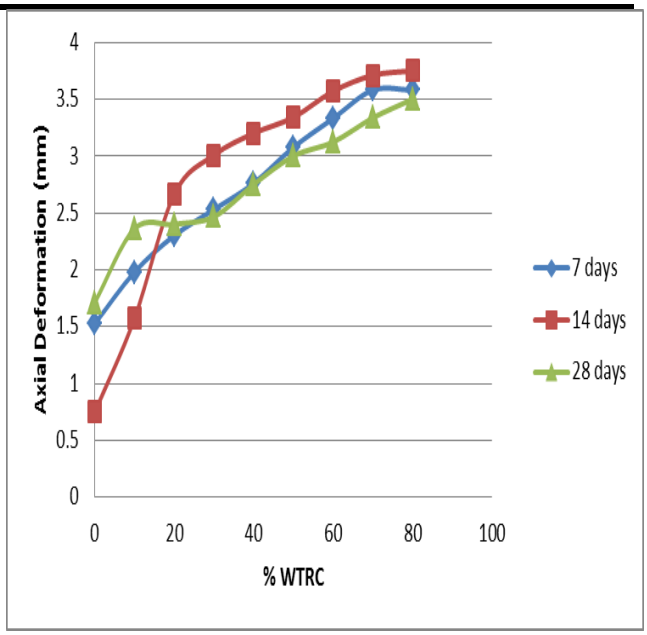


*Fig.2.8: Axial deformation of confined concrete cylinders vs % WTRC*

## III. CONCLUSION

### 3.1 Summary

High ductility and strength were both achieved in this research through replacement of coarse aggregate with WTRC and through confinement by the use of waste cement sacks. Findings can be summarized as follows:

- The slump decreased with increasing WTRC content. However, the mix with 10% WTRC gave a fair degree of workability.
- There was a proportional decrease in the unit weight of concrete with increasing WTRC content.
- A general reduction in strength was observed with increase of WTRC content.
- The flexural strength of beams with 20% and 40% WTR chips replacement fall within the range of flexural strength of ordinary Portland cement concrete. The flexural strength generally decreased with increased amount of WTRC content.
- Confinement to improve the structural performance of the WTRC concrete through the use of waste cement sacks is feasible.
- Ductile mode of failure was exhibited by concrete containing WTRC. The concrete tends to withstand further loading after failure.
- Concrete with 0% WTRC exhibited a sudden and brittle mode of failure
- Concrete with WTRC exhibit higher deformation than the control concrete (0% WTRC).
- The confined concrete could regain up to 95% of its original height after compression. This

*https://dx.doi.org/10.22161/ijaers.5.1.7* *ISSN: 2349-6495(P) | 2456-1908(O)*

also implies enhanced flexibility, ductility and energy dissipation of the concrete.

### 3.2 Conclusion

From the experimental study, it can be concluded that

- The strength properties of rubberized concrete can be greatly enhanced in concrete through the use of waste cement sacks-confinement of WTRC concrete.
- Waste cement sacks pose a cheaper alternative to all other materials used for confinement of concrete elements.
- The WTRC concrete can enhance the structure ductility, damping ratio, and the energy dissipation which are the most important parameters in structures built for earthquakes.
- This type of confinement is feasible for strengthening concrete columns and beams of houses built in rural areas with poor quality control.
- The light unit weight qualities of rubberized concrete also makes it suitable for architectural application, false facades, stone baking, interior construction, foundation pads for machinery, railway stations where vibration damping is required and in areas where resistance to impact is needed, such as in jersey barrier, railway buffers, bunkers and for trench filling.

### 3.3 Recommendations

Future studies on this work will seek to investigate the strength properties of waste cement sacks. For the purpose of this research, the confinement wraps were limited to 3 layers. More layers of confinement wrap will be investigated. Finally, time-dependent strength behaviours of the waste cement sacks will be investigated in future works.

## REFERENCES

[1] Rui, L. (2013): "Recycle Tyre as Coarse Aggregate in Concrete Pavement Mixtures", Report No. CDOT-2013-1. Mat. in Civil Eng, Vol. 19, pp173-178.

[2] Tarun R. N. and Rafat, S. (2002): "Properties of Concrete Containing Scrap Tire Rubber – An Overview", Report No. CBU-2002-06, REP-459

[3] Momoh Emmanuel Owoichoechi, Kypros Pilakoutas (2017) *"Highly Deformable Energy-Dissipating Reinforced Concrete Elements in Seismic Design of Reinforced Concrete Structures"*Vol. 7 - Issue 6 (June - 2017), International Journal of Engineering Research and Applications (IJERA) , ISSN: 2248-9622 , www.ijera.com

[4] Albano, C., Camacho, N., Reyes, J., Feliu, J. and Hernández, M. (2005): *Influence of Scrap Rubber Addition to Portland Concrete Composites: Destructive and Non-destructive Testing*, Compos. Struct. Vol. 71, pp439–446.

[5] Eldin, N.N. and Senouci, A.B. (1993): *Rubber-Tire Particles as Concrete Aggregates*. Journal of Materials in Civil Engineering, ASCE. Vol. 5, No. 4, 1993, pp. 478- 496.

[6] Topcu, I.B. and Avcular, N. (1997a): *Analysis of Rubberized Concrete as a Composite Material*, Cement and Concrete Research. Vol. 27, No. 8, pp1135-1139.

[7] Kotresh K.M and Mesfin G. B. (2014): *Study on Waste Tyre Rubber as Concrete Aggregates.* International Journal of Scientific Engineering and Technology. Vol.3, No.4, pp433-436

[8] Sathiparan, N., & Meguro, K. (2015). Strengthening of adobe houses with arch roofs using tie-bars and polypropylene band mesh. *Construction and Building Materials*, *82*, 360-375.

[9] Garcia, R., Hajirasouliha, I., & Pilakoutas, K. (2010). Seismic behaviour of deficient RC frames strengthened with CFRP composites. *Engineering Structures*, *32*(10), 3075-3085.

[10] Garcia, R., Pilakoutas, K., Guadagnini, M., Helal, Y., Jemaa, Y., Hajirasouliha, I., & Mongabure, P. (2012). Seismic strengthening of deficient RC buildings using post-tensioned metal straps: an experimental investigation. *Proceedings of the 15WCEE, Lisbon, Portugal*.

[11] Li, G., Pang, S. S., & Ibekwe, S. I. (2011). FRP tube encased rubberized concrete cylinders. *Materials and structures*, *44*(1), 233-243.

[12] Mirmiran, A., & Shahawy, M. (1997). Behavior of concrete columns confined by fiber composites. *Journal of Structural Engineering*, *123*(5), 583-590.

[13] Youssf, O., ElGawady, M. A., Mills, J. E., & Ma, X. (2014). An experimental investigation of crumb rubber concrete confined by fibre reinforced polymer tubes. *Construction and Building Materials*, *53*, 522-532.

[14] Neville, A. M. and Brooks, J. J. (2010): **Concrete Technology.** 2nd edition, Long Man Group UK Limited, Tottenham, London

[15] Batayneh, M., Marie, I. and Asi I. (2008): *Promoting the Use of Crumb Rubber Concrete in Developing Countries*, Waste Manag. Vol. 28, pp 2171–2176.

[16] Ganjian, E., Khorami, M., and Maghsoudi, A. (2009): *Scrap-Tyre-Rubber Replacement for*

*https://dx.doi.org/10.22161/ijaers.5.1.7* *ISSN: 2349-6495(P) | 2456-1908(O)*

*Aggregate and Filler in Concrete*, Constr. Build Mat. Vol. 23, pp1828-1836.

[17] Parveen, Sachin D. and Ankit S. (3013): *Rubberized Concrete: Needs of Good Environment (Overview).* International Journal of Emerging Technology and Advanced Engineering Website: www.ijetae.com (ISSN 2250-2459, ISO 9001:2008 Certified Journal), Vol. 3, No. 3.

[18] Farhad, A. (2015): *Mechanical Properties of Waste Tyre Rubber*. Journal of Materials in Civil Engineering. https://www.researchgate.net/publication/282120797

*https://dx.doi.org/10.22161/ijaers.5.1.8* *ISSN: 2349-6495(P) | 2456-1908(O)*

# Facies analysis and stratigraphic development of the Albian Succession in Nasiriyah Oil Field, Southern Iraq

Aiad Ali Al-Zaidy, Marwah Hatem Khudhair

University of Baghdad, College of Science, Department of Geology

***Abstract—*** *The Carbonate - Clastic succession in this study is represented by the Nahr Uamr and Mauddud Formations deposited during the Albian Sequence. This study includes facies analysis and stratigraphic development for this succession in 5 boreholes within Nasiriyah oil field.*

*There are several types of microfacies were recognized in the succession of the Mauddud Formation. Their characteristic grain types and depositional texture enabled the recognition of six facies associations (depositional environments) were distinguished in the Mauddud Formation, they are: shallow open marine, restricted, reef, slope, deep open marine and basinal.*

*Two types of rocks are observed within the Nahr Umr Formation; the first is the upper part which characterized by shale dominated rocks and the second (lower part) is characterized by sand dominated rocks. Four facies associations (depositional environments) were distinguished in the Nahr Umr Formation, they are: delta plain, prodelta, bay fill, and distributary channels.*

*The microfacies analysis and reconstructed the paleoenvironments of the Albain basin in the studied area; there are three stages of the deposition: - during the first stage the sea level was rise which led to progress prodelta facies (retrogradation) and onlapping the unconformity. This part is represented by TST stage in all studied boreholes. The prodelta facies was changed to distributary channel facies up-wared to mark the mfs between these two facies. This refers to deposition during the high stand period as two cycles. The sea level was reactivated to progress after the last step of Nahr Umr deposition, to start the Mauddud Formation deposition.*

*At second stage the facies change was shown three steps of the sea level rise (TST) to deposition the restricted, reef-back reef and shallow open marine/slope. Overlying the slope facies to the shallow marine and then deposited the shallow marine refer to maximum flooding surfaces after deposition the last ones. Therefore, the shallowing up-ward succession which deposition later was represented the high stand stage (HST).*

*The final stage is represented by reactivated the sea level rise to deposition the basinal facies within the Mauddud Formation. The continued rise in sea level during the period of transgression (TST) is a preparation for the Ahmadi basin, which is characterized by deposition in a deep environment and conformable lower contact with the Mauddud Formation.*

***Keywords— Petrophysical Properties, Reservoir development, Albian Succession and Nasiriyah Oil Field.***

## I. INTRODUCTION

Clastic-carbonate succession which including the Nahr Umr and Mauddud Formations are represented a part of Albian-Early Turonian Sequence (Wasi`a Group), (Cretaceous period). The present study includes five boreholes (Ns-1, 2, 3, 4 and5) within the Nasiriyah oil field. The study area is located in the South of Iraq. This field is representing a subsurface anticline with Northwest to Southeast direction axis within the Mesopotamian Zone, figure (1).

The Nahr Umr Formation was defined by Glynn Jones in 1948[1] from the Nahr Umr structure in South Iraq. The two major depocentres in central and South Iraq correspond to areas which received clastics from the Rutba Uplift and the Arabian Shield. In its type area in Southern Iraq, the Nahr Umr Formation comprises black shale bedded with medium to fine grained sandstones with lignite, amber, and pyrite [1]. The proportion of sand in the formation increases towards the Salman Zone.

The Mauddud Formation includes the Upper part of Qamchuqa Formation and is the most widespread Lower Cretaceous formation in Iraq. Its thickness varies due to lateral facies changes and erosional truncation. At outcrop in NE Iraq the Qamchuqa Formation comprises organodetrital, detrital and locally argillaceous limestones with variable degrees of dolomitization. In some areas fresh- or brackish-water limestone beds were reported [1]. In Southern Iraq, the Mauddud Formation comprises frequently dolomitised organodetrital limestone.

*https://dx.doi.org/10.22161/ijaers.5.1.8* *ISSN: 2349-6495(P) | 2456-1908(O)*

The present study involves petrophysical properties of the Nahr Umr and Mauddud Formations, and the effects of diagenetic development on reservoir properties, with construction of a reservoir model for these formations.

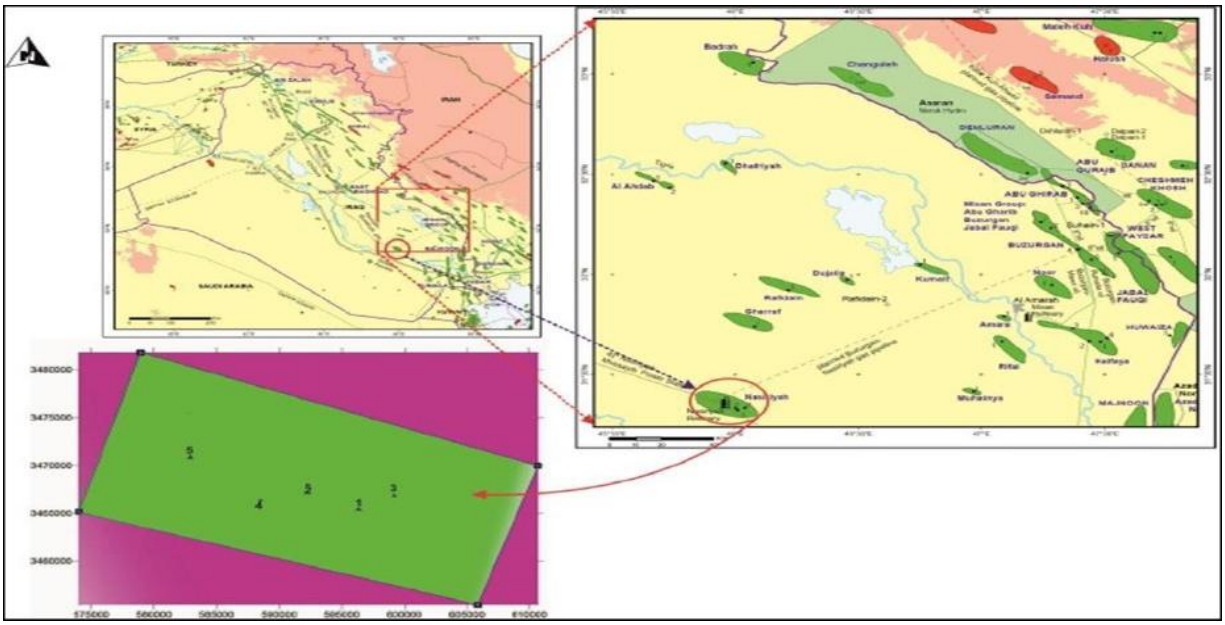

*Fig.1: Location map of Study area*

## II. FACIES ANALYSIS OF MAUDDUD FORMATION

The textures and fabric of the carbonate rocks for Mauddud Formation are classified according to Embry and Klovan"s classification [2] modified from Dunham [3]. The approach of Burchette and Brittons [4] in grouping facies types as "association" rather than a single type or class was followed. The facies associations were compared with the models of standard microfacies and depositional environment belt of carbonates proposed by Wilson [5] and Flugel [6].

There are several types of microfacies were recognized in the succession of the Mauddud Formation; their characteristic grain types and depositional texture enabled the recognition of paleoenvironment.

**Microfacies (A):-** Orbitolina - wackestone to packstone

This facies is mainly composed of Orbitiolina and shell fragments (mollusk), echinoderms, pellets and calcareous algae (Plt 1.a). Such microfacies reflect a shallow open marine.

**Microfacies (B):-** Textularia/hedenbergella wackestone

The second most common microfacies is the textularia, and hedenbergella limestone. With echinoderm and calcareous algae (Plt 1.b). This may reflect an open marine.

**Microfacies (C):-** Globigerina wackestone to packestone

The main constituents are Globigerina and small benthic foraminifera with few red algae (Plt 1.c). This microfacies reflects a deep open marine environment.

**Microfacies (D):-** Peloidal wackestone to packstone

This microfacies consists mainly of peloids with rudist fragments, calcareous algae and miliolids being the less abundant. It can be divided into:-

- Peloidal wackestone to packstone rounded grains are inferred, from their biform size, ovoid shape where the dominance of relatively coarse to fine (sand sized) and moderate sorted peloids (Plt 1.d).
- pelletal wackestone to packstone is characterized by the abundance of the uniformly of small particle size and consistent shape of these grains (silt sized well sorted pellets) (Plt 1.e).

**Microfacies (E):-** Intraclasts packstone

Two types of this microfacies were distinguished in the succession Bioclasts (Rudist and other shell fragments) (Plt 1.f), and Mudstone to wackstone shell fragment packstone with micro convolute structure (Plt 1.g). This may reflect to brecciated slope deposits.

**Microfacies (F):-** Rudist boundstone to rudstone .

This is a less common microfacies distinguished in most wells. It is composed of rudist fragments and other shell fragments (gastropod and mollusk) (Plt 1.h). This microfacies is identified as backreef to reef environment.

**Microfacies (G):-** Basinal green shale

These facies is appeared in the upper part of Mauddud Formation as Globigerinal and calcisphere shale and shaly limestone. This faceis is observed in the reflected by gamma ray log response addition to thin section diagnostic (Plt 1.i).

*https://dx.doi.org/10.22161/ijaers.5.1.8* *ISSN: 2349-6495(P) | 2456-1908(O)*

**Plate- 1**

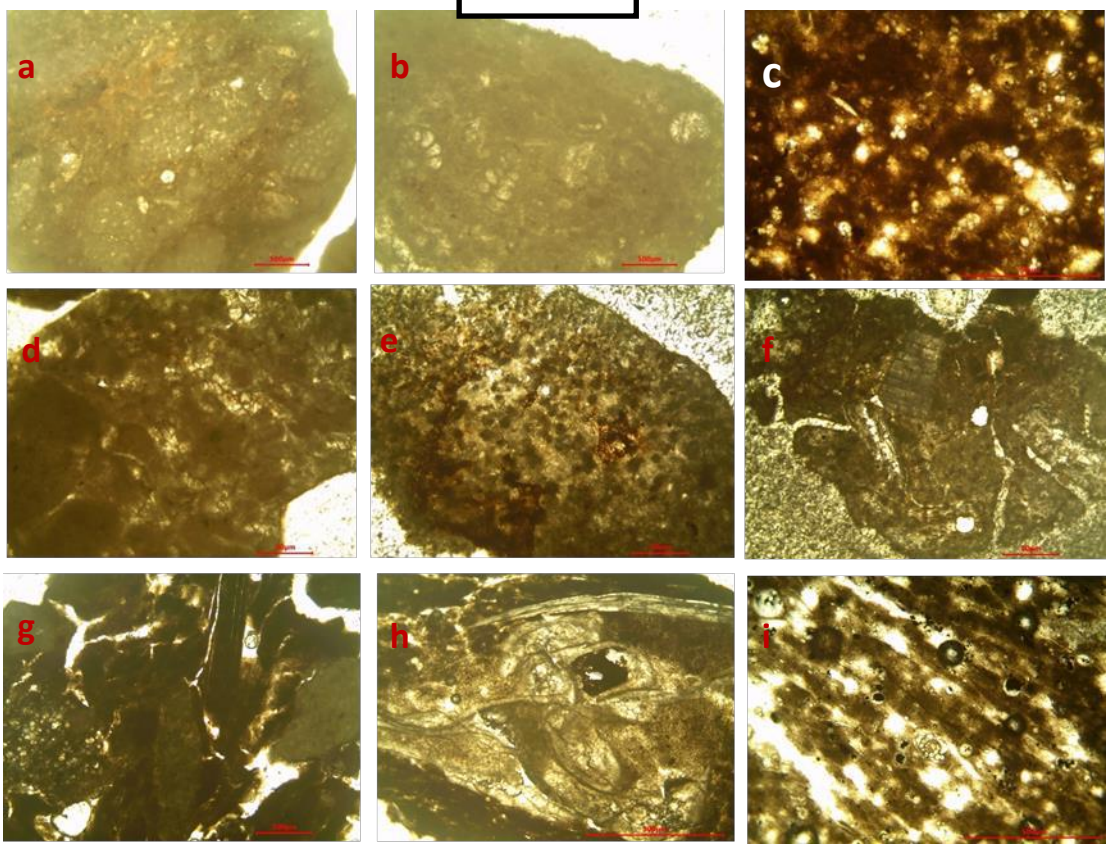


a. Orbitolina - wackestone to packstone
b. Textularia/hedenbergella wackestone
c. Globigerina wackestone to packestone
d. Peloidal wackestone to packstone
e. Pelletal wackestone to packstone
f. Rudist intraclasts packstone
g. Mudstone to wackstone intraclasts packstone
h. Rudist boundstone to rudstone.
i. Basinal marl to marly limestone

## III. PALEOENVIRONMENTS OF MAUDDUD FORMATION

Six facies associations (depositional environments) were distinguished in the Mauddud Formation, they are: shallow open marine, restricted, reef, slope, deep open marine and basinal (Fig.2).

- Facies association 1:- shallow open marine

The Orbitolina wackstone to packstone is the main microfacies which reflect the open marine conditions. It is characterized by high diversity in components where contained upon the Orbitolina as major component addition to Echinoderms, gastropods fragments, small benthic foraminifera and lithothamnium algae.

- Facies association 2:- restricted shallow marine

The restricted shallow marine facies association is largely consisting of peloidal and pelletal wackestone-packestone. Other important compounds are rudist fragments, and mollusk, echinoderm and green algae.

- Facies association 3: reef and back reef environment

This associated is represented by Rudist boundstone to rudstone which composed of rudist as a main compound. Also consists of Mollusca (pelecypoda and gastropoda) and algae.

- Facies association 4: slope environment

This is the less common facies association in the Mauddud Formation. It is characterized by various microfacies such as Intraclasts packstone - wackestone, bioclastic-Orbitolinid- packstone, and foraminiferal - rudistid wackestone - packstone. The main components of these environments are intraclasts rudist fragments, and Mollusc fragments.

- Facies association 5: deep open marine

The planktonic mudstone to wackstone with abundant Globigerina sp. With few small benthic foraminifera reflects deposition in a deep marine environment of the outer ramp.

*https://dx.doi.org/10.22161/ijaers.5.1.8* *ISSN: 2349-6495(P) | 2456-1908(O)*

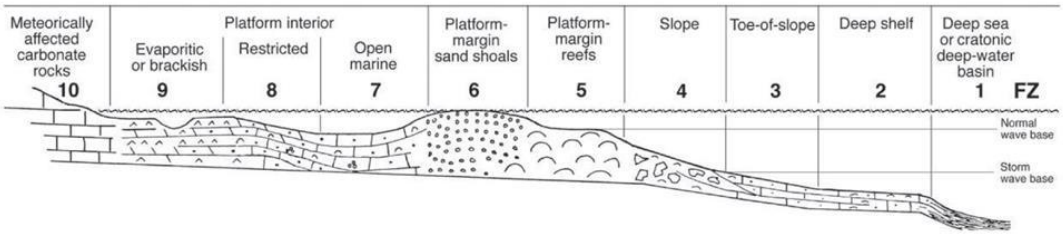


*Fig. 2: Rimmed carbonate platform: The Standard Facies Zones of the modified Wilson model[7].*

- Facies association 6: basinal environment

This facies association is represented by planktonic foraminifera and calcisphere marl and marly limestone. This facies is reflected to deposition in the basinal environment. The high value of gamma ray log response referred to clay compound in this facies.

## IV. FACIES ANLYSIS AND PALEOENVIRONMENTS OF NAHR UMR FORMATION

Two types of rocks are observed within the Nahr Umr Formation; the first is the upper part which characterized by shale dominated rocks and the second (lower part) is characterized by sand dominated rocks. Five major lithofacies were recognized in the succession of the Nahr Umr Formation according to the petrographic observation with gamma ray and spontaneous potential well logs to determine the paleoenvironment.

- Well sorted Quartz arenite Lithofacies (1):- Its represents the fine grained sandstone dominated rocks of Nahr Umr Formation. This characterized by well sorted quartz arenite, with very low gamma ray values with box shape of GR log (Plt 2.a).
- Poorly sorted Quartz arenite Lithofacies (2):- Its represents wide range of grain size of sandstone (fine-coarse), within the sandstone dominated rocks of Nahr Umr Formation. This characterized by poorly sorted quartz arenite, with very low gamma ray values with box shape of GR log (Plt 2.b).
- Poorly sorted graywacke Lithofacies (3):- This lithofacies represents the upper part of the sandstone member, and characterized by poorly sorted graywacke sandstone with moderate values of gamma ray (funnel shape) (Plt 2.c).
- Sandy shale Lithofacies (4):-This facies is appeared in the lower part of the shale member of Nahr Umr Formation, which characterized by high gamma ray values with funnel shape and sand lenses. high gamma ray values with box shape (Plt 2.d).
- Shale Lithfacies (5):- This facies represent the lower part of Nahr Umr Formation. Its characterized by high gamma ray values with bell to funnel shape (Plt 2.e).

## V. PALEOENVIRONMENTS OF NAHRUMR FORMATION

In the present study, four facies associations (depositional environments) were distinguished in the Nahr Umr Formation, they are: delta plain, prodelta, bay fill, and distributary channels. This distinguished was according to Coleman, and Prior (1981), Emery (1996), Kindall (2003) and Rachmawati (2011).

1. Delta plain

These shallow inland-restricted inter distributary lakes constitute an important environment in many upper delta plains and occur in all climatic settings. The delta-fill forms a wedge of coarse clastics within an overall deposit consisting of fine-grained organic-rich clays from lacustrine and back swamp deposits, which normally displays a coarsening-upward trend.

2. Delta front

Prodelta silts and clays grade landward and upward vertically into the coarser silts and sands of distal bar. Directly at the mouths of the active distributaries lie the coarsest sand deposits. These deposits are commonly referred to as the distributary-mouth bar. If sediments deposited seaward of the river mouth accumulates faster than subsidence or removal of sediments by marine processes occurs, deltaic progradation will take place and the subaerial deltaic deposits will overlie the uppermost parts of the subaqueous delta, forming a complete delta sequence[8].

3. Bay fill

Bay-fill sequence and variations in log response that can occur within such a sand body. The sand body generally displays a fan-shaped wedge, with the thickest sands generally being found near the initial break in the distributary channel. Often, sands in this vicinity display a sharp base scoured into the underlying inter distributary bay and marsh deposits (Coleman, and Prior, 1981). Away from the initial break, however, the typical coarsening-upward sequence (or inverted bell-shaped logs) becomes clearly the type of log response.

*https://dx.doi.org/10.22161/ijaers.5.1.8* *ISSN: 2349-6495(P) | 2456-1908(O)*

**Plate- 2**

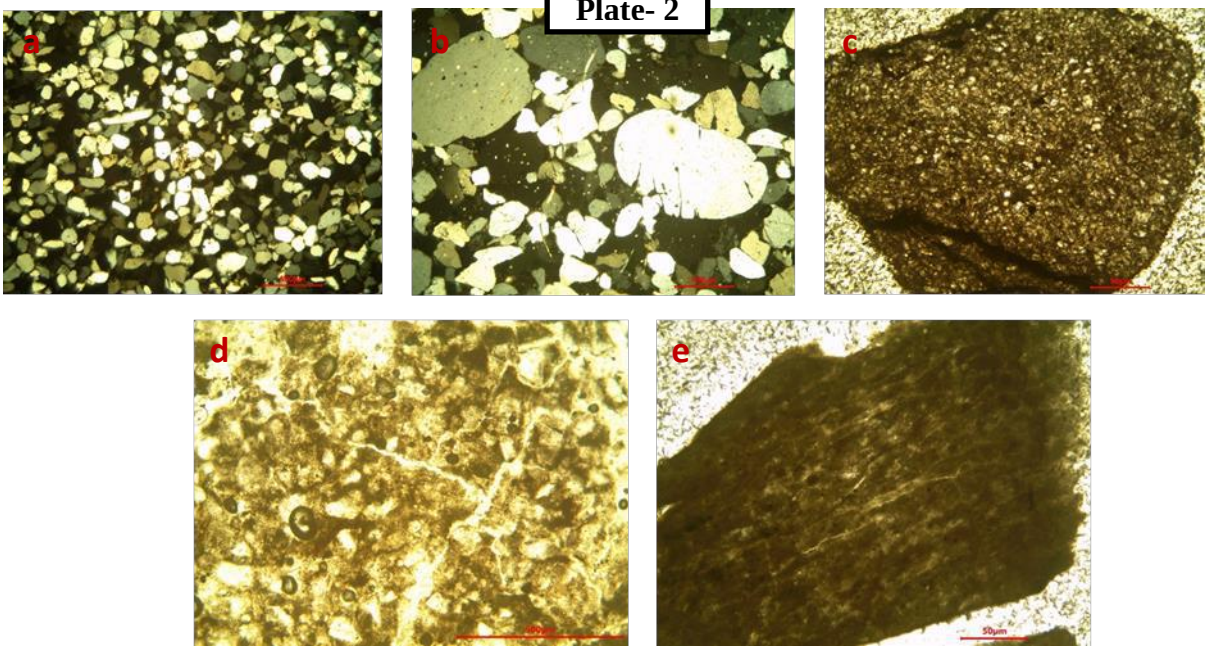


a. Well sorted Quartz arenite Lithofacies
b. Poorly sorted Quartz arenite Lithofacies
c. Poorly sorted graywacke Lithofacies
d. Sandy shale Lithofacies
e. Shale Lithfacies

4. Distributary channels

Braided Rivers exhibit numerous channels that split off and rejoin each other to give a braided appearance. They typically carry fairly coarse-grained sediments down a fairly steep gradient. Deposits of Braided Rivers tend to be coarse-grained and contain abundant amalgamated channels. The vertical sequence shows a fining-upward grain size relationship; a few coarser layers are found near the upper one-third of the sand body. The sand body has a scoured base, and often coarse, organic trash (logs, limbs and clay clasts) is found intercalated with the sandy units. Thin clay and silt layers often separate coarse.

## VI. BASIN DEVELOPMENT

The studied succession was deposited during the Albian age, after the sea level was made the unconformable surface between the Shuaiba Formation and Nahr Umr Formation. The microfacies analysis and reconstructed the paleoenvironments of the Albain basin in the studied area; there are three stages of the deposition: -

- The first stage: During this stage the sea level was rise which led to progress prodelta facies (retrogradation) and onlapping the unconformity. This part is represented by TST stage in all studied boreholes. The prodelta facies was changed to distributary channel facies up-wared to mark the mfs between these two facies. This refers to deposition during the high stand period as two cycles (Fig. 4).

The sea level was reactivated to progress after the last step of Nahr Umr deposition, to start the Mauddud Formation deposition.

- The second stage: the facies change during this stage was shown three steps of the sea level rise (TST) to deposition the restricted, reef-back reef and shallow open marine/slope.

Overlying the slope facies to the shallow marine and then deposited the shallow marine refer to maximum flooding surfaces after deposition the last ones. Therefore, the shallowing up-ward succession which deposition later was represented the high stand stage (HST).

- The third stage: This stage is represented by reactivated the sea level rise to deposition the basinal facies within the Mauddud Formation. The continued rise in sea level during the period of transgression (TST) is a preparation for the Ahmadi basin, which is characterized by deposition in a deep environment and conformable lower contact with the Mauddud Formation.

*https://dx.doi.org/10.22161/ijaers.5.1.8* *ISSN: 2349-6495(P) | 2456-1908(O)*

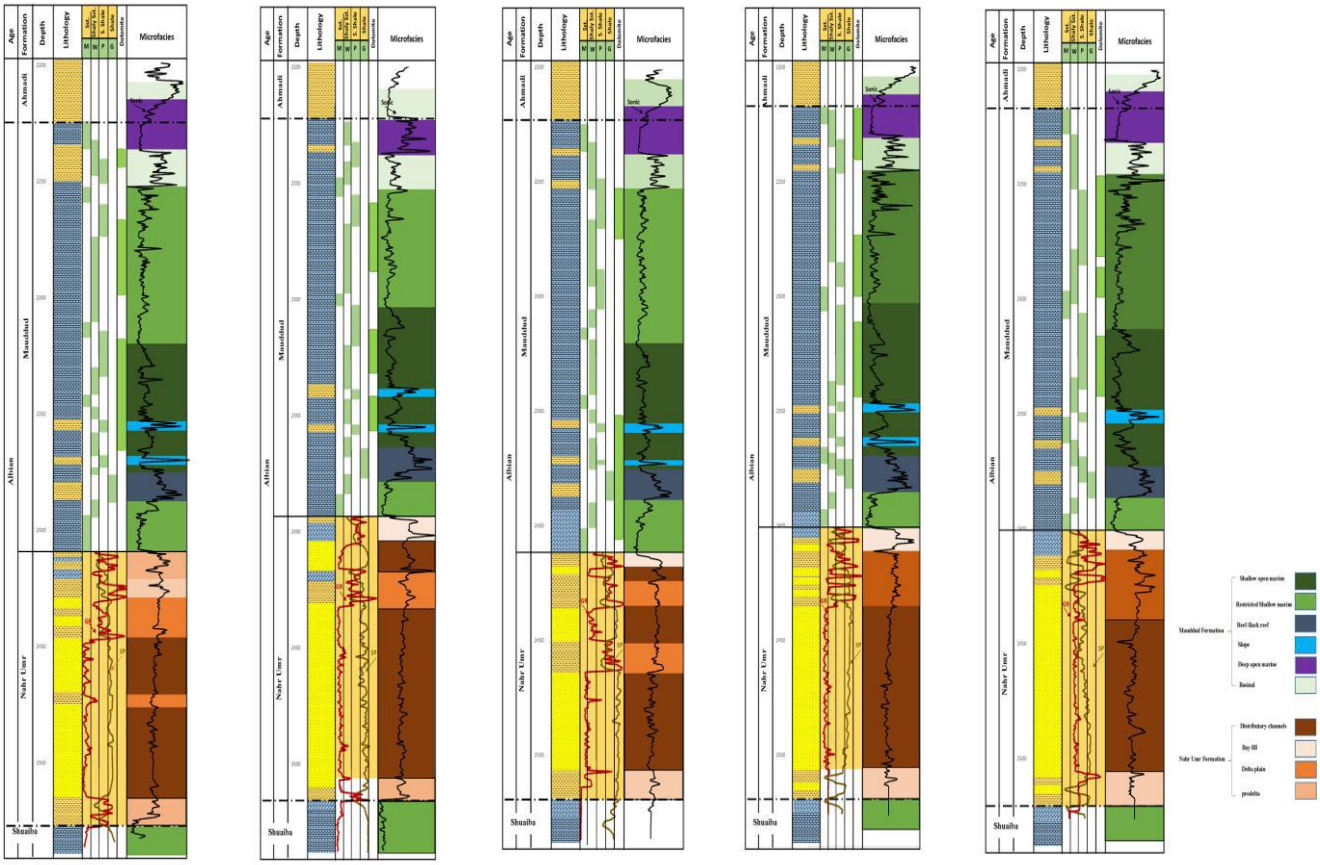


*Fig. 3: Lithology and Microfacies of the five wells Ns-1, 2, 3, 4, and 5.*

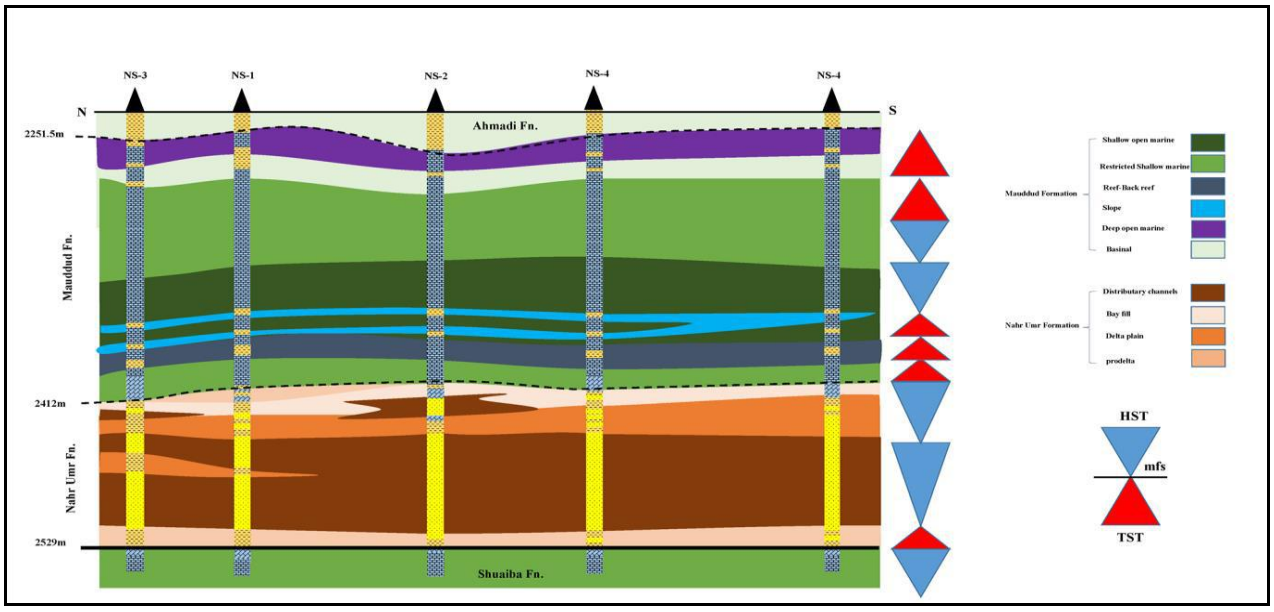


*Fig. 4: Depositional model of the studied section*

## REFERENCES

[1] Bellen, R. C. Van, Dunnington, H. V., Wetzel, R. and Morton, D., 1959 Lexique Stratigraphique, Interntional. Asie, Iraq, vol. 3c. 10a, 333p.

[2] Emery, D., Myers, K. J., 1996. Sequence stratigraphy, published by Blackwell Science Ltd, P.297.

[3] Dunham, R.J.,1962, Classification of carbonate according to depositional texture, in Ham, W.E. (ed.),

*https://dx.doi.org/10.22161/ijaers.5.1.8* *ISSN: 2349-6495(P) | 2456-1908(O)*

Classification of carbonate rocks. AAPG Memoir 1, p.108-121.

[4] Burchette, T.P. and S.R.Britton 1985. Carbonate facies analysis in the exploration for hydrocarbons: a case study from the Cretaceous of the Middle East. In, P.J. Brenchley and B.P.J. Williams (Eds.), Sedimentology: Recent Developments and Applied Aspects, p. 311-338.

[5] Wilson, J. l., 1975. Carbonate facies in the geological history. Springer-Verlag, New York, 439pp.

[6] Flugel, E., 2004, Microfacies of Carbonate Rocks, Springer, 976 p.

[7] Flugel, E., 2004. Microfacies analysis of limestone, Translated by Christensen, K., Springer-Verlag, Berlin, 633pp.

[8] Coleman, J. M. and Prior, D.B. (1980). Deltaic sand bodies; A 1980 education short course. AAPG Note Series No.14.Company, Pub., San Francisco and London, 724P.Conference and Exhibition, p. 152-155.

[9] Emery, D., Myers, K. J., 1996. Sequence stratigraphy, published by Blackwell Science Ltd, P.297.

[10] Kindall, 2003 in Kenneth, 2013.

[11] Rachmawati, 2011 in Kenneth, 2013.

https://dx.doi.org/10.22161/ijaers.5.1.9 *ISSN: 2349-6495(P) | 2456-1908(O)*

# Towards a Music Algebra: Fundamental Harmonic Substitutions in Jazz

Carmine Cataldo

Independent Researcher, PhD in Mechanical Engineering, Jazz Pianist and Composer, Battipaglia (SA), Italy
Email: catcataldo@hotmail.it

***Abstract*****—***In this paper the most common harmonic substitutions, at least as far as jazz music is concerned, are unconventionally addressed. The novelty consists in introducing a new method finalized to formally defining and logically applying all the fundamental harmonic substitutions, by exploiting an unusually rigorous notation. After defining the substitutions and discussing their applicability, we resort to them in order to modify some simple harmonic progressions substantially based upon a banal major turnaround. As explicitly suggested by the title, the modifications are carried out by following an extremely formal line of reasoning: all the logic passages are accurately described by resorting to a notation so similar to the one commonly employed in mathematics and physics, that the harmonic analysis of a song turns out to be de facto comparable to the demonstration of a theorem.*

***Keywords—Music Algebra, Unconventional Notation, Harmonic Substitutions, Ionian Scale, Turnaround.***

## I. INTRODUCTION

In this paper, all the fundamental harmonic substitutions [1] [2] are discussed by resorting to a notation, generally employed in fields such as mathematics and physics, extremely formal and rigorous. We herein exclusively refer to a single harmonization, the *Ionian* one: consequently, for the sake of clarity, we reveal in advance that the so-called *"Modal Interchange"* is not addressed in this article. Obviously, the line of reasoning we exploit can be equally followed starting from other scales, such as the *Natural Minor Scale* (that can be obtained from the *Ionian Scale* by means of a banal translation), the *Ipoionian Scale* (*Bach Minor Scale*), the *Harmonic Scales* (Major and Minor).

## II. DIATONIC SUBSTITUTIONS

Two chords that arise from the harmonization of the same scale are interchangeable if the distance between them (between the roots) is equal to a diatonic third (both ascending and descending). [1] [2] Exclusively referring to the *Ionian Harmonization*, the *Diatonic Substitutions* in their entirety can be effectively summarized by means of the following relations:

$$VIm7 \leftrightarrow Imaj7 \leftrightarrow IIIm7 \tag{1}$$

$$VII\emptyset \leftrightarrow IIm7 \leftrightarrow IVmaj7 \tag{2}$$

$$Imaj7 \leftrightarrow IIIm7 \leftrightarrow V7 \tag{3}$$

$$IIm7 \leftrightarrow IVmaj7 \leftrightarrow VIm7 \tag{4}$$

$$IIIm7 \leftrightarrow V7 \leftrightarrow VII\emptyset \tag{5}$$

$$IVmaj7 \leftrightarrow VIm7 \leftrightarrow Imaj7 \tag{6}$$

$$V7 \leftrightarrow VII\emptyset \leftrightarrow IIm7 \tag{7}$$

If we set, for example, $I = C$, from the foregoing relations we immediately obtain the following:

$$Am7 \leftrightarrow Cmaj7 \leftrightarrow Em7 \tag{8}$$

$$B\emptyset \leftrightarrow Dm7 \leftrightarrow Fmaj7 \tag{9}$$

$$Cmaj7 \leftrightarrow Em7 \leftrightarrow G7 \tag{10}$$

$$Dm7 \leftrightarrow Fmaj7 \leftrightarrow Am7 \tag{11}$$

$$Em7 \leftrightarrow G7 \leftrightarrow B\emptyset \tag{12}$$

$$Fmaj7 \leftrightarrow Am7 \leftrightarrow Cmaj7 \tag{13}$$

$$G7 \leftrightarrow B\emptyset \leftrightarrow Dm7 \tag{14}$$

The *Diatonic Substitutions* can be described, with obvious meaning of the notation, by resorting to a matrix of chords (that represents the *Diatonic Tensor*):

$$Dia^{Ion}(I) = \begin{bmatrix} I^{\Delta} & 0 & IIIm7 & 0 & 0 & VIm7 & 0 \\ 0 & IIm7 & 0 & IV^{\Delta} & 0 & 0 & VII\emptyset \\ I^{\Delta} & 0 & IIIm7 & 0 & V7 & 0 & 0 \\ 0 & IIm7 & 0 & IV^{\Delta} & 0 & VIm7 & 0 \\ 0 & 0 & IIIm7 & 0 & V7 & 0 & VII\emptyset \\ I^{\Delta} & 0 & 0 & IV^{\Delta} & 0 & VIm7 & 0 \\ 0 & IIm7 & 0 & 0 & V7 & 0 & VII\emptyset \end{bmatrix} \tag{15}$$

https://dx.doi.org/10.22161/ijaers.5.1.9 *ISSN: 2349-6495(P) | 2456-1908(O)*

Evidently, the *Diatonic Substitutions* can be summarized exploiting the following simple relation:

$$Dia_{ij}^{Ion} \leftrightarrow Dia_{ji}^{Ion} \tag{16}$$

From *(15)*, by setting, for example, $I = C$, we obtain:

$$Dia^{Ion}(C) = \begin{bmatrix} C^{\Delta} & 0 & Em7 & 0 & 0 & Am7 & 0 \\ 0 & Dm7 & 0 & F^{\Delta} & 0 & 0 & B\emptyset \\ C^{\Delta} & 0 & Em7 & 0 & G7 & 0 & 0 \\ 0 & Dm7 & 0 & F^{\Delta} & 0 & Am7 & 0 \\ 0 & 0 & Em7 & 0 & G7 & 0 & B\emptyset \\ C^{\Delta} & 0 & 0 & F^{\Delta} & 0 & Am7 & 0 \\ 0 & Dm7 & 0 & 0 & G7 & 0 & B\emptyset \end{bmatrix} \tag{17}$$

In *Figure 1* a useful graphic representation of the *Diatonic Substitutions* is provided.

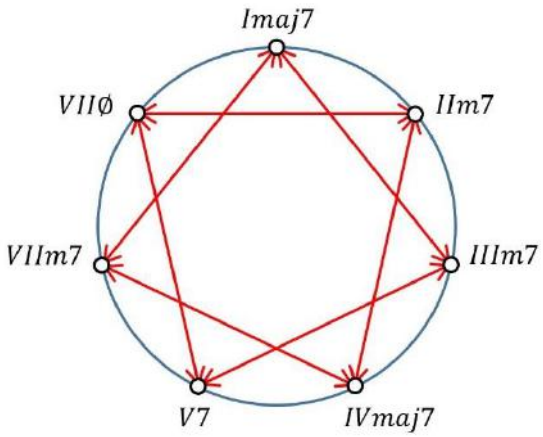


*Figure 1. Diatonic Substitutions*

## III. SECONDARY DOMINANTS

Any chord, even if it arises from a previous harmonic substitution, can be converted into a *Dominant Seventh Chord*. [1] [2] [3] [4] Referring, once again, to the chords obtained from the *Ionian Harmonization*, we have:

$$Imaj7 \rightarrow I7 = V(IV) \tag{18}$$

$$IIm7 \rightarrow II7 = V(V) \tag{19}$$

$$IIIm7 \rightarrow III7 = V(VI) \tag{20}$$

$$IVmaj7 \rightarrow IV7 = V(bVII) \tag{21}$$

$$V7 = V(I) = Primary\ Dominant(I) \tag{22}$$

$$VIm7 \rightarrow VI7 = V(II) \tag{23}$$

$$VII\emptyset \rightarrow VII7 = V(III) \tag{24}$$

If we set, for example, $I = C$, from the foregoing relations we immediately obtain the following:

$$Cmaj7 \rightarrow C7 = V(F) \tag{25}$$

$$Dm7 \rightarrow D7 = V(G) \tag{26}$$

$$Em7 \rightarrow E7 = V(A) \tag{27}$$

$$Fmaj7 \rightarrow F7 = V(B^{b}) \tag{28}$$

$$G7 = V(C) = Primary\ Dominant(I) \tag{29}$$

$$Am7 \rightarrow A7 = V(D) \tag{30}$$

$$B\emptyset \rightarrow B7 = V(E) \tag{31}$$

From *(28)* we immediately deduce that the dominant seventh chord obtained from the fourth degree (*F7*, in the specific case) leads towards a note, to extremely simplify, that does not belong to the *C Ionian Scale* (*Bb*, in the specific case). Consequently, the *Secondary Dominant* that arises from the forth degree is to be regarded as *non-functioning* (or *non-functional*).

## IV. TRITONE SUBSTITUTION

Any *Dominant Seventh Chord*, especially in the case it is altered and even if it arises from a previous harmonic substitution, can be replaced by a chord of the same kind (a dominant seventh chord) distant three whole tones from the initial chord. [1] [2] [3] [4] [5] Generally, if we denote with $X$ a generic note belonging to the *Chromatic Scale*, and with $t$ a *Whole Tone Interval*, we can write:

$$X7 \rightarrow Y7 \tag{32}$$

$$Y = X + 3t \tag{33}$$

If we set, for example, $X = C$, from the foregoing relations we immediately obtain the following:

$$C7 \rightarrow G^{b}7 \equiv F^{\#}7 \tag{34}$$

## V. DIMINISHED SUBSTITUTION

Any *Dominant Seventh Chord*, especially if it is provided with the flat ninth and even if it arises from a previous harmonic substitution, can be replaced by a *Diminished Chord* distant a major third, a perfect fifth, a minor seventh or a flat ninth from the initial chord. [2] [3] [4] [5] [6] [7] All the above-mentioned intervals are implicitly regarded as ascending. In other terms, we can concisely write, with obvious meaning of the notation, as follows:

$$X7^{(b9)} \rightarrow Ydim7 \tag{35}$$

$$Y = X + 2t + \frac{3n}{2}t \qquad n = 0,1,2,3 \tag{36}$$

More explicitly, we have:

https://dx.doi.org/10.22161/ijaers.5.1.9 ISSN: 2349-6495(P) | 2456-1908(O)

$$X7^{(b9)} \rightarrow \begin{cases} \langle X + 2t \rangle dim7 & n = 0, major\ third \\ \langle X + \frac{7}{2}t \rangle dim7 & n = 1, perfect\ fifth \\ \langle X + 5t \rangle dim7 & n = 2, minor\ seventh \\ \langle X + \frac{13}{2}t \rangle dim7 & n = 3, flat\ ninth \end{cases} \quad (37)$$

By setting, for example, $X = C$, from *(37)* we obtain:

$$C7^{(b9)} \rightarrow \begin{cases} Edim7 & n = 0, major\ third \\ Gdim7 & n = 1, perfect\ fifth \\ B^b dim7 & n = 2, minor\ seventh \\ D^b dim7 & n = 3, flat\ ninth \end{cases} \quad (38)$$

## VI. EXPANSION

The *Dominant 9sus4* and *b9sus4 Chords* can be expressed by resorting to the so-called *Slash Chords*. In very formal terms, with obvious meaning of the notation, we can write:

$$V7^{9sus4}(X) = \frac{II - 7(X)}{\langle X + \frac{7}{2}t \rangle} \quad (39)$$

$$V7^{b9sus4}(X) = \frac{II - 7b5(X)}{\langle X + \frac{7}{2}t \rangle} \quad (40)$$

By virtue of *(39)* and *(40)*, we can state that, in a certain measure, any *Dominant Seventh Chord* can be imagined as being preceded by a *Minor Seventh Chord* or a *Half-Diminished Chord* distant a descending perfect fourth. [3] Consequently, employing a vertical line to separate two consecutive beats or bars, we have:

$$V7 \rightarrow \begin{cases} II - 7 \ \ | V7 \\ II - 7b5 \mid V7 \end{cases} \quad (41)$$

If we set, for example, $X = C$, from *(39)* and *(40)* we obtain:

$$G7^{9sus4} = \frac{Dm7}{G} \quad (42)$$

$$G7^{b9sus4} = \frac{D\emptyset}{G} \quad (43)$$

Coherently with the setting ($X = C$), from *(41)* we have:

$$G7 \rightarrow \begin{cases} Dm7 \mid G7 \\ D\emptyset \mid G7 \end{cases} \quad (44)$$

## VII. SOME NOTEWORTHY CASES

***Case 1: Rhythm Changes (Bridge)***

Let's consider the following simple harmonic progression:

| | | | |
|---|---|---|---|
| *Imaj7* | *Imaj7* | *VIm7* | *Vm7* |
| *IIm7* | *IIm7* | *V7* | *V7* |

*Harmonic Progression 1.1*

If we set $I = B^b$, we immediately obtain:

| | | | |
|---|---|---|---|
| $B^b$maj7 | $B^b$maj7 | Gm7 | Gm7 |
| Cm7 | Cm7 | F7 | F7 |

*Harmonic Progression 1.2*

Taking into account the previous progression, let's carry out the following substitutions:

$$bars\ 1,2: B^b maj7 \xrightarrow{diat.} Dm7 \xrightarrow{sec.\ dom.} D7 \quad (45)$$

$$bars\ 3,4: Gm7 \xrightarrow{sec.\ dom.} G7 \quad (46)$$

$$bars\ 5,6: Cm7 \xrightarrow{sec.\ dom.} C7 \quad (47)$$

From the *Harmonic Progression 1.2*, by virtue of *(45)*, *(46)* and *(47)*, we finally obtain:

| | | | |
|---|---|---|---|
| D7 | D7 | G7 | G7 |
| C7 | C7 | F7 | F7 |

*Harmonic Progression 1.3*

***Case 2: I'm Getting Sentimental Over You (first 8 bars)***

Let's now consider the following harmonic progression:

| | | | |
|---|---|---|---|
| *Imaj7* | *V7* | *Imaj7* | *IVm7* |
| *IIm7* | *V7* | *Imaj7 VIm7* | *IIm7 V7* |

*Harmonic Progression 2.1*

By setting $I = F$, we immediately obtain:

| | | | |
|---|---|---|---|
| Fmaj7 | C7 | Fmaj7 | Dm7 |
| Gm7 | C7 | Fmaj7 Dm7 | Gm7 C7 |

*Harmonic Progression 2.2*

Taking into account the foregoing progression, let's carry out the following substitutions:

$$bar\ 2: C7 \xrightarrow{diat.} E\emptyset \xrightarrow{sec.\ dom.} E7 \xrightarrow{exp.} Bm7 \mid E7 \quad (48)$$

$$bar\ 3: Fmaj7 \xrightarrow{sec.\ dom.} F7 = V(B^b) \xrightarrow{diat.} A\emptyset \quad (49)$$

$$bars\ 4,6: Dm7 \xrightarrow{sec.\ dom.} D7 \quad (50)$$

$$bars\ 5,8: Gm7 \xrightarrow{sec.\ dom.} G7 \quad (51)$$

https://dx.doi.org/10.22161/ijaers.5.1.9 *ISSN: 2349-6495(P) | 2456-1908(O)*

From the *Harmonic Progression 2.2*, by virtue of *(48)*, *(49)*, *(50)* and *(51)*, we immediately obtain:

| | | | |
|---|---|---|---|
| Fmaj7 | Bm7 E7 | Am7$^{b5}$ | D7 |
| G7 | C7 | Fmaj7 D7 | Gm7 C7 |

*Harmonic Progression 2.3*

It is worth underlining that, in some cases, a desired chord (or a harmonic progression in its entirety) can be obtained by following various lines of reasoning. Just to provide an example, it is easy to verify how the third bar of the *Harmonic Progression 2.3* could have been alternatively deduced by resorting to the following simple substitutions:

$$bar\ 3\text{: } Fmaj7 \xrightarrow{diat.} Dm7 \xrightarrow{sec.\ dom.} D7 \tag{52}$$

$$bars\ 4\text{: } Dm7 \xrightarrow{sec.\ dom.} D7 \tag{53}$$

$$bars\ 3{,}4\text{: } D7 \xrightarrow{exp.} A\emptyset \mid D7 \tag{54}$$

***Case 3: Stella by Starlight (first 8 bars)***
Let's consider the following harmonic progression:

| | | | |
|---|---|---|---|
| *IIm7* | *IIm7* | *V7* | *V7* |
| *Imaj7* | *Imaj7* | *IIm7* | *V7* |

*Harmonic Progression 3.1*

If we set $I = B^b$, we immediately obtain:

| | | | |
|---|---|---|---|
| Cm7 | Cm7 | F7 | F7 |
| B$^b$maj7 | B$^b$maj7 | Cm7 | F7 |

*Harmonic Progression 3.2*

Taking into account the progression we have just obtained, let's carry out the following substitutions:

$$bars\ 1{,}2\text{: } Cm7 \xrightarrow{diat.} A\emptyset \xrightarrow{sec.\ dom.} A7 \xrightarrow{exp.} E\emptyset \mid A7 \tag{55}$$

$$bars\ 3{,}4\text{: } F7 \xrightarrow{exp.} Cm7 \mid F7 \tag{56}$$

$$bars\ 5{,}6\text{: } B^bmaj7 \xrightarrow{sec.\ dom.} B^b7 \xrightarrow{exp.} Fm7 \mid B^b7 \tag{57}$$

$$bar\ 7\text{: } Cm7 \xrightarrow{diat.} E^bmaj7 \tag{58}$$

$$bar\ 8\text{: } F7 \xrightarrow{diat.} Dm7 \xrightarrow{sec.\ dom.} D7 \xrightarrow{trit.} A^b7 \tag{59}$$

From the *Harmonic Progression 3.2*, exploiting *(55)*, *(56)*, *(57)*, *(58)* and *(59)*, we finally obtain:

| | | | |
|---|---|---|---|
| Em7$^{b5}$ | A7 | Cm7 | F7 |
| Fm7 | B$^b$7 | E$^b$maj7 | A$^b$7 |

*Harmonic Progression 3.3*

The chord obtained in the eight bar ($A^b7$) leads towards $B^bmaj7$ (ninth bar, not displayed in the *Harmonic Progression 3.3*). The progression $^bVII7 \mid Imaj7$ is commonly named *"Back-Door Solution"*. [5]

***Case 4: Easy Living (first 8 bars)***
Let's consider the following banal harmonic progression:

| | | | | | | | |
|---|---|---|---|---|---|---|---|
| *Imaj7* | *VIm7* | *IIm7* | *V7* | *Imaj7* | *VIm7* | *IIm7* | *V7* |
| *Imaj7* | *VIm7* | *IIm7* | *V7* | *Imaj7* | *VIm7* | *IIm7* | *V7* |

*Harmonic Progression 4.1*

If we set $I = A^b$, from the foregoing progression we obtain:

| | | | | | | | |
|---|---|---|---|---|---|---|---|
| A$^b$maj7 | Fm7 | B$^b$m7 | E$^b$7 | A$^b$maj7 | Fm7 | B$^b$m7 | E$^b$7 |
| A$^b$maj7 | Fm7 | B$^b$m7 | E$^b$7 | A$^b$maj7 | Fm7 | B$^b$m7 | E$^b$7 |

*Harmonic Progression 4.2*

Taking into account the previous harmonic progression, let's carry out the following substitutions:

$$bar\ 1\text{: } Fm7 \xrightarrow{sec.\ dom.} F7 \xrightarrow{dim.} Adim7 \tag{60}$$

$$bar\ 2\text{: } E^b7 \xrightarrow{diat.} G\emptyset \xrightarrow{sec.\ dom.} G7 \xrightarrow{dim.} Bdim7 \tag{61}$$

$$bars\ 3{,}6\text{: } A^bmaj7 \xrightarrow{diat.} Cm7 \tag{62}$$

$$bar\ 3\text{: } Fm7 \xrightarrow{diat.} A^bmaj7 \xrightarrow{sec.\ dom.} A^b7 \tag{63}$$

$$bar\ 4\text{: } B^bm7 \xrightarrow{diat.} D^bmaj7 \tag{64}$$

$$bar\ 4\text{: } E^b7 \xrightarrow{diat.} Cm7 \xrightarrow{sec.\ dom.} C7 \xrightarrow{trit.} G^b7 \tag{65}$$

$$bar\ 7\text{: } Fm7 \xrightarrow{sec.\ dom.} F7 \tag{66}$$

From the *Harmonic Progression 4.2*, taking into account *(60)*, *(61)*, *(62)*, *(63)*, *(64)*, *(65)* and *(66)*, we finally obtain:

| | | | | | | | |
|---|---|---|---|---|---|---|---|
| A$^b$maj7 | Ao7 | B$^b$m7 | Bo7 | Cm7 | A$^b$7 | D$^b$maj7 | G$^b$7 |
| A$^b$maj7 | Fm7 | B$^b$m7 | E$^b$7 | Cm7 | F7 | B$^b$m7 | E$^b$7 |

*Harmonic Progression 4.3*

https://dx.doi.org/10.22161/ijaers.5.1.9 ISSN: 2349-6495(P) | 2456-1908(O)

The second chord in the fourth bar ($G^b7$) leads towards $A^bmaj7$: once again, a typical *"Back-Door Solution"*.

***Case 5: Giant Steps***

Let's now consider the following harmonic progression:

| | | | |
|---|---|---|---|
| *Imaj7 VIm7* | *IIm7 V7* | *Imaj7* | *VIm7* |
| *IIm7 V7* | *Imaj7 V7* | *Imaj7* | *V7* |
| *Imaj7* | *VIm7* | *IIm7* | *V7* |
| *Imaj7* | *V7* | *Imaj7* | *V7* |

*Harmonic Progression 5.1*

By setting $I = B$, we immediately obtain:

| | | | |
|---|---|---|---|
| Bmaj7 G#m7 | C#m7 F#7 | Bmaj7 | G#m7 |
| C#m7 F#7 | Bmaj7 F#7 | Bmaj7 | F#7 |
| Bmaj7 | G#m7 | C#m7 | F#7 |
| Bmaj7 | F#7 | Bmaj7 | F#7 |

*Harmonic Progression 5.2*

Taking into account the previous progression, let's carry out the following substitutions:

$$bar\ 1: G^{\#}m7 \xrightarrow{sec.\ dom.} G^{\#}7 \equiv A^b7 \xrightarrow{trit.} D7 \quad (67)$$

$$bars\ 2,5,11: C^{\#}m7 \xrightarrow{sec.\ dom.} C^{\#}7 \equiv D^b7 \xrightarrow{trit.} G7 \quad (68)$$

$$bars\ 2,5: F^{\#}7 \xrightarrow{diat.} A^{\#}\emptyset \xrightarrow{sec.\ dom.} A^{\#}7 \equiv B^b7 \quad (69)$$

$$bars\ 3,6,9,15: Bmaj7 \xrightarrow{diat.} D^{\#}m7 \xrightarrow{sec.\ dom.} D^{\#}7 \equiv E^b7 \quad (70)$$

$$bars\ 4,10: G^{\#}m7 \xrightarrow{sec.\ dom.} A^b7 \xrightarrow{trit.} D7 \xrightarrow{exp.} Am7 \mid D7 \quad (71)$$

$$bars\ 8,14: F^{\#}7 \xrightarrow{diat.} A^{\#}\emptyset \xrightarrow{sec.\ dom.} B^b7 \xrightarrow{exp.} Fm7 \mid B^b7 \quad (72)$$

$$bars\ 12,16: F^{\#}7 \xrightarrow{exp.} C^{\#}m7 \mid F^{\#}7 \quad (73)$$

From the foregoing harmonic progression, by virtue of *(67)*, *(68)*, *(69)*, *(70)*, *(71)*, *(72)* and *(73)*, we obtain:

| | | | |
|---|---|---|---|
| Bmaj7 D7 | G7 B♭7 | E♭7 | Am7 D7 |
| G7 B♭7 | E♭7 F#7 | Bmaj7 | Fm7 B♭7 |
| E♭7 | Am7 D7 | G7 | C#m7 F#7 |
| Bmaj7 | Fm7 B♭7 | E♭7 | C#m7 F#7 |

*Harmonic Progression 5.3*

The *Harmonic Progression 5.3*, clearly, does not represent the desired result yet. In order to obtain the original Coltrane progression, we have to further modify all the chords written in red. On this purpose, we introduce a banal harmonic substitution (often simply named *"Quality Substitution"*) that allows to instantly transform a *Dominant Seventh Chord* into a *Major Seventh*, without resorting to the so-called *"Modal Interchange"*. In this regard, suffice it to bear in mind that the two above-mentioned chords are characterized by the same triad (the same *chordal notes*): in other terms, they only differ in the seventh (that can be considered, at least in a certain sense, as being a *fundamental tension*). It is worth highlighting how, by exploiting this very method, the well-known *"Tadd Dameron* (or *Coltrane*) *Turnaround"* [4] [8] can be obtained. Ultimately, we can write:

$$bars\ 2,5,11: G7 \xrightarrow{dom.\ to\ maj.} Gmaj7 \quad (74)$$

$$bar\ 3,6,9,15: E^b7 \xrightarrow{dom.\ to\ maj.} E^bmaj7 \quad (75)$$

Taking into account *(74)* and *(75)* we finally obtain:

| | | | |
|---|---|---|---|
| Bmaj7 D7 | Gmaj7 B♭7 | E♭maj7 | Am7 D7 |
| Gmaj7 B♭7 | E♭maj7 F#7 | Bmaj7 | Fm7 B♭7 |
| E♭maj7 | Am7 D7 | Gmaj7 | C#m7 F#7 |
| Bmaj7 | Fm7 B♭7 | E♭maj7 | C#m7 F#7 |

*Harmonic Progression 5.4*

## VIII. FINAL REMARKS

Let's start from a banal sequence of four bars (or beats, or sets composed of an equal number of beats) characterized by the same chord (in our case, a *Major Seventh Chord*):

| | | | |
|---|---|---|---|
| *Imaj7* | *Imaj7* | *Imaj7* | *Imaj7* |

*Harmonic Progression 6.1*

Although it cannot be formally regarded as a harmonic substitution, we are clearly allowed to resort to the so-called *"Tonicization"* [9] [10] [11] [12] [13] in order to create a first, simple harmonic motion (nothing but an *Authentic Cadence*):

| | | | |
|---|---|---|---|
| *Imaj7* | *Imaj7* | *V7* | *V7* |

*Harmonic Progression 6.2*

Let's now carry out the following substitutions:

https://dx.doi.org/10.22161/ijaers.5.1.9 *ISSN: 2349-6495(P) | 2456-1908(O)*

$$bars\ (beats)\ 3{,}4\colon V7 \overset{exp.}{\longrightarrow} IIm7 \mid V7 \tag{76}$$

$$bar\ (beat)\ 2\colon Imaj7 \overset{diat.}{\longrightarrow} VIm7 \tag{77}$$

From the *Harmonic Progression 6.2*, by virtue of *(76)* and *(77)*, we immediately obtain:

| | | | |
|---|---|---|---|
| *Imaj7* | *VIm7* | *IIm7* | *V7* |

*Harmonic Progression 6.3*

It is evident that, starting from a single *Major Seventh Chord*, we can easily obtain a *Major Turnaround*. In other terms, we are implicitly stating that all the harmonic progressions we have obtained in the previous section may be imagined as arising from a single chord. In a certain sense, we could even state that, net of some progressions explicitly based upon the so-called *"Pure Plagal Cadence"* (*IVmaj7* | *Imaj7*), all the *Popular Jazz Songs*, as far as the harmonic structure is concerned, may be considered as originating from a single chord (a *Major Seventh Chord* or, exploiting the harmonization of whatever minor scale, a *Minor Seventh*). It is worth underlining that we have explicitly referred to the *"Pure Plagal Cadence"*, since the "*Authentic"* or *"Extended"* one (*IVmaj7* | *V7* | *Imaj7*) can be immediately deduced, by simply resorting to a banal *Diatonic Substitution*, from a *IIm7* | *V7* | *Imaj7* harmonic progression which, in turn, can be obtained from a single *Major Seventh Chord* by exploiting a *"Tonicization"* and, taking into account *(76)*, an *Expansion*.

## ACKNOWLEDGEMENTS

This paper is dedicated to my father, Antonio Cataldo, who unexpectedly passed away on the 11th of June 2016.
I would like to thank my friends Francesco D'Errico, Giulio Martino, and Sandro Deidda, excellent Italian jazz musicians and esteemed teachers at the Conservatory of Salerno, for their precious suggestions.

## REFERENCES

[1] D'Errico, F. (2017). Armonia Funzionale e Modalità – Rudimenti per l'Improvvisazione a Indirizzo Jazzistico. Naples, Italy: Editoriale Scientifica.

[2] Cho, G. J. (1992). Theories and Practice of Harmonic Analysis. Lewiston, NY: Edwin Mellen Press.

[3] Levine, M. (2009). The Jazz Theory Book (Italian Edition by F. Jegher). Milan, IT: Curci Jazz.

[4] Lawn, R., Hellmer, J. L. (1996). Jazz: Theory and Practice. Los Angeles, CA: Alfred Publishing Co. Inc.

[5] Coker, J. (1997). Elements of the Jazz Language for the Developing Improvisor. Los Angeles, CA: Alfred Publishing Co. Inc.

[6] Cataldo, C. (2017). The Art of Improvising: the Be-Bop Language and the Dominant Seventh Chords. Art and Design Review, 5, 181-188. http://doi.org/10.4236/adr.2017.53014

[7] Cataldo, C. (2017). Il Linguaggio Be-Bop e gli Accordi di Settima di Prima Specie [The Be-Bop Language and The Dominant Seventh Chords]. Journal of Science, Humanities and Arts (JOSHA) 4(4). https://dx.doi.org/10.17160/josha.4.4.340

[8] Coker, J., Casale, J., & Campbell, G. (1982). Patterns for Jazz – A Theory Text for Jazz Composition and Improvisation: Treble Clef Instruments. Los Angeles, CA: Alfred Publishing Co. Inc.

[9] Dobbins, B. (2010). Jazz Arranging and Composing – L'Approccio Lineare (Italian Ed. by Roberto Spadoni). Italy: Volontè & Co.

[10] Cataldo, C. (2017). The Art of Improvising: the Be-Bop Language and the Minor Seventh Chords. Art and Design Review, 5, 213-221. https://doi.org/10.4236/adr.2017.54017

[11] Cataldo, C. (2017). Il Linguaggio Be-Bop e gli Accordi di Settima di Seconda Specie [The Be-Bop Language and The Minor Seventh Chords]. Journal of Science, Humanities and Arts (JOSHA), 4(4). https://dx.doi.org/10.17160/josha.4.4.339

[12] Cataldo, C. (2017). The Art of Improvising: the Be-Bop Language and the Major Seventh Chords. Art and Design Review, 5, 222-229. https://doi.org/10.4236/adr.2017.54018

[13] Cataldo, C. (2017). Il Linguaggio Be-Bop e gli Accordi di Settima di Quarta Specie [The Be-Bop Language and The Major Seventh Chords]. Journal of Science, Humanities and Arts (JOSHA), 4(4). https://dx.doi.org/10.17160/josha.4.4.341

https://dx.doi.org/10.22161/ijaers.5.1.10 ISSN: 2349-6495(P) | 2456-1908(O)

# Solar Resource Assessment in Jammu and Kashmir State

Nasir Ul Rasheed Rather[1], Anju Singh[2], Asghar Samoon[3]

[1]PhD Renewable Energy Engineering Shuats, Allahabad, India
[2]Senior Research Scientist, NISE, Ministry of New & Renewable Energy, New Delhi
[3]IAS (Principal Secretary), Higher Education Department J&K Govt.
Received on: 15, Nov, 2017 | Published on: 18, Jan, 2018

***Abstract*****—***The state of Jammu and Kashmir has diverse agro-climatic zones. The present paper on solar resource assessment in the state of Jammu and Kashmir is based on ten years of average data taken from NREL and SRRA stations. The state is blessed with huge solar potential, both for thermal generation as well as photovoltaic. The same energy can be used for electricity and process heat generation to mitigate growing energy crisis particularly in winter. The data as obtained from NREL and C-WET through SRRA stations revealed that the state is receiving more than 5 kWh/m$^2$/day of average DNI and GHI every month which in itself can be harnessed for solar thermal energy and photovoltaic power. The average DNI and GHI received from last ten years varied from (1 kWh/day/m$^2$) to (8kWh/day/m$^2$) per day.*

***Keywords— Solar resource assessment, Jammu and Kashmir, Solar, photovoltaic, thermal, Direct normal radiation, Global horizontal radiation, National Renewable Energy Laboratory.***

## I. INTRODUCTION

Jammu and Kashmir has extensive energy needs and increasing difficulty in meeting those needs through traditional means of power generation. Jammu and Kashmir is energy starved state though it has one of the best potentials in Renewable Energy viz. Solar Energy, bioenergy, geothermal energy, alternate hydro energy and other alternate sources of energy. The potential energy sources have not been harnessed till date resulting in low capita per energy availability forcing people to use wood, coal and LPG cylinders for heating purpose in winter and switching to kerosene, LPG and other fossil fuels for electricity generation. Developing and encouraging proper resource assessment of all renewable energy sources in state is important in present scenario where there has been acute shortage of energy and electricity. Among all Renewable Energy sources, solar energy can also play an important role in mitigating energy crisis in state. It can provide secure energy supply with additional income to state and shall generate employment in state.

The state of Jammu and Kashmir has large scope of solar energy, however there is wide gap between estimated potential and the cumulative achievements made so far (1). The state is situated in northern Himalayas spreading over 33$^0$-37$^0$N latitude and 70$^0$- 80 $^0$E longitude **(2).** The state comprises of 6.7 percent of total geographical area of country covering over 2.22 lakh square km, of which 30 percent is under cultivation. The mean ambient temperature in Jammu ranges between 13 -33 degree Celsius, in Kashmir the mean ambient temperature ranges in between 0 to 25 degree Celsius and in Leh, region, which actually receives highest DNI in India has average ambient temperature of -8 to 18 degrees Celsius temperature (figure 1). The low ambient temperature gives rise to huge energy requirement. The same energy is needed for power generation (electricity) and heating, which are also either run on traditional electricity and is mostly met through burning coal, firewood and LPG.

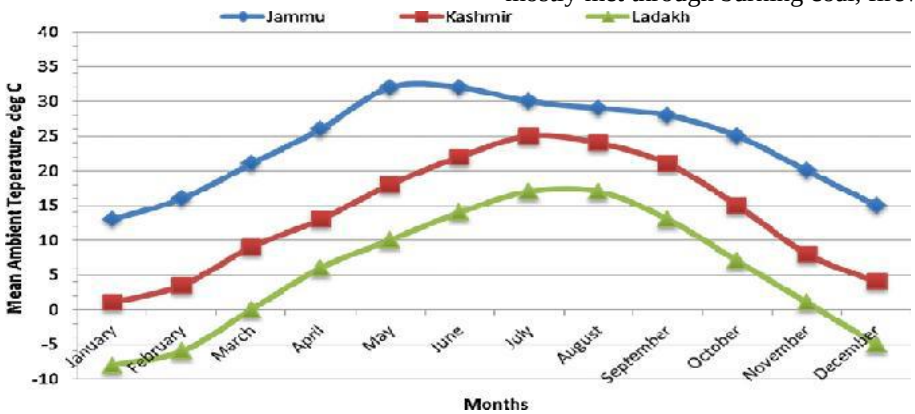


*Fig.1: Mean ambient temperature of Jammu, Kashmir and Leh division (10 years data)*

*https://dx.doi.org/10.22161/ijaers.5.1.10* *ISSN: 2349-6495(P) | 2456-1908(O)*

However, the low ambient temperature is an important factor in deciding efficiency of CST technologies. Low ambient temperature and high DNI can give best efficiency in solar thermal production. Leh region in Jammu and Kashmir receives highest sunshine days in whole country and can be one of the best places for solar cooking, solar drying and solar thermal electricity generation through trough collectors or CST technology. The same technologies can even be used for process heat design to ensure heat flow through HVAC systems. Higher DNI ensures higher efficiencies in solar cooking, solar water heating systems and solar green houses. The present studies shall evaluate DNI and GHI for three regions of Jammu and Kashmir. i,e Jammu ,kashmir and Ladakh. The average data of 10 years has been evaluated, the same data has been obtained from NREL and SSRA C-WET data stations. Solar energy is an important renewable energy source that is expected to play a significant role in the future energy supply mix [3–6].

Solar technologies could be characterised as either passive solar or active solar depending on the way they capture, convert, and distribute solar energy. An active solar technique includes using photovoltaic panels and solar thermal collectors to harness the energy. A passive solar technique includes orienting a building to the sun, selecting materials with positive thermal mass or light dispersing properties, and designing buildings that naturally circulate air.

## II. ASSESSMENT OF SOLAR ENERGY IN J&K STATE

Electricity and heat can be generated by radiation either through solar photovoltaic route or through solar thermal route. Availability of reliable solar radiation data is vital for the success of solar energy installations in different sites of the country. For solar collectors which are flat in nature, solar radiation data in the form of Global Horizontal Irradiance (GHI) is useful whereas for solar collectors which are concentrating in nature Direct Normal Irradiance (DNI) data is required. Solar thermal power plants are essentially Concentrating Solar Power (CSP) units. For designing solar thermal power plants, DNI data is therefore a pre-requisite. For solar energy needs we mainly differ between Global Horizontal Irradiance, which consist of Direct Irradiance of the sun and the scattered Irradiance and Direct Normal Irradiance (DNI), which is the Direct Irradiance reaching a surface that is always perpendicular to the sun. GHI is important factor to determine efficacy for photovoltaics, while DNI is of special importance for solar thermal applications. Solar energy can be important source of energy in state which is traditionally harnessing hydro energy and dependent on hydel projects or diesel gensets only.

*Fig.2: SRRA station by Centre of Wind Energy Technology (MNRE) at Leh for assessment of solar radiation data.*

CPV(Concentrated photovoltaic ) systems use optics to concentrate a large area of sunlight onto a small solar cell and are either refractive (with lenses) or reflective (with mirrors). To achieve high concentration ratios, the optics have a narrow field of view and only make use of direct normal irradiance (DNI) from the sun. DNI is most accurately measured by a high quality pyrheliometer

*https://dx.doi.org/10.22161/ijaers.5.1.10* *ISSN: 2349-6495(P) | 2456-1908(O)*

mounted on a precise automatic sun tracker to provide reliable data about the solar radiation input.

Thermal systems use the direct normal irradiance (DNI) from the sun to generate heat, which can be used as the energy source for steam turbine electricity generators. These systems use mirrors to concentrate solar radiation. Unlike PV cells, they can take advantage of the full spectrum of solar radiation, including ultraviolet and near infrared light, leading to high efficiencies. For such systems it is extremely important to monitor the broadband solar radiation with high precision, because sky conditions have a strong influence on the performance of a CSP plant. To predict the energy yield of a CSP system with a minimum of uncertainty it is crucial to measure solar radiation locally. Satellite measurements and related models don't take into account theof local climatic conditions, such as clouds, nor do they include local aerosols (dust, sand and other particles). Two CSP plants in different locations with equal direct irradiance totals, according to satellite data, may have very different energy outputs, due to differences in clouds and aerosols in the particular locations, which block the incoming radiation. To ensure the reliability and redundancy of the data, a typical CSP solar monitoring station uses high precision instruments with low uncertainty for the measurements of direct, diffuse and global irradiance. This way the direct radiation measurement can be compared with values derived from the global and diffuse radiation.

The amount of solar radiation available over time under the local environmental conditions is a key input for choosing the optimal location, technology and size of a solar energy project. Feasibility studies and technical calculations of a solar energy project always start with energy resource assessment. High precision on-site measurements of solar radiation provide the lowest uncertainty for bankable data about the energy resource and the possible energy yield. Such measurements are performed by a high quality solar radiation monitoring station that measures all three components of solar radiation: direct normal irradiance (DNI), diffuse horizontal irradiance (DHI) and global horizontal irradiance (GHI). Also, other meteorological parameters relevant to the project, such as air temperature, humidity, precipitation, wind speed and direction need to be monitored by a dedicated weather station. The GHI and DNI data obtained and calculated shows a great scope of both solar thermal technology (through CST) and photovoltaic systems. The photovoltaic systems can be developed and installed on both off grid and on grid mode. The Smart grids can be developed to feed this energy (electricity) and the same can be sent to consumer use.

## III. RESULTS AND DISCUSSION

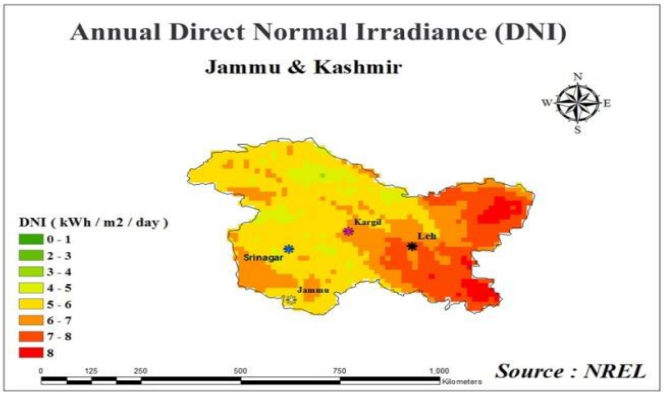


| Direct Normal Irradiance ( kWh /m²/ day ) | | | | | |
|---|---|---|---|---|---|
| Sl.No | Month | Jammu | Srinagar | Kargil | Leh |
| 1. | January | 3.44 | 2.78 | 2.27 | 4.78 |
| 2. | February | 4.38 | 2.52 | 2.40 | 3.77 |
| 3. | March | 5.31 | 3.85 | 3.69 | 6.13 |
| 4. | April | 5.65 | 4.63 | 5.29 | 6.76 |
| 5. | May | 6.37 | 5.83 | 6.34 | 6.97 |
| 6. | June | 5.21 | 6.15 | 5.83 | 6.68 |
| 7. | July | 3.88 | 5.69 | 5.65 | 6.49 |
| 8. | August | 4.31 | 5.62 | 5.33 | 6.45 |
| 9. | September | 5.40 | 6.07 | 6.04 | 7.43 |
| 10. | October | 5.65 | 6.48 | 7.03 | 7.95 |
| 11. | November | 4.49 | 4.89 | 6.48 | 7.58 |
| 12. | December | 3.95 | 2.99 | 3.33 | 6.05 |
| 13. | Annual | 4.84 | 4.80 | 4.98 | 6.43 |

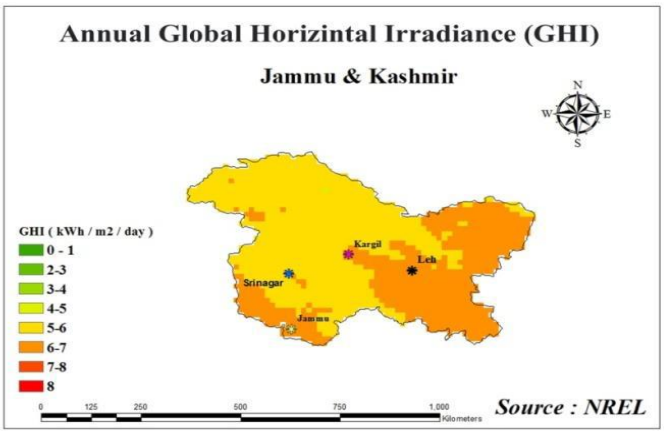


| Global Horizontal Irradiance ( kWh /m²/ day ) | | | | | |
|---|---|---|---|---|---|
| Sl.No | Month | Jammu | Srinagar | Kargil | Leh |
| 1. | January | 2.97 | 2.60 | 2.25 | 2.95 |
| 2. | February | 3.88 | 3.06 | 2.98 | 3.39 |
| 3. | March | 5.31 | 4.59 | 4.17 | 5.31 |
| 4. | April | 6.46 | 5.67 | 5.94 | 6.01 |
| 5. | May | 7.32 | 6.81 | 7.10 | 7.35 |
| 6. | June | 7.00 | 7.20 | 7.27 | 7.52 |
| 7. | July | 6.00 | 6.70 | 6.90 | 7.34 |
| 8. | August | 5.70 | 6.17 | 6.32 | 6.72 |
| 9. | September | 5.60 | 5.71 | 5.81 | 6.22 |
| 10. | October | 4.97 | 4.92 | 4.99 | 5.26 |
| 11. | November | 3.74 | 3.56 | 3.83 | 4.09 |
| 12. | December | 2.99 | 2.60 | 2.34 | 3.15 |
| 13. | Annual | 5.17 | 4.97 | 5.00 | 5.50 |

*Fig.3: Annual Direct Normal Irradiance (DNI) and Annual Global Horizontal Irradiance (GHI) for Jammu and Kashmir state based on 10 years NREL data.*

*https://dx.doi.org/10.22161/ijaers.5.1.10* *ISSN: 2349-6495(P) | 2456-1908(O)*

The annual solar radiation received in all the regions of Jammu & Kashmir is relatively high. Based on hourly estimate of 10 years (2002-11) radiation data collected from geostationary orbit satellites with a resolution of 10 kms, by NREL and ground data, radiation is being estimated. Solar radiation has huge seasonal/monthly fluctuation. Solar radiation is directly linked with day length (no of day hours/day) and angle between sun radiation and surface. During summer sun radiation is more perpendicular than winter. And also, summer day length is longer than winter. The month wise values recorded for the last ten years by NREL along with radiation maps for DNI and GHI, along with annual total are given below. Green colour illustrates lowest range of radiation (0-1 kWh/day/$m^2$) and red highest (8kWh/day/$m^2$). For solar energy, January is a very bad month while June is excellent. Monthly variation of DNI and GHI are given in figure 3.

The monthly global horizontal radiation (GHI) for the state of Jammu and Kashmir based on 10 years of average data from NREL is given below:

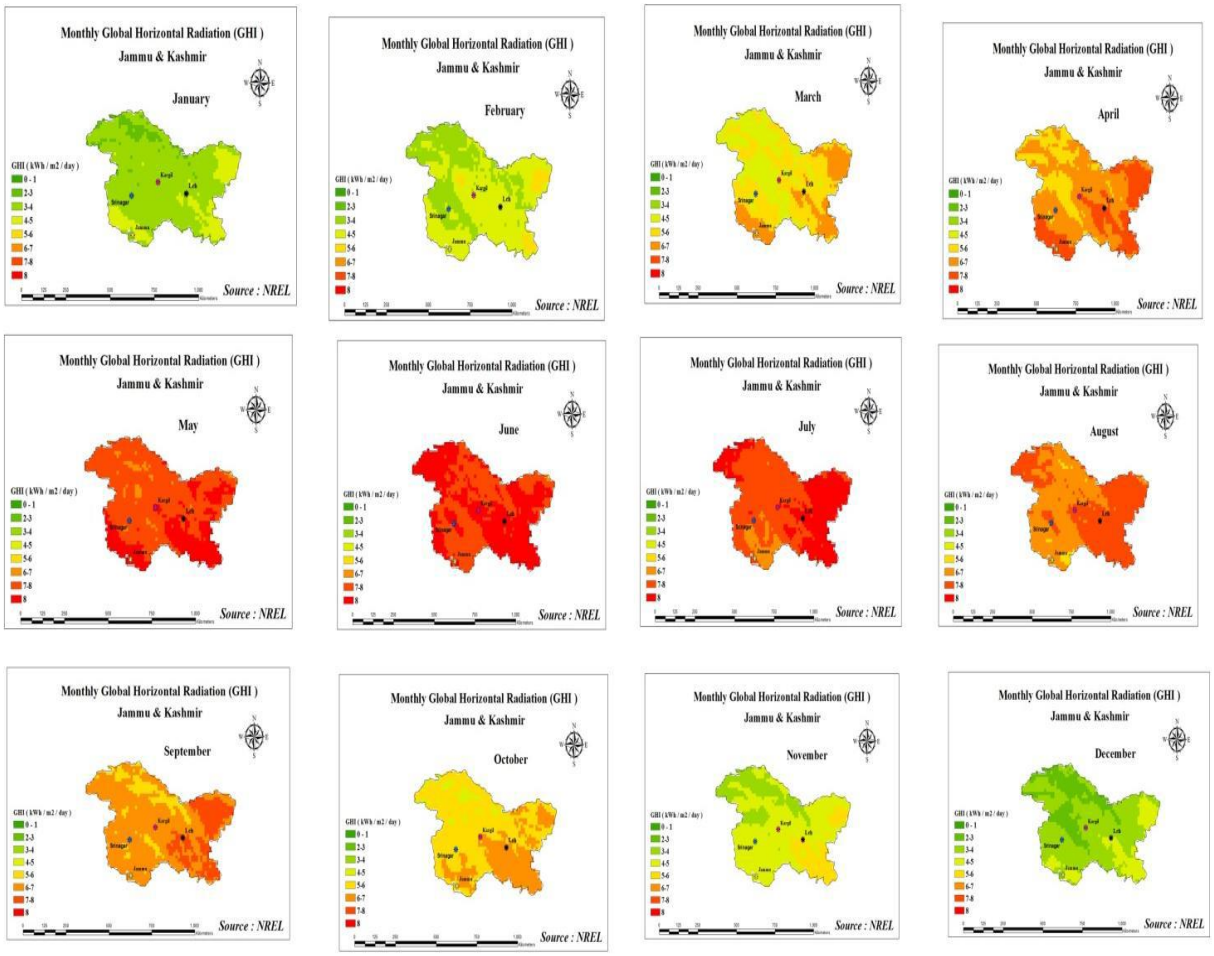


*Fig.4: Average monthly global horizontal radiation data for the state of Jammu and Kashmir.*

The monthly direct normal radiation (DNI) for the state of Jammu and Kashmir based on 10 years of average data from NREL is given below:

*https://dx.doi.org/10.22161/ijaers.5.1.10* *ISSN: 2349-6495(P) | 2456-1908(O)*

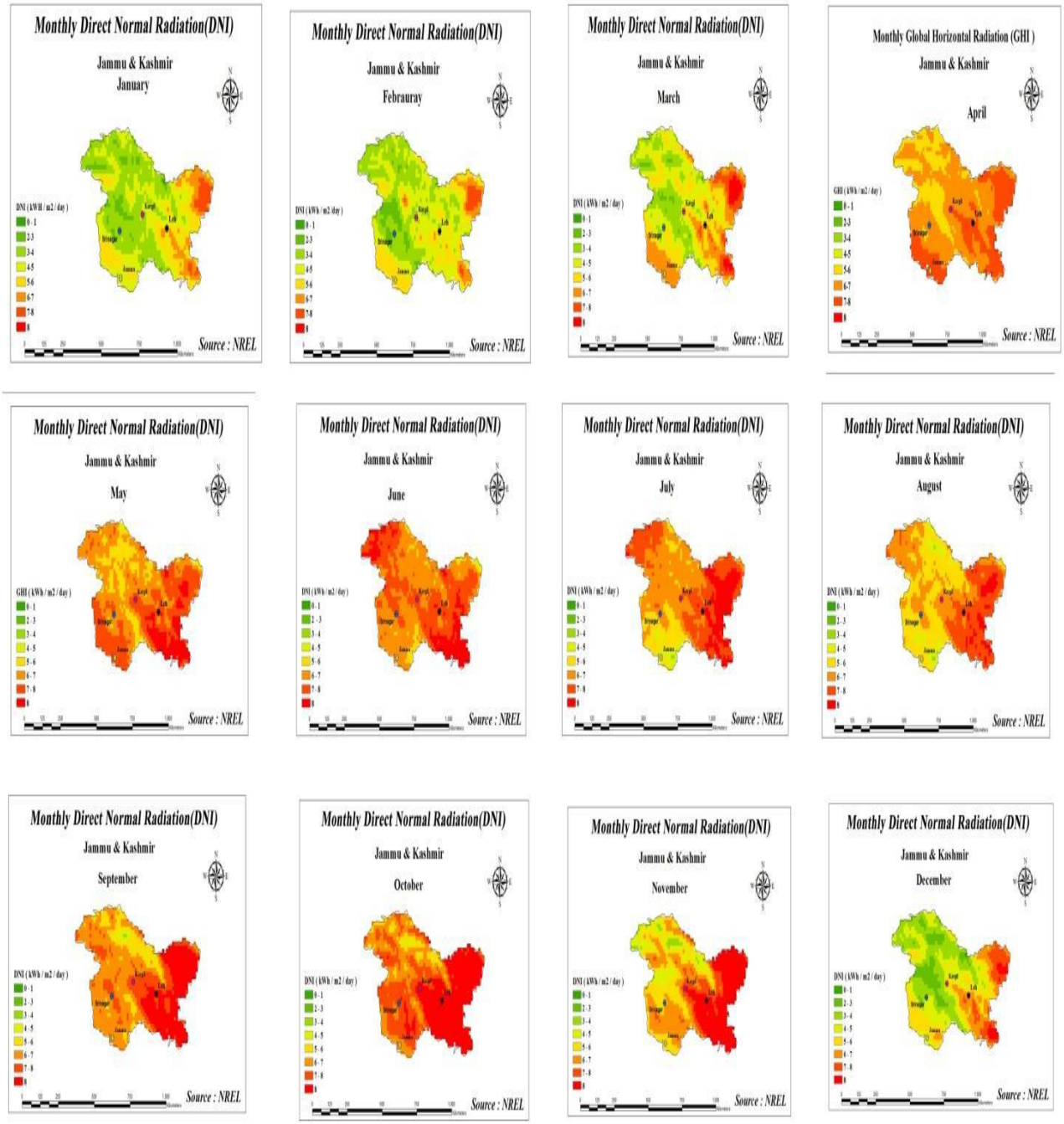


*Fig.5: Average monthly direct normal radiation data for the state of Jammu and Kashmir.*

During winter, tilt radiation is almost double than the horizontal whereas in summer there is a good horizontal radiation which is helpful in photovoltaic electricity generation. Low ambient temperature with high GHI ensures higher efficiency of solar panels and thus higher efficiency of solar photovoltaic electricity. The Annual global radiation at latitude is around 25% greater than horizontal, especially in Ladakh region. The higher values of DNI in Jammu and Kashmir ensures high efficiency of concentrated solar technologies like parabolic trough and dish collectors have high grade heat application. From the above DNI & GHI map of J&K, it is clear that Leh has highest DNI and GHI. Kargil has second highest DNI in state. Overall, solar radiation is always good in summer months when the demand is comparatively high. During winter months, the demand of electricity can be made available by hybridizing solar photovoltaic and solar thermal technology. This will ensure both electricity and

*https://dx.doi.org/10.22161/ijaers.5.1.10* *ISSN: 2349-6495(P) | 2456-1908(O)*

heat is made available to areas like Leh, Kargil and Kashmir and parts of Jammu which have inadequate energy solutions at present. The process heat can be utilized by using Flat plate collectors as well as evacuated tube collectors which are mainly used for low grade heat application (under 50- $70^0$C). The Solar concentrated technologies (parabolic trough, Parabolic dish collector etc.) are good for high grade heat application (above $100^0$C). By switching to appropriate solar energy technologies, the Jammu and Kashmir state can mitigate its growing energy demands based on Clean and green energy.

The results reveal that average GHI and DNI for all regions vary in between 4-8 kWh per square per metre per day. Thus, investment in solar energy is a natural choice for Jammu and Kashmir and for solar resource assessment is mandatory at all locations for proper selection of solar energy technology.

## ACKNOWLEDGEMENT

The authors would like to acknowledge the inputs and review by Dr Arun K Tripathi (Director General, National Institute of Solar Energy MNRE) and Sh. S K Singh (Advisor/Scientist 'G', Ministry of New & Renewable Energy) in preparation of this manuscript.

## REFERENCES

[1] Ramachandra T. V, Renewable Energy Transition-peresepective and challenges in India,Saket power projects, Ahamadabad ;2011:175-183.
[2] Renewable Energy status global report update,Paris. 2009 p.11.
[3] Tsoutsos T, Gekas V, Marketaki K. Technical and economical evaluation of solar thermal power generation. Renew Energy 2003;28(6):873–86.
[4] Brakmann G, Aringhoff R, Geyer M, Teske S. Concentrated solar thermal power – now. Amsterdam: Green peace International; 2005.
[5] McKinsey. The economics of solar power. The McKinsey Quarterly, June 2008.
[6] European Commission. Concentrating solar power – from research to implementation. Luxembourg: European Commission; 2007.
[7] Singh A. Power sector reform in India: current issues and prospectus. EnergyPolicy 2006;34:2480–90.
[8] Ministry of Power. Available: http://www.powermin.nic.in [online].
[9] Ministry of New and Renewable Energy source (MNRE),http://www.mnre.gov.in/achievements.htm; 2011 [accessed August 2011].
[10] Government of India. Annual Report 2009–10. New Delhi, India: Ministry ofNew and Renewable Energy, Government of India; 2010 [online].
[11] Bhattacharyya CS. An overview of problems and prospects for the Indian power sector. Energy 1999;19:795–803.
[12] Garud S, Purohit I. Making solar thermal power generation in India a reality– overview of technologies, opportunities and challenges, The Energy and Resources Institute (TERI), Darbari Seth Block, IHC Complex, Lodhi Road, NewDelhi 110003, India.

*https://dx.doi.org/10.22161/ijaers.5.1.11* *ISSN: 2349-6495(P) | 2456-1908(O)*

# Weighted Moving Average of Forecasting Method for Predicting Bitcoin Share Price using High Frequency Data: A Statistical Method in Financial Cryptocurrency Technology

Nashirah Abu Bakar[1], Sofian Rosbi[2]

[1]Islamic Business School, College of Business, Universiti Utara Malaysia, Malaysia
[2]School of Mechatronic Engineering, Universiti Malaysia Perlis, Malaysia

***Abstract*****—** *Bitcoin is a type of cryptocurrency that implemented decentralized digital currency method. The transaction is monitored and validated by peer-to peer system using hash programming. These transactions are verified by network nodes through the use of cryptography and recorded in a public distributed ledger called a blockchain. The objective of this study is to forecast the Bitcoin exchange rate using weighted moving average method. Data selected in this study are selected hourly from 14th December 2017 until 18th December 2017. The forecasting method is using weighted moving average. Then, the validity of the forecasting model is validated using mean absolute percentage error (MAPE) calculation. Results indicated mean absolute percentage error is 0.72%. Therefore, the moving average method is considered as reliable forecasting method for Bitcoin exchange rate. The finding of this study will help investors to make best decision regarding suitable portfolio for their investment.*

***Keywords*****— Bitcoin, Financial technology, Forecasting method, Statistical approach, Cryptocurrency***

## I. INTRODUCTION

Bitcoin is a type of cryptocurrency that implemented decentralized digital currency method. The transaction is monitored and validated by peer-to peer system using hash programming. These transactions are verified by network nodes through the use of cryptography and recorded in a public distributed ledger called a blockchain.

Bitcoin become popular when the price for 1 Bitcoin was aggressively increased. This condition was attracted more investors to invest in Bitcoin cryptocurrency transaction. Bitcoin was developed by Satoshi Nakamoto. Bitcoin is a crypto-currency based on open-source software and protocols that operates in peer-to-peer networks as a private irreversible payment mechanism. The protocol allows cross-border payments, for large and small items, with little or no transactional costs (Nakamoto, 2009).

The bitcoin transactional system is often described as an anonymous system, although it might be more accurate to describe the system as one in which users can invoke privacy. The ledger of account for all Bitcoin transactions is public and distributed (Simser, 2015). According to Christopher (2014) Bitcoin operates via a peer-to-peer (P2P) network. P2P networks are created when multiple individuals run the necessary software on their individual computers and connect to each other.

Bitcoin is different with traditional method of payment. Abu Bakar et al. (2017) highlight several main differences between traditional digital currency and cryptocurrency transaction process. In definition, current fiat money is money in any form when in actual use or circulation as a medium of exchange, especially circulating banknotes and coins. This type of money is government-issued currencies. Comparing to cryptocurrency, Bitcoin is digital currency in which encryption techniques are used to regulate the generation of units of currency.

Even there are many advantage using a Bitcoin cryptocurrency but the problem arises is either Bitcoin cryptocurrency can be a good medium of exchange due to high volatility and risk. Therefore, this study tries to fulfill this gap by forecasting Bitcoin exchange rate using weighted moving average.

## II. LITERATURE REVIEW

Over the last few years, a wide range of digital currencies, such as BitCoin, LiteCoin, PeerCoin, AuroraCoin, DogeCoin and Ripple, have emerged (Ciaian et al., 2014). The most popular is Bitcoin. It has been getting a lot of media attention, and its total market value has reached 20 billion USD in March 2017 (Chiu and Koeppl, 2017). The price of the Bitcoin cryptocurrency has risen from December 2016, moving to USD 13282.29 in early December 2017. This value show the Bitcoin

*https://dx.doi.org/10.22161/ijaers.5.1.11* *ISSN: 2349-6495(P) | 2456-1908(O)*

cryptocurrency was attracted more investors to involved in this transaction. As investors, the main objective of the investment is to get high profit. Therefore, Bitcoin cryptocurrency are looking as a good platform for investment (Abu Bakar and Rosbi, 2017).

Bitcoin is a type of digital coins (cryptocurrency) which is not issued by any government, bank or organization. However, bitcoin is relying on cryptographic protocols and a distributed network of users to perform mining, storing, and transferring activities. Bitcoin currency is a monetary value that is accepted for payment purposes by persons other than the issuer, with the unit of account matching that of the physical currency (Ram, et al., 2016; Bal, 2013).

Wijk, (2017) stated the main users of the Bitcoin are technologically interested geeks who want to use the newest innovations, anarchists who have lost trust in the governments and the banking systems, and speculative risk-seekers looking for a new gamble. However, this is quickly changing due to the increase in the value of the Bitcoin and the attention that it gets in the news.

Abu Bakar and Rosbi (2017) show a statistical analysis, for Bitcoin return is 0.006 (mean) and the deviation is 0.04458. The standard error indicates the volatility for Bitcoin is 4.458 %. This value is considered as high value of volatility. High value of volatility indicates the investment in Bitcoin is categorical as high risk investment. The important of this study is to assist investors to develop better investment portfolio in targeting better profit and lowering the loss. While Buchholz , et al. (2012) show the strong explanation and validation of the existence of a market bubble in the bitcoin currency market.

Abu Bakar and Rosbi (2017) shows the distribution of Bitcoin exchange rate with first difference is follow normal distribution with probability of 0.722. The result show the distribution of data after second stages of outlies deletion treatments is high normal distribution characteristics. This finding concludes that Bitcoin data is highly volatile with existence of many outliers.

## III. RESEARCH METHODOLOGY

This section describes normality test, weightage moving average method and mean absolute percentage error calculation.

### 3.1 Shapiro Wilk Normality test

This section describes the mathematical procedure to perform normality test (Shapiro and Wilk, 1965).

Consider $m' = (m_1, m_2, ..., m_n)$ as the vector of expected values of standard normal statistics. Then, $V = (v_{ij})$ is represented as $n \times n$ covariance matrix.

Next, $x_1 \le x_2 \le ...x_n$ denotes as ordered random sample of size $n$ from a normal distribution data with mean 0 and variance 1. Therefore, below equations were derived.

$$E(x)_i = m_i \text{ , where } (i = 1,2,...,n) \text{ ...}\ldots\ldots\ldots\ldots\ldots \text{ (1)}$$

$$\operatorname{cov}(x_i, x_j) = v_{ij} \text{ , where } (i, j = 1,2,...,n) \text{ ...}\ldots\ldots\ldots \text{ (2)}$$

Then, consider $y' = (y_1,..., y_n)$ represents as a vector of ordered random observation. The objective of this test is to derive a test for the hypothesis that this is a sample from a normal distribution data with unknown value of mean $\mu$ and unknown variance $\sigma^2$.

Clearly, if $\{y_i\}$ is a normal sample, then $y_i$ may be expressed as:

$$y_i = \mu + \sigma x_i \text{ , where } (i = 1,2,...,n) \ldots\ldots\ldots\ldots\ldots\ldots \text{ (3)}$$

Utilizing the generalized least-squares theorem that the best linear unbiased estimates of $\mu$ and $\sigma$ are those quantities that minimize the quadratic form:

$$(y - \mu 1 - \sigma m)' V^{-1} (y - \mu 1 - \sigma m) \ldots\ldots\ldots\ldots\ldots\ldots \text{ (4)}$$

where, $1' = (1,1,...,1)$.

Next, the estimates of $\mu$ and $\sigma$ are described as below equation.

$$\hat{\mu} = \frac{m'V^{-1}(m1' - 1m')V^{-1}y}{1'V^{-1}1m'V^{-1}m - (1'V^{-1}m)^2} \ldots\ldots\ldots\ldots\ldots\ldots\ldots\ldots\ldots\ldots \text{ (5)}$$

$$\hat{\sigma} = \frac{1'V^{-1}(1m' - m1')V^{-1}y}{1'V^{-1}1m'V^{-1}m - (1'V^{-1}m)^2} \ldots\ldots\ldots\ldots\ldots\ldots\ldots\ldots\ldots\ldots \text{ (6)}$$

The symmetric data distribution indicates,

$$1'V^{-1}m = 0 \ldots\ldots\ldots\ldots\ldots\ldots\ldots\ldots\ldots\ldots\ldots\ldots\ldots\ldots \text{ (7)}$$

Therefore,

$$\hat{\mu} = \frac{1}{n}\sum_{i=1}^{n} y_i = \bar{y} \ldots\ldots\ldots\ldots\ldots\ldots\ldots\ldots\ldots\ldots\ldots\ldots\ldots\ldots \text{ (8)}$$

$$\hat{\sigma} = \frac{m'V^{-1}y}{m'V^{-1}m} \ldots\ldots\ldots\ldots\ldots\ldots\ldots\ldots\ldots\ldots\ldots\ldots\ldots\ldots \text{ (9)}$$

Next, let

$$S^2 = \sum_{i=1}^{n} (y_i - \bar{y})^2$$

denote the usual symmetric unbiased estimate of $(n-1)\sigma^2$.

Therefore, the *W* test statistic for normality is defined by

$$W = \frac{R^4\hat{\sigma}^2}{C^2S^2} = \frac{b^2}{S^2} = \frac{(a'y)^2}{S^2}$$

$$W = \frac{\left(\sum_{i=1}^{n} a_i y_i\right)^2}{\sum_{i=1}^{n} (y_i - \bar{y})^2} \ldots\ldots\ldots\ldots\ldots\ldots\ldots\ldots\ldots\ldots\ldots\ldots\ldots\ldots \text{ (10)}$$

where,

*https://dx.doi.org/10.22161/ijaers.5.1.11* *ISSN: 2349-6495(P) | 2456-1908(O)*

$$R^2 = m'V^{-1}m$$
$$C^2 = m'V^{-1}V^{-1}m$$
$$a' = (a_1,...,a_n) = \frac{m'V^{-1}}{\left(m'V^{-1}V^{-1}m\right)^{\frac{1}{2}}}$$
$$b = \frac{R^2\hat{\sigma}}{C}$$

Thus, $b$ is, up to the normalizing constant $C$, the best linear unbiased estimate of the slope of a linear regression of the ordered observations, $y_i$ , on the expected values, $m_i$ , of the standard normal order statistics. The constant C is so defined that the linear coefficients are normalized.

It may be noted that if one is indeed sampling from a normal population then the numerator, $b^2$, and denominator, $S^2$, of $W$ are both, up to a constant , estimating the same quantity, namely $\sigma^2$.

### 3.2 Weighted moving average

This section describes the forecasting method using weighted moving average. Weighted moving average is a forecasting method that more responsive to changes because more recent periods may be more heavily weighted.

A weighted moving average may be expressed mathematically as:

$$Weighted\ moving\ average = \frac{\sum\left((Weight\ for\ period\ n)(Exchange\ rate\ in\ period\ n)\right)}{\sum Weights}$$

In this study, we assigned the weightage according to next equation.

$$EXF_t = \alpha EX_{t-1} + \beta EX_{t-2} + \gamma EX_{t-3} \quad \text{..... (11)}$$

where,

$EXF_t$ is forecast value of exchange rate at period *t*,

$EX_{t-1}$ is actual value of exchange rate at period *t*-1,

$\alpha$ is weightage for $EX_{t-1}$, we set as 0.8,

$EX_{t-2}$ is actual value of exchange rate at period *t*-2,

$\beta$ is weightage for $EX_{t-2}$, we set as 0.1,

$EX_{t-3}$ is actual value of exchange rate at period *t*-3, and

$\gamma$ is weightage for $EX_{t-3}$, we set as 0.1.

### 3.3 Mean absolute percentage error calculation

One of the indicators for detecting a reliable and robust model of forecasting is using mean absolute percentage error (MAPE). The MAPE is computed as the average of the absolute difference between the forecasted and actual values, expressed as a percentage of the actual values.

That is, if we have forecasted and actual values for *n* periods, the MAPE is calculated as:

$$MAPE(\%) = \frac{\sum_{i=1}^{n}\left(\frac{|Actual_i - Forecast_i|}{Actual_i} \times 100\right)}{n} \quad \text{..... (12)}$$

The MAPE has advantage that easily interpreted in term of percentage to the actual values.

## IV. RESULT AND DISCUSSION

This study performed analysis of normality for data distribution and performed weighted moving average as prediction method.

### 4.1 Dynamic behavior of Bitcoin exchange rate

This study analyzed hourly data of Bitcoin exchange rate starting from 14th December 2017 until 18th December 2017. The starting value for Bitcoin exchange rate on 14th December 2017, 01:00 is USD 16600 for each Bitcoin. The minimum value of Bitcoin exchange rate is USD 16169 on 14th December 2017, 03:00. Meanwhile, the maximum value of Bitcoin exchange rate is USD 19704.80 on 17th December 2017, 12:00. The ending value of Bitcoin exchange rate on 18th December 2017, 24:00 is USD 18960.52.

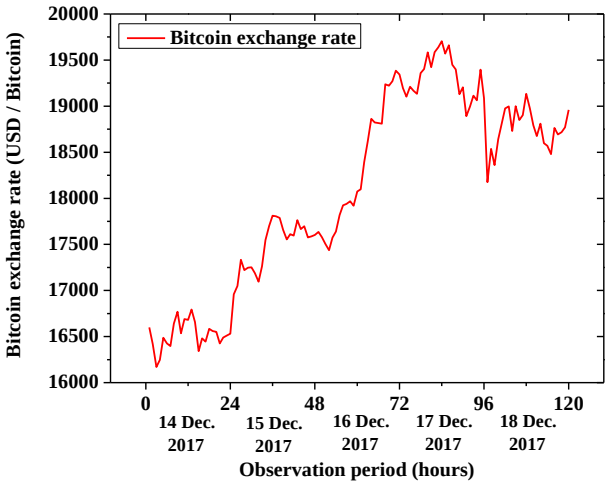


*Fig. 1: Dynamic behavior of Bitcoin exchange rate*

### 4.2 Normality test for first difference of Bitcoin exchange rate

Then, this study calculated the changes of Bitcoin exchange rate. The changes are calculated by difference between current observations with previous observation of Bitcoin exchange rate. The calculation is represented by Equation (13).

$$\Delta EXC_t = EXC_t - EXC_{t-1} \quad \text{..... (13)}$$

Where:

$\Delta EXC_t$ is first difference of exchange rate;

$EXC_t$ is Bitcoin exchange rate on period *t*;

$EXC_{t-1}$ is Bitcoin exchange rate on period *t*-1.

*https://dx.doi.org/10.22161/ijaers.5.1.11* *ISSN: 2349-6495(P) | 2456-1908(O)*

Figure 2 shows changes of Bitcoin exchange rate. The mean of the data is 19.83. The standard deviation is 179.25.The maximum value of changes is USD 427.17. There is one outliers exists which is 97th observation. The value of outliers is -912.15. This finding is validated with normal percentiles plot in Figure 3. A normal percentile plot shows one outliers exists in Figure 3. This value is considered as outliers because that observation is deviated far from normal reference line.

Then, this study performed numerical normality test using Shapiro-Wilk method. The probability value is 0.000 less than 0.05. Therefore, the distribution of data follows non-normal distribution.

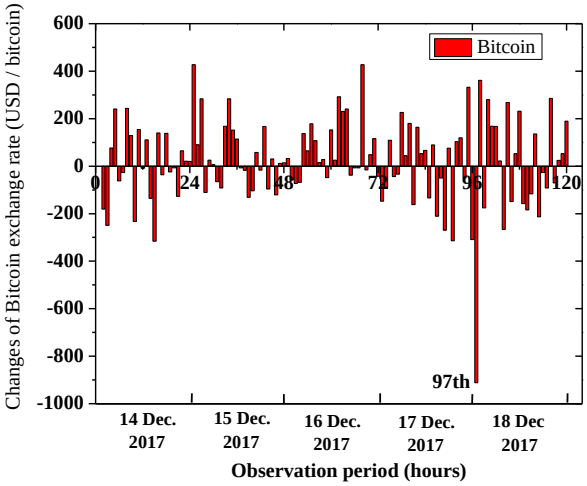


*Fig. 2: Changes of Bitcoin exchange rate*

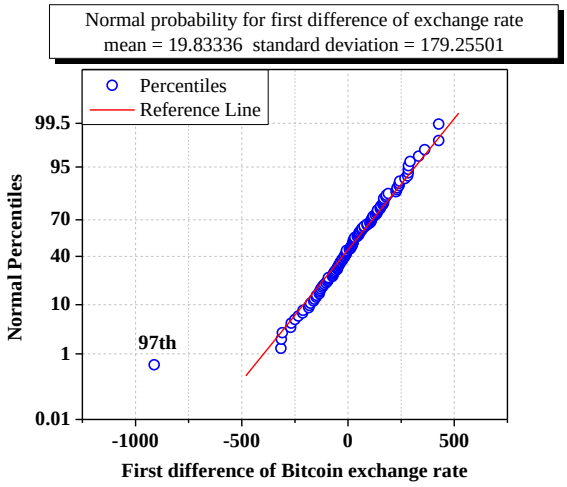


*Fig. 3: Normal Percentiles*

*Table 1: Statistical normality test*

| Shapiro-Wilk test | | |
|---|---|---|
| Statistics | Degree of freedom | Probability value |
| 0.939 | 119 | 0.000 |

**4.3 Normality transformation for data**

This section describes the normality transformation for first difference of exchange rate data. This study started with detecting outliers. Therefore, the 97$^{th}$ observation (18$^{th}$ December 2017, 01:00, with value -912.15) is considered as outliers. This study eliminated this data point to evaluate the effect to the normality characteristics.

This study validated the normality characteristics using graphical method and numerical method. Graphical method is implemented using histogram and normal probability plot. Figure 4 shows the histogram for first difference of Bitcoin exchange rate. The distribution of data is near to normal distribution line (red line). Therefore, distribution of data follows normal distribution.

In addition, this study performed the second graphical method namely normal probability plot. Figure 5 shows the normal percentiles for first difference of Bitcoin exchange rate. Result shows all the data points are distributed closely to normal reference line (red line). Therefore, the distribution of first difference of Bitcoin exchange rate follows normal distribution.

Then, we performed numerical testing to validate the normality characteristics of data distribution. Table 2 shows the Shapiro-Wilk normality test for first difference of Bitcoin exchange rate. The null hypothesis of this test is that the sample data is normally distributed. Table 2 shows the probability value is 0.795. This value is larger than chosen alpha (0.05).Therefore, this study fail to reject null hypotheses. The distribution of data is normally distributed.

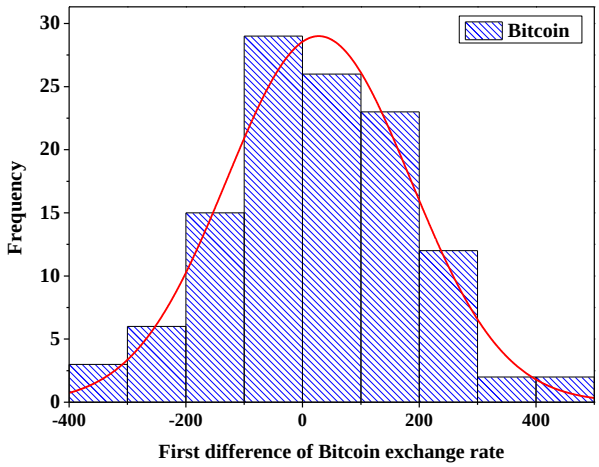


*Fig. 4: Histogram for first difference of Bitcoin exchange rate*

*https://dx.doi.org/10.22161/ijaers.5.1.11* *ISSN: 2349-6495(P) | 2456-1908(O)*

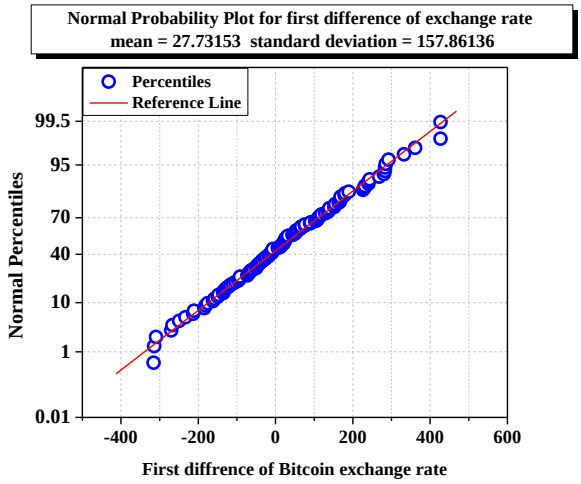


*Fig. 5: Normal probability plot for first difference of Bitcoin exchange rate*

*Table 2: Statistical normality test for first difference of Bitcoin exchange rate*

| Shapiro-Wilk test | | |
|---|---|---|
| Statistics | Degree of freedom | Probability value |
| 0.993 | 118 | 0.795 |

### 4.4 Forecasting method using weighted moving average

This section describes the result of forecasting using weighted moving average. Figure 6 shows the comparison between actual data and forecast data using weighted moving average. Forecast data is represented by red line. The maximum value of forecast data is USD 19686.26 for each Bitcoin on 17th December 2017, 13:00. Meanwhile, the minimum value of forecast data is USD 16237.75 for each Bitcoin on 14th December 2017, 04:00.

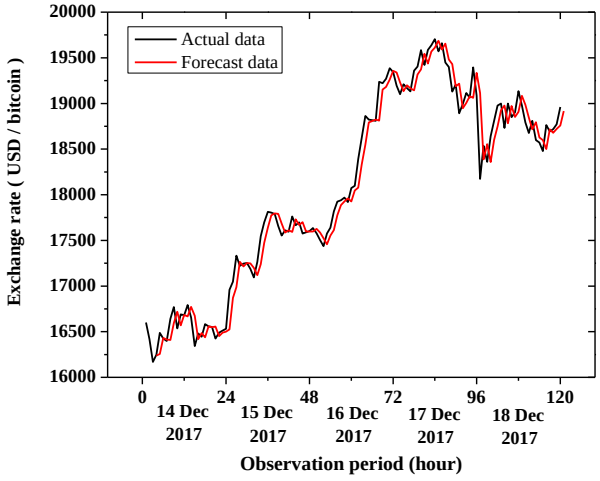


*Fig. 6: Forecasting using weighted moving average*

Then, this study developed residual plot to evaluate the reliability of the forecasting model. Figure 7 shows the residual plot for forecasting method using weighted moving average. Figure 7 shows one data (97th observation, 18th December 2017, 01:00) that shows large residual. This data point is the outliers in the data set. Therefore, it contributes to large residual between actual value and forecast value.

Mean value for residual is USD 29.68 for each Bitcoin. The standard deviation for data is USD 179.49 for each Bitcoin. Figure 7 indicates the distribution of residual is follows white noise pattern. Therefore, the residual analysis shows the moving average model is a reliable forecasting method.

Then, this study performed the calculation of absolute percentage error analysis. Figure 8 shows the absolute percentage error for each of the observations. The mean absolute percentage error is 0.72%. Therefore, the moving average method is considered as reliable forecasting method for Bitcoin exchange rate.

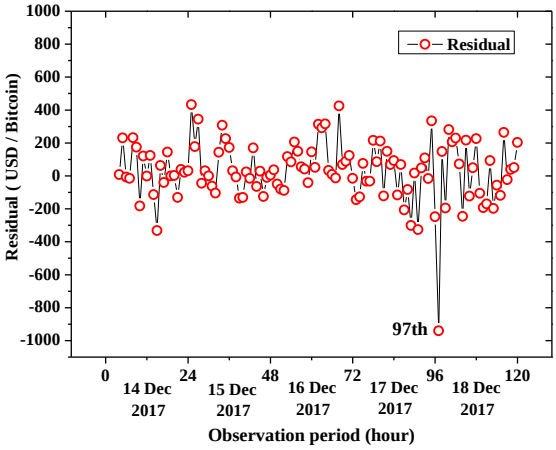


*Fig. 7: Residual plot for forecasting method using weighted moving average*

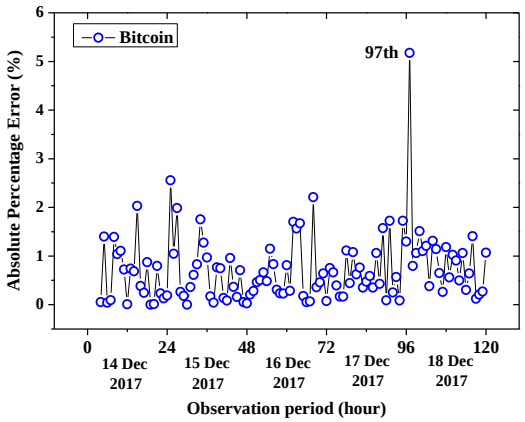


*Fig. 8: Absolute percentage error analysis*

## V. CONCLUSION

The objective of this study is to develop forecasting methos for high frequency data for Bitcoin exchange rate data. This study proposed weighted moving average to forecast the dynamic movement of Bitcoin exchange rate.

*https://dx.doi.org/10.22161/ijaers.5.1.11* *ISSN: 2349-6495(P) | 2456-1908(O)*

The main findings concluded from this study are:

(a) This study analyzed hourly data of Bitcoin exchange rate starting from 14th December 2017 until 18th December 2017. The starting value for Bitcoin exchange rate on 14th December 2017, 01:00 is USD 16600 for each Bitcoin. The minimum value of Bitcoin exchange rate is USD 16169 on 14th December 2017, 03:00. Meanwhile, the maximum value of Bitcoin exchange rate is USD 19704.80 on 17th December 2017, 12:00. The ending value of Bitcoin exchange rate on 18th December 2017, 24:00 is USD 18960.52.

(b) Next, this study performed analysis to first difference of Bitcoin exchange rate. The mean of the data is 19.83. The standard deviation is 179.25.The maximum value of changes is USD 427.17. There is one outliers exists which is 97th observation. The value of outliers is -912.15.

(c) Then, this study performed numerical normality test for first difference of Bitcoin exchange rate using Shapiro-Wilk method. The probability value is 0.000. Therefore, the distribution of data follows non-normal distribution.

(d) In addition, this study performed the forecast using weighted moving average. The maximum value of forecast data is USD 19686.26 for each Bitcoin on 17th December 2017, 13:00. Meanwhile, the minimum value of forecast data is USD 16237.75 for each Bitcoin on 14th December 2017, 04:00.

(e) Mean value for residual is USD 29.68 for each Bitcoin. The standard deviation for data is USD 179.49 for each Bitcoin. Result indicates the distribution of residual is follows white noise pattern. Therefore, the residual analysis shows the moving average model is a reliable forecasting method.

(f) The mean absolute percentage error is 0.72%. Therefore, the moving average method is considered as reliable forecasting method for Bitcoin exchange rate.

## REFERENCES

[1] Abu Bakar, N. and Rosbi, S. (2017), High Volatility Detection Method Using Statistical Process Control for Cryptocurrency Exchange Rate: A Case Study of Bitcoin, The International Journal of Engineering and Science, Vol. 6(11), pp. 39-48.

[2] Abu Bakar, N. and Rosbi, S. (2017), Robust Statistical Normality Transformation method with Outlier Consideration in Bitcoin Exchange Rate Analysis, International Journal of Advances in Scientific Research and Engineering, Vol.3 (9), pp. 80-91.

[3] Abu Bakar, N., Rosbi, S. and Uzaki, K., (2017) Cryptocurrency Framework Diagnostics from Islamic Finance Perspective: A New Insight of Bitcoin System Transaction, International Journal of Management Science and Business Administration, Vol. 4 (1), pp.19-28.

[4] Abu Bakar, N. and Rosbi, S., (2017) High Volatility Detection Method Using Statistical Process Control for Cryptocurrency Exchange Rate: A Case Study of Bitcoin, The International Journal of Engineering and Science, Vol. 6(11), pp. 39-48.

[5] Buchholz, M., Delaney, J. and Warren, J. (2012) Bits and Bets Information, Price Volatility, and Demand for Bitcoin, available at: http://www.bitcointrading.com/pdf/bitsandbets.pdf

[6] Ciaian, P., Rajcaniova, M. and Kancs, D., The Economics of BitCoin Price Formation,available at: https://arxiv.org/ftp/arxiv/papers/1405/1405.4498.pdf

[7] Chiu, J. and Koeppl, T., (2017) The Economics of Cryptocurrencies - Bitcoin and Beyond, available at: https://www.chapman.edu/research/institutes-and-centers/economic-science-institute/_files/ifree-papers-and-photos/koeppel-april2017.pdf

[8] Nakamoto, S. (2009) "Bitcoin: A peer-to-peer electronic cash system", Retrieved from http://www.bitcoin.org

[9] Ram, A., Maroun, W. and Garnett, R., (2016) Accounting for the Bitcoin: accountability, neoliberalism and a correspondence analysis, Meditari Accountancy Research, 24 (1), pp. 2-35.

[10] Shapiro, S.S. and Wilk, M.B. (1965), An Analysis of Variance Test for Normality (Complete Samples), Biometrika, Vol. 52, No.3/4.

[11] Simser, J.,(2015), Bitcoin and modern alchemy: in code we trust, Journal of Financial Crime, Vol. 22 (2), pp. 156-169.

[12] Wijk, D.V. (2013), What can be expected from the BitCoin?, Working Paper No. 345986, Erasmus Rotterdam Universiteit

*https://dx.doi.org/10.22161/ijaers.5.1.12* *ISSN: 2349-6495(P) | 2456-1908(O)*

# The Creation of a Vortex in Sea water through the MHD

Osvaldo Missiato[1], Celso Luis Levada[2], Alexandre Luis Magalhães Levada[3]

[1]Universities Integrated Einstein of Limeira- Brazil
[2]Hermínio Ometto Foundation- Uniararas- Brazil
[3]Federal University of São Carlos- Brazil

***Abstract***— *The Magneto hydrodynamics equations, MHD, are discussed for weakly conductive fluids of electricity, and then an analytical solution is presented. An MHD vortex is generated using seawater in a cylindrical vessel, where external electromagnetic fields are conveniently applied. Some physical quantities of interest are discussed and measured by well-known techniques.*

***Keywords— MHD, Magneto hydrodynamics equations, cylindrical vessel, Vortex.***

## I. INTRODUCTION

Weak electrically conductive fluids, when subjected to electromagnetic forces, may respond somewhat surprisingly depending on how the force in the fluid volume applies.

Even though the fluid is weakly conductive, the density of electromagnetic force, $\vec{f} = \vec{j} \times \vec{B}$, being $\vec{j}$ the current density and B the externally applied magnetic field may be sufficient to induce large movements. For this, it is necessary that the magnetic field be of relatively great intensity, because the currents that are induced in these, in general, are very small since the electrical conductivity is relatively small, as indicated by BRAGINSKII(1).

The rotationality of the magnetic force, that is, $\nabla \times \vec{f} \neq \vec{0}$ is critical to generate fluid movement and thus create MHD vortex.

In the experiment, the fluid is considered to be at rest at the instant the electromagnetic force (Lorentz force) is applied. The establishment of the vortex in the fluid occurs after a few seconds of force application and is visualized quite clearly. The vorticity, given by the rotational velocity vector, is a physical quantity of great interest and is associated with the concept of angular velocity. A rotational speed meter, called a measurement rotor, was introduced into a vessel containing the liquid in rotational motion. By means of the stroboscopic technique, it was possible to measure the angular velocity. Values of the order of 1000 RPM are common for magnetic fields of the order of 0.3 Tesla and applied voltage of the order of 400 V/m.

It is possible to emphasize the importance of the Hartmann layer in the mechanism of generation of the rotational movement of the fluid; the electric current tends to circulate in the mentioned layer giving the maximum force applied, since in this case the field is axial and forms an angle of 90º with the current intensity.

THE IMPORTANCE OF VORTICITY

Consider an incompressible conducting fluid subjected to the influence of external electromagnetic fields, initially at rest. Consider, also, the second law of Newton per unit volume, expressed by:

$$\rho\vec{a} = -\nabla p + \vec{f} \quad (1)$$

where ρ is the specific mass, $\vec{a}$ is the acceleration vector, p is the pressure and $\vec{f}$ is the force field. Applying the rotational operator on equation (1), the pressure p and the force $\vec{f}$ are mathematically eliminated if it is irrotational or conservative. If the force $\vec{f}$ is rotational (viscous or Lorentz), i.e. if it has the tendency to induce a rotation about the fluid element or to modify its rotational state, then a path for solving the fluid motion may be found in function of the vorticity $\vec{\omega}$. It should be noted that the vorticity $\vec{\omega}$ is a measure of the average rotation at each point of the fluid. It can also be shown that the movement of a fluid of uniform mass, occupying a closed vessel, does not occur without the presence of vorticity (MOFFAT(2)).

## II. FAILED DRIVER FLUIDS : BASIC EQUATIONS

According to LEWELLEN(3), the equations that describe the behavior of an incompressible conductive fluid, subject to the influence of external electromagnetic fields in the low frequency regime, where the displacement current is neglected, are given by:

$$\nabla \cdot \vec{V} = 0 \quad (2)$$

$$\rho \frac{D\vec{V}}{Dt} = -\nabla p + \rho\vec{g} + \vec{j} \times \vec{B} + \eta \nabla^2 \vec{V} \quad (3)$$

*https://dx.doi.org/10.22161/ijaers.5.1.12* *ISSN: 2349-6495(P) | 2456-1908(O)*

$$\nabla \times \vec{E} = -\frac{\partial \vec{B}}{\partial t} \quad (4)$$

$$\vec{j} = \frac{1}{\mu} \nabla \times \vec{B} \quad (5)$$

$$\vec{j} = \sigma\left(\vec{E} + \vec{V} \times \vec{B}\right) \quad (6)$$

where $\vec{V}$ is the velocity vector, p is the pressure, ϱ is the specific mass, $\vec{J}$ is the current density, $\vec{B_o}$ is the magnetic field, $\vec{E}$ is the electric field, σ is the electrical conductivity, η is the viscosity and μ is the magnetic permeability.

Consider, however, that

$$\frac{D}{Dt} = \frac{\partial}{\partial t} + \vec{V} \cdot \nabla \quad (7)$$

Let $R_m = \mu\sigma UL$ be the Magnetic Reynolds number, which is defined by the ratio between convection and diffusion of the magnetic field by the fluid. On the other hand, using equations (4), (5) and (6), it can be shown that

$$\frac{\partial \vec{B}}{\partial t} = \nabla \times \left(\vec{V} \times \vec{B}\right) + \eta \nabla^2 \vec{B}, \eta = \frac{1}{\mu\sigma}$$

And so it comes that

$$Rm = \frac{\left|\nabla \times \left(\vec{V} \times \vec{B}\right)\right|}{\left|\eta \nabla^2 \vec{B}\right|} = \mu\sigma UL$$

In this development, U is a characteristic velocity and L is a characteristic length. Considering that $\mu = 4\pi 10^{-7} SI$ and σ ≈4S/m, we find that in this work we have $R_m << 1$, since U≈ 1m/s and L≈ 1m. On the other hand, by theory, we know that although the fluid is initially at rest, the force $\vec{f} = \vec{j} \times \vec{B}$ imposes a movement on it. Then, due to this movement, an induced electromotive force of the order of VB is generated in the fluid, as well as a current of magnitude equal to σVB. The magnetic field $B_1$, produced by this current, is approximately equal to the product of the magnetic Reynold number, Rm, by the externally applied magnetic field, B. That is, $B_1 \approx R_m.B$. In contrast, considering that $R_m << 1$, we can say that $B_1$ is negligible. Analogous reasoning can be established for the induced electric field, whose value E1 is given by the product of Rm by the module of the velocity vector V, by the module of the external magnetic field B, that is, $E_1 \approx R_m$ VB. Again, because $R_m << 1$, this induced electric field is also discarded. Thus, the resulting magnetic field is the applied external magnetic field itself. Since, by hypothesis, B is assumed to be uniform, Landau shows that ∇XB = 0 and that ∇.B = 0.

It is noted, then, that the Law of Ampere does not apply, so that the electric currents are determined by the Law of Ohm. Thus, the Lorentz force is given by

$$\vec{f} = \vec{j} \times \vec{B} = \left[\sigma\left(\vec{E} + \vec{V} \times \vec{B}\right) \times \vec{B}\right] \quad (8)$$

## III. SIMPLIFIED SOLUTION

A very simple solution of the problem is one in which, in a cylindrical coordinate system (r, Θ, z), only the azimuth velocity $V_\Theta$ is considered, making $V_r = V_z = 0$.

The justification for such a hypothesis is based on the application of a strong external magnetic field on the fluid. Thus, everything happens as if the fluid were suspended in the applied field.

It is a completely different situation from a sink vortex, for example, where radial and axial velocities are considerable.

Assuming the flow as stationary and with axial symmetry,

$$\left(\frac{\partial}{\partial t} = 0\right) \quad \text{e} \quad \left(\frac{\partial}{\partial \theta} = 0\right)$$

Besides that, it is considered that $E_z = E_\Theta = 0$; $B_z = B_o \approx$ constant.

Thus, the system of equations proposed in the previous section becomes:

$$j_r \cong \sigma Er \quad ; \quad j_\theta = 0 \quad (9)$$

$$-\frac{V_\theta^2}{r} + \frac{1}{\rho}\frac{\partial p}{\partial r} = 0 \quad (10)$$

$$\rho g + \frac{\partial p}{\partial z} = 0 \quad (11)$$

$$\frac{\eta}{\rho}\left(\frac{\partial^2 V_\theta}{\partial r^2} + \frac{1}{r}\frac{\partial V_\theta}{\partial r} - \frac{V_\theta^2}{r}\right) - \frac{1}{\rho} Boj_r = 0 \quad (12)$$

The conservation of the electric charge or continuity of the electric current ensures that

$$\frac{1}{r}\frac{\partial}{\partial r}(rj_r) = 0 \quad (13)$$

With this we have that rJr is constant.

Taking into account that rJr is constant, in equation (12) and considering that

$$J = \frac{xjr}{\sigma Bo V_{\theta_o}}$$

e

$$x = \frac{r}{r_o}, V = \frac{V_\theta}{V_{\theta_o}}, V^* = \frac{E}{Bo V_{\theta_o}}, H = Bor_o\left(\frac{\sigma}{\eta}\right)^{1/2}$$

*https://dx.doi.org/10.22161/ijaers.5.1.12* *ISSN: 2349-6495(P) | 2456-1908(O)*

We arrive at the dimensionless form of equation (12), given by:

$$x^2\frac{\partial^2 V}{\partial x^2}+x\frac{\partial V}{\partial x}-V=xH^2J \tag{13}$$

The resolution of this linear and second-order differential equation is

$$V(x)=C_1\,x+\frac{C_2}{x}+\frac{H^2J}{2}x\ln x \tag{14}$$

The last term of equation (14) represents the electromagnetic driving force. The integration constants C1 and C2 are determined by the boundary condition given by:

1) V(x=1) = 0
2) $V(x=x_0) = V_0 \approx 0$, pois $x = \frac{r}{r_0} << 1$

Substituting the boundary conditions 1) and 2) in equation (13), we find

$$C_1=\frac{H^2j}{2}x_o^2\ln x_o \tag{15}$$

$$C_2=-\frac{H^2j}{2}x_o^2\ln x_o \tag{16}$$

It can be seen that the current density is related to the potential difference applied through the quantities explained by Eq. (9). In addition, taking into account the definition of V*, and making the necessary transformations[4], we have

$$V^*=\frac{1}{r_o Bo V_{\theta_o}}\int_{x_o}^{1}E_r dr=J\ln x_o \tag{17}$$

On the other hand, considering that $\vec{\omega}=\nabla\times\vec{V}$, taking the relations of Eq. (10), expressions for pressure and vorticity are easily found.

## IV. EXPERIMENTAL PART

In the specialized literature, there are few experimental works on the generation, measurement and analysis of vortexes by magneto hydrodynamics. Even so, most of them, like SOMMERIA[5], treat with relatively high electrical conductivity fluids, such as mercury, sodium and various liquid metal alloys, where the effects of induction play a relevant role and many approaches made in this paper do not apply. Then, with the purpose of adding something more relevant to the mentioned literature, we will present next an experiment that deals with the generation of a forced vortex, using as a working fluid the sea water and electromagnetic fields chosen in a convenient way.

### DESCRIPTION OF THE EXPERIMENT

In a cylindrical vessel, shown in fig. 1, two electrodes are fitted, one of which, of gold, is installed in the center of the vessel, is hemispherical 4 mm in diameter. The other is of stainless steel in ring format of variable diameter and concentric to the first. That is, sea water is added to the height of approximately 10cm. The cylinder with water rests on the basis of a solenoid of 50cm in diameter so as to benefit to the maximum from the intensity of the applied magnetic field which on average is of the order of 0.35 Tesla and is located very close to the center of the system. The solenoid is powered by a source, generating a current of the order of 90 A. Another electrical device provides an adjustable voltage that is applied between the two gold electrodes and stainless steel to establish a potential difference and hence an electric current in the liquid. The applied electric field ranges from zero to approximately 1000V / m.

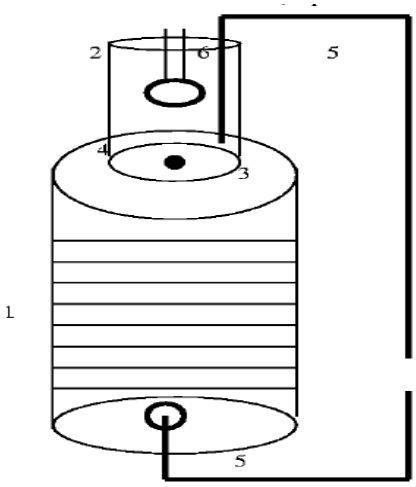


1- solenoid

2- cylinder with water

3-Gold Electrode

4- Ring Electrode

5- electrical circuit

6- Measuring rotor

*Fig.1: Experimental apparatus*

*https://dx.doi.org/10.22161/ijaers.5.1.12* *ISSN: 2349-6495(P) | 2456-1908(O)*

**SOME FINDINGS**

When only the electric field is acting, there is no movement of the liquid, however, at the instant it is applied, also, the magnetic field, starts to act the magnetic force. In this case, such force acts in the tangential direction and accelerates the fluid. In contrast, the Hartmann layer acts in order to conduct the electric current more easily in the radial direction, contributing to make the tangential force more intense. As can be deduced from the texts of SHERCLIFF and HUNT[6], under the conditions mentioned in the previous paragraph, an increase in the electric current density occurs. An experimental verification of the current circulation by the Hartmann layer can be inferred by moving the ring-shaped electrode along the axis of symmetry. It is noted[7], therefore, that the vortex continues to be formed and loses little intensity even when the ring-shaped electrode is displaced vertically.

## V. RESULTS

**Experiment-1**

In this case, for a pair of gold and brass electrodes, the following values were used: Fixed magnetic field, equal to B = 0.39T Rotor - R = 2.9 cm; Radius = 5.25 cm; Fluid column in cylinder - 6cm of water column; Rotor apparatus placed 1.5 cm from the surface; Room temperature.

In this way, the data of table 1

| ΔU (v) | Ω (c/s) | Ω (R.P.M.) |
|---|---|---|
| 25 | 21 | 1260 |
| 30 | 21,5 | 1290 |
| 35 | 22 | 1320 |
| 40 | 23 | 1380 |
| 50 | 24 | 1440 |
| 60 | 24,5 | 1470 |

*Tabela 1 – Valores de ΔU, Ω(Hz),Ω(RPM).*

The values of ΔU in volts and Ω, in RPM, allowed the sketch of graph 1.

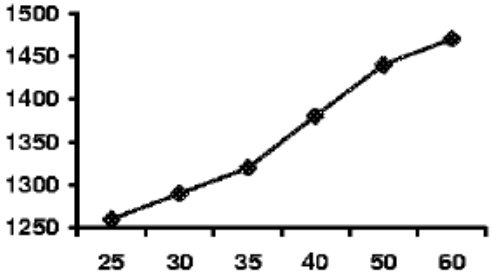


*Graph 1 of ΔU (Volt) and Ω (RPM).*

**Experiment 2:**

Magnetic field B = 0,39Tlas; water level 6cm; Radius = 5,25cm, with the measuring device 1.5cm from the surface; Temperature = 70C. In view of this, the data in table 2

| ΔU (v) | Ω (c/s) | Ω (R.P.M.) |
|---|---|---|
| 22 | 21,5 | 1290 |
| 30 | 23,5 | 1410 |
| 40 | 24,0 | 1440 |
| 50 | 24,0 | 1560 |

*Table 2 - Values of ΔU (V), Ω (Hz), Ω (RPM).*

The values of ΔU in volts and Ω, in RPM, allowed the sketch of graph 2.

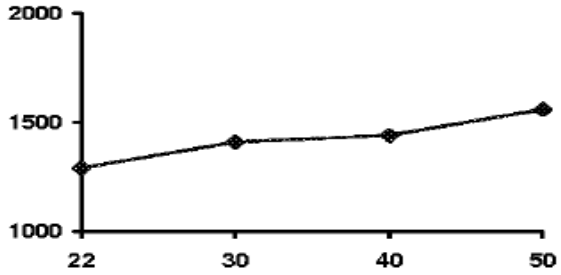


*Graph 2 of ΔU (Volt) and Ω (RPM).*

**Experiment 3:**

Measurement of vortex rotation using cork stopper; Magnetic field B = 0.36 Tesla; Gold and brass electrode; Container with 5cm of water column; Ring electrode placed on the bottom of the vessel; Radius = 5.25 cm

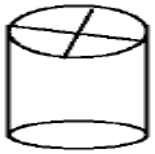

cork stopper

Therefore, the data presented in table 3

| ΔU (v) | Ω (R.P.M.) |
|---|---|
| 20 | 350 |
| 30 | 615 |
| 40 | 1100 |
| 50 | 1400 |

*Table 3 - Values of ΔU (V) and Ω (RPM)*

The values of ΔU in volts and Ω, in RPM, allowed the sketch of graph 3.

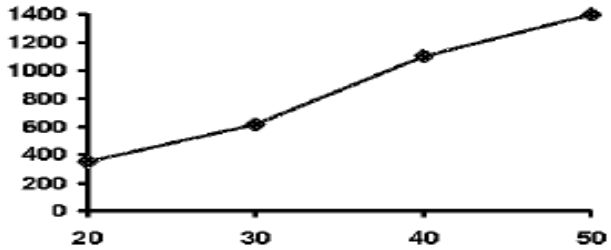


*Graph 3 of ΔU (Volt) and Ω (RPM).*

*https://dx.doi.org/10.22161/ijaers.5.1.12* *ISSN: 2349-6495(P) | 2456-1908(O)*

**Experiment 4:**

Keeping the voltage constant and varying the magnetic field. By doing this, we obtained the data from table 4

| TENSÃO | | VALORES MÉDIOS (CORRENTE) | CAMPO B |
|---|---|---|---|
| ΔU = 30V | $R_1 = 9,14\Omega$ | I = 3,28 A | $B_1 = 0,376$ T |
| ΔU = 30V | $R_2 = 9,43\Omega$ | I = 3,18 A | $B_2 = 0,365$ T |
| ΔU = 30V | $R_3 = 9,64$ | I = 3,11 A | $B_3 = 0,375$ T |
| ΔU = 30V | $R_1 = 9,80\Omega$ | I = 3,06 A | $B_4 = 0,39$ T |

Table 4 - Values of voltage, resistance, current and magnetic field

From table 4 was constructed the graph n.4 referring to the values of the electric resistance as a function of the magnetic field.

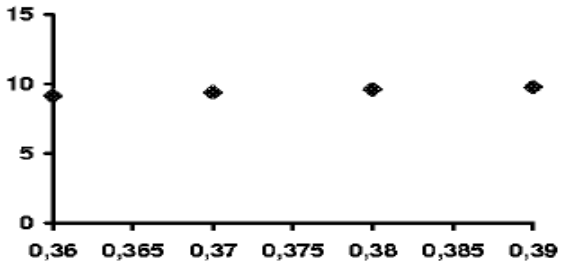


Graph 4 - Electrical resistance as a function of the magnetic field.

## VI. CONCLUSIONS

This work shows that seawater behaves in a somewhat surprising way as MHD working fluid. It can be concluded that the increase of the magnetic field intensity and the reduction of the electric current are of extreme importance for the increase of the speed of rotation and also of the efficiency of the experiment, since, the reduction of the electrical current causes the decrease of the Joule effect. The obtaining of new data, point by point, with more refined techniques, will be necessary to be able to compare the results with the proposed theoretical model and to change it in a compatible way, if it is the case. It was also verified an increase of the electric resistance as a function of the increase of the applied magnetic field. Theoretically, as SOMMERIA[5] indicates, the formula for resistance is:

$$R = \frac{Bo}{2\pi\sqrt{\sigma\eta}} \ln\left(\frac{Ro}{a}\right)$$

Since the constant a represents the radius of the core of the vortex and R0 corresponds to the radius of the cylindrical vessel.

Finally, some comments can be made between the theoretical model and the experimental part.

1. In the flow core, at first approximation, the viscosity can be neglected. Thus, by the Work - Energy theorem, we have that the velocity at a point of the fluid is given by:

$$V = \left(\frac{4\pi\sigma|\Delta\Phi|B_o}{\rho}\right)^{1/2}$$

Considering that:

$$\sigma = 4{,}3\frac{S}{m}$$

$|\Delta\emptyset| = 160V$ a 1,2 cm from the center of the container

$B_0 = 0{,}3$ Teslas $\qquad \rho = 1030\frac{kg}{m^3}$

The measured value of velocity V = 1.5 m / s, which can be compared with the theoretical value given by V = ωr, is obtained.

Taking the mean value for the angular velocity ω ≈ 1300RPM and, where r = 1.2 cm, we reached the value V = 1.6 m / s, being very close to the value measured experimentally.

At the core of the flow, the electric current tends to flow through the Hartmann layer, so we have j≈0, so it turns out that

$$\nabla\Phi' \approx \vec{V}\times\vec{B} \quad \text{e} \quad V \approx \frac{1}{B}\frac{\Delta\Phi}{\Delta r}$$

Substituting the velocity value V = 1.6 m / s and using a mean magnetic field value equal to 0.3 Teslas

$$\frac{\Delta\emptyset}{\Delta r} \approx 0{,}5\frac{V}{m}$$

That is within the expected value.

## REFERENCES

[1] BRAGINSKII, S.I. Magneto hydrodynamics of Weakly Conducting Liquids, Soviet Physics, JETP, v.37; n.5, 1960

[2] MOFFAT, H.K. Some problems in the Magneto hydrodynamics of Liquids Metal, ZAMM, v.58; 1978

[3] LEWELLEN, W.S.; Magneto hydrodinamically Driven Vortices, Proc. Heat Transf. Fluid Mech. Inst. Stanford University Press, v.1, 1960

[4] LANDAU,L. &LIEFCHITZ, E.; Electro Dynamics of Continuous Media, v.VIII, Ed.Mir, 1969.

[5] SOMMERIA,J.; Electrically Driven Vortices in a Strong Magnetic Field, J.Fluid Mech.v.189, 1988

*https://dx.doi.org/10.22161/ijaers.5.1.12* *ISSN: 2349-6495(P) | 2456-1908(O)*

[6] HUNT, J.C. & SHERCLIFF, J.A., 1971, Magneto hydrodynamics at High Hartmann Number, Ann. Rev. Fluid Mech., vol. 3, pp. 37-62.
[7] SHERCLIFF, J. A., 1970, Fluid Mechanics due to a electric current source, J. Fluid Mech., vol. 40, part 2, pp. 241-250.

https://dx.doi.org/10.22161/ijaers.5.1.13 ISSN: 2349-6495(P) | 2456-1908(O)

# Simulation model of the flow in the drainage system of Ambon city withexplicit finite difference method

Lenora Leuhery, Godfried Lewakabessy, Obednego D Nara

Lecturer Polytechnic Ambon, Jl. Ir Putuhena Wailela – Ambon Indonesia

***Abstract—*** *Analysis of flood modeling scenarios conducted on the simulation of urban drainage systems in Ambon city based on mathematical equations finite difference method which allows analyzing the water depth and flowing rate as a function of space and time. In order to study the propagation of flooding in the drainage channel with the 1D model of Saint Venant hydrodynamic equations are approximated by explicit MacCormack numerical method which is used as a simulation model. Numerical solution with MacCormack discretization technique on the parameters that influence the system can provide stable and final results that can be trusted. The purpose of this model is that it can reduce the volume of puddles on the local channel of drainage system area.*

***Keywords— Drainage System, Saint Venant, Mac Cormack, Ambon City.***

## I. INTRODUCTION

Flow in open channels can be classified in a steady flow and unsteady flow. The steady stream flow is classified in the absence of changes in water level over time. While the flow unsteady flow is characterized by a change in elevation and velocity with respect to time and changes in discharge or velocity against distance. Flow that occurs in nature almost cannot be classified in anunsteady flow.

Unsteady flow is classified into two types, they are unsteady flow that gradually varied flowand the rapidly varied flow. Unsteady flow phenomena can be formulated into mathematical equations in one, two, or three dimensions. The mathematical equation resulting is quite complicated and difficult to be solved analytically. So the common solution is to use numerical methods, one of which is the finite difference. One of the finite difference method is a method that has been known as Mac Cormak explicit.

In an open channel flow river / canal there are some common model to use in order to describe the flow of the channel as Saint Venant models [1,2,3,4,8,9,10] patterns of flood flow in open channel which can be approximated by differential equations partial and derived from of Saint Venat equation [13]. Hydraulics model is based on two forms of the equation is the equation of conservation of mass and momentum conservation equations [11] (Chow, 1988). The purpose of this study is to simulate case of one-dimensional flow in the drainage network system in Ambon city.

## II. METHODOLOGY

### 2.1 The Study Area

Ambon city is located on the coast and has a flat topography with elevation of 0 meters - 10 meters from the sea level and has a catchment area covering an area of 1.43 km2. Drainage system in the city of Ambon has 5 parts water catchment area with 3 small rivers which can directly flow from the drainage to dispose of the body directly into the river or sea. In accordance with the characteristics of the system area the climatic conditions in the city of Ambon has daily rainfall maximum of 455 mm which occurred on 28 August 1988 for data analysis rainfall 29 years and temperature maximum temperature that occurred was in January of 2004 at 30 º C and The minimum in February 2001 of 21.6 º C. During the period of the last six years (2007 - 2013) Ambon City area experienced flooding in the area and eventually the system impact of material and human losses. Causes of flooding caused changes in the function of land use, poor drainage system and will be less conscious of the impact of flood hazards.

*https://dx.doi.org/10.22161/ijaers.5.1.13* *ISSN: 2349-6495(P) | 2456-1908(O)*

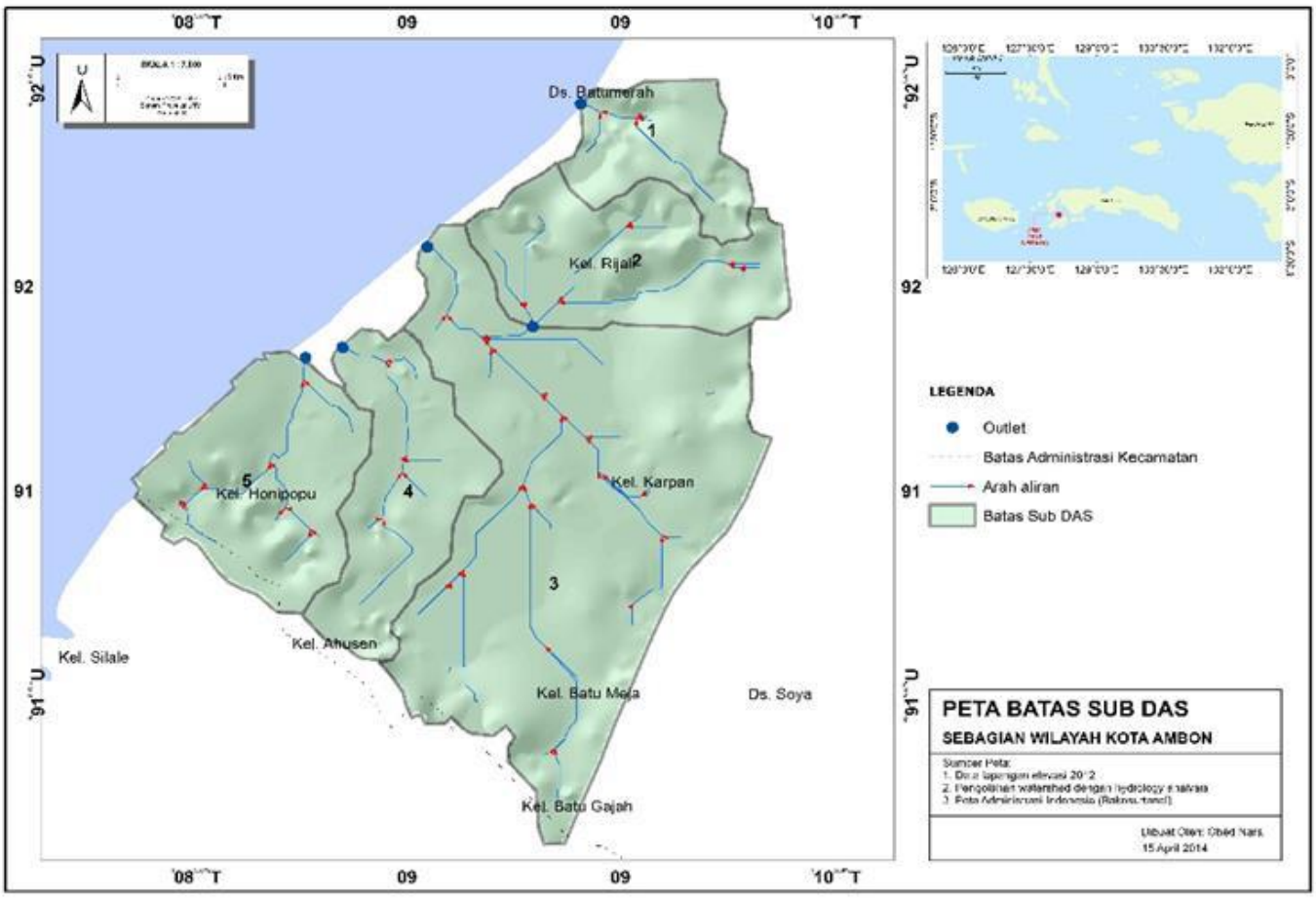


*Fig.1: Catchments areain Ambon city*

## 2.2 Numerical Model

The concept of a mathematical model used for the simulation of Ambon city drainage network system is a collection of mathematical description of the components hodrologi and hydraulics. The structure of the model and is determined by the objectives of development planning models. To facilitate the solution of mathematical model, then the model reduces to the numerical model. The purpose of the simulation model to learn a numeric behavior that is an event that occurs which is influenced by variables modifiers and other components as described in the concept of a model like image 2 below.

*https://dx.doi.org/10.22161/ijaers.5.1.13* *ISSN: 2349-6495(P) | 2456-1908(O)*

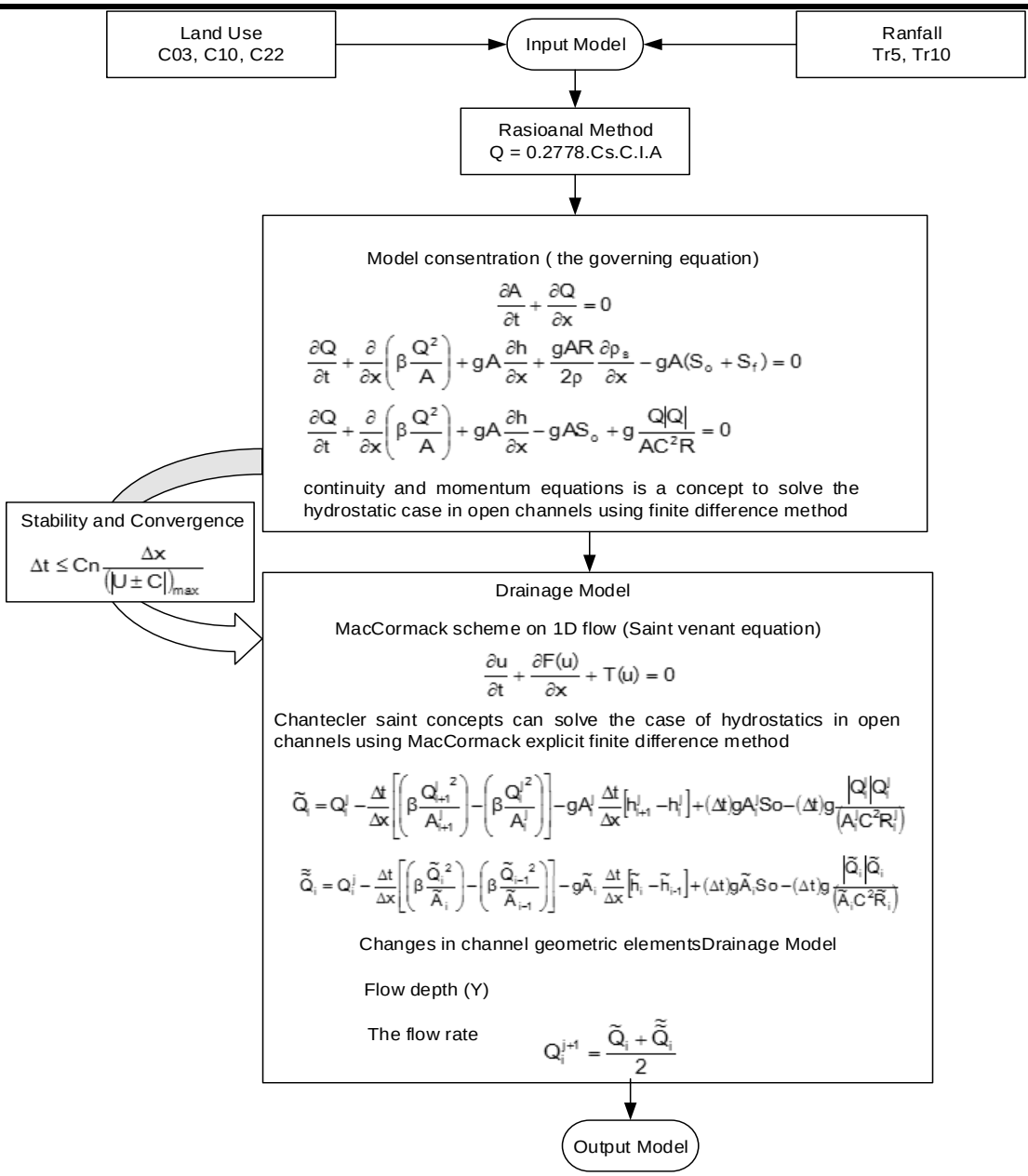


*Fig.2: Framework numerical of modeling scenarios*

**2.2.1 The governing equationsThe continuity equation**

The continuity equation [1,3,11] for unsteady flow there can be structured based on the mass conservation of a teller space, that is the mass rate of water entering the space look - mass flow of water coming out the room look the same as the rate of increase in volume / mass in the eye chamber , for the assumption of the continuity equation as follows:

- For the entire cross section of the channel

$$\frac{\partial A}{\partial t}+\frac{\partial Q}{\partial x}=q \qquad (1)$$

- If q = 0, then ;

$$\frac{\partial A}{\partial t}+\frac{\partial Q}{\partial x}=0 \qquad (2)$$

**Momentum Equation**

Momentum equation [7] derived from the concept of conservation of momentum, where the net rate of momentum entering the room look + Number of the forces acting on the space look = The rate of accumulation of momentum in the eye chamber.

The momentum equation taking into account the net rate of momentum, hydrostatic force, changes in fluid density and friction force, with the simplifying assumptions stated earlier, is obtained as follows:

*https://dx.doi.org/10.22161/ijaers.5.1.13* *ISSN: 2349-6495(P) | 2456-1908(O)*

$$\frac{\partial Q}{\partial t}+\frac{\partial}{\partial x}\left(\beta\frac{Q^2}{A}\right)+gA\frac{\partial h}{\partial x}+\frac{gAR}{2\rho}\frac{\partial \rho_s}{\partial x}-gA(S_o+S_f)=0 \quad (3)$$

$$\frac{\partial Q}{\partial t}+\frac{\partial}{\partial x}\left(\beta\frac{Q^2}{A}\right)+gA\frac{\partial h}{\partial x}+\frac{gAR}{2\rho}\frac{\partial \rho_s}{\partial x}-gAS_o+g\frac{Q|Q|}{AC^2R}=0 \quad (4)$$

if the fluid density is assumed constant, then we obtain :

$$\frac{\partial Q}{\partial t}+\frac{\partial}{\partial x}\left(\beta\frac{Q^2}{A}\right)+gA\frac{\partial h}{\partial x}-gAS_o+g\frac{Q|Q|}{AC^2R}=0 \quad (5)$$

### 2.2.2 Model discretization and MacCormack Schemes

One of the schemes that are commonly used for analysis of variable explicitly on the channel is the difference until MacCormack method [5]. After using the shape derivative approach to explicit difference, that enter the differential equation, the price of a time function on the grid point interval = t + Δt waktut along the x-axis and y-axis can be calculated directly by using the values of the function at the point near him at the time interval t = Δt known. Development explicitly have a weakness, because it is necessary to obtain stability calculation restrictions interval Δt.

The concept models of the flow in the drainage system are;

- The time interval (Δt): By using the MacCormack explicit finite difference equation where the price function of a lattice point at time interval = t + Δt along the x-axis and y-axis can be calculated directly by using the values of the function at a nearby point on the hose time t = Δt known. Development explicitly have a weakness, because it is necessary to obtain stability calculation restrictions interval Δt.
- The interval distance (Δx): Changes in the distance added to the terms of the initial conditions along the drainage of free water level.
- Volume Control: The volume control is used to control the continuity and momentum equations in fluid density changes in hydrostatic force and the friction force on the liquid. In the picture above is the Qin discharge Qout incoming volume control which is a discharge coming out of the control volume where Δx is the length of the control volume PIAs ∂ Q / ∂ x which is the change in the value of Q along Δx.
- Stabilization flow: In order to assert a condition where the flow conditions are considered stable, then Cn (Courant number) is a necessary condition.
- Elements of geometric channel
  Channel width (b), High water in the channel (h), channel length (L) is a parameter used in modeling the flow.
  In general, explicit MacCormack numerical scheme is divided into two phases: phase predictor and corrector. For more details can be seen In Figure 3 below;

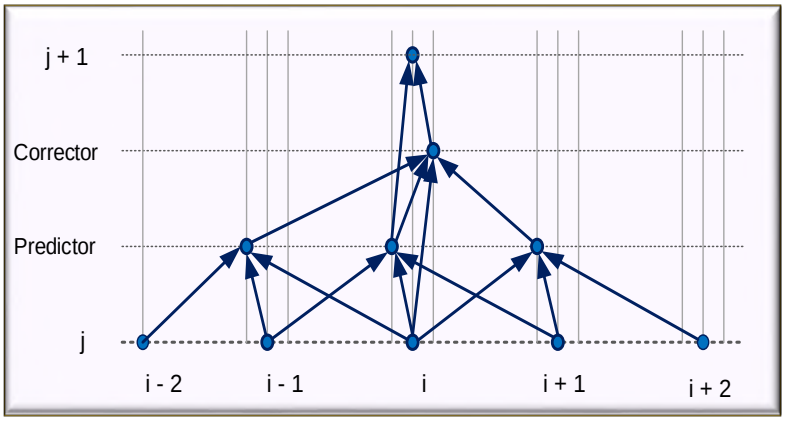


*Fig.3: MacCormack scheme*

Application of the MacCormack scheme Flow Equation 1 Dimensions (Saint Venant Equation) will be as follows:

*https://dx.doi.org/10.22161/ijaers.5.1.13* *ISSN: 2349-6495(P) | 2456-1908(O)*

$$\frac{\partial u}{\partial t}+\frac{\partial F(u)}{\partial x}+T(u)=0 \quad (6)$$

fittings flow equation above with Mac Cormack gives [1,2,5]

Predictor:

$$\tilde{U}_i = U_i^j \frac{\Delta t}{\Delta x}\left[F(u)_{i+1}^j - F(u)_i^j\right] - \Delta t T(u)_i^j \quad (7)$$

Corrector:

$$\bar{\bar{U}} = U_i \frac{\Delta t}{\Delta x}\left[F(\tilde{u})_i - F(\tilde{u})_{i-1}\right] - \Delta t \tilde{T}(u)_i \quad (8)$$

$U_i^{j+1}$ = 0.5*(Upredictor + Ucorrector) (9)

The continuity equation for a wide cross-section per unit

$$U_i^{n+1} = \frac{\tilde{U}_i + \bar{\bar{U}}_i}{2} \quad (10)$$

The continuity equation for a wide cross-section per unit

$$\frac{\partial h}{\partial t}+\frac{\partial uh}{\partial x}=0 \quad (11)$$

$$\frac{\partial h}{\partial t}+h\frac{\partial u}{\partial x}+u\frac{\partial h}{\partial x}=0 \quad (12)$$

Pengepingan equation (12) with Mac Cormack: $\tilde{h}_i = h_i^j - h_i^j \frac{\Delta t}{\Delta x}\left[u_{i+1}^j - u_i^j\right] - u_i^j \frac{\Delta t}{\Delta x}\left[h_{i+1}^j - h_i^j\right]$

(13)

$$\tilde{\tilde{h}}_i = h_i^j - \tilde{h}_i \frac{\Delta t}{\Delta x}\left[\tilde{u}_i - \tilde{u}_{i-1}\right] - \tilde{u}_i \frac{\Delta t}{\Delta x}\left[\tilde{h}_i - \tilde{h}_{i-1}\right]$$

$$h_i^{j+1} = \frac{\tilde{h}_i + \tilde{\tilde{h}}_i}{2} \quad (14)$$

$$h_i^{j+1} = \frac{\tilde{h}_i + \tilde{\tilde{h}}_i}{2}$$

$$= \frac{1}{2}\left\{h_i^j - h_i^j \frac{\Delta t}{\Delta x}\left[u_{i+1}^j - u_i^j\right] - u_i^j \frac{\Delta t}{\Delta x}\left[h_{i+1}^j - h_i^j\right] + h_i^j - \tilde{h}_i \frac{\Delta t}{\Delta x}\left[\tilde{u}_i - \tilde{u}_{i-1}\right] - \tilde{u}_i \frac{\Delta t}{\Delta x}\left[\tilde{h}_i - \tilde{h}_{i-1}\right]\right\}$$

$$= h_i^j - \frac{\Delta t}{2\Delta x}\left\{h_i^j\left[u_{i+1}^j - u_i^j\right] + u_i^j\left[h_{i+1}^j - h_i^j\right] + \tilde{h}_i\left[\tilde{u}_i - \tilde{u}_{i-1}\right] + \tilde{u}\left[\tilde{h}_i - \tilde{h}_{i-1}\right]\right\}$$

$$h_i^{j+1} = hj - \frac{\Delta t}{2\Delta x}\left\{h_i^j\left[u_{i+1}^j - u_i^j\right] + u_i^j\left[h_{i+1}^j - h_i^j\right] + \tilde{h}_i\left[\tilde{u}_i - \tilde{u}_{i-1}\right] + \tilde{u}\left[\tilde{h}_i - \tilde{h}_{i-1}\right]\right\} \quad (15)$$

- In state n, t, dx = 0 then all the parameters on the node (i, j) are the values that are used as initial conditions in terms of this model.
- In state n, t, dx> 0; high value of water in the channel (h) is proportional to the width of the channel cross section (b) in (i, j).

Momentum equation cross-section per unit width

$$\frac{\partial uh}{\partial t}+\frac{\partial}{\partial x}\left(\beta u^2 h\right)+gh\frac{\partial h}{\partial x}+g\frac{hR}{\rho}\frac{\partial \rho_s}{\partial x}-gh(So-Sf)=0$$

The above equation is the momentum equation in the absence of adverse runoff. If the hydrostatic force due to density differences are ignored then the equation (11) becomes

*https://dx.doi.org/10.22161/ijaers.5.1.13* *ISSN: 2349-6495(P) | 2456-1908(O)*

$$\frac{\partial uh}{\partial t}+\frac{\partial}{\partial x}\left(\beta u^2 h\right)+gh\frac{\partial h}{\partial x}-gh(So-Sf)=0 \quad (16)$$

$$u\frac{\partial h}{\partial t}+h\frac{\partial u}{\partial t}+\frac{\partial}{\partial x}\left(\beta u^2 h\right)+gh\frac{\partial h}{\partial x}-gh(So-Sf)=0 \quad (17)$$

By using equations (2) and (4) to pengepingan to equation (1) the importance of the equation (18) and (19) below;

$$\tilde{Q}_i=Q_i^j-\frac{\Delta t}{\Delta x}\left[\left(\beta\frac{Q_{i+1}^{j\,2}}{A_{i+1}^j}\right)-\left(\beta\frac{Qj^2}{A_i^j}\right)\right]-gA_i\frac{\Delta t}{\Delta x}\left[h_{i+1}^j-h_i^n j\right]+(\Delta t)gA_i^j So-(\Delta t)g\frac{\left|Q_i^j\right|Q_i^j}{\left(A_i^n C^2 R_i^j\right)} \quad (18)$$

$$\tilde{\tilde{Q}}_i=Q_i^j-\frac{\Delta t}{\Delta x}\left[\left(\beta\frac{\tilde{Q}_i^{\,2}}{\tilde{A}_i}\right)-\left(\beta\frac{\tilde{Q}_{i-1}^{\,2}}{\tilde{A}_{i-1}}\right)\right]-g\tilde{A}_i\frac{\Delta t}{\Delta x}\left[\tilde{h}_i-\tilde{h}_{i-1}\right]+(\Delta t)g\tilde{A}_i So-(\Delta t)g\frac{\left|\tilde{Q}_i\right|\tilde{Q}_i}{\left(\tilde{A}_i C^2\tilde{R}_i\right)} \quad (19)$$

Equation (18) and (19) become equation (20)

$$Q_i^{j+1}=\frac{\tilde{Q}_i+\tilde{\tilde{Q}}_i}{2} \quad (20)$$

The above equation is the equation of the predictor and corrector MacCormack explicit numerical methods for simulation of 1D flow in the channel [5].

Value Debit (Q) on the initial conditions at each node (i, j) is the same as using the Manning equation whereas the discharge value (n +1) has the same value as the initial condition and the condition (i, j +1) value obtained discharge initial conditions of discharge for discharge predictions in total the correction divided by two or discharge (Qp + Qc) / 2.

### 2.2.3 Initial Conditions and Boundary Conditions

Mac Cormack method is the explicit calculation of the non-staggerred **pembaganan** scheme. To resolve the above discrete equation with this method required some values that are known / defined. These values are called the boundary condition (boundary condition) and the initial conditions (initial condition) [5,6,]

Initial conditions (initial condition) is the determination of the initial values, good water level (h) and discharge (Q), at any point in time the calculation was first started. Making this initial value arranged for not too much with the actual conditions. Intake values are much different from the true value will make the calculations more iterations, so the calculation time is longer (time consuming).

Boundary condition (boundary condition) that is required consists of the downstream boundary condition (down stream boundary) and upstream boundary conditions (up stream boundary) to a fluctuating water level h = f (t) or can also discharge data (water inflow) at any time, Q = f (t).

### 2.2.4Stability Criteria

Figures from the Courant-Friedrichs-Lewy (CFL) condition express a necessary condition for the convergence of the explicit finite difference scheme dependence domain. Where the issue involves discrete domain differential equations in finite difference boundary is close to zero. Conditions Courant-Friedrichs-Lewy (CFL condition) is a necessary condition for stability while in order to solve certain partial differential equations (PDE usually hyperbolic) numerically with a finite difference method. This figure appears in an explicit numerical analysis of time-based scheme, when it is used for numerical solution. For MacCormack scheme on time step as other explicit scheme, must meet the Courant stability criterion Friedrich-Lewy (CFL) [6,11] as the following equation:

$$\Delta t\le Cn\frac{\Delta x}{\left(\left|U\pm C\right|\right)_{max}} \quad (21)$$

## III. APPLICATION SIMULATION MODEL

In order to determine the effect of water level and discharge in the channel as shown in figure 5 below the channel that is used as a model for in simulate with the red line. The parameters in the model are defined as the channel length (L) = 112 m, channels with a rectangular cross-section of the channel width (b) = 2 m; the slope of the line (S0) = 0.00071; cross-section correction factor (β) = 1; channel wall roughness (n) = 0.025. Simulations performed with the number of nodes on the line segment by 21 grid so that the channel is divided into several sections with Δx = 5.6 m and the interval Δt = 1 sec. With the Courant number (Cn) = 0.583. In this case the initial value of high water in saluran1, 163 m obtained by using the Manning equation [12]. Boundary condition on the

*https://dx.doi.org/10.22161/ijaers.5.1.13* *ISSN: 2349-6495(P) | 2456-1908(O)*

steady flow case is to set the flow rate at the upstream (x = 0) at Q = 1.062 m3/sec. The results of the simulation model can be seen in the table Q and Q predictor corrector below.

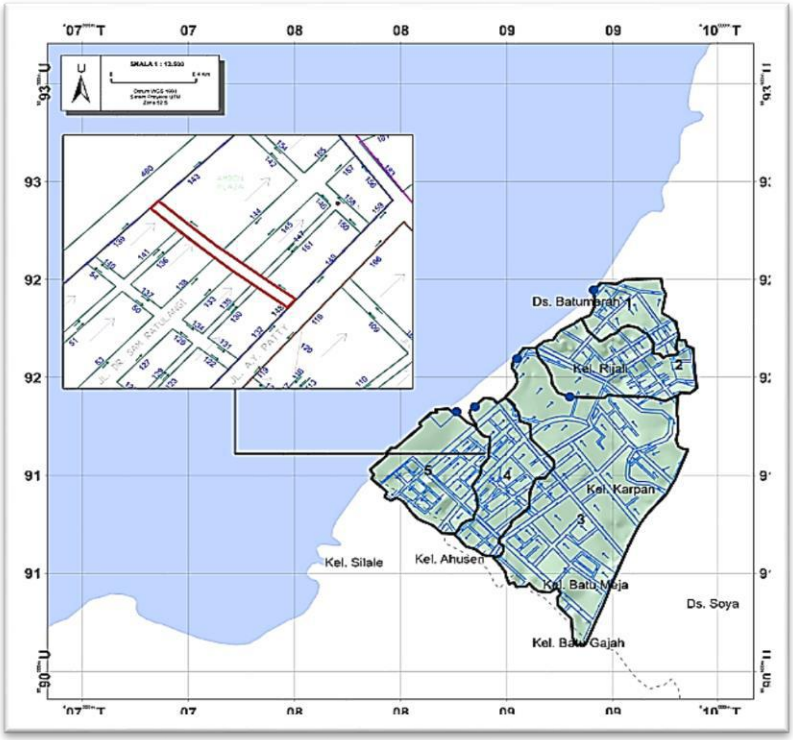


*Fig.4: Layout of drainage network distribution system*

*Table.1: Initial conditions stedy flow*

| t=0 | Node | | | | | | | | | | | | | | | | | | | | |
|---|---|---|---|---|---|---|---|---|---|---|---|---|---|---|---|---|---|---|---|---|---|
| | 1 | 2 | 3 | 4 | 5 | 6 | 7 | 8 | 9 | 10 | 11 | 12 | 13 | 14 | 15 | 16 | 17 | 18 | 19 | 20 | 21 |
| h | 0,758 | 0,758 | 0,758 | 0,758 | 0,758 | 0,758 | 0,758 | 0,758 | 0,758 | 0,758 | 0,758 | 0,758 | 0,758 | 0,758 | 0,758 | 0,758 | 0,758 | 0,758 | 0,758 | 0,758 | 0,758 |
| Q | 1,062 | 1,062 | 1,062 | 1,062 | 1,062 | 1,062 | 1,062 | 1,062 | 1,062 | 1,062 | 1,062 | 1,062 | 1,062 | 1,062 | 1,062 | 1,062 | 1,062 | 1,062 | 1,062 | 1,062 | 1,062 |

*Table.2: Conditions steady simulation models*

| Node | n | t | dx | h | A | P | R | C2 | Q | Ap | Qp | hp | Pp | Rp | (C2)p | Ac | Qc |
|---|---|---|---|---|---|---|---|---|---|---|---|---|---|---|---|---|---|
| 1 | | | | 0,758 | 1,516 | 3,516 | 0,43 | 1208,8 | 1,0624 | 1,516 | 1,06 | 0,758 | | | | | 1,0624 |
| 5 | | | | 0,758 | 1,516 | 3,516 | 0,43 | 1208,8 | 1,0624 | 1,516 | 1,06 | 0,758 | 3,516 | 0,43 | 1209 | 1,516 | 1,0627 |
| 10 | 0 | 0 | 0 | 0,758 | 1,516 | 3,516 | 0,43 | 1208,8 | 1,0624 | 1,516 | 1,06 | 0,758 | 3,516 | 0,43 | 1209 | 1,516 | 1,0627 |
| 15 | | | | 0,758 | 1,516 | 3,516 | 0,43 | 1208,8 | 1,0624 | 1,516 | 1,06 | 0,758 | 3,516 | 0,43 | 1209 | 1,516 | 1,0627 |
| 21 | | | | 0,758 | 1,516 | 3,516 | 0,43 | 1208,8 | 1,0624 | | | | | | | | 1,0624 |

*Table.3: Analysis of numerical models*

*https://dx.doi.org/10.22161/ijaers.5.1.13* *ISSN: 2349-6495(P) | 2456-1908(O)*

| t | dx | h | A | P | R | C2 | Q | Ap | Qp | hp | Pp | Rp | (C2)p | Ac | Qc |
|---|---|---|---|---|---|---|---|---|---|---|---|---|---|---|---|
| 5 | 28 | 0,759 | 1,516 | 3,516 | 0,43 | 1208,8 | 1,062 | 1,516 | 1,06 | 0,758 | | | | | 1,062 |
| | | 0,759 | 1,516 | 3,516 | 0,43 | 1208,8 | 1,0636 | 1,516 | 1,06 | 0,758 | 3,516 | 0,43 | 1209 | 1,516 | 1,0639 |
| | | 0,759 | 1,516 | 3,516 | 0,43 | 1208,8 | 1,0636 | 1,516 | 1,06 | 0,758 | 3,516 | 0,43 | 1209 | 1,516 | 1,0639 |
| | | 0,759 | 1,516 | 3,516 | 0,43 | 1208,8 | 1,0636 | 1,516 | 1,06 | 0,758 | 3,516 | 0,43 | 1209 | 1,516 | 1,0639 |
| | | 0,759 | 1,516 | 3,516 | 0,43 | 1208,8 | 1,0636 | | | | | | | | 1,062 |

| t | dx | h | A | P | R | C2 | Q | Ap | Qp | hp | Pp | Rp | (C2)p | Ac | Qc |
|---|---|---|---|---|---|---|---|---|---|---|---|---|---|---|---|
| 10 | 56 | 0,767 | 1,516 | 3,516 | 0,431 | 1208,8 | 1,062 | 1,516 | 1,06 | 0,758 | | | | | 1,062 |
| | | 0,767 | 1,516 | 3,516 | 0,431 | 1208,8 | 1,0652 | 1,516 | 1,07 | 0,758 | 3,516 | 0,43 | 1209 | 1,516 | 1,0656 |
| | | 0,767 | 1,516 | 3,516 | 0,431 | 1208,8 | 1,0652 | 1,516 | 1,07 | 0,758 | 3,516 | 0,43 | 1209 | 1,516 | 1,0655 |
| | | 0,767 | 1,516 | 3,516 | 0,431 | 1208,8 | 1,0652 | 1,516 | 1,07 | 0,758 | 3,516 | 0,43 | 1209 | 1,516 | 1,0655 |
| | | 0,767 | 1,516 | 3,516 | 0,431 | 1208,8 | 1,0652 | | | | | | | | 1,062 |

| t | dx | h | A | P | R | C2 | Q | Ap | Qp | hp | Pp | Rp | (C2)p | Ac | Qc |
|---|---|---|---|---|---|---|---|---|---|---|---|---|---|---|---|
| 15 | 84 | 0,779 | 1,516 | 3,516 | 0,431 | 1208,8 | 1,062 | 1,516 | 1,06 | 0,758 | | | | | 1,062 |
| | | 0,779 | 1,5164 | 3,5164 | 0,431 | 1208,8 | 1,0672 | 1,516 | 1,07 | 0,758 | 3,516 | 0,43 | 1209 | 1,517 | 1,068 |
| | | 0,779 | 1,516 | 3,516 | 0,431 | 1208,8 | 1,0668 | 1,516 | 1,07 | 0,758 | 3,516 | 0,43 | 1209 | 1,516 | 1,0671 |
| | | 0,779 | 1,516 | 3,516 | 0,431 | 1208,8 | 1,0668 | 1,516 | 1,07 | 0,758 | 3,516 | 0,43 | 1209 | 1,516 | 1,0671 |
| | | 0,779 | 1,516 | 3,516 | 0,431 | 1208,8 | 1,0684 | | | | | | | | 1,062 |

| t | dx | h | A | P | R | C2 | Q | Ap | Qp | hp | Pp | Rp | (C2)p | Ac | Qc |
|---|---|---|---|---|---|---|---|---|---|---|---|---|---|---|---|
| 20 | 112 | 0,800 | 1,516 | 3,516 | 0,431 | 1208,8 | 1,062 | 1,517 | 1,06 | 0,759 | | | | | 1,062 |
| | | 0,800 | 1,5179 | 3,5179 | 0,431 | 1208,8 | 1,0713 | 1,518 | 1,07 | 0,759 | 3,518 | 0,43 | 1208 | 1,518 | 1,0736 |
| | | 0,800 | 1,516 | 3,516 | 0,431 | 1208,8 | 1,0684 | 1,516 | 1,07 | 0,758 | 3,516 | 0,43 | 1209 | 1,516 | 1,0687 |
| | | 0,800 | 1,516 | 3,516 | 0,431 | 1208,8 | 1,0684 | 1,516 | 1,07 | 0,758 | 3,516 | 0,43 | 1209 | 1,516 | 1,0687 |
| | | 0,800 | 1,5555 | 3,5555 | 0,437 | 1208,8 | 1,1736 | | | | | | | | 1,062 |

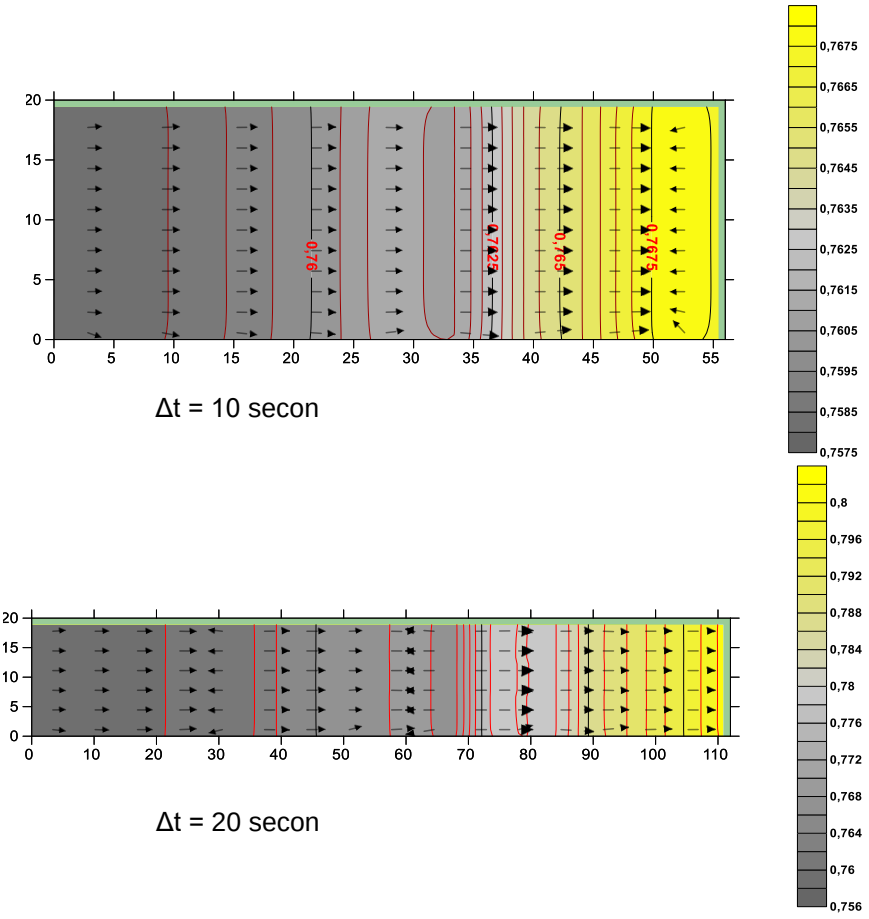


*Fig.5: Contours of flow and change the time on the channel at node 148*

*https://dx.doi.org/10.22161/ijaers.5.1.13* *ISSN: 2349-6495(P) | 2456-1908(O)*

From the results of numerical experiments running on the channel at node 148 with the boundary condition is the condition of high water in the channel on condition of t = 0; h = 0.78 meters and the inflow at node 1 = Q at the beginning and the end node 21 = Q. Channel propagation process that occurs at node 148 provides an overview to the fluctuation of water level changes resulting from a change in the distance and the change of time increase

The results of numerical calculations for changes in overtime 10 seconds and 20 seconds at a distance equal to the channel at node 148 which gives an overview of the direction of flow has distributed nearly perpendicular to the flow pattern in a cross section of the channel and the water surface contour changes in longitudinal cross section gives an overview of where each channel presence increment Δx and Δt, the closer the contour lines which led to increased fluctuations in discharge and water level in the channel will be higher than normal.

## IV. Conclusion

The use of explicit MacCormack method provides an easy to model analysis but has a weakness in the interval (Δt) in the simulation.

- Determination of boundary conditions and initial conditions must be adapted to the geometry of the channel element because in this case the channel cross section is relatively small.
- The more grids used in the simulation indicates a condition will be stable flow conditions

## REFERENCES

[1] Amanda J. Crossley, Nigel G. Wright and Chris D. Whitlow ., *Local Time Stepping for Modeling Open Channel Flows* DOI: 10.1061/(ASCE)0733-9429(2003)129:6(455).2003

[2] Cevza Melek Kazezyılmaz-Alhan, A.M.ASCE, and Miguel A. Medina Jr., F.ASCE., *Kinematic and Diffusion Waves: Analytical and Numerical Solutions to Overland and Channel Flow*. DOI: 10.1061/(ASCE)0733-9429(2007)133:2(217). 2007.

[3] Chad M. Cristina, A.M.ASCE, and John J. Sansalone, M.ASCE ; *Kinematic Wave Model of Urban Pavement Rainfall-Runoff Subject to Traffic Loadings* DOI: 10.1061 /(ASCE) 0733-9372(2003)129:7(629).2003.

[4] D. Ga˛siorowski a, R.Szymkiewicz., *Mass and momentum conservation in simplified flood routing models*. Journal homepage: www.elsevier.com /locate/jhydrol. Received 7 March 2007; Received in revised form 10 August 2007; accepted 21 August 2007.

[5] D. Pantelakis, Th. Zisis A.D. Nikolaou , E. Anastasiadou Partheniou E. Baltas.,*Hydraulic models for the simulation of flow routing in drainage canals*. Global NEST Journal, Vol 15, No 3, pp 315-323, 2013.

[6] G. Akbari , B. Firoozi.,*Implicit and Explicit Numerical Solution of Saint-Venent Equations for Simulating Flood Wave in Natural Rivers*.5th National Congress on Civil Engineering, May 4-6, 2010, Ferdowsi University of Mashhad, Mashhad, Iran. 2010.

[7] Han Dong, Fang Hong-wei, Bai Jing, He Guo-jian., *A coupled 1-d and 2-D channel network mathematical model used for flow calculation in the middle reaches of the yangtze river*. DOI: 10.1016/S1001-6058(10)60145-X .ScienceDirect.Received June 27, 2010, Revised May 28, 2011.

[8] Pantelakis D., Zissis Th., Anastasiadou-Partheniou E., Baltas e.Simulation of flow routing in a network of drainage canals at northern greece.Protection and restoration of the environment XI. 2013

[9] P. Mirzazadeh,G Akbari., A case study of flood dynamic wave simulation in natural waterways using numerical solution of unsteady flows . Comp. Meth. Civil Eng., Vol. 3, 2 (2012) 67-77. Received 13 March 2013; accepted in revised form 24 July 2013.

[10] Prasada Rao., *Numerical modeling of open channels flows with moving fronts using a variable boundary formulation*. www.elsevier.com/locate/amc. Applied Mathematics and Computation 182 92006) 369-282.and Computation 161 (2005) 599–610. 2005.

[11] Stephen Boon Kean Tan, Lloyd Hock Chye Chua,Eng Ban Shuy, Edmond Yat-Man Lo, A.M.ASCE, and Lai Wan Lim.,*Performances of Rainfall-Runoff Models Calibrated over Single and Continuous Storm Flow Events*. DOI: 10.1061/(ASCE) 1084-0699(2008) 13:7(597). 2008.

[12] Xin Liu, Abdolmajid Mohammadian and Julio Angel Infante Sedano.,*One Dimensional Numerical Simulation of Bed Changes in Irrigation Channels using Finite Volume Method*. Irrigation & Drainage Systems Engineering. http://dx.doi.org/10.4172/2168-9768.1000103. 2012 .

*https://dx.doi.org/10.22161/ijaers.5.1.14* *ISSN: 2349-6495(P) | 2456-1908(O)*

# Water Quality Considerations in Rainwater Harvesting Case Study of Heavy Metal Contamination in Kampala City

Ono Felix Tebangula[1], Mulindi Solomon Adekhela[2]

[1]Department of Agriculture Livestock and Fisheries Development, Agriculture Mechanization Services - Siaya County, P.O. Box 803-40600 Siaya.

[2]Department of Agriculture and Bio systems Engineering, University of Eldoret, P.O. Box 1125-30100 Eldoret

***Abstract—*** *Past studies have established a link between industrialization and heavy metal contamination of rainwater. However, no such study has been done in Kampala, or elsewhere in Uganda. In view of industrialization and the proliferation of iron roofs, this study aimed at addressing the suitability of rainwater harvesting and its quality as an alternative source of drinking water supply. The specific objectives were; to identify the predominant roof-covering materials in use in Kampala; to determine the level of heavy metal contamination obtained from each of these roof materials; and to compare the quality of water obtained, with various accepted standards for drinking water. The roof coverings considered were clay tiles, plain Galvanized Corrugated Iron (GCI) sheets and painted GCI sheets. In each of these types, they were further classified as relatively new, medium age and the relatively older. Samples were collected from each of the five divisions, including a control sample that was intercepted directly from open space. In the laboratory, heavy metal tests were performed on these samples, using a Flame Atomic Absorption Spectrophotometer. The metals tested were Cadmium, Copper, Lead, Zinc and Nickel.*

***Keywords***— ***Rainwater, Kampala City, Heavy Metal***

## I. INTRODUCTION

The Development Technology Unit (DTU) [2] appreciates the fact that much research work has been done in the world on domestic Rainwater Harvesting (RWH). They, however, contend that there is a lot more to be researched in humid tropics, especially in regard to health concerns associated with domestic RWH; storage capacity versus cost; and implementing domestic RWH in the sphere of integrated water resource management. In order to change the attitude by which RWH is treated as "second class" water supply source, a wide-sweeping awareness and sensitization campaign targeting users, promoters and planners is necessary. If widely practiced in urban areas, RWH helps reduce runoff, hence less flooding and ultimately saving on cost of extending storm water drainage infrastructure [5].

According to [3], wastewater released by some Ugandan industries into agricultural land has heavy metal content above internationally accepted concentration levels, thus posing a health risk to consumers. Soil was sampled from thirty-five sites with a history of waste disposal and was subsequently tested for Cadmium, Copper, Lead, Zinc and Nickel contents using a Flame Atomic Absorption Spectrophotometer.

Consequently, analytical results showed that vegetables sampled from the industrial area have higher concentrations of zinc, lead and copper than those grown at sites irrigated by municipal wastewater and solid waste from dumping sites. The high heavy metal content in these vegetables was attributed to multiple exposure routes (contaminated soil, soil splash onto leafy vegetables, absorption from aerial emissions, and direct contact with effluents during the rainy season). This view has given this study the impetus to further pursue the possibility that heavy metal-laden aerial emissions remain in the atmosphere for long enough to mix with the rain-causing clouds, and thus contaminate the rain.

The comparison of RWH to other technologies that provide the same level of service can be properly appreciated when approached in a wider context in which in addition to cost considerations, encompasses other concerns that may include social, economic technical and environmental aspects. RWH systems provide appropriate and economically attractive technologies in regard to operation and maintenance requirements, horizon of service and environmental concerns. The technology has very minimal environmental impact and is predicated on the use of a renewable resource, unlike other sources, which are subject to depletion and increased pollution. As such, RWH is commensurate development in the new world order [5].

Further, the piped water from the Ggaba Water Treatment Plant might not in the future be feasible due to either the

*https://dx.doi.org/10.22161/ijaers.5.1.14* *ISSN: 2349-6495(P) | 2456-1908(O)*

chemical content, or its prohibitive costs of treatment, should the Nakivubo wetland's deterioration continue unabated [6]

Kampala is known to receive at least 1000 mm of rainfall a year which makes RWH a viable alternative to provide drinking water, in addition to other domestic requirements.

## II. METHODOLOGY

### 2.1 Geographical Area

The study confined itself to areas in Kampala City. Each of the administrative divisions in Kampala, which are, Kawempe, Makindye, Nakawa, Rubaga and Central, were represented in the study. The main reasons for the choice of this geographical area were the budgetary and time constraints, as well as keeping the study relevant.

### 2.2 Sampling Population and Strategies

The population of the study included the three predominant different types of roof coverings in use in Kampala. Hence, the study essentially confined itself to clay tiles; plain galvanized corrugated iron sheets and painted galvanized corrugated iron sheets. In each of these types, there was a further sub-classification of the relatively new, medium age and the relatively older. Samples were collected from each of the five divisions, including a control sample that was intercepted directly from open space, from each division. There were therefore fifty rainwater samples in all for the study. The random sampling strategy was engaged to pick the sampling sites. Maps of each Kampala administrative division were obtained, where each parish was clearly marked out. Each parish was assigned a number, and the ten sites for sample collection were randomly picked from a set of random numbers. This was done for each of the five divisions. Each of the fifty rainwater samples was tested for five heavy metals.

### 2.3 Data Collection

The samples of rainwater were collected in appropriately coded plastic anaesthised sampling bottles. The codes for each sample were formulated in the following manner: The code for each sample contained three digits. The first digit of the code would give the administrative division where the sample was collected. The second digit would give the roof covering material. It would also denote the control sample if labeled appropriately. The third digit would denote the age of the roof. For example, "KX1" refers to Kawempe New Clay Tile roof. The coding scheme was as shown in Table 1, below:

*Table.1: Coding Scheme for Data Collection*

| ***Location*** | ***Material*** | ***Age*** |
|---|---|---|
| Kawempe – K | Clay Tiles – C | New (1-2 yrs) – 1 |
| Central – C | Plain GCI Sheets – Y | Medium Age (2-10 yrs) – 2 |
| Nakawa – N | Painted GCI Sheets – Z | Old (>10 yrs) |
| Rubaga - R | Control - O | |

For each sample, a Sample Collection Form (Appendix 3) was completed and thereafter taken to the laboratory for analysis of the various heavy metal concentrations. Thereafter, comparison with various guideline values was done, and appropriate conclusions drawn. The following procedures were generally followed for sampling:

1. The sampling bottle was ensured clean and with nothing inside except the water to be sampled to come into contact with the inside or cap of the bottle.
2. The rainwater was allowed to run for an ample period of time, approximately 2-3 minutes, to ensure a simulation of standard domestic rainwater collection principle, that the debris from the roof have been washed off before collecting the water. Care was taken to ensure that the water does not make contact with any object before running into the bottle. This entailed holding the bottle just below the eave, and trapping the water between the eave and the ground.
3. For the control sample, it involved situating a bottle with a funnel approximately 1 metre above the ground, to prevent the splashed raindrops from getting into the bottle. Each sample was immediately preserved by acidifying with concentrated nitric acid to a pH less than 2.
4. The sample was then capped immediately to preserve volatile compounds in the water and prevent atmospheric contamination. Samples were then refrigerated to await analysis.

https://dx.doi.org/10.22161/ijaers.5.1.14 ISSN: 2349-6495(P) | 2456-1908(O)

*Fig.1: KX3*

*Fig.2: RZ3*

**2.4 Data Quality Control, Analysis and Interpretation**

As a first measure, the research assistants were educated on the research aims in general, and specifically on the need to obtain unadulterated samples. They were trained on the correct procedures to follow during collection, preservation and storage of samples.

All the plastic bottles used for collection of the samples were sterilized using the following procedure. They were first cleaned with a laboratory detergent and rinsed with tap water. Next, the container was rinsed in 1:1 hydrochloric acid solution. The container was then rinsed with de-ionized water three times and allowed to air dry.

At the lab, suitable tests were carried out using a Flame Atomic Absorption Spectrophotometer and the results represented in Test Result Sheets (Appendix 3). During the analysis, the treated water samples were directly aspirated on the Flame Atomic Absorption Spectrophotometer.

*https://dx.doi.org/10.22161/ijaers.5.1.14* *ISSN: 2349-6495(P) | 2456-1908(O)*

Matrix interference was eliminated by standard addition, that is, they were also acidified by addition of nitric acid to a pH of less than 2. Two different models of the Spectrophotometer were used; Perkin-Elmer 2380 model at the Geology Department, Makerere University; and Shimadzu 6200 model at the Government Chemist & Analytical Laboratory, Wandegeya.

The detection limits on the Perkin-Elmer 2380 model were higher than the WHO limits; hence it was necessary to use the Shimadzu 6200 model, due to its higher sensitivity.

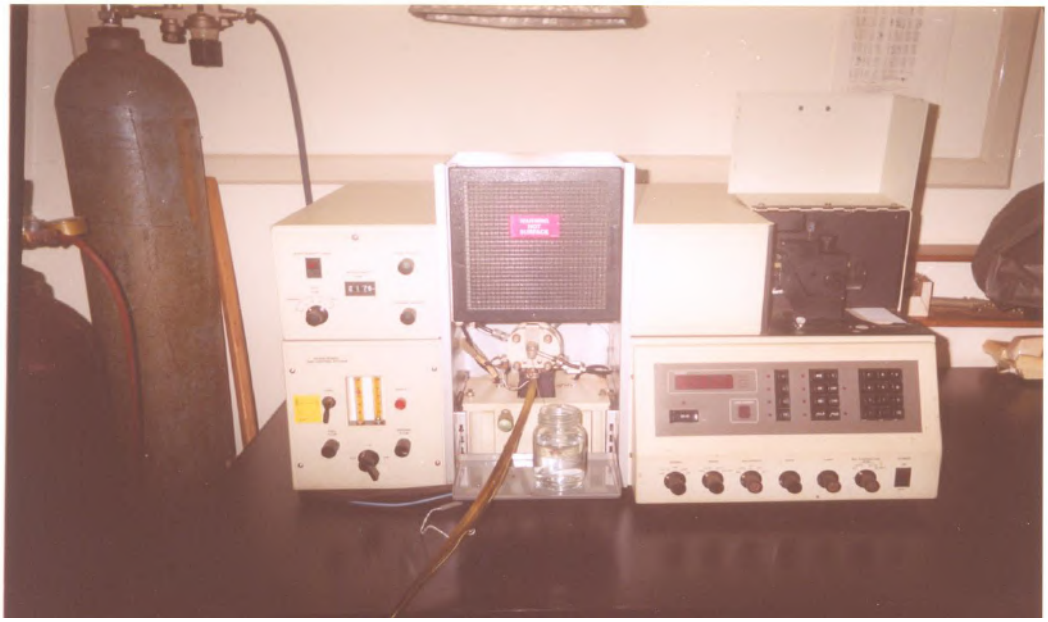

*Fig.3: Flame Atomic Absorption Spectrophotometer*
The Perkin-Elmer 2380 model at the Geology Department, Makerere University.

The detection limits, wavelengths and slit width used for the various elements by the Perkin-Elmer 2380 model were:

*Table.2: Settings for Perkin-Elmer 2380 model*

| | Zinc | Copper | Nickel | Cadmium | Lead |
|---|---|---|---|---|---|
| Detection Limit (mg/L) | 0.01 | 0.01 | 0.1 | 0.01 | 0.1 |
| Wavelength, λ, (nm) | 213.9 | 324.8 | 352.5 | 228.8 | 217.0 |
| Slit width (nm) | 0.7 | 0.2 | 0.2 | 0.7 | 0.7 |

The wavelengths and detection limits used for Lead, Cadmium and Nickel by the Shimadzu 6200 model were:

*Table.3: Settings for Shimadzu 6200 model*

| | Lead | Cadmium | Nickel |
|---|---|---|---|
| Detection Limits (mg/L) | 0.001 | 0.001 | 0.001 |
| Wavelength, λ, (nm) | 283.3 | 228.8 | 232.0 |

### 2.5 Presentation of Results

The WHO Drinking Water Guideline values; the Draft UNBS Standard (1999) for Bottled/Packaged Waters Other Than Natural Mineral Waters; and NEMA Standards for the Discharge of Effluent into Water or on Land are also indicated for each metal, for comparison, as shown in Table 4 [1]; [7];[8].

https://dx.doi.org/10.22161/ijaers.5.1.14 ISSN: 2349-6495(P) | 2456-1908(O)

*Fig.4: Heavy Metal Tests Being Run Using Perkin-Elmer 2380 model*

*Table.4: Water Quality Guidelines Used*

| | Zn (mg/l) | Cu (mg/l) | Ni (mg/l) | Cd (mg/l) | Pb (mg/l) |
|---|---|---|---|---|---|
| WHO limits | 3.0 | 2.0 | 0.02 | 0.003 | 0.01 |
| Draft UNBS Standard | 0.5 | 1.0 | 0.02 | 0.003 | 0.05 |
| NEMA Limits | 5.0 | 1.0 | 1.0 | 0.1 | 0.1 |

The results of the analysis of the samples were presented in result sheets, as seen in Appendix 4. However, they have been simplified as follows;

*Table.5: Kawempe Division Results*

| Sample Code | Zn (mg/l) | Cu (mg/l) | Ni (mg/l) | Cd (mg/l) | Pb (mg/l) |
|---|---|---|---|---|---|
| KX1 | 0.03 | < 0.01 | < 0.001 | < 0.001 | < 0.001 |
| KX2 | 0.10 | 0.02 | < 0.001 | < 0.001 | < 0.001 |
| KX3 | 0.77 | < 0.01 | < 0.001 | < 0.001 | < 0.001 |
| KY1 | 0.12 | < 0.01 | < 0.001 | < 0.001 | < 0.001 |
| KY2 | 1.59 | 0.01 | < 0.001 | < 0.001 | < 0.001 |
| KY3 | 0.24 | < 0.01 | < 0.001 | < 0.001 | < 0.001 |
| KZ1 | 0.01 | < 0.01 | < 0.001 | < 0.001 | < 0.001 |
| KZ2 | 0.04 | < 0.01 | < 0.001 | < 0.001 | < 0.001 |
| KZ3 | 0.24 | 0.01 | < 0.001 | < 0.001 | < 0.001 |
| KO | 0.10 | 0.01 | < 0.001 | < 0.001 | < 0.001 |

Where Cd – Cadmium, Cu – Copper, Pb – Lead, Zn – Zinc, Ni – Nickel, mg/l – milligrams per litre, or parts per million

*https://dx.doi.org/10.22161/ijaers.5.1.14* *ISSN: 2349-6495(P) | 2456-1908(O)*

*Table.6: Central Division Results*

| Sample Code | Zn (mg/l) | Cu (mg/l) | Ni (mg/l) | Cd (mg/l) | Pb (mg/l) |
|---|---|---|---|---|---|
| CX1 | 0.22 | 0.02 | < 0.001 | < 0.001 | < 0.001 |
| CX2 | 0.02 | 0.01 | < 0.001 | < 0.001 | < 0.001 |
| CX3 | 0.26 | < 0.01 | < 0.001 | < 0.001 | < 0.001 |
| CY1 | < 0.01 | < 0.01 | < 0.001 | < 0.001 | < 0.001 |
| CY2 | 1.06 | 0.02 | < 0.001 | < 0.001 | < 0.001 |
| CY3 | 0.02 | 0.01 | < 0.001 | < 0.001 | < 0.001 |
| CZ1 | 1.55 | 0.01 | < 0.001 | < 0.001 | < 0.001 |
| CZ2 | < 0.01 | < 0.01 | < 0.001 | < 0.001 | < 0.001 |
| CZ3 | 1.56 | 0.01 | < 0.001 | < 0.001 | < 0.001 |
| CO | < 0.01 | 0.01 | < 0.001 | < 0.001 | < 0.001 |

*Table.7: Rubaga Division Results*

| Sample Code | Zn (mg/l) | Cu (mg/l) | Ni (mg/l) | Cd (mg/l) | Pb (mg/l) |
|---|---|---|---|---|---|
| RX1 | 0.61 | 0.01 | < 0.001 | < 0.001 | < 0.001 |
| RX2 | 0.02 | 0.01 | < 0.001 | < 0.001 | < 0.001 |
| RX3 | 0.01 | 0.01 | < 0.001 | < 0.001 | < 0.001 |
| RY1 | 1.01 | 0.02 | < 0.001 | < 0.001 | < 0.001 |
| RY2 | 0.40 | 0.01 | < 0.001 | < 0.001 | < 0.001 |
| RY3 | 0.43 | < 0.01 | < 0.001 | < 0.001 | < 0.001 |
| RZ1 | 0.42 | 0.01 | < 0.001 | < 0.001 | < 0.001 |
| RZ2 | 0.13 | 0.02 | < 0.001 | < 0.001 | < 0.001 |
| RZ3 | 0.42 | < 0.01 | < 0.001 | < 0.001 | < 0.001 |
| RO | 0.98 | < 0.01 | < 0.001 | < 0.001 | < 0.001 |

*Table.8: Nakawa Division Results*

| Sample Code | Zn (mg/l) | Cu (mg/l) | Ni (mg/l) | Cd (mg/l) | Pb (mg/l) |
|---|---|---|---|---|---|
| NX1 | 0.69 | < 0.01 | < 0.001 | < 0.001 | < 0.001 |
| NX2 | 0.05 | < 0.01 | < 0.001 | < 0.001 | < 0.001 |
| NX3 | 0.72 | 0.01 | < 0.001 | < 0.001 | < 0.001 |
| NY1 | 0.02 | < 0.01 | < 0.001 | < 0.001 | < 0.001 |
| NY2 | 0.01 | < 0.01 | < 0.001 | < 0.001 | < 0.001 |
| NY3 | 0.10 | 0.02 | < 0.001 | < 0.001 | < 0.001 |
| NZ1 | 0.01 | 0.02 | < 0.001 | < 0.001 | < 0.001 |
| NZ2 | 0.01 | < 0.01 | < 0.001 | < 0.001 | < 0.001 |
| NZ3 | 6.77 | 0.02 | < 0.001 | < 0.001 | < 0.001 |
| NO | 1.47 | < 0.01 | < 0.001 | < 0.001 | < 0.001 |

*Table.9: Makindye Division Results*

| Sample Code | Zn (mg/l) | Cu (mg/l) | Ni (mg/l) | Cd (mg/l) | Pb (mg/l) |
|---|---|---|---|---|---|
| MX1 | 1.21 | < 0.01 | < 0.001 | < 0.001 | < 0.001 |
| MX2 | < 0.01 | 0.01 | < 0.001 | < 0.001 | < 0.001 |
| MX3 | 0.01 | < 0.01 | < 0.001 | < 0.001 | < 0.001 |
| MY1 | 0.15 | 0.01 | < 0.001 | < 0.001 | < 0.001 |
| MY2 | 0.31 | 0.01 | < 0.001 | < 0.001 | < 0.001 |
| MY3 | 0.36 | 0.01 | < 0.001 | < 0.001 | < 0.001 |
| MZ1 | 0.15 | 0.01 | < 0.001 | < 0.001 | < 0.001 |

*https://dx.doi.org/10.22161/ijaers.5.1.14* *ISSN: 2349-6495(P) | 2456-1908(O)*

| Sample Code | Zn (mg/l) | Cu (mg/l) | Ni (mg/l) | Cd (mg/l) | Pb (mg/l) |
|---|---|---|---|---|---|
| MZ2 | 0.13 | < 0.01 | < 0.001 | < 0.001 | < 0.001 |
| MZ3 | 0.75 | < 0.01 | < 0.001 | < 0.001 | < 0.001 |
| MO | 0.02 | < 0.01 | < 0.001 | < 0.001 | < 0.001 |

## III. ANALYSIS, INTERPRETATION AND DISCUSSION OF RESULTS

### 3.1 General Descriptions

From the test result sheets, some general determinations were made, regarding the presence of some of the heavy metals in a particular division. These have been arranged for the individual heavy metals.

#### 3.1.1 Lead

Lead detection limit was 0.001 mg/L. Lead concentrations in all the samples obtained from the study were in such small quantities that they were not detected. The lead concentration in the samples thus appears to be more than ten times lower than the WHO drinking water guideline value, and more than one hundred times lower than the NEMA Effluent Discharge Standards. The Lead level is still safe enough compared to the Draft UNBS Standard.

#### 3.1.2 Cadmium

The detection limit for Cadmium was 0.001 mg/L. As with Lead above, Cadmium was not detected in any of the samples in the study. This implies that the Cadmium concentration in the water is less than 0.001 mg/L. Cadmium concentration thus is at least three times lower than the WHO guideline value and Draft UNBS Standard, and one hundred times lower than the NEMA Effluent Discharge standards.

#### 3.1.3 Nickel

The Nickel detection limit was 0.001 mg/L. In no instance was Nickel detected, implying that any Nickel present was in levels less than 0.001 mg/L. Nickel concentration is therefore at least twenty times lower than the WHO guideline value and Draft UNBS Standard, and one thousand times lower than the NEMA Effluent Discharge standards.

#### 3.1.4 Copper

The detection limit for Copper was 0.01 mg/L. In Kawempe division, Copper was detected in the medium age clay tile roof sample; medium age plain GCI sheet roof sample; old painted GCI sheet roof sample and in the control sample. In Central division, Copper was detected in every sample, except the old clay tile roof sample; the new plain GCI sheet roof sample and the medium age painted GCI sheet roof sample. In Rubaga division, Copper was also detected in every sample, except the old plain GCI sheet roof sample; the old painted GCI sheet roof sample and the control sample. In Nakawa division, Copper was detected the old clay tile roof sample; the old plain GCI sheet roof sample; and the new and old painted GCI sheet roof samples.

In Makindye division, Copper was detected in the medium age clay tile roof sample; all the plain GCI sheet roof samples, and the new painted GCI sheet roof sample. However, even the highest contamination level obtained, of 0.02 mg/L, was still one hundred timed lower than the WHO guideline value, and fifty times lower than the NEMA Effluent Discharge standards and Draft UNBS Standard.

#### 3.1.5 Zinc

The detection limit was 0.01 mg/L. In Kawempe, Rubaga and Nakawa divisions, Zinc was detected in all the samples. In Central division, no zinc was detected in the new plain GCI sheet roof sample; medium age painted GCI sheet roof sample, and the control sample. In Makindye division, Zinc was not detected in the medium age clay tile roof sample. Zinc was detected in much higher concentrations than the other heavy metals. There was one case that more than doubled the WHO guideline value. Only 36 cases had Zinc levels lower than the Draft UNBS Standard. Hence, Zinc represents a real challenge to the drinking water quality; in as far as heavy metal contamination is concerned.

*https://dx.doi.org/10.22161/ijaers.5.1.14* *ISSN: 2349-6495(P) | 2456-1908(O)*

### 3.2 Overall Distribution of Contaminants

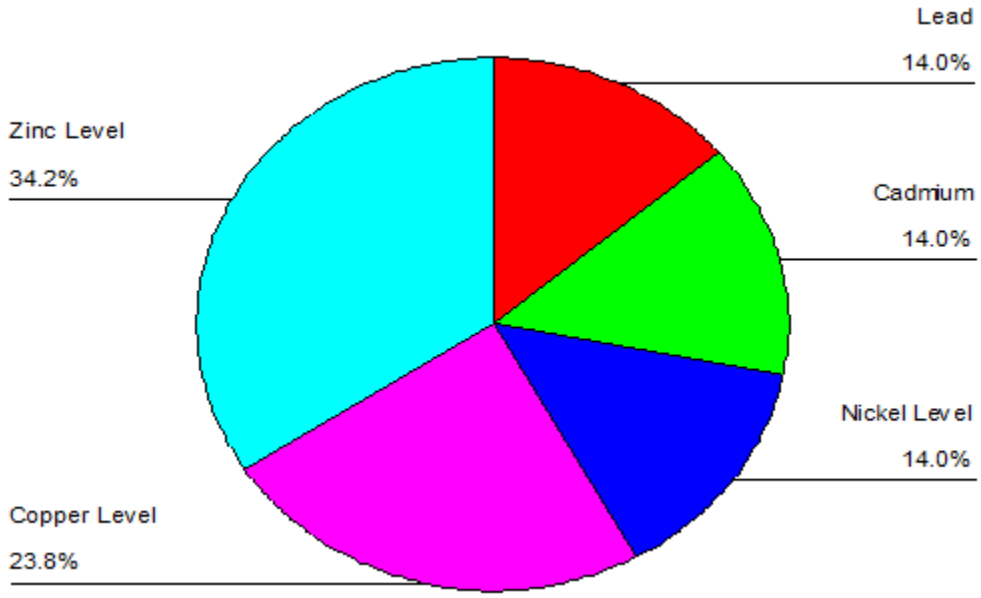


*Fig.5: Overall Distribution of Heavy Metals*

Overall, Zinc was the overwhelming contaminant with 34.2% of the distribution chart, as can be seen from the figure above. Copper was second likely to detect, while Lead, Cadmium and Nickel had equal chances of occurrence, at 14% chance each.
All Lead, Cadmium and Nickel values were in the range "less than 0.001 mg/L". The frequency distribution for Copper and is as shown in Tables 10 and 11;

*Table.10: Copper Overall Frequency Distribution*

| | Frequency | Percent | Cumulative Percent |
|---|---|---|---|
| less than 0.01 | 23 | 46.0 | 46.0 |
| 0.01 | 19 | 38.0 | 84.0 |
| 0.02 | 8 | 16.0 | 100.0 |
| Total | 50 | 100.0 | |

46% of the total number of samples had Copper values of less than 0.01 mg/L; 38% of the total number had values of 0.01 mg/L; whereas the remaining 16% had values of 0.02 mg/L. Therefore, most of the samples had Copper concentration of less than 0.01 mg/L. It is also clear that 84% of the samples had a concentration of 0.01 mg/L, or less.

*Table.11: Zinc Overall Frequency Distribution*

| | Frequency | Percent | Cumulative Percent |
|---|---|---|---|
| less than 0.01 | 4 | 8.0 | 8.0 |
| 0.01 to 0.49 | 32 | 64.0 | 72.0 |
| 0.50 to 0.99 | 6 | 12.0 | 84.0 |
| 1.00 to 1.49 | 4 | 8.0 | 92.0 |
| Over 1.50 | 4 | 8.0 | 100.0 |
| Total | 50 | 100.0 | |

Here, 64% of the total number of samples had Zinc concentration of between 0.01to 0.49 mg/L; 12% have a concentration of between 0.50 to 0.99 mg/L; and with 8% each, are those with concentrations of less than 0.01 mg/L; 1.00 to 1.49 mg/L; and over 1.5 mg/L. It is thus safe to conclude that the majority of samples have Zinc concentrations of between 0.01 to 0.49 mg/L.

### 3.3 Interpretation & Discussion on Contamination

Various analyses for each of the heavy metal contamination were made. From the analyses, inferences were made from

*https://dx.doi.org/10.22161/ijaers.5.1.14* *ISSN: 2349-6495(P) | 2456-1908(O)*

the results. For Lead, Cadmium and Nickel, all samples returned values of less than 0.001 mg/l, that is, below the detection limit of the spectrophotometer. Therefore, no further interpretation was deemed necessary.

**Copper Contamination**

On the vertical axes on Figures 8, 9 and 10, '1.0' represents 'less than 0.01 mg/l'; '2.0' represents 0.01 mg/l; '3.0' represents 0.02 mg/l, as used to input the raw data into the SPSS statistical program.

**Copper Contamination Vs. Roof Type by Location**

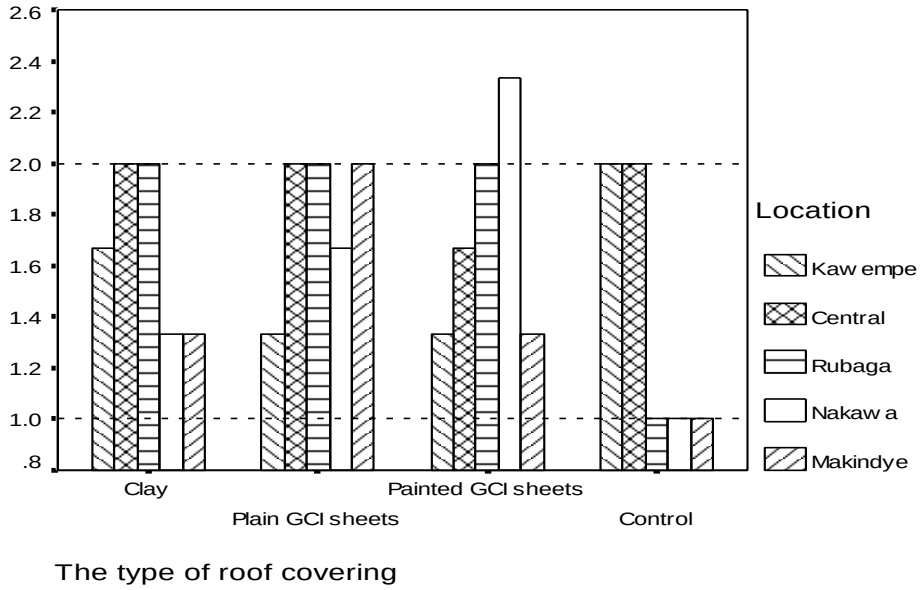


*Fig.6: Mean Copper Level against Roof Type by Location*

From the Figure 8 above, mean Copper levels here showed a slightly different variation, as compared to previous heavy metals. The control samples from Rubaga, Nakawa and Makindye divisions showed a uniform mean level of less than 0.01 mg/L; while the control samples from Kawempe and Central divisions gave mean Copper levels of 0.01 mg/L. For the painted GCI sheet roof samples, none of them gave a mean level of less than 0.01 mg/L; only Nakawa division had a mean level of more than 0.01 mg/L. None of the samples from plain GCI sheet roofs gave a mean Copper level of less than 0.01 mg/L; Central, Rubaga, Nakawa and Makindye samples all having concentrations of 0.01 mg/L. All of the clay tile roof samples had means of 0.01 mg/L.

**Copper Contamination Vs. Roof Age by Location**

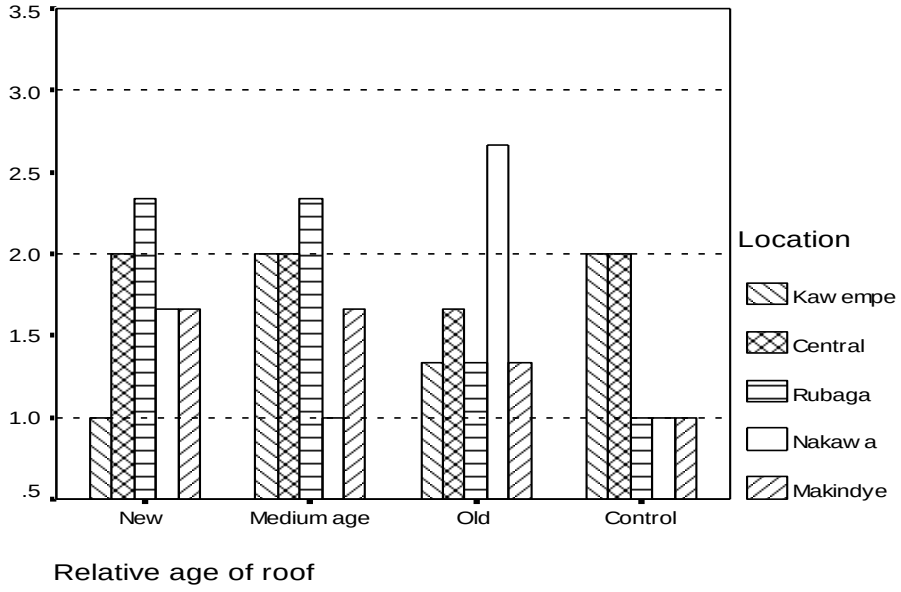


*Fig.7: Mean Copper Level against Roof Age by Location*

*https://dx.doi.org/10.22161/ijaers.5.1.14* *ISSN: 2349-6495(P) | 2456-1908(O)*

For old roofs, there was no sample with a mean less than 0.01 mg/L. They all lay generally at 0.01 mg/L, except Nakawa division, where the mean was around 0.02 mg/L. For the medium age roofs, only Nakawa division had a mean of less than 0.01 mg/L; while the Kawempe, Central and Makindye divisions had means of 0.01 mg/L, with Kawempe and Central divisions having uniform concentrations for all roof types. Rubaga division had a mean of 0.02 mg/L. For new roofs, Kawempe division had the lowest mean of less than 0.01 mg/L. Rubaga division had the highest mean of 0.02 mg/L; while the rest had 0.01 mg/L.

**Copper Contamination Vs. Roof Age by Roof Type**

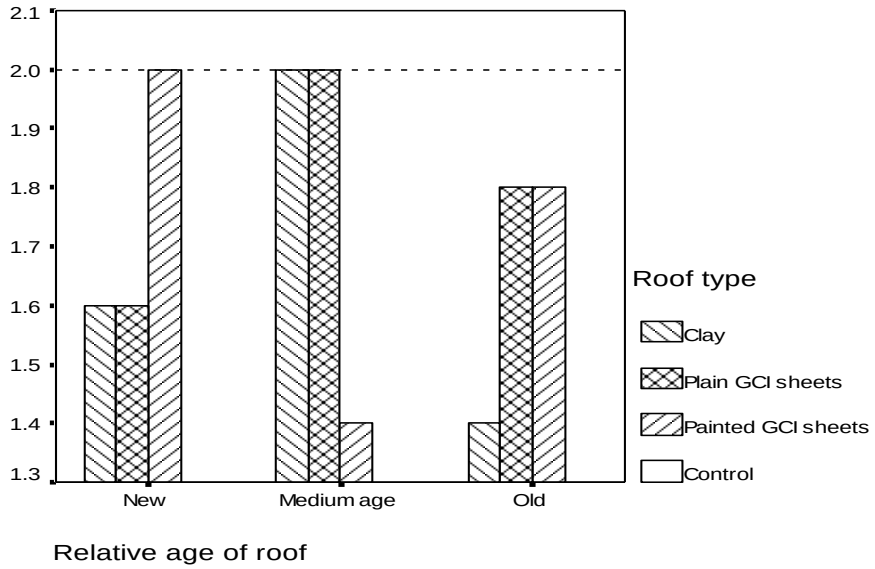


*Fig.8: Mean Copper Level against Roof Age by Roof Type*

The mean copper levels, based on the relative age of the roof, were all at 0.01 mg/L. Among the new roofs, painted GCI sheet roofs had a uniform copper concentration, while for medium age roofs, clay tiled and plain GCI sheet roofs had uniform copper concentrations.

**Zinc Contamination**

During the analysis of Zinc, the data was grouped. Therefore, on the vertical axes on Figures 11, 12 and 13, the bar graphs on Zinc contamination, '1.0' represents 'less than 0.01 mg/l'; '2.0' represents '0.01 to 0.49 mg/l'; '3.0' represents '0.50 to 0.99 mg/l', and '4.0' represents the group '1.00 to 1.49 mg/l', as used to input the raw data into the SPSS statistical program.

**Zinc Contamination Vs. Roof Type by Location**

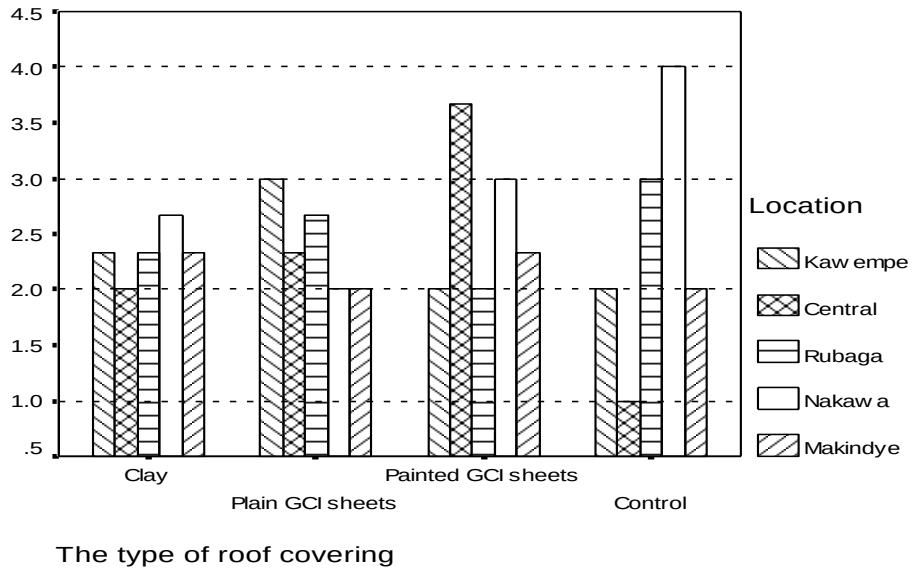


*Fig.9: Mean Zinc Level against Roof Type by Location*

*https://dx.doi.org/10.22161/ijaers.5.1.14* *ISSN: 2349-6495(P) | 2456-1908(O)*

Central division control samples showed a uniform mean level of less than 0.01 mg/L; Kawempe and Makindye divisions exhibited a uniform mean level of 0.01 to 0.49 mg/L; Rubaga division showed a uniform mean level of 0.50 to 0.99 mg/L; and Nakawa division had the highest mean, at 1.00 to 1.49 mg/L. There was a mean level of 0.01 to 0.49 mg/L for Kawempe and Rubaga painted iron sheets; while in Nakawa and Makindye divisions the mean was 0.50 to 0.99 mg/L. Central division painted iron sheets had the highest mean of 1.00 to 1.49 mg/L. Makindye plain iron sheets had a mean of 0.01 to 0.49 mg/L, while the rest had means of 0.50 to 0.99 mg/L. Central division clay tiles had a mean of 0.01 to 0.49 mg/L, while the rest had means of 0.50 to 0.99 mg/L.

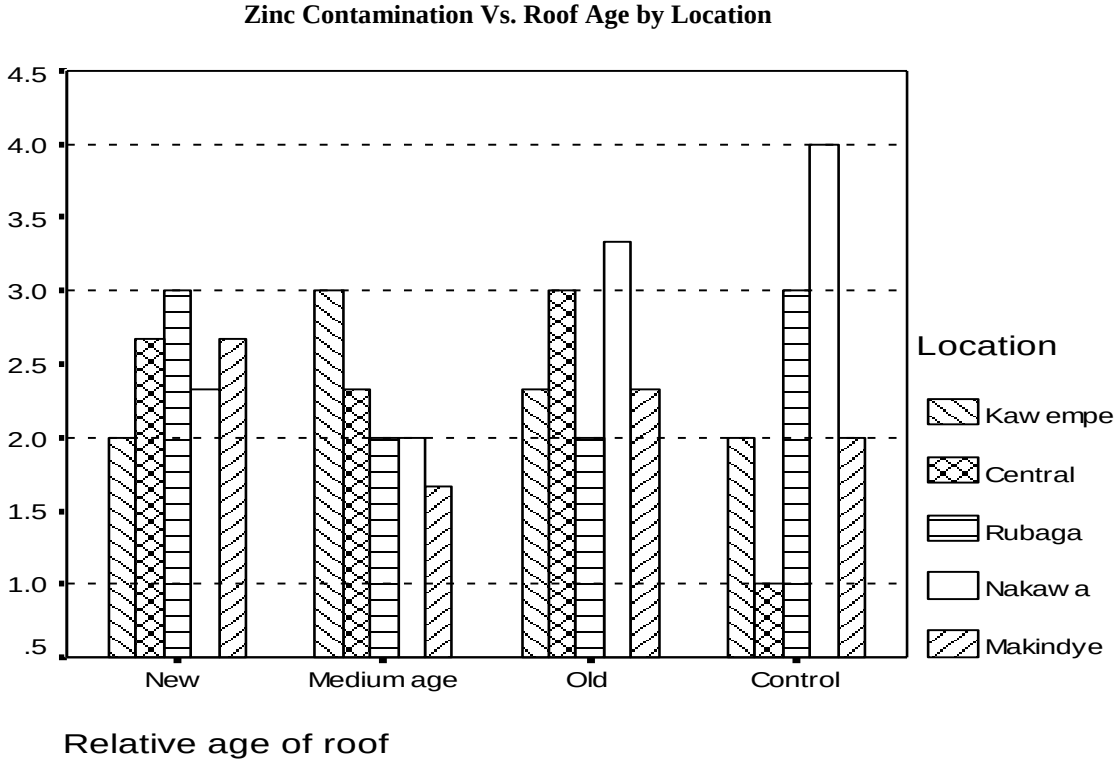


*Fig.10: Mean Zinc Level against Roof Age by Location*

For the old roofs, Rubaga division had a mean level of 0.01 to 0.49 mg/L; Kawempe, Central and Makindye had a mean of 0.50 to 0.99 mg/L; while in Nakawa had a mean of 1.00 to 1.49 mg/L. For medium age roofs, Rubaga, Nakawa and Makindye had a mean level of 0.01 to 0.49 mg/L; while Kawempe and Central had a mean of 0.50 to 0.99 mg/L. For new roofs, Kawempe had a mean level of 0.01 to 0.49 mg/L; while the rest had a mean of 0.50 to 0.99 mg/L.

*https://dx.doi.org/10.22161/ijaers.5.1.14* *ISSN: 2349-6495(P) | 2456-1908(O)*

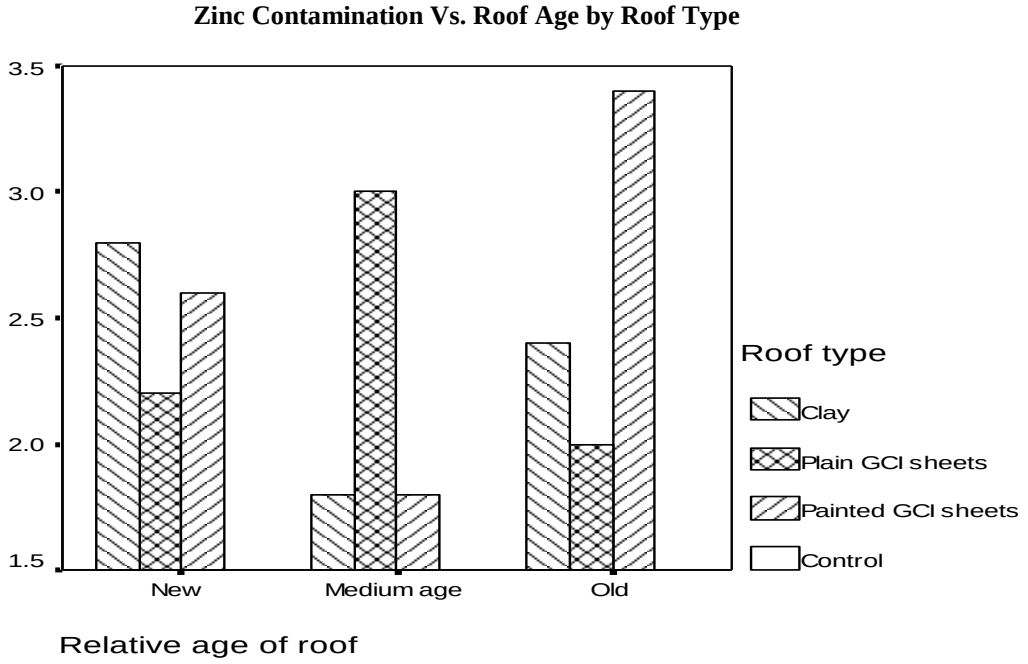


*Fig.11: Mean Zinc Level against Roof Age by Roof Type*

For new roofs, the mean level was 0.50 to 0.99 mg/L. For medium age roofs, clay and painted GCI sheet roofs had mean levels of 0.01 to 0.49 mg/L, while plain GCI sheets had a mean of 0.50 to 0.99 mg/L. For old roofs, plain GCI sheet roofs had a mean of 0.01 to 0.49 mg/L; clay tile roofs had a mean level of 0.50 to 0.99 mg/L; while painted GCI sheet roofs had a mean of 1.00 to 1.49 mg/L.

**Discussion of Means**

These tests were not many enough to justify the use of statistical tests of significance. Therefore, judgment and deductions have been majorly used in this analysis.

*Table.12: Comparison of Statistics*

| | | Lead Level | Cadmium Level | Nickel Level | Copper Level | Zinc Level |
|---|---|---|---|---|---|---|
| N | Valid | 50 | 50 | 50 | 50 | 50 |
| | Missing | 50 | 50 | 50 | 50 | 50 |
| Mean | | 1.00 | 1.00 | 1.00 | 1.70 | 2.44 |
| Median | | 1.00 | 1.00 | 1.00 | 2.00 | 2.00 |
| Mode | | 1 | 1 | 1 | 1 | 2 |
| Std. Deviation | | .00 | .00 | .00 | .74 | 1.03 |
| Minimum | | 1 | 1 | 1 | 1 | 1 |
| Maximum | | 1 | 1 | 1 | 3 | 5 |

The mean levels of the heavy metals Lead, Nickel and Cadmium did not really need any further analysis since the levels in all the samples were identical; hence the mean, mode, median, minimum and maximum values were the same and standard deviation, zero.

However, Copper and Zinc had varying values. Zinc had a higher mean than Copper. The median Copper level is 0.01 mg/L, while the median Zinc level is in the group, '0.01 to 0.49 mg/L'. The modal Copper level is less than 0.01 mg/L, while the modal Zinc level is still in the '0.01 to 0.49 mg/L' group. This is quite clear from Tables 10 and 11. Zinc varies more from its mean than Copper. The mean heavy metal level values were also compared by location, roof type and roof age. The results are as shown in the Tables 13 – 18.

*https://dx.doi.org/10.22161/ijaers.5.1.14* *ISSN: 2349-6495(P) | 2456-1908(O)*

### 3.4.1 Means by Location

*Table.13: Mean Copper Levels by Location*

| Sampling Location | Mean | N | Std. Deviation | Median |
|---|---|---|---|---|
| Kawempe | 1.50 | 10 | 0.71 | 1.00 |
| Central | 1.90 | 10 | 0.74 | 2.00 |
| Rubaga | 1.90 | 10 | 0.74 | 2.00 |
| Nakawa | 1.70 | 10 | 0.95 | 1.00 |
| Makindye | 1.50 | 10 | 0.53 | 1.50 |
| Mean | 1.70 | 10 | 0.74 | 2.00 |

The means in this case, cannot be fully interpreted, since this is grouped data, which is in discrete steps, 1, 2 and 3. It is only clear that Kawempe and Makindye have lower levels than the mean, while Central and Rubaga have higher levels than the mean. The median Copper level for Kampala was 0.01 mg/L. Again from this, it is evident that Central and Rubaga divisions have the higher media.

*Table.14: Mean Zinc Levels by Location*

| Sampling Location | Mean | N | Std. Deviation | Median |
|---|---|---|---|---|
| Kawempe | 2.40 | 10 | 0.97 | 2.00 |
| Central | 2.50 | 10 | 1.58 | 2.00 |
| Rubaga | 2.40 | 10 | 0.70 | 2.00 |
| Nakawa | 2.70 | 10 | 1.06 | 2.00 |
| Makindye | 2.20 | 10 | 0.79 | 2.00 |
| Mean | 2.44 | 10 | 1.03 | 2.00 |

Again, since this is grouped data represented in discrete steps, the means here, having decimals, cannot be fully interpreted. However, it can be seen that Nakawa division had the highest dispersion from the mean, while Rubaga, the least. The mean level in Makindye seems lower than the overall mean.

### 3.4.2 Means by Roof Type

*Table.15: Mean Copper Levels by Roof Type*

| Type of roof covering | Mean | N | Std Deviation | Median |
|---|---|---|---|---|
| Clay | 1.67 | 15 | 0.72 | 2.00 |
| Plain GCI Sheets | 1.80 | 15 | 0.77 | 2.00 |
| Painted GCI Sheets | 1.73 | 15 | 0.80 | 2.00 |
| Control | 1.40 | 5 | 0.55 | 1.00 |
| Mean | 1.70 | | 0.74 | 2.00 |

Plain GCI sheet roofs had the highest dispersion from the mean, with clay tiles, the least. Plain GCI Sheets have the highest contamination mean levels. The fact that the control samples had the least levels, even lower than the overall mean, points to the deduction that Copper actually is on the roofs.

*Table.16: Mean Zinc Levels by Roof Type*

| Type of roof covering | Mean | N | Std Deviation | Median |
|---|---|---|---|---|
| Clay | 2.33 | 15 | 0.72 | 2.00 |
| Plain GCI Sheets | 2.40 | 15 | 1.06 | 2.00 |
| Painted GCI Sheets | 2.60 | 15 | 1.30 | 2.00 |
| Control | 2.40 | 5 | 1.14 | 2.00 |
| Mean | 2.44 | | 1.03 | 2.00 |

*https://dx.doi.org/10.22161/ijaers.5.1.14* *ISSN: 2349-6495(P) | 2456-1908(O)*

The means were highest among the heavy metals. Zinc also had the highest standard deviations among the metals tested. Painted GCI sheet roofs had the highest dispersion, and clay tiles, the least. Overall, it seems painted GCI Sheets have higher means than the rest.

**3.4.3 by Roof Age**

*Table.17: Mean Copper Levels by Roof Age*

| Relative age of roof | Mean | N | Std. Deviation | Median |
|---|---|---|---|---|
| New | 1.73 | 15 | 0.80 | 2.00 |
| Medium Age | 1.80 | 15 | 0.77 | 2.00 |
| Old | 1.67 | 15 | 0.72 | 2.00 |
| Control | 1.40 | 5 | 0.55 | 1.00 |
| Mean | 1.70 | | 0.74 | 2.00 |

The values appear very close to each other. However, new roofs showed marginally higher deviations for the mean value. Among the roofs there is a uniform median at 0.01 mg/l. Due to the lower value returned by the control samples, there seems to be a case for a part played by age on the contamination levels.

*Table.18: Mean Zinc Levels by Roof Age*

| Relative age of roof | Mean | N | Std. Deviation | Median |
|---|---|---|---|---|
| New | 2.53 | 15 | 1.06 | 2.00 |
| Medium Age | 2.20 | 15 | 1.01 | 2.00 |
| Old | 2.60 | 15 | 1.06 | 2.00 |
| Control | 2.40 | 5 | 1.14 | 2.00 |
| Mean | 2.44 | | 1.03 | 2.00 |

Zinc showed the highest dispersion of all the metals. However, it seems that Zinc is also found in the atmosphere, since control values are higher than the values from some of the roofs.

**3.5 General Discussions**

Generally, the presence of some heavy metals in the rain drops reaching the ground surface, as well as rainwater collected from roofs around Kampala City is not in doubt. Rather, the issue as remains the degree of contamination. The study has endeavored to ascertain this contamination level as best as possible, and present it in well understood terms. Overall, Zinc was found to be the most prevalent metal, with a probability of 34.2% of being detected. Copper was second, while the rest of the metals; Lead, Nickel and Cadmium, were detected with the same chance of occurrence.

The study did note a consistent pattern in Lead levels in that in all instances, the levels were less than 0.001 mg/L. This is much lower than that given by the WHO value of 0.01 mg/L. Thus there is no immediate danger of lead poisoning. From the NEMA guideline value for effluent discharge into water or land, and Draft UNBS Standard, the rainwater is also within the limits. However, the exact Lead concentration was not known, due to the detection limits of the spectrophotometer used. From these findings, it was not possible to infer any relationship between either age or location of a sampling location and Lead contamination therein.

Like Lead, Cadmium showed a consistent presence in levels of less than 0.001 mg/L. The WHO and Draft UNBS Standard guideline value of 0.003 mg/L is, however, a small quantity in itself. The seriousness of the consequence of this type of contamination can be seen from the small value of WHO and Uganda Standards level.

Therefore, in as far as ascertaining the drinking quality, with respect to Cadmium levels, there is no immediate danger of Cadmium poisoning. The NEMA standard for effluent discharge stands at 0.1 mg/L. Thus, the cadmium level in the rainwater is safe to discharge to the ground. Similarly to Lead, from these findings it is not possible to infer any relationship between either age or location of a sampling location and Cadmium contamination therein.

Nickel levels are generally also less than 0.001 mg/L. In comparison to the WHO and Draft UNBS Standard guideline value of 0.02 mg/L, the amount of Nickel in the rainwater need not cause any alarm. However, the exact level of Nickel was also not established due to the detection limits of the spectrophotometer. Also, it is within the NEMA effluent discharge guidelines. The same comment as above applies.

Copper was registered in varying levels in some of the control samples. This can be taken to mean that Copper is

*https://dx.doi.org/10.22161/ijaers.5.1.14* *ISSN: 2349-6495(P) | 2456-1908(O)*

present to some degree in the atmosphere. Actually, it would seem that in the case of Kawempe division, the mean levels in the atmosphere were higher than from the roofs; while in Central division, the levels in the roofs were quite comparable to the levels in the atmosphere. However, this would seem random at best. In Rubaga and Makindye, a clear pattern of decrease in levels with age is discerned. Such a scenario is also almost replicated in Nakawa, but the levels shoot up in the old roofs. This observation, however, does not mean a general increase of copper levels with age. More samples would be needed for such a generalization.

These appear random observations, as they are no consistent in all the sampling sites, and yet no reasonable explanation is apparent. The observations of the different roof materials with age do also show any consistency, hence difficult to make generalizations. The WHO limit is 2 mg/L, whereas the Draft UNBS Standard guideline value is 1 mg/L. None of the samples gave a value of more than 0.02 mg/L. Thus, the maximum concentration recorded is only 1% of the WHO limit and 0.5% of the Draft UNBS Standard. With the discernible pattern of reduction of levels with age, then there is no danger currently of unsafe Copper contamination of rainwater in Kampala. The detected values are also way below the recommended NEMA level of 1 mg/L.

Most Zinc detected, being in the range of 0.01 to 0.49 mg/L, is below the WHO limit of 3 mg/L. The atmosphere around Kampala also seems to have some Zinc in it. In Nakawa and Rubaga divisions, there is more Zinc in the atmosphere than from the roofs. This may be attributed to the industries therein. There is still no clear discernible relationship between contamination and either location or roof age. The levels are generally so much lower than the NEMA guideline value of 5 mg/L. Since 14 cases (28% of the samples) reported levels of Zinc above the Draft UNBS Standard, then Zinc requires intervention. As mentioned earlier elsewhere in this report, unlike the other heavy metals which accumulate in the human body to achieve their lethal levels, Zinc does not accumulate; rather, it is fatal in lethal doses taken at once. Measures have to be taken to ensure that the Zinc does not reach these lethal contamination levels.

### 3.6 Significance of Output

This study sought to investigate the levels of heavy metal contamination of rainwater as collected from various roofs. Several drinking water quality standards were used in this. These findings will be very helpful in the establishment of a rainfall heavy metal contamination database for Kampala in particular, and Uganda in general. As of now, such a document does not exist. Policy makers can use these findings to issue appropriate guidelines and make fitting laws regarding the RWH for drinking purposes. All other stakeholders promoting RWH, especially NGOs, local women organizations, the church and individuals can make use of these findings to better their knowledge of heavy metal contamination in rainwater, and together with the recommendations issued hereafter, better the quality of this water, if it to be used for drinking purposes.

## IV. CONCLUSION

Rain water, as it is, is largely safe for human consumption in as far as heavy metal contamination is concerned, when compared to the various national and international standards. If proper water quality control and efficient management structures like proper storage facilities and first flush diversion systems are in place, RWH can provide good quality water free from heavy metal contamination.

The various types of roof covering materials predominantly in use in Kampala were identified as clay tiles, plain and painted GCI sheets. Coated metal roofs and organic roofs are also in use, but to a small extent. Clay tile roofs and painted iron sheet roofs were observed to be in use on some commercial and office buildings, high and middle income households, and government and private institutions. Plain iron sheet roofs were also observed on commercial and office buildings to a small extent; some middle income and most low income households. On the low income households, they were generally characteristically well rusted.

The study has determined the quality suitability of the rainwater from these roofs, in terms of heavy metal contamination. For Lead, Cadmium and Nickel the levels were below 0.001 mg/L. 46% of Copper cases had a contamination level of less than 0.01 mg/L, whereas 38% of the cases were at a level of 0.01 mg/L, while the rest was at 0.02 mg/L. The modal Zinc level was 0.01 to 0.49 mg/L.

The quality of the rainwater in terms of heavy metal contamination was assessed with various accepted standards for drinking water. These were WHO Drinking Water Guidelines; NEMA Uganda Standards for Discharge of Effluent into Water or on Land; and the Uganda National Bureau of Standards Draft Standard for Bottled Waters Other than Natural Mineral Waters. It has been found that heavy metal contamination is largely minimal, except for Zinc, which is lower than WHO limits in 98% of the cases, but has surpassed the Draft UNBS Standard limits in 28% of the instances.

## REFERENCES

*https://dx.doi.org/10.22161/ijaers.5.1.14* *ISSN: 2349-6495(P) | 2456-1908(O)*

[1] Anon (1999). *National Environment (Standards for Discharge of Effluent into Water or On Land) Regulations*. Statutory Instruments Supplement, No. 5, To the Uganda Gazette No. 7, Vol. XCII.

[2] Development Technology Unit (2002). *Very Low Cost Domestic Roofwater Harvesting in the Humid Tropics: Constraints and Problems*. DFID KaR Contract R7833, pages 3-4, 16-17.

[3] Nabulo Grace (2004). Assesment of heavy metal contamination of food crops and vegetables from motor vehicles emissions in Kampala City, Uganda. *A Technical paper submitted to IDRC,* Agropolis, pages 1 – 40

[4] Khatiwada, N.R., Takizawa, S., Tran, T.V.N. and Inoue, M. (2002). Groundwater contamination assessment for sustainable water supply in Kathmanandu Valley, Nepal, Water Science and Technology, Vol 46 (9), pages 147-154.

[5] Mugisha, S., Berg, S.V. and Katashaya, G.N. (2004). Short-term initiatives to improve Water Utility Performance in Uganda: The case of National water and Sewerage Corporation

[6] NWSC (2002). Cost of Kampala Water Will Rise. (2002, October 2) http://www.nwsc.co.ug/news.php.?StoryId=124. Accessed on 27th March 2004.

[7] UNBS (1994) standard specification for Drinking (Portable) Water: US201: 1994. Uganda UDC 543.341

[8] World Health Organization (2004), Drinking water Quality: Recommendations, Vol.1, 3rd Edition, Geneva

https://dx.doi.org/10.22161/ijaers.5.1.15 ISSN: 2349-6495(P) | 2456-1908(O)

# Evaluation of the Potential use of Bagasse and Sugar Millswaste Water as Substrate for Biogas Production

Mulindi S.A., Odhiambo B. O.

Department of Agriculture and Bio systems Engineering- University of Eldoret,; P.O. Box 1125-30100, Eldoret,

***Abstract*****—***Biogas is a sustainable alternative source of energy to fossil fuels. Its production also serves as sink for biological wastes and it is a pollution control measure. Most of biogas generation units in Kenya utilize animal wastes as the substrate. However, the bio fuel potential of bagasse, the abundant crop residues like co-products in sugarcane-based industries remain underutilized. The idea of converting bagasse into additional energy is gaining attention, especially through government commitments on increasing the renewable energy generation combined with the reduction of carbon dioxide emissions. In this study bagasse samples collected from Chemelil sugar mills were passed through multiple sieves of different sizes to obtain different particle sizes. Mills waste water was also collected from Chemelil sugar factory and analyzed for pH and Total Dissolved Solids (TDS) to establish their biogas production potential, the analyzed mills waste water was then mixed with different particle sizes of bagasse and allowed to be digested anaerobically. Volume of the gas collected from each flask containing different particle sizes of bagasse was measured to identify the optimum conditions for biogas production. The study showed that the mills waste water that had the highest TDS (130g/L) yielded relatively higher volumes of biogas when mixed with bagasse of different particle sizes. Bagasse of particle size ≤0.600mm produced the highest volume when mixed with the mills waste water with TDS and pH of130g/l and 4.67 respectively. Designing and installing a digester system that allows for the control of TDS and pH in mills wastewater and utilizes bagasse of particle size ≤0.600mm would be expected to produce reasonable amount of biofuel and put a check on environmental pollution problems associated with bagasse and sugar mill waste waters in sugar factories.*

***Keywords*****— Bagasse, biogas, mill waste water, pH and TDS.**

## I. INTRODUCTION

Biogas refers to a mixture of different gases produced by the breakdown of organic matter in the absence of oxygen. Biogas can be produced from raw materials such as agricultural wastes (e.g. Sugarcane bagasse, animal excreta), domestic wastes and industrial wastewaters. Bagasse is the fibrous matter that remains after sugarcane is crushed to extract its juice. Sugarcane based industries are among the most promising agricultural sources of biogas energy in Kenya from abundant co-products of bagasse and waste water. However, the Kenyan Sugar industries are yet to embrace technologies that could utilize the wastes in the production of biogas and fertilizers. The bagasse waste is often left to decompose outside the sugar factories (Figure 1.1), thus contributing to environmental pollution and consume the much needed space in and around the factories.

The accumulated bagasse are common features in and around sugar milling facilities putting water bodies around the factories under constant threat of pollution by both leachates from the bagasse and waste water from the factories. Anaerobic digestion of sugarcane waste can be considered a promising strategy since the slurry could still be used to partially replace the mineral fertilizers on the sugarcane fields and the produced biogas could be upgraded to bio methane and sold as a new energy product by the sugarcane manufacturing firms. The sum of these being a fermentation which converts a wide array of substrate materials, having carbon atoms at various oxidation/reduction states, to molecules containing one carbon in its most oxidized ($CO_2$) and the most reduced ($CH_4$) state. Minor quantities of nitrogen, hydrogen, ammonia and hydrogen sulphide(usually less than 1% of the total gas volume) are also generated [13].The principal objectives of recycling bagasse and waste water are generally to allow industrial effluents to be disposed of without posing risk to human health and to prevent unacceptable damage to the natural environment. Since cost effectiveness is one of the key considerations in any production process, it is imperative to identify and profile the major waste products from sugar industries that could be used for other economic gains as a way of environmental pollution control.

https://dx.doi.org/10.22161/ijaers.5.1.15 ISSN: 2349-6495(P) | 2456-1908(O)

*Fig,1.1: Accumulated bagasse waste outside Sony sugar factory*

Similarly waste water from the sugar production processes and cleaning operations in the factories end up into surface water bodies. The recipient water bodies are at risk of chemical pollution, thermal pollution and eutrophication (Figure 1.2) shows accumulating wastewater from Chemelil sugar factory, in Kisumu County.

*Fig.1.2: Waste water around Chemelil sugar factory*

Bagasse is the fibrous matter that remains after sugarcane is crushed to extract its juice. According to [4], accumulation of greenhouse gasses in the atmosphere and limited fossil fuel reserves, a transition away from fossil fuel is necessary. Bagasse has got the potential for being used for biogas generation as studied by [6] and can reduce the reliance on fossil fuel. Study by [10] show that the annual production of dry cut sugarcane is about 328 million tons and after sugars have been extracted about 180 million tons of bagasse remain which could be used in biogas production However, in Kenya some bagasse is burned for process heat in sugar mills and distillers [1].

https://dx.doi.org/10.22161/ijaers.5.1.15 ISSN: 2349-6495(P) | 2456-1908(O)

Excess bagasse is left to decompose outside the industries and is likely to be a source of environmental pollution.

Bagasse is a lignocellulosic biomass primarily composed of cellulose (38 to 45%) hemicellulose (23 to 27%) and lignin (19 to 32%) [5]. Today new enzyme cocktails developed for scarification of lignocellulose contain high β glycosidase activity and lytic polysaccharides mono oxygenases, LPMOs [3],[9],[4] and may also include better and more stable cellulose. Overall these improvements have led to considerably more efficient enzyme cocktails [2] that will help in the digestion of bagasse to generate biogas.

For optimum biogas production, sugarcane bagasse residues should be harvested within their growing period as fresh. The drier and straw-like the plant, the less biogas it produces [7]. [11]Stated that Bagasse substrate should be chopped into smaller pieces in order to increase the surface area for hydrolytic enzymes to attack and thus to release more soluble components. However, they never specified the specific size in which the bagasse particles should be chopped. In this work the optimum size of bagasse was determined and recommendations made. Recently, the concept of the bio refinery has received considerable attention as an alternative route for biomass exploitation, based on integrated combined processes for the simultaneous generation of energy, fuel, and value – added products [8]. As an abundant waste, bagasse could be used for production of sig Wastewater is any water that has been adversely affected in quality by anthropogenic influence.

This water are collected and channeled into a common treatment plant after which they are being discharged back to the river. This waste water contains a lot of sugar that can aid fermentation process.

## II. METHODOLOGY

### 2.1.1. Area of study

Study was carried in University of Eldoret School of Agriculture Chemistry laboratory at 2,100 meters above sea level. At 00 34' 43"N and 350 18' 21" E.

The project samples were collected from Chemelil Sugar Company located in in Kisumu County, Kenya. The field work involved visiting the company and collecting samples of the waste water from the five sources of the waste water in the industries i.e. sugar process house, juice treatment, mills water, V – notch water, anaerobic pond. The samples were collected on 23rd May 2016

### 2.2. Types of tests on industrial waste water

Waste water was collected in a clean three litre tin from five locations of the sugar mill and was carried to the University laboratory for analysis. The locations were; Sugar process house, Juice treatment house, Mill waters, V – Notch water and anaerobic pond.

### 2.2.1 Determining Total Dissolved Solids (TDS)

Total dissolved solids (TDS) is defined as "the combined content of all inorganic and organic substances contained in a liquid that are present in a molecular, ionized or micro granular suspended form." TDS is measured on a quantity scale, either in mg/L or, more commonly, in parts per million (ppm). In this study the TDS was determined in the laboratory using the following setup and procedure.

### 2.2.2Apparatus

Porcelain dish, Hot plates, Measuring cylinder, Beaker,Weighing balance.

### 2.2.3 Procedure

The empty porcelain dish was weighed and weight recorded. Using the measuring cylinder equal volume of 50ml of the industrial water was measured and added to the pre-weighed porcelain dishes labelled differently for different samples. The samples were then placed on hot plate until all the water evaporated. The set up was as shown in figure 3.1 below

*Fig.2.1: sample of waste waters on hot plate*

### 2.3 pH

The term pH refers to the measure of hydrogen ion concentration in a solution and defined as the negative logarithm of hydrogen ions concentration ($-Log_{10}$ [H+] in water, wastewater or a solution. The values of pH 0 to a little less than 7 are termed as acidic and the values of pH a little above 7 to 14 are termed as basic. When the concentration of H+ and OH– ions are equal then it is termed as neutral pH, and corresponds to a value of 7.

Wastewater was collected in cleaned tins from different sources in the factory and labelled using stickers. Their pH was measured using pH meter using the procedure shown below.

### 2.3.1 Procedure.

- 15mL of each of industrial waste water was poured into separate 30mL beakers.
- pH electrode was then connected to the meter

https://dx.doi.org/10.22161/ijaers.5.1.15 ISSN: 2349-6495(P) | 2456-1908(O)

- The protective cap was then removed from the electrode and rinsed. The electrode was shaken gently to remove excess water
- The electrode was then immersed into the waste water. The electrode should be submerged at least 1.5cm into the water poured in the beakers.
- The electrode cap was then rinsed with deionized water to remove any residues and to dry in air.
- Press the "ON/OFF" button. Note that buttons have a delayed response and holding down lightly for a couple of seconds is required to get a response.
- If "CAL" does not appear on the left of the screen, press and hold down the "CAL" button and the left side of the screen will flash "NOT READY "until the meter reading stabilizes.
- Repeat the procedure for other samples

The set up was as shown in figure 3.2 below.

*Fig.2.2: pH meter being used to measure sample pH*

**2.4. Determination of the bagasse particle size**

The bagasse sample was collected in clean dry polythene from Chemelil sugar factory and was carried to the university laboratory for analysis. The sample was dried inside glass green house as shown in figure 3.3 below prevent the smaller particles from being carried away by wind.

*Fig.2.3: Bagasse being dried before grinded.*

**2.4.1 Apparatus and materials**

Mechanical shaker, Bagasse, Brass, Sieves of the different sizes(1.0mm, 0.6mm, 0.425mm, 0.3mm, 0.212mm, 0.15mm),Pastle and mortar.

**2.4.2 Procedure**

The sieves were cleaned to remove all residues from previous experiments. Small portions of bagasse were added to the mortar and ground using into smaller sizes. The sieves were then arranged in descending order of sizes and the bagasse was added in the top sieve then clamped on the mechanical shaker. The set up was the shaken thoroughly for 20 minutes. The set up was as shown in figure 3.4 below.

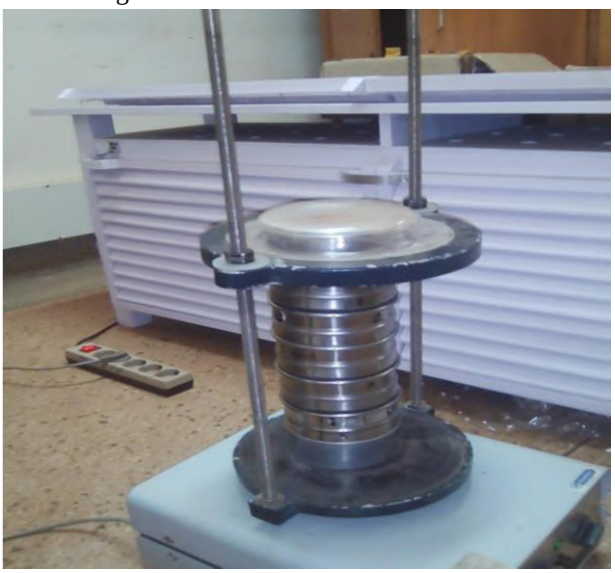

*Fig.3.4: Mechanical shaker and sieves*

**2.5 Experimental set up for biogas production**

The various samples of waste water obtained from various sources in the factory and different particle sizes of bagasse were mixed to react in order to produce biogas.

https://dx.doi.org/10.22161/ijaers.5.1.15 ISSN: 2349-6495(P) | 2456-1908(O)

**2.5.1 Procedure**

Five conical flasks were cleaned and rinsed thoroughly using clean distilled water and labelled using stickers, labelling was done in descending order of particle sizes. The bagasse sample was then weighed and poured into different conical flask as shown in the table below.

*Table.2.1: Particle size and water added*

| Labelled | Particle size of bagasse | Water added |
|---|---|---|
| Flask 1 | 1.000mm | Sugar process house |
| Flask 2 | 0.600mm | Juice treatment house |
| Flask 3 | 0.425mm | Mills waters |
| Flask 4 | 0.300mm | V – Notch water |
| Flask 5 | 0.215mm | Anaerobic pond. |

The mills waste water collected from various sources was then measured using measuring cylinder and added to the conical flask in and stirred using stirrer in order to mix with the bagasse, the conical flask was then closed using a cork fitted with a straw that allows the delivery of the gas generated. The gas was collected using non – porous plastic polythene bags, the set up was then stored in a safe place for twenty days to react and generate the gas. The set up was as shown in the image below.

*Fig.2.5: Set up for biogas production*

The set up was monitored daily and the reaction rate was observed and changes in the conical flask were noted, increase in size of the polythene bag and accumulation of moisture on the walls of some conical flask were also observed as shown in figure 2.6 below

https://dx.doi.org/10.22161/ijaers.5.1.15 ISSN: 2349-6495(P) | 2456-1908(O)

*Fig.2.6: vapour condensing on walls of conical flask*

After the retention period was attained, the gas collected in the polythene bag was carefully removed from the setup, its mass was measured and the volume was estimated through assuming the density of methane to be 0,656Kg/$m^3$ since it is the most abundant gas in the mixture. The results obtained were as shown in table 4.1.

## III. RESULTS AND DISCUSSIONS

### 3.1 Determination of TDS.

The results of the experiment to determine the TDS of various water samples collected from the factory is as shown in the table 4.1 below. The values of TDS we calculated; For example, for sample 1

TDS = 0.032 x 1000 = 32g/l

Calculation was repeated for the entire to obtain various values of TDS of the remaining samples and results

*Table.3.1: TDS values for wastewater samples from Chemelil Sugar Factory*

| Sample | Weight of empty tin (g) | Resultant weight after evaporation (g) | Weight difference | TDS (g/l) |
|---|---|---|---|---|
| Sample 1 | 25.5 | 27.1 | 1.6g | 32g/l |
| Sample 2 | 33.6 | 40.1 | 6.5g | 130g/1 |
| Sample 3 | 33.2 | 34.5 | 1.3g | 26g/l |
| Sample 4 | 24.8 | 27.6 | 2.8g | 56g/l |
| Sample 5 | 33.1 | 34.9 | 1.8g | 36g/l |

### 3.2 Results of pH of the waste waters.

*Table.3.2: pH values for wastewater samples from Chemelil Sugar Factory*

| Sample | Source of the sample | pH value |
|---|---|---|
| Sample 1 | Sugar process house | 4.28 |
| Sample 2 | Juice treatment house | 4.67 |
| Sample 3 | Mills waters | 5.14 |
| Sample 4 | V – Notch water | 5.44 |
| Sample 5 | Anaerobic pond. | 5.60 |

https://dx.doi.org/10.22161/ijaers.5.1.15 ISSN: 2349-6495(P) | 2456-1908(O)

*Table.3.3: Results of volume of gas generated*

| Flask | Particle size | Weight of gas generated + polythene bag (g) | Weight of the gas (g) | Volume of the gas ($cm^3$) |
|---|---|---|---|---|
| Flask 1 | 1.000mm | 0.08g | 0.07g | 10.67$cm^3$ |
| Flask 2 | 0.600mm | 0.10g | 0.09g | 13.72 $cm^3$ |
| Flask 3 | 0.425mm | 0.07g | 0.06g | 9.15$cm^3$ |
| Flask 4 | 0.300mm | 0.06g | 0.05g | 7.62$cm^3$ |
| Flask 5 | 0.215mm | 0.02g | 0.01g | 1.52$cm^3$ |

Assumptions made in this calculation was that the overall density of the biogas was taken to be 0.656kg/m3 which is the density of methane since it is the highest portion of the gas generated i.e.
68% of the total volume.

**3.4 Data presentation**

3.4.1 Particle size against volume

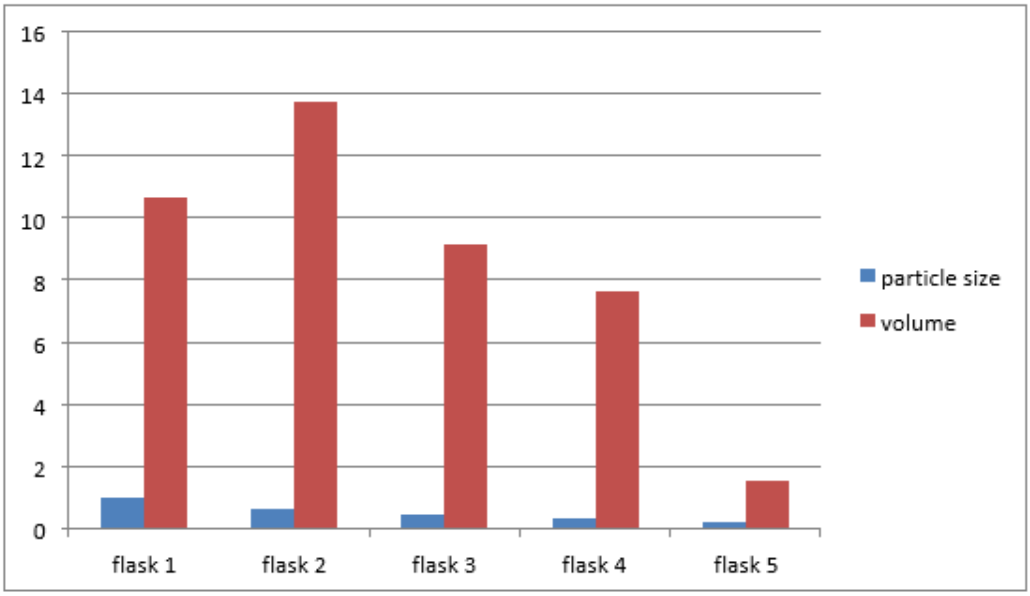


*Fig.3.1: Graph showing particle size against volume*

3.4.2 TDS against volume

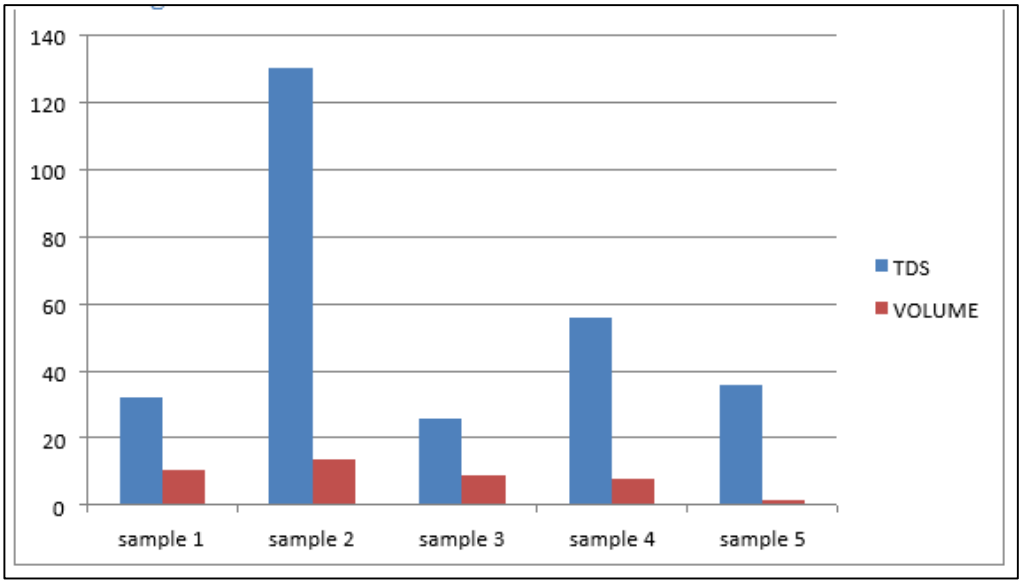


*Fig.3.2: Graph showing TDS against Volume.*

https://dx.doi.org/10.22161/ijaers.5.1.15 ISSN: 2349-6495(P) | 2456-1908(O)

3.4.3 pH Against Volume

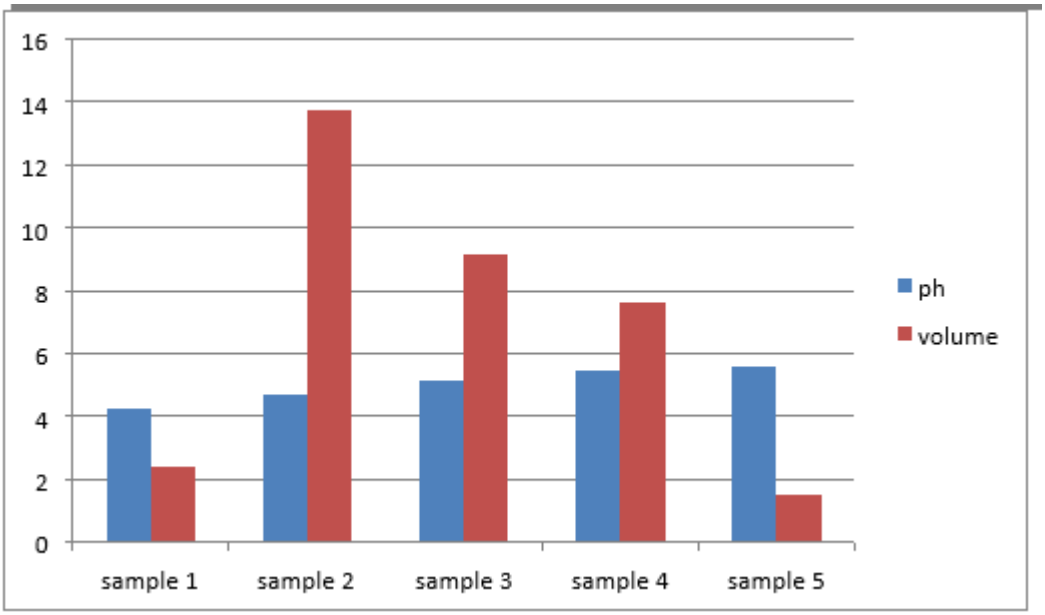


*Fig 3.3: Graph showing pH against volume*

3.4.4 Comparison of pH, particle size, TDs and volume

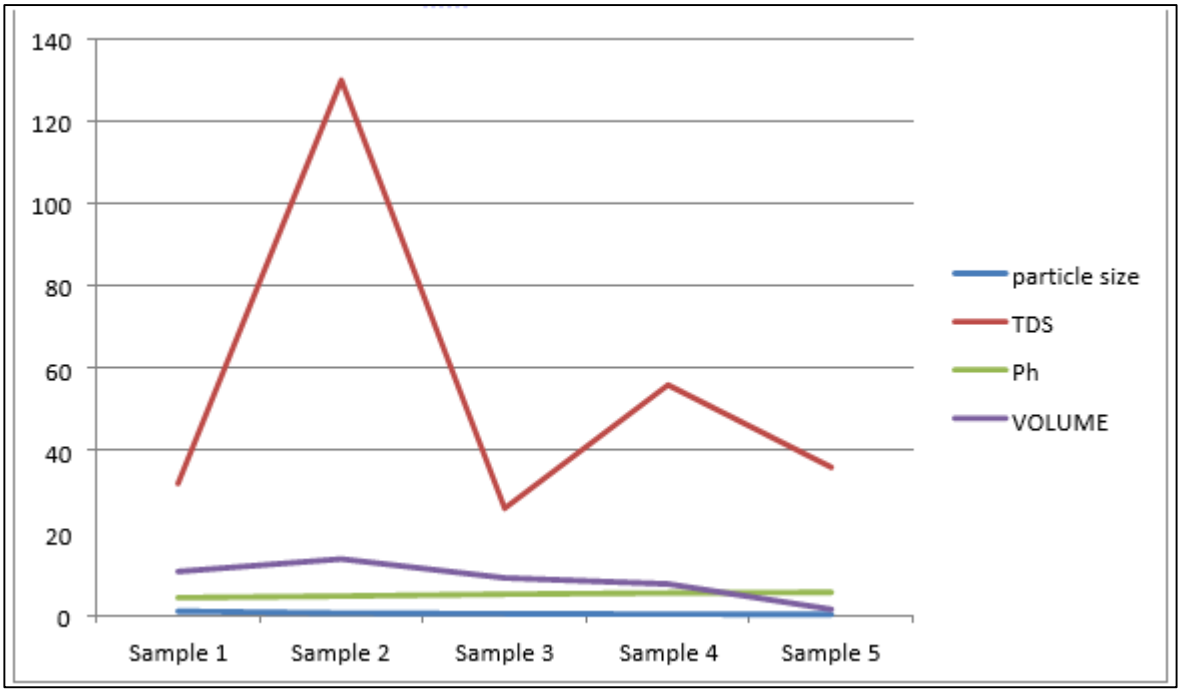


*Fig.3.4: Graph showing comparison of pH, particle size and TDS against volume of biogas*

**3.5 Discussions**

The biogas components and biogas yield depend on feed materials due to the difference of material characteristics in each raw material [12]. Different particle sizes of bagasse and different quality of waste water were investigated to determine characteristics of biogas production. In this study, the experiment had been done in natural condition. The characteristics of biogas production using different particle sizes and different quality of mills waste water are discussed as follow.

**3.5.1 Influence of pH on biogas production**

At pH 4.67, the volume of biogas generated was more compared to pH of 6.69, this was because the mills waste water was probably in the initial stage of fermentation due to presence of sugar and the bacteria present were already active to digest bagasse particle sizes. In this study the

*https://dx.doi.org/10.22161/ijaers.5.1.15* *ISSN: 2349-6495(P) | 2456-1908(O)*

optimum pH ranges from 4.67 – 5.44, this confirms the study by [14]on influence of pH on anaerobic process.

**3.5.2 Influence of particle size on biogas production**

Particle sizes of bagasse play an important role in biogas production. The smaller particle sizes are readily digested by anaerobic bacteria than the larger ones. In this experiment the optimum particle size that yielded high volume of biogas is observed to be 0.6mm. This is because this size contains less fibers and dust particle hence can easily be digested by anaerobes bacteria to generate biogas. Smaller particle sizes were observed to generate less volume of biogas due to the fact that they are mixed with other smaller particles like soil that don't contain nitrogen element which is responsible anaerobic digestion. Particle size of 1.00mm produced good volume of biogas due the influence of the waste water used which contained high level of microorganism that digested portion of the bagasse substrate.

There is a general trend of decrease in volume of biogas produced as the particle sizes of bagasse reduces as shown in (Figure 4.1.), in the second conical flask the volume was observed to be high due other factors.

**3.5.3 Influence of TDS on volume of biogas production**

The volume of biogas generated was observed to be high in flask 2 which contained water with a TDS of 130g/l. This is because high TDS shows high presence of microorganism and other impurities that will generate maximum biogas. In the flask where water of low TDS was added less volume of gas was generated due to presence of less number of anaerobes that digest bagasse particles as shown in Figure 4.2

**3.5.4: Comparison of the TDS, pH, TDS, particle size on volume of gas produced**.

As can be seen in Figure 4.4 the volume of biogas generated varied in different direction depending on the parameters that was observed. The volume of gas produced was observed to be highest in wastewater sample, drawn from juice treatment house, which had TDS of 130g/l, pH of 4.67, mixed with Bagasse of particle size of 0.600mm. This can be taken as the optimum conditions for the use of bagasse and industrial waste water.

## IV. CONCLUSION

Anaerobic fermentation for biogas production is very complex reactions which involve many intermediate compounds and microorganisms that play important role in the process. This study evaluated the potential of different particle sizes of bagasse and different qualities of waste water in terms of TDS, pH of the mills waste water, in production of biogas.

The result can be concluded as follows:

a) High level of TDS in mills waste water catalyzes biogas production when mixed with different particle sizes of bagasse.
b) The biogas production was highest when using bagasse of particle size 0.6mm due absence of foreign particles and absence of fibrous matter content that has less nitrogen content hence this size appeared to be the most suitable to be used in digesters.
c) The variation in volume of biogas produced in various set up was mainly dependent on TDS level and pH.

## REFERENCES

[1] Alsonso P., Luengo W., andAlberteries A.M. (2011). "Energy recovery from sugarcane trash in the light of second generation biofuels. Part 1.

[2] Canella, D., and Jorgensen, H. (2014). Do new cellulytic enzyme preparations affect the indusrial strategies for high solid lignocellulosic ethanol production? Biotechnol. Boieng. Vol 111 (1), pages 59 – 68.

[3] Vaaje- Kolstad G., Westareng B., Horn S.J., Liu Z., Zhai H. and Sorlie M., (2010).An oxidative enzyme boosting the enzymatic conversion of recalcitrant polysaccharides, Science, vol. 330, pages 219-222

[4] Horn S.J., Estevez M.M., Neilsen (2011). Biogas production and sacchrification of salix pretreated at different steam explosion condition, Bio resource. Technol. 102(17), pages 7932 – 7936.

[5] Canihla L., Chandel A. L., Milessi T. S., Antunes F. A., Freitas W. L., Felipe M. and Silva S., (2012), Bioconversion of sugarcane Biomass into ethanol: An overview about composition, pretreatment methods, Detoxification of hydrolysates, Enzymatic Saccharification and ethanol fermentation, Journal of Biomedicine and Biotechnology

[6] Malik Badshah, Duong Minh Lam, Jing Liu and Bo Mattiason, (2012). Use of an automatic methane potential test system for evaluating the biomethane potential of sugar bagasse after different treatment, Bioresource Technology, vol. 114, pages 262-269

[7] Seppala M., Paavola T., Lehtomaki A. and Rintala J. (2009). Biogas production from boreal herbaceous grasses-specific methane yield per hectare, Bioresource technology, vol. 106 (12),pages 2952-2958

[8] Ragauskas A.J., Williams C. K., Davinson, B.H., Britovsek (2006). The path forward for biofuels and Biomaterials, Science, vol 311 (5760), pp 484 – 489

[9] Quinlan R.J., Sweeney M.D., Leggio L., Otten H., Poulsen J.C, K.S. Johansen,…& Walton P. (2011), Insights into the oxidative degradation of cellulose by a copper metalloenzyme that exploits biomas component, Proceedings of The National Academy of Science, Vol. 108 (37), pages 15079-15084

*https://dx.doi.org/10.22161/ijaers.5.1.15* *ISSN: 2349-6495(P) | 2456-1908(O)*

[10] Seungdo Kim and Bruce E. Dale, (2004). Global potential bioethanol production from waste crops and crop residue, Biomass and bioenergy, vol 26(4), pages 361-371

[11] Molano D.P., Liliana, G.L. Carolina and Hernandez E., (2012). Influence of particle size and Temperature on methane production from Fique's Bagasse, Heckne, vol 9(2), pages72-77

[12] Wantanee Anunputtikul and Sureelak Rodtong,(2004). Laboratory experiments for biogas production from Cassava tubers, The joint international conference on "Sustainable Energy and Environment (SEE)

[13] Angelidaki, I., Alves M., Bolzonella D., Borzacconi L., Campos J.L., Guwy A.J., Kalyuzhnyi S., Jenicek P. &Van Lier J.B, (2009). Defining the Biomethane Potential [BMP] of solid organic Wastes and Energy crops: A proposed protocol for batch assays, Water science and Technology, Vol 59(5), pages 927-934

[14] Speece, R.E.,(1996). Anaerobic Technology for Industrial Wastewater, Archae Press, USA.

https://dx.doi.org/10.22161/ijaers.5.1.16 *ISSN: 2349-6495(P) | 2456-1908(O)*

# A Simplified Introduction to Music Algebra: from the Scale Vectors to the Modal Tensor

Carmine Cataldo

Independent Researcher, PhD in Mechanical Engineering, Jazz Pianist and Composer, Battipaglia (SA), Italy
Email: catcataldo@hotmail.it

***Abstract*—***In this paper we take a step forward towards the attainment of a formalism that allows to establish a deeper connection between Music and Algebra. Starting from the writing of the Ionian Scale as a Vector, we define the Ionian Modal Tensor. We prove that all the Scales that derive from the Ionian Mode, as well as all the corresponding Seventh Chords, herein considered as being Scalars, can be obtained from the above-mentioned Tensor by resorting to the concepts of Standard Basis and Dot Product. Moreover, by opportunely summing the Vectors of the Standard Basis to each other, we define some interesting Fundamental Vectors such as the "Monk – Powell" Vector and the "Guide Notes" one.*

***Keywords*—Music Algebra, Scale Vector, Modal Tensor, Harmonization, Standard Basis, Matrix, Dot Product.**

## I. BRIEF INTRODUCTION

We start by defining the *Ionian scale* a *vector* whose *components* are nothing but the *degrees* of the *scale*. The same procedure is applied to all the *scales* that derive from the above-mentioned. Subsequently, we define the *Ionian Modal Tensor* and, by resorting to the concepts of *standard basis* and *dot product*, we deduce the *seventh chords vector*. A reasonable mastery of the fundamental notions concerning *vectors* and *matrices* is required.

## II. SCALES AS VECTORS

If we denote with $X$ a generic note belonging to the *Chromatic scale*, and with $t$ a *whole tone interval* [1] [2], we can represent the *Ionian scale* as a *vector*:

$$\boldsymbol{s}^{Ion}(X) = \left(X, X+t, X+2t, X+\frac{5}{2}t, X+\frac{7}{2}t, X+\frac{9}{2}t, X+\frac{11}{2}t\right) \quad (1)$$

For example, by setting $X = C$, from *(1)* we banally obtain:

$$\boldsymbol{s}^{Ion}(C) = (C, D, E, F, G, A, B) \quad (2)$$

Obviously, whatever scale can be represented as a vector. In this regard, let's consider all the *modes* (or *scales*) that can be deduced from the *Ionian* one (*Dorian*, *Phrygian*, *Lydian*, *Mixolydian*, *Aeolian*, *Locrian*) [3] [4]. Bearing in mind the *Ionian harmonization*, and denoting with $\boldsymbol{s}^{Ion,n}$ the *scale vector* derived from the *n-th degree* of the *Ionian scale* ($n$ is a positive integer that runs from 1 to 7), we can write, with obvious meaning of the notation, the following:

$$\boldsymbol{s}^{Ion,1}(X) = \boldsymbol{s}^{Ion}(Y) \qquad Y = X \quad (3)$$

$$\boldsymbol{s}^{Ion,2}(X) = \boldsymbol{s}^{Dor}(Y) \qquad Y = X + t \quad (4)$$

$$\boldsymbol{s}^{Ion,3}(X) = \boldsymbol{s}^{Phr}(Y) \qquad Y = X + 2t \quad (5)$$

$$\boldsymbol{s}^{Ion,4}(X) = \boldsymbol{s}^{Lyd}(Y) \qquad Y = X + \frac{5}{2}t \quad (6)$$

$$\boldsymbol{s}^{Ion,5}(X) = \boldsymbol{s}^{Mix}(Y) \qquad Y = X + \frac{7}{2}t \quad (7)$$

$$\boldsymbol{s}^{Ion,6}(X) = \boldsymbol{s}^{Aeo}(Y) \qquad Y = X + \frac{9}{2}t \quad (8)$$

$$\boldsymbol{s}^{Ion,7}(X) = \boldsymbol{s}^{Loc}(Y) \qquad Y = X + \frac{11}{2}t \quad (9)$$

Clearly, the opposite procedure can be easily followed: in other terms, we can choose any *mode* (among those to date considered) and determine the *Ionian scale* from which it derives (if we select a *mode* and set $Y$, we can determine $X$). For example, since the *Dorian mode* arises from the *second degree* of the *Ionian scale* [3] [4] [5] [6] [7], taking into account *(4)*, we can immediately write:

$$\boldsymbol{s}^{Dor}(Y) = \boldsymbol{s}^{Ion,2}(X) \qquad X = Y - t \quad (10)$$

If we set $X = C$, from *(3)*, *(4)*, *(5)*, *(6)*, *(7)*, *(8)* and *(9)* we obtain, respectively:

$$\boldsymbol{s}^{Ion,1}(C) = \boldsymbol{s}^{Ion}(C) = (C, D, E, F, G, A, B) \quad (11)$$

$$\boldsymbol{s}^{Ion,2}(C) = \boldsymbol{s}^{Dor}(D) = (D, E, F, G, A, B, C) \quad (12)$$

$$\boldsymbol{s}^{Ion,3}(C) = \boldsymbol{s}^{Phr}(E) = (E, F, G, A, B, C, D) \quad (13)$$

$$\boldsymbol{s}^{Ion,4}(C) = \boldsymbol{s}^{Lyd}(F) = (F, G, A, B, C, D, E) \quad (14)$$

$$\boldsymbol{s}^{Ion,5}(C) = \boldsymbol{s}^{Mix}(G) = (G, A, B, C, D, E, F) \quad (15)$$

$$\boldsymbol{s}^{Ion,6}(C) = \boldsymbol{s}^{Aeo}(A) = (A, B, C, D, E, F, G) \quad (16)$$

$$\boldsymbol{s}^{Ion,7}(C) = \boldsymbol{s}^{Loc}(B) = (B, C, D, E, F, G, A) \quad (17)$$

https://dx.doi.org/10.22161/ijaers.5.1.16 ISSN: 2349-6495(P) | 2456-1908(O)

## III. THE MODAL TENSOR

*Taking into account (11), (12), (13), (14), (15), (16) and* (17), we instantly obtain a matrix of notes whose rows and columns are nothing but the scale vectors that derive from the *Ionian mode*:

$$\boldsymbol{M}^{Ion}(C) = \begin{bmatrix} C & D & E & F & G & A & B \\ D & E & F & G & A & B & C \\ E & F & G & A & B & C & D \\ F & G & A & B & C & D & E \\ G & A & B & C & D & E & F \\ A & B & C & D & E & F & G \\ B & C & D & E & F & G & A \end{bmatrix} \quad (18)$$

The above-mentioned matrix represents the *Ionian modal tensor* denoted by $\boldsymbol{M}^{Ion}$. We highlight that the "$\boldsymbol{M}$" is written in bold, since we do not deal with a s*calar*, and in upper-case in order to create a distinction between tensors and vectors. The latter are herein written, in fact, in lower-case. The *Ionian modal tensor* is *symmetric*: consequently, with obvious meaning of the notation, we have:

$$M_{ij}^{Ion} = M_{ji}^{Ion} \quad (19)$$

As a consequence, if, once again, we denote with $\boldsymbol{s}^{Ion,n}$ the *scale vector* derived from the *n-th degree* of the *Ionian scale*, we can evidently write:

$$\boldsymbol{s}^{Ion,n} = \left(M_{n1}^{Ion}, M_{n2}^{Ion}, M_{n3}^{Ion}, M_{n4}^{Ion}, M_{n5}^{Ion}, M_{n6}^{Ion}, M_{n7}^{Ion}\right) \quad (20)$$

$$\boldsymbol{s}^{Ion,n} = \left(M_{1n}^{Ion}, M_{2n}^{Ion}, M_{3n}^{Ion}, M_{4n}^{Ion}, M_{5n}^{Ion}, M_{6n}^{Ion}, M_{7n}^{Ion}\right) \quad (21)$$

Let's now consider the *standard basis* of the 7-dimensional *Euclidean space* ($\mathscr{R}^7$):

$$\boldsymbol{d^1} = (1,0,0,0,0,0,0) \quad (22)$$

$$\boldsymbol{d^2} = (0,1,0,0,0,0,0) \quad (23)$$

$$\boldsymbol{d^3} = (0,0,1,0,0,0,0) \quad (24)$$

$$\boldsymbol{d^4} = (0,0,0,1,0,0,0) \quad (25)$$

$$\boldsymbol{d^5} = (0,0,0,0,1,0,0) \quad (26)$$

$$\boldsymbol{d^6} = (0,0,0,0,0,1,0) \quad (27)$$

$$\boldsymbol{d^7} = (0,0,0,0,0,0,1) \quad (28)$$

The *standard basis* consists in seven *fundamental vectors*. Evidently, every *fundamental vector* is characterized by having all the *components* null except for the one specified in the superscript, which is equal to 1.

At this point, it is easy to imagine how a generic *scale vector* $\boldsymbol{s}^{Ion,n}$ can be obtained by means of the *dot product* between the *modal tensor* and the *n-th fundamental vector*:

$$\boldsymbol{s}^{Ion,n}(X) = \boldsymbol{M}^{Ion}(X) \cdot \boldsymbol{d^n} \quad (29)$$

For example, taking into account *(5)* and *(29)*, we have:

$$\boldsymbol{s}^{Phr}(Y) = \boldsymbol{s}^{Ion,3}(X) = \boldsymbol{M}^{Ion}(X) \cdot \boldsymbol{d^3} \qquad Y = X + 2t \quad (30)$$

From *(30)*, by setting $X = C$, we immediately obtain:

$$\boldsymbol{s}^{Phr}(E) = \boldsymbol{s}^{Ion,3}(C) = \boldsymbol{M}^{Ion}(C) \cdot \boldsymbol{d^3} \quad (31)$$

$$\boldsymbol{s}^{Phr}(E) = \begin{bmatrix} C & D & E & F & G & A & B \\ D & E & F & G & A & B & C \\ E & F & G & A & B & C & D \\ F & G & A & B & C & D & E \\ G & A & B & C & D & E & F \\ A & B & C & D & E & F & G \\ B & C & D & E & F & G & A \end{bmatrix} \begin{bmatrix} 0 \\ 0 \\ 1 \\ 0 \\ 0 \\ 0 \\ 0 \end{bmatrix} = \begin{bmatrix} E \\ F \\ G \\ A \\ B \\ C \\ D \end{bmatrix} \quad (32)$$

Obviously, the *fundamental vectors* can be summed to each other. According to our notation, the vectors we obtain are characterized by superscripts that reveal the non-null components (the components equal to 1). We have:

$$\boldsymbol{d^1} + \boldsymbol{d^7} = \boldsymbol{d^{17}} = (1,0,0,0,0,0,1) \quad (33)$$

$$\boldsymbol{d^3} + \boldsymbol{d^7} = \boldsymbol{d^{37}} = (0,0,1,0,0,0,1) \quad (34)$$

$$\boldsymbol{d^1} + \boldsymbol{d^3} + \boldsymbol{d^5} = \boldsymbol{d^{135}} = (1,0,1,0,1,0,0) \quad (35)$$

$$\boldsymbol{d^1} + \boldsymbol{d^3} + \boldsymbol{d^5} + \boldsymbol{d^7} = \boldsymbol{d^{1357}} = (1,0,1,0,1,0,1) \quad (36)$$

We can now name the vectors we have just deduced. Very intuitively, $\boldsymbol{d^{17}}$ may be named *"Monk-Powell" fundamental vector* (since both *Thelonious Monk* [8] [9] and *Bud Powell* [10] [11] used to play *dyads*, exclusively consisting of the *root* and the *seventh* of the *chord*, with the left hand), $\boldsymbol{d^{37}}$ *"guide notes" fundamental vector*, $\boldsymbol{d^{135}}$ *triad fundamental vector*, $\boldsymbol{d^{1357}}$ *seventh chord fundamental vector*.

In particular, the vector $\boldsymbol{d^{1357}}$ may be exploited to obtain seventh chords (that we regard as *scalars*) from scales, by resorting, once again, to the *dot product*. If $\boldsymbol{s}^{Ion,n}(X)$ is the *vector* that represents the *mode* derived from the *n-th degree* of the *Ionian Scale* of *X*, the corresponding *seventh chord* can be immediately obtained, with obvious meaning of the notation, as follows:

$$c^{Ion,n}(X) = \boldsymbol{s}^{Ion,n}(X) \cdot \boldsymbol{d^{1357}} = \sum_{i=1}^{7} s_i^{Ion,n}(X)\, d_i^{1357} \quad (37)$$

For example, taking into account *(6)* and *(37)*, we have:

$$c^{Lyd}(Y) = \boldsymbol{c}^{Ion,4}(X) = \boldsymbol{s}^{Ion,4}(X) \cdot \boldsymbol{d^{1357}} \qquad Y = X + \frac{5}{2}t \quad (38)$$

From *(38)*, by setting $X = C$, we obtain:

https://dx.doi.org/10.22161/ijaers.5.1.16 *ISSN: 2349-6495(P) | 2456-1908(O)*

$$c^{Lyd}(F) = \boldsymbol{s}^{Ion,4}(C) \cdot \boldsymbol{d}^{\mathbf{1357}} = F + A + C + E = Fmaj7 \quad (39)$$

As it can be easily imagined, we can also consider *vectors* whose *components* consist in *chords*. On this subject, let's denote with $\boldsymbol{h}^{Ion}(X)$ the *vector* whose *components* are nothing but the *seventh chords* that arise from the *harmonization* of the *Ionian Scale* of *X*. It is very easy to verify that the above-mentioned vector can be banally obtained as follows:

$$\boldsymbol{h}^{Ion}(X) = \boldsymbol{M}^{Ion}(X) \cdot \boldsymbol{d}^{\mathbf{1357}} \quad (40)$$

From the previous identity, by setting, for example, $X = C$, we instantly obtain:

$$\boldsymbol{h}^{Ion}(C) = \boldsymbol{M}^{Ion}(C) \cdot \boldsymbol{d}^{\mathbf{1357}} \quad (41)$$

More explicitly, from *(41)* we can write:

$$\boldsymbol{h}^{Ion}(C) = \begin{bmatrix} C & D & E & F & G & A & B \\ D & E & F & G & A & B & C \\ E & F & G & A & B & C & D \\ F & G & A & B & C & D & E \\ G & A & B & C & D & E & F \\ A & B & C & D & E & F & G \\ B & C & D & E & F & G & A \end{bmatrix} \begin{bmatrix} 1 \\ 0 \\ 1 \\ 0 \\ 1 \\ 0 \\ 1 \end{bmatrix} = \begin{bmatrix} Cmaj7 \\ Dm7 \\ Em7 \\ Fmaj7 \\ G7 \\ Am7 \\ B\emptyset \end{bmatrix} \quad (42)$$

## IV. FINAL REMARKS

Although the approach herein briefly described can be considered, at least to a certain measure, concretely innovative, we underline, for the sake of clarity, that the representation of a scale as a vector (a *Pitch-Class Set*) is anything but a novelty. [12] [13] For example, the *Ionian Scale* can be alternatively represented as follows:

$$\boldsymbol{s}^{Ion} = \{0,2,4,5,7,9,11\} \quad (43)$$

The *elements* of the *set* (the *components* of the *vector*) represent the *distance* between the *scale degrees* (from the first to the seventh) and the *Tonic*: the first is null since the *distance* between the *Tonic* and itself is obviously equal to zero, the second is equal to 2 since the distance between the *Supertonic* and the *Tonic* is equal to 2 *semitones*, the third is equal to 4 since the distance between the *Mediant* and the *Tonic* is equal to 4 *semitones*, and so on.

Finally, it is worth highlighting that the line of reasoning herein followed can be applied to whatever heptatonic scale: by starting, for example, from the *Ipoionian Scale*, we can easily obtain the corresponding *Modal Tensor* $\boldsymbol{M}^{Ipo}$ and the *Harmonization Vector* $\boldsymbol{h}^{Ipo}$.

## ACKNOWLEDGEMENTS

This paper is dedicated to my mother, Giuseppina, who has always encouraged me to play piano with passion and devotion.

I would like to thank my friends Francesco D'Errico, Giulio Martino, and Sandro Deidda, excellent Italian jazz musicians and esteemed teachers at the Conservatory of Salerno, for their precious suggestions.

## REFERENCES

[1] Cataldo, C. (2018). Towards a Music Algebra: Fundamental Harmonic Substitutions in Jazz. International Journal of Advanced Engineering Research and Science (IJAERS), 5(1), 52-57. https://dx.doi.org/10.22161/ijaers.5.1.9

[2] Cataldo, C. (2018). Jazz e Sostituzioni Armoniche: Verso un Nuovo Formalismo [Jazz and Harmonic Substitutions: Towards a New Formalism]. Journal of Science, Humanities and Arts (JOSHA) 5(1). https://dx.doi.org/10.17160/josha.5.1.381

[3] D'Errico, F. (2017). Armonia Funzionale e Modalità – Rudimenti per l'Improvvisazione a Indirizzo Jazzistico. Naples, Italy: Editoriale Scientifica.

[4] Levine, M. (2009). The Jazz Theory Book (Italian Edition by F. Jegher). Milan, IT: Curci Jazz.

[5] Lawn, R., Hellmer, J. L. (1996). Jazz: Theory and Practice. Los Angeles, CA: Alfred Publishing Co. Inc.

[6] Cho, G. J. (1992). Theories and Practice of Harmonic Analysis. Lewiston, NY: Edwin Mellen Press.

[7] Coker, J., Casale, J., & Campbell, G. (1982). Patterns for Jazz – A Theory Text for Jazz Composition and Improvisation: Treble Clef Instruments. Los Angeles, CA: Alfred Publishing Co. Inc.

[8] Monk, T. (2006). Thelonious Monk Collection: Piano Transcriptions (Artist Transcriptions). Milwaukee, WI: Hal ·Leonard.

[9] Monk, T. (2006). The Best of Thelonious Monk: Piano Transcriptions (Artist Transcriptions). Milwaukee, WI: Hal ·Leonard.

[10] Powell, B. (2002). The Bud Powell Collection: Piano Transcriptions (Artist Transcriptions). Milwaukee, WI: Hal ·Leonard

[11] Powell, B. (1998). Bud Powell Classics (Artist Transcriptions). Milwaukee, WI: Hal ·Leonard.

[12] Schuijer, M. (2008). Analyzing Atonal Music: Pitch-Class Set Theory and Its Contexts. University of Rochester. [ISBN 978-1-58046-270-9]

[13] Lewin, D. (1960). The Intervallic Content of a Collection of Notes, Intervallic Relations between a Collection of Notes and its Complement: an Application to Schoenberg's Hexachordal Pieces. Journal of Music Theory, 4(1), 98-101.

https://dx.doi.org/10.22161/ijaers.5.1.17 ISSN: 2349-6495(P) | 2456-1908(O)

# Modeling, and FEA of Multi-Plate Clutches by Varying Materials for Optimum Torque Transfer Capacity of TCT System of Green, And Light Vehicles

Seyoum Kebede[1], Hailemariam Nigus Hailu[2]

[1]Addis Ababa science and Technology University, Addis Ababa, Ethiopia
[2]Federal TVET Institute, Addis Ababa, Ethiopia

***Abstract*****—** *This paper addresses Modeling and analysis of easily applicable multi-plate clutches to use in twin clutch transmission (TCT) system for green and Light Weight Vehicle. The static and dynamic analysis were developed for a clutch plate by using finite element analysis (FEA). The 3D solid model was done using SOLID WORK 2016 and imported to ANSYS work bench 16 for model analysis. The mathematical modelling was also done using different vastly available materials (i.e. Aluminum alloy 6061, E-Glass Epoxy, and Gray Cast iron); then, by observing the results, comparison was carryout for materials to validate better lining material for multi plate clutches using ANSYS workbench 16 and finally concluded that composite material E-Glass Epoxy has a better friction material for design of multi-plate clutches in TCT system.*

***Keywords— Green Vehicle, Modeling multi-plate clutches, TCT, Clutch materials, MPC.***

## I. INTRODUCTION

Clutches are projected for transferring the greatest amount of torque with less heat generation and is one part of the transmission system. Twin clutch transmissions (TCT) have emerged as a viable alternative to conventional planetary automatics and continuously variable transmissions with the development of precise control strategies. TCT can be considered as two lay shaft transmissions in one, Odd gears are connected to first shaft while the even gears are connected to the other shaft. Light Weight and Green Vehicles that use TCT has developed be an excellent and competitive in every situation [1].

Multi-plate clutches in a twin clutch transmission system are the most efficient and to be employed in vehicles to achieve better vehicle fuel economy and comfort. Vehicles that use a manual clutch has not been the preferred choice; due to recently developed automatic twin clutch transmission. Evidences show that racing cars, most electric vehicles, Honda cars and motorcycles have been available with automatic transmission systems [2].

The idea behind automatic Twin-clutch is that a vehicle requires less driver input for any transmission system. The TCT as its name implies uses two clutches to change gears. The transmission can be used in fully automatic mode, with a computer determining gear shifts.

TCT, is available both in Wet and dry type Twin clutch transmission system, is more preferable, and has been developed to meet the very high torque capacity and to have more efficiency. Comparison of Wet, and Dry type clutches with their advantages and disadvantages has been done in [3, 5-8].

Good Characteristics of Clutches with high torque capacity, low weight, easy packaging, less noise, vibrations and Harshness (Good NVH characteristics), Longlife and High energy density as described in [4]

## II. MATERIAL OF MULTI-PLATE CLUTCH

To specify and limit number of materials to be used for the clutch analysis have be done by comparison of some material properties; Material selection property is used for the expected clutch disc materials and its mechanical property mostly used by different literatures.

*https://dx.doi.org/10.22161/ijaers.5.1.17* *ISSN: 2349-6495(P) | 2456-1908(O)*

*Table.1: comparison of better materials based on its Mechanical property [9].*

| Material types | Specific Strength | Yield Strength (Mpa) | Elastic Modulus(GPa) |
|---|---|---|---|
| E-Glass Epoxy | 28.4 | 1270 | 28 |
| Aluminum Alloy | 4.8 | 275 | 69.7 |
| ceramics | 6.7 | 457 | 33 |
| Gray Cast Iron | 19.1 | 720 | 24.1 |
| Silicon Carbide | 57 | 1710 | 63 |
| Kevlar 49 | 23.8 | 370 | 72 |
| organics | 17 | 270 | 28 |

The material property shown in Table1indicates that E-Glass Epoxy, Silicon Carbide, and Alloy Materials are better materials in resisting for yield when load is applying on them. But, it is clear that Silicon Carbide is a tool material which is very costly. So, it is not recommended to use in clutch.

From the above listed materials Aluminum Alloy, Gray Cast Iron and E-Glass Epoxy were better candidate materials for design of friction clutches of TCT. But, this is not the only way for selection. Beside, Finite element analysis should be done using ANSYS Work Bench depending on the properties of materials to identify which material is better. The properties of the frictional lining are important factors in the design of the clutches. So, typical characteristics of some widely used friction linings materials are given in table 2. The mechanical property of the selected materials are also shown in table 3. As shown in table 3 of properties of material, the density of E-glass Epoxy UD is lower than that of Aluminum alloy, and Gray Cast Iron. Since the density is the ratio of mass to it volume ($\rho$= m/v), and increase in mass is proportional to the density. So, Gray Cast Iron has more weight than aluminum alloy, and E-Glass Epoxy with the lowest weight of materials [10].

*Table.2: properties of candidate clutch lining materials.*

| Materials combination | | Aluminum Alloy 6061 | Gray Cast Iron | E-Glass Epoxy |
|---|---|---|---|---|
| Dynamic coefficient of friction | Dry | 0.25 – 0.45 | 0.15 – 0.25 | 0.25 – 0.45 |
| | Wet | 0.06 – 0.09 | 0.03 – 0.06 | 0.06 – 0.09 |
| Maximum pressure MPa | | 345 - 690 | 690 -720 | 345 -690 |
| Maximum temperature 0C | | 2104 -260 | 260 | 204 - 206 |

*Table.3: Mechanical properties of selected materials*

| Materials combination | Aluminum Alloy 6061 | Gray Cast Iron | E-Glass Epoxy |
|---|---|---|---|
| Young's Modulus (Mpa) | 68900 | 120000 | 27600 |
| Density(Kg/m3) | 2700 | 7200 | 1900 |
| Poisson's ratio | 0.33 | 0.29 | 0.34 |
| Friction coefficient | 0.23 | 0.28 | 0.48 |
| Tensile strength (Mpa) | 276 | 220 | 124 |

## III. NUMERICAL OF ANALYSIS

The numerical analysis of the TCT multi plate clutch was done in which theapplied force can keep the members together with a uniform pressure all over its contact area and the consequent analysis is based on uniform pressure condition. However as the time progresses some wear takes place between the contacting members and this may alter or vary the contact pressure appropriately and uniform pressure condition may no longer prevail. Hence the analysis was calculated based on uniform wear condition and uniform pressure theory.

The maximum torque which can be transmitted by the friction clutch for uniform pressure theory is given bythe formula in equation1.

$$T_{\max} = n\pi\mu p_a r(R^2 - r^2) \quad (1)$$

Where Rand r are external and internal radius of the clutch respectively.

*https://dx.doi.org/10.22161/ijaers.5.1.17* *ISSN: 2349-6495(P) | 2456-1908(O)*

The objective function, F1 and new objective function in deterministic $F_d$ is also formulated in equation 2 and 3 as:

$$F_1 = \left(\frac{1}{T_{\max}}\right) = \frac{1}{n\pi\mu p_a r\left(R^2 - r^2\right)} \qquad (2)$$

$$F_d = F_1 + \left[\sum_{i=1}^{n}\left(\frac{\partial F_1}{\partial R_j}\right)^2 \sigma^2{}_{Rj}\right]^{\frac{1}{2}} \qquad (3)$$

The Constrained equation also formulated in equation 4, if the constraint equation $g_j$ in equation 4 is satisfied with a probability $p_j$ then the normal variation for probability $p_j$ is given then, the new constraint equation in deterministic form is given in equation. And finally problem reduces to minimize the objective function given by equation (2) satisfying constraint equation (4).

$$g_j = \Phi_j\left(\rho_j\right)\left[\sum_{i=1}^{n}\left(\frac{\partial g_j}{\partial R_j}\right)^2 \sigma^2{}_{Rj}\right]^{\frac{1}{2}} \qquad (4)$$

To design the multi plate friction clutch for maximum torque transmitting capacity, given by equation 1 and 2 can be calculated from a given values i.e.μ= 0.48, n=1, $P_a = 0.35N/mm^2$

$$F1 = \frac{1}{1*0.48*\pi*0.35*10^6*r(R^2 - r^2)} = 7.8 * 10^{-7} / (R^2r - r^3)$$

If the design parameters D and d are taken as random variables following normal distribution and the standard deviations are $\sigma_D$ = 0.01D and $\sigma_d$ = 0.01d respectively, then the new objective function in deterministic form, from equation 3 is:

$$F_d = \frac{7.8*10^{-7}}{(R^2r - r^3)} + \frac{0.03*10^{-6}R^2r}{(R^2r - r^3)} + \frac{7.8*10^{-6}(R^2r - r^3}{(R^2r - r^3)^2} = \frac{7.8*10^{-7}}{(R^2r - r^3)}$$

Substitute the calculated parameters in to equation 4 and gives; $g_j = \frac{1.73r}{R}$ (5)

If the constraint equation is satisfied with a probability of 99.99%, then for $p_j$ = 99.99%.The normal variants from table is 5. Using equation (12) the constraint equation in deterministic form is:$g_j d = 1.733\ r/R - 0.087R \leq 1$

Hence the problem reduces to minimize objective function given by equation (4) satisfying constraint equation (5). If the torsion is only considered as active constraint then the degree of difficulty will be zero.

The number of friction surfaces,since there are two multi plate clutches the number of friction surface is (n + n – 1) which is 1; then the maximum torque increased n times. So, to deliver 5KW power, 135Nm torque, at a speed of 1000-5000rpm, using the candidate materials, design calculations include,

Let's use the power delivery of the vehicle as 5KW and at a specified initial speed of 5000rpm. But the torque transferred by the clutch would be calculated for analysis of loads and maximum pressure with new specifications.

So, using twin multi-plate clutch is using the number of friction surfaces to be one. Then, the total torque transfer would be; $T_t = \frac{60P}{2\pi\omega}$. (6)

Where $T_t$ = a total torque transfer, P = a maximum power carried by a clutch, $\omega$ = speed in rpm

Then using eq.6 above;

Then, using the number of friction surfaces n=1: $T = T_t/n$ = 10/1 = 10Nm (7)

Now, from uniform wear theory, the clumping force W

$W = 2\ \pi\ (P_{max} x\ D_1)\ x\ (D_2 - D_1)$ (8)

*Table.4: numerical results and given parametric with different materials from the above formulas*

| Material | Maximum pressure (P) | Clumping force (W) | Torque Transfer (T) | Coefficient of friction μ | No of friction surface (n) | Mean radius of friction surface (R) | Speed |
|---|---|---|---|---|---|---|---|
| E-Glass Epoxy | 0.00037MPa | 119 N | 10Nm | 0.48 | 1 | 0.175m | 5000rpm |
| Gray cast iron | **0**.0043Mpa | 204 N | 10Nm | 0.28 | 1 | 0.175m | 5000rpm |
| Aluminum alloy | 0.0053MPa | 248N | 10Nm | 0.23 | 1 | 0.175m | 5000rpm |

*https://dx.doi.org/10.22161/ijaers.5.1.17* *ISSN: 2349-6495(P) | 2456-1908(O)*

## IV. RESULTS AND DISCUSSIONS

The maximum pressure obtained by numerical analysis as tabulated in table 4 was applied on the friction plate and results were obtained in Ansys work bench and stress and deformation values in figure -----are compared for the said materials. Figure 1 shows that the exploded and the meshed model of the plate. The boundary condition and load of the plate is applied as depicted in figure 2 below like applied the pressure and fixed supports.

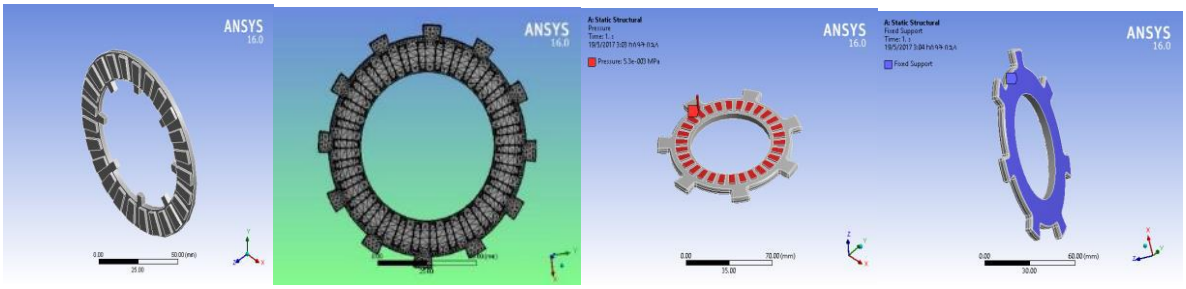


*Fig.1: Export and Meshed Figure 2: Load and boundary conditions*

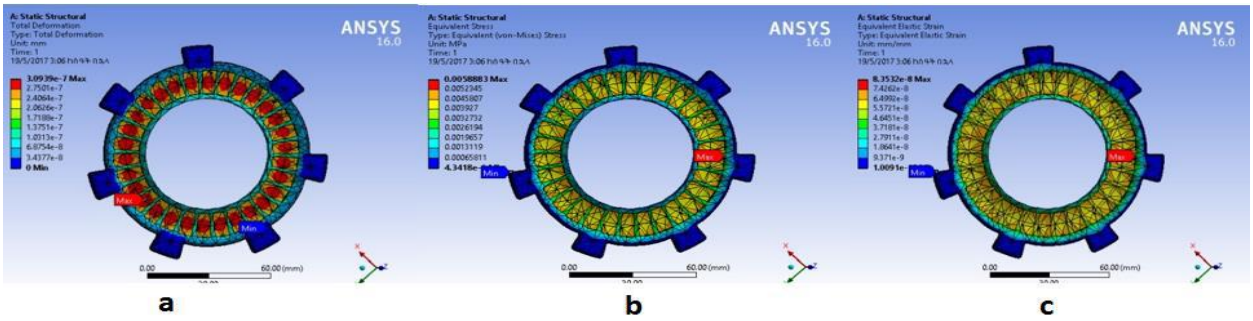


*Figure 3: Aluminum alloy as friction material for external spline (a) Total deformation; (b) Equivalent Stress;(c) Equivalent strain*

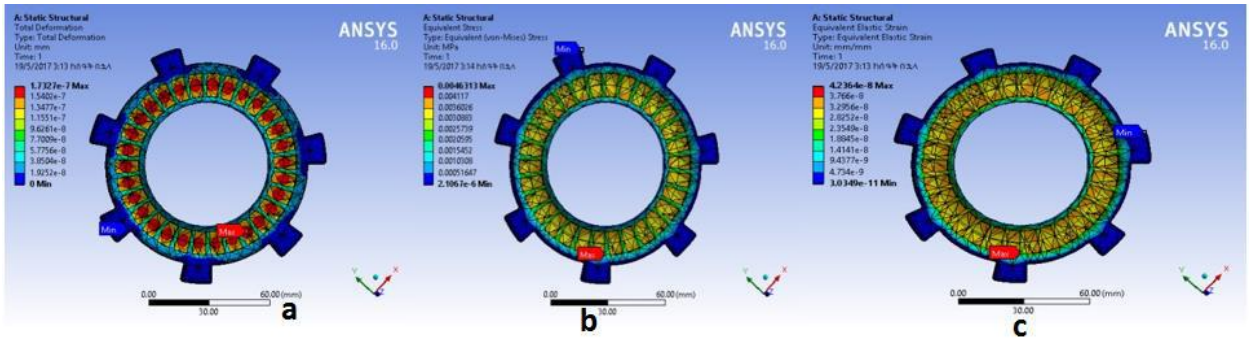


*Fig.4: Gray Cast Iron as friction material for external splines MPC (a) applied maximum pressure; (b) total deformation; (c) Equivalent stress*

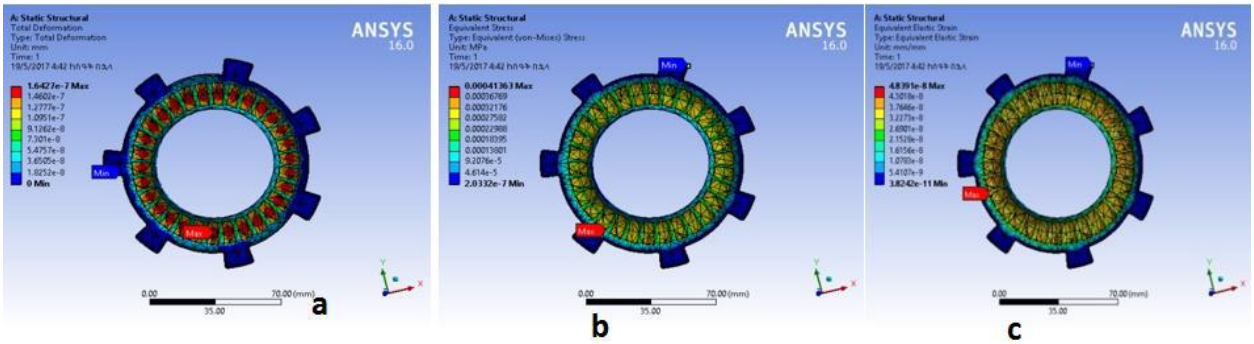


*Fig.5: E-Glass Epoxy as friction material for external splines MPC (a) Applied maximum pressure; (b) total deformation; (c) Equivalent stress*

*https://dx.doi.org/10.22161/ijaers.5.1.17* *ISSN: 2349-6495(P) | 2456-1908(O)*

The same case for dynamic analysis was done and the static and dynamic analysis of external spline values are tabulated in the table 5 and 6 respectively.

*Table.5: External spline FEA /Ansys result (static)*

| Selected materials | Total deformation (mm) | Equivalent elastic strain (mm/mm) | Equivalent Stress (MPa) |
|---|---|---|---|
| Aluminum alloy | $3.0939 * 10^{-7}$ | $8.3532 * 10^{-8}$ | 0.00588 |
| E-glass Epoxy UD | $1.6427 * 10^{-7}$ | $4.8391 * 10^{-8}$ | 0.00041 |
| Gray Cast Iron | $1.7327 * 10^{-7}$ | $4.2364 * 10^{-8}$ | 0.00463 |

*Table.6: External spline FEA/ANSYS result (Dynamic)*

| Selected materials | Total deformation (mm) | Equivalent elastic strain (mm/mm) | Equivalent Stress (MPa) |
|---|---|---|---|
| Aluminum alloy | $3.0433 * 10^{-5}$ | $7.0744 * 10^{-7}$ | 0.0487 |
| E-glass Epoxy UD | $1.6118 * 10^{-5}$ | $4.9203 * 10^{-7}$ | 0.0049 |
| Gray Cast Iron | $1.6702 * 10^{-5}$ | $4.0124 * 10^{-7}$ | 0.0432 |

The above analysis is the external spline friction material for different candidates of material, in the same case the internal spline of friction material will analyzed both static and dynamic once. From figure 6 – figure 9 shown the static analysis of internal spline for aluminum alloy, gray cast iron and E-glass Epoxy using Ansy workbench. In same manner dynamic analysis is tabulated below.

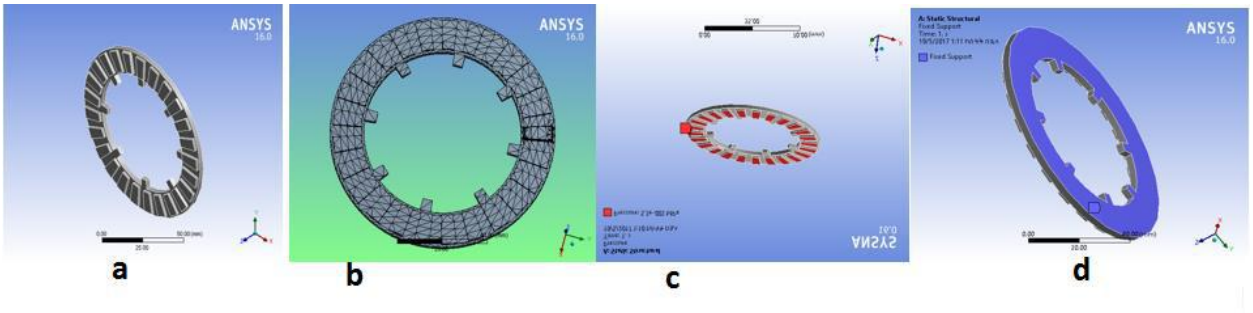


*Fig.6: internal splines MPC a) Export from Solid work b) meshed model C) boundary conditions fixed support d) applied Load*

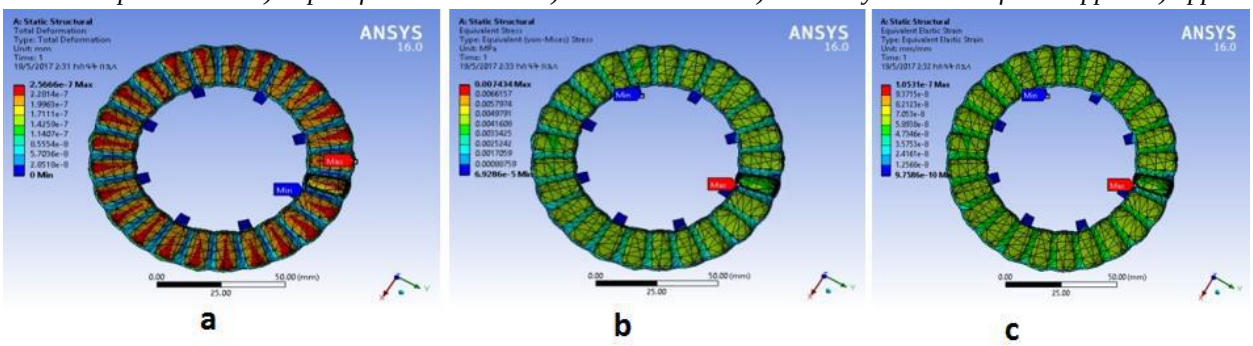


*Fig.7: aluminum alloy as a friction material for internal splines MPC; (a) Total deformation; (b) Equivalent stress; (c) Equivalent strain*

*https://dx.doi.org/10.22161/ijaers.5.1.17* *ISSN: 2349-6495(P) | 2456-1908(O)*

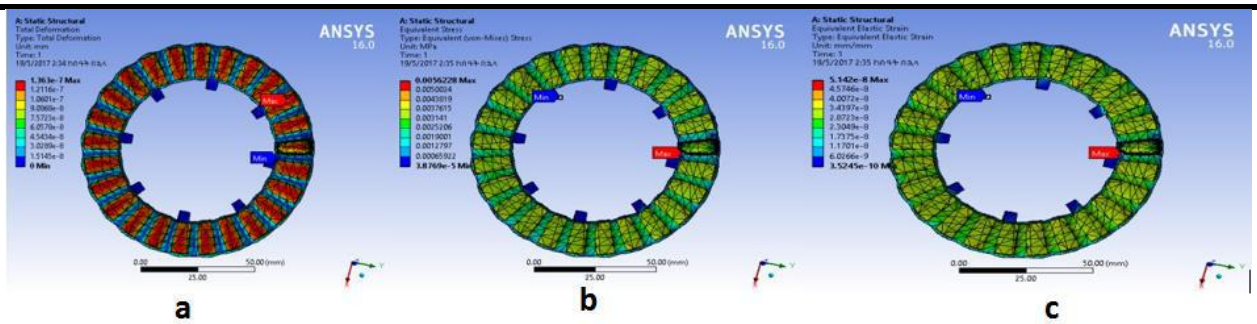


*Fig.8: Gray cast iron as a friction material for internal splines MPC (a) total deformation; (b) Equivalent stress; (c) Eq. strain*

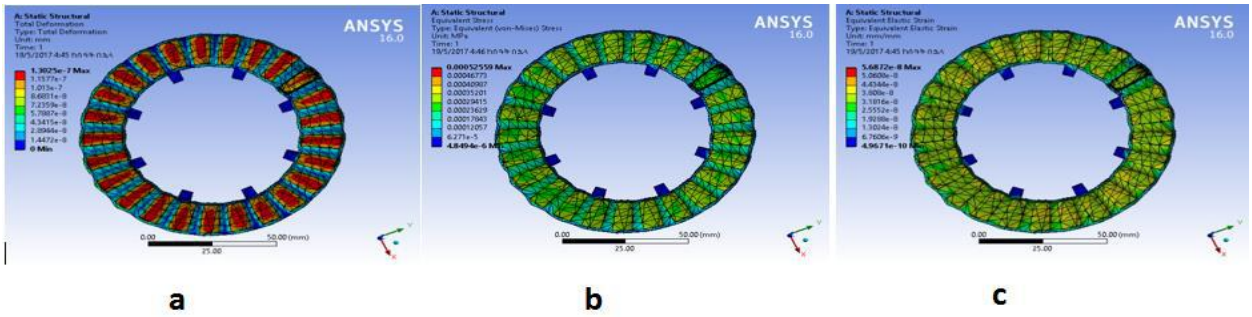


*Fig.9: E-Glass Epoxy as a friction material for internal spline (a) total deformation; (b) Equivalent stress; (c) equivalent strain*

The static and dynamic analysis of internal spline of friction material values were tabulated in the table 7 and 8 respectively.

*Table.7: internal spline FEA/ANSYS result (static)*

| Selected materials | Total deformation (mm) | Equivalent elastic strain (mm/mm) | Equivalent Stress (Mpa) |
|---|---|---|---|
| Aluminum alloy | $2.5666 * 10^{-7}$ | $1.0531 * 10^{-7}$ | 0.007434 |
| E-glass Epoxy UD | $1.3025 * 10^{-7}$ | $5.6872 * 10^{-8}$ | 0.000525 |
| Gray Cast Iron | $1.363 * 10^{-7}$ | $5.142 * 10^{-8}$ | 0.005623 |

*Table.8: internal spline FEA/ANSYS result (Dynamic)*

| Selected materials | Total deformation (mm) | Equivalent elastic strain (mm/mm) | Equivalent Stress (MPa) |
|---|---|---|---|
| Aluminum alloy | $5.94 * 10^{-5}$ | $2.633 * 10^{-6}$ | 0.18659 |
| E-glass Epoxy UD | $3.22 * 10^{-5}$ | $1.717 * 10^{-6}$ | 0.01658 |
| Gray Cast Iron | $3.21 * 10^{-5}$ | $1.408 * 10^{-6}$ | 0.15456 |

As we can observed from the tabulated results shown in table 5,6,7 and 8of external and internal spline MPCs of the selected materials that; the total deformation, equivalent strain, equivalent stress for clutch plate with E-Glass Epoxy as a friction material has less than that of Aluminum alloy and Gray Cast Iron. For same input torque stress developed in clutch plate with friction material of E-Glass Epoxy has less compared to Cast Iron and aluminum alloy not only this but also Epoxy UD has the lowest in weight than that of existing commercial clutch materials mostly Gray Cast Iron. Hence it is concluded that the clutch plate with friction material E-Glass Epoxy UD gives better performance than that of Gray Cast Iron and Aluminum alloy.

It is also observed that total deformation, equivalent stress and equivalent strain of E-glass Epoxy UD material were in the permissible range for the ideal friction material

*https://dx.doi.org/10.22161/ijaers.5.1.17* *ISSN: 2349-6495(P) | 2456-1908(O)*

compared to the theoretical calculations. E-glass Epoxy UD has the low total deformation when compared to the existing conventional Gray Cast Iron friction material. Hence, it is concluded that E-glass Epoxy UD serves as a better friction material than Gray Cast Iron, and aluminum alloy and gives better clutch performance.

## V. CONCLUSION

From the ANSYS Workbench structural simulation and analysis in FEM is a key to facilitate the assessment of structural analysis of clutch plate which provides relatively simple method for analyzing of material strength. Besides, the analysis shows that increase in tensile yield strength of material, the maximum equivalent stress decrease and similarly the deformation rate decreases. The final result shows that E-Glass Epoxy materials have minimum deformation in their applied load and pressure conditions than other materials used, it also have high wear resistance property and lower weight than existing Gray Cast Iron, and aluminum alloy materials. Besides these, the weight of E-Glass Epoxy material is 72% lower than that of Gray Cast Iron and 26% lower than Aluminum Alloy Materials. So, this makes Epoxy Materials to be better for clutching.

## REFERENCES

[1] A. Senatore, Advances in the Automotive Systems: “An Overview of Dual-Clutch Transmissions", Recent Patents on Mechanical Engineering, vol. 2, pp. 93{101, 2 2009, issn: 2212-7976.) (Accessed on: Dec.8,2016)

[2] Adam ADAMOWICZ, and Piotr GRZES, “FINITE ELEMENT ANALYSIS OF THERMAL STRESSES IN A PAD-DISC BRAKE SYSTEM (A REVIEW)”*actamechanica et automatica, vol.7 no.4 (2013), DOI 10.2478/ama-2013-0032* (Accessed on: Nov.10,2016)

[3] Audi, S.-S.P. (2006) *6-speed twin-clutch gearbox 02E (S-Tronic) Self-Study Programme386*.Available,at:http://training.avme.net/admin/Upload/SSP/4800_386%206%20speed%20twin%20clutch%20DSG%20s_tronic%20Audi.pdf(Accessed:on Dec.9,2016)

[4] Chang-Yeon Cho, Jeong-HeonKam, Han-Ki Hong, and Dilp.-Ing. CarstenLovenich, “More Efficiency with the Dry Seven-speed Dual-clutch Transmission by Hyundai”, Development transmissions and Clutches. ATZ 0612016, Vol. 118.p3-8 (retrieved on Dec. 12,2016),

[5] Mario Pisaturo, “Dry clutch for automated manual Transmissions” Structural analysis and control strategies, PhD. Thesis in Mechanical Engineering, cycle XII(2011-2013) (Accessed: on Dec.16,2016)

[6] Mrs.Ch.Vasantha Lakshmi, and SandhyaRani.V, “Design and Structural Analysis of Composite Coated Clutch Plate by using Composite Materials”, international journal and Magazine of Engineering, Technology, Management and Research, A peer Reviewed Open Access International Journal. ISSN No: 2348-4845. P1-4, (retrived on, Dec. 12,2016)

[7] P. Janssen, and K. Govindswamy, “Future Automatic Transmission Requirements”, Submission_VDI_Transmission_IV_02.p5-8.

[8] Suyog Vitnor1, and MukundKavade, “Finite Element Analysis of Friction Plate of Diaphragm Spring Clutch for TD-3250 Vehicle” International Journal of Science and Research (IJSR) ISSN (Online): 2319-7064 Index Copernicus Value (2013): 6.14 | Impact Factor (2015): 6.391

[9] IEEE Terms and conditions, AA/IADS,AMS, and ASTM/ASME STANDARDS metals and their alloys,

[10] Ferro ceramic grinding inc.,Wakefield, mass.,www.ferroceramic.com

*https://dx.doi.org/10.22161/ijaers.5.1.18* *ISSN: 2349-6495(P) | 2456-1908(O)*

# Plaster Layout Process in Civil Works with a Focus on Clean Production

Claiton Mesacasa, Felipe Crestani, Lidiane Canofre, Marina Junges, Josiane Maria Muneron de Mello, Francieli Dalconton, Sideney Becker Onofre

Universidade Comunitária da Região de Chapecó - UNOCHAPECÓ - Graduate Program in Technology and Innovation Management - PPGTI - Av. Sen. Atílio Fontana, 591 E - Efapi - 89809-000 - Chapecó – Santa Catarina – Brazil.
Email: diretor@c2.eng.br

***Abstract—*** *The constant expansion of civil construction and the increasing use of plaster gives rise to a solid waste generation problem causing difficulties for the disposal or reuse of this material. The generation of plaster waste represents an economic problem, with serious consequences and impacts. In order to contribute to sustainability, this study sought to evaluate the reduction of plaster waste in an apartment construction project, employing the layout method. With the adequate arrangement of plates, a reduction of 4.41% in the use of plaster could be obtained, This reduction will consequently result in the minimization of waste from civil works, bringing invaluable economic and environmental benefits.*

***Keywords—Drywall, layout, sustainability, waste minimization.***

## I. INTRODUCTION

The gypsum mineral, the raw material for the production of plaster, is composed of calcium sulfate dihydrate ($CaSO_4 \cdot 2H_2O$), occurring naturally in various regions of the world and having a broad and diversified field of uses. The great interest in gypsum is attributed to a peculiar characteristic, which consists in the ease of its dehydration and rehydration. When mixed with water, it can be molded and worked before hardening and acquiring the mechanical consistency of the dehydrated and stable form (Baltar; Bastos; Luz, 2008).

Currently, gypsum has numerous applications, and is intensely used in the construction industry. Plaster is the product of the thermal dehydration of gypsum and of its subsequent grinding with temperature limits (Follner et al., 2002). It can be used to line walls and ceilings; build partition walls in block form or drywalls.

According to data presented by the Brazilian Drywall Association (2013), the figures relating to the commercial performance of drywall in the country are growing. With regard to the use of this constructive system, Brazil occupies a modest position in the international scenario, placed 12th in the ranking of plaster consumption with 0.25 $m^2$ per inhabitant per year, representing a total of 50 million $m^2$ of panels used in 2013.

The use of plaster is closely related to population growth and changes in markets, technologies and products, accelerating the industry around the world. The constant expansion of civil construction and the increasing use of plaster gives rise to a solid waste generation problem causing difficulties for the disposal or reuse of this material. The generation of plaster waste in construction represents an economic problem, with serious environmental consequences if the disposal isn't done correctly. Resolution no. 431 from CONAMA classifies the plaster residue as class B, which means it is considered recyclable waste for other destinations, (Conama, 2011).

According to Campbell (2008), in the US the construction industry's losses due to the drywall cutting activities becoming waste is estimated to be between 10 to 12%. In Brazil, the losses in construction are also significant, with 5% of the drywall being estimated to be turned into waste during construction (Sindusgesso, 2006).

The disposal of plaster in landfills is not a recommended practice, except when enclosed and kept out of contact with organic matter and water. The reason is that plaster in contact with moisture and in anaerobic conditions, with low pH, and in contact with sulphate-reducing bacteria - conditions present in many landfills and dumps - may form hydrogen sulfide gas ($H_2S$), which has a characteristic rotten egg odor and is toxic and flammable (Melo, 2012). It is known that some vermiculite deposits can contain asbestos, and there are also records of the presence of heavy metals, but the presence of boron is the most worrying, since it is a toxic element (Munhoz; Renofio, 2007).

Despite the notorious problems related to the toxicity of the plaster waste, in most cases these residues are not treated and/or reused, being disposed in an environmentally inadequate way and making environmental mitigation measures necessary. A first step would be to reduce the generation of plaster waste. In relation to the losses in the use of drywall and in the manufacture of pre-molded panels, the most important thing is to improve the product technology, the quality of labor and especially a proper layout of the panels available on the market. Studies in this field are still incipient, however, and it is not possible to find layout methods seeking to reduce waste in the literature.

https://dx.doi.org/10.22161/ijaers.5.1.18 ISSN: 2349-6495(P) | 2456-1908(O)

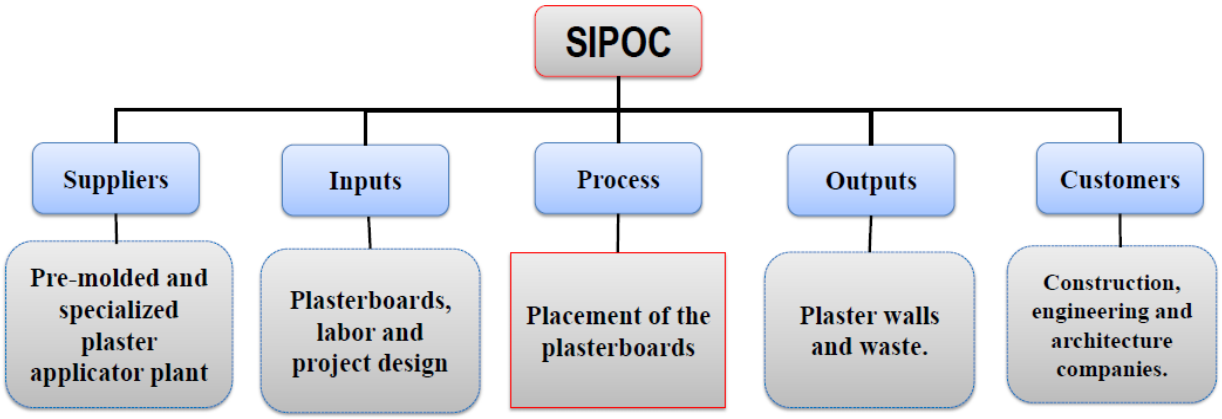


*Fig. 1 - SIPOC map - SIPOC for layout*

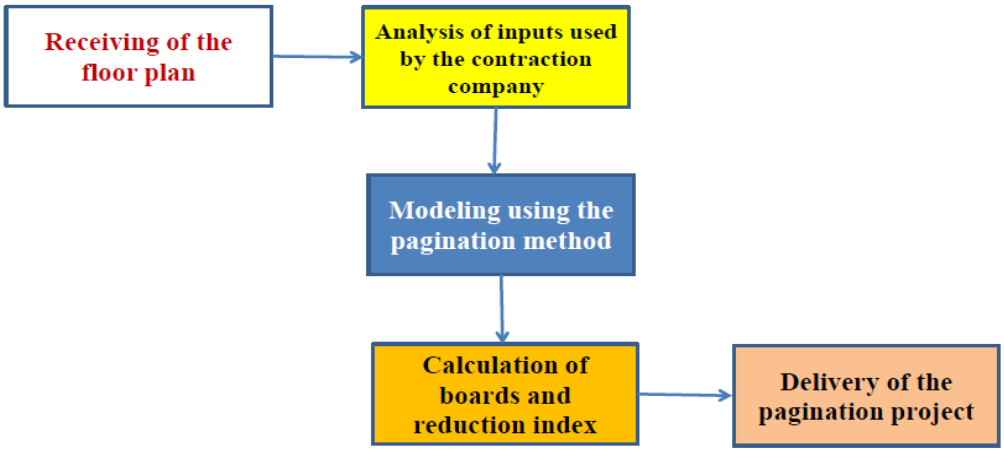


*Fig. 2: Flowchart of the developed activities.*

*Table 1: Actions to be undertaken in the short term.*

| Name of the Action | Description | Indicators | U/M |
|---|---|---|---|
| Plaster Layout | Plaster layout analysis in civil works with a focus on waste reduction | Waste minimization in civil construction | % |

U/M = Unit of Measurement.

In view of concerns regarding the final disposal of plaster waste to minimize environmental pollution, and to contribute to sustainability and the lack of technical/scientific information regarding plasterboard layouts, this study therefore sought to evaluate the reduction of plaster waste in apartments using the layout method.

## II. THE IMPLEMENTATION OF CLEANER PRODUCTION

### 2.1. Diagnosis of the Production Activity

The representation of the process through the SIPOC map (Figure 1) reveals the inter-relationships within the plasterboard layout method, from the suppliers who are responsible for the design of the layout, aiming to reduce waste, until the target customer of the proposal. In Figure 2 the flowchart is shown summarizing the suggested activities to achieve the result.

## III. INTERVENTION PROPOSALS / OPPORTUNITIES

Table 1 shows an indicator that was used for the actions undertaken in the short term. The plaster layout method for waste reduction in civil construction is done individually according to the characteristics of each project. To this end, an analysis is performed by the responsible party, the indicator used for monitoring is the minimization of waste at the end of the work calculated in percentages.

## IV. ADOPTED METHODOLOGY

In order to analyze the plaster layout with a focus on waste minimization, the floor plan of an apartment (Figure 3) in a residential building with 20 apartments was used, located in Rua Travessa Angelica, 120C - Maria Goretti, Chapecó - Santa Catarina - Brazil, with a private area of 165.00 $m^2$.

*https://dx.doi.org/10.22161/ijaers.5.1.18* *ISSN: 2349-6495(P) | 2456-1908(O)*

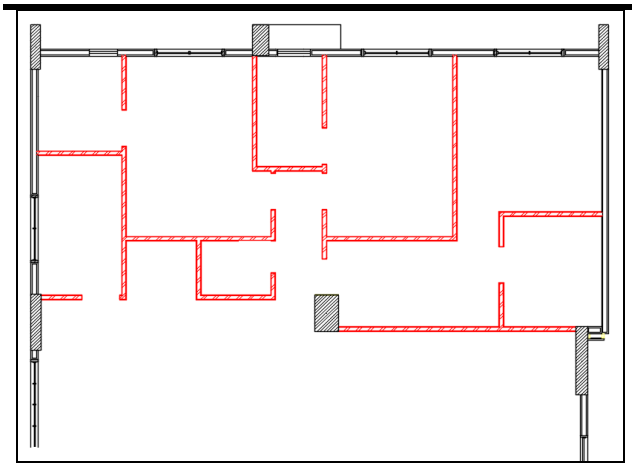

*Fig. 3 - Apartment floor plan (internal plaster wall*

The modeling software SketchUp Pro was used to develop the layout of the panels, with them being set up for the most efficient cutting. For a better visualization of this study, colors were used for the distribution of the drywalls, as a sequence to this step, there was a greater concern with the layout of the seams and gaps.

The design implementation was planned with assembly details for each wall, as starting points for the drywall layout and the required cuts. Figures 4 and 5 show the finished layout to be implemented. The total number of panels used in the layout was summed to estimate the rate of reduction.

The executive version of the drywall layout project was guided by the use of numbering on the plates and letters for the cutouts, e,g., Panel 01, Panel 02, Panel 02-A, Banel 02-B, and so forth.

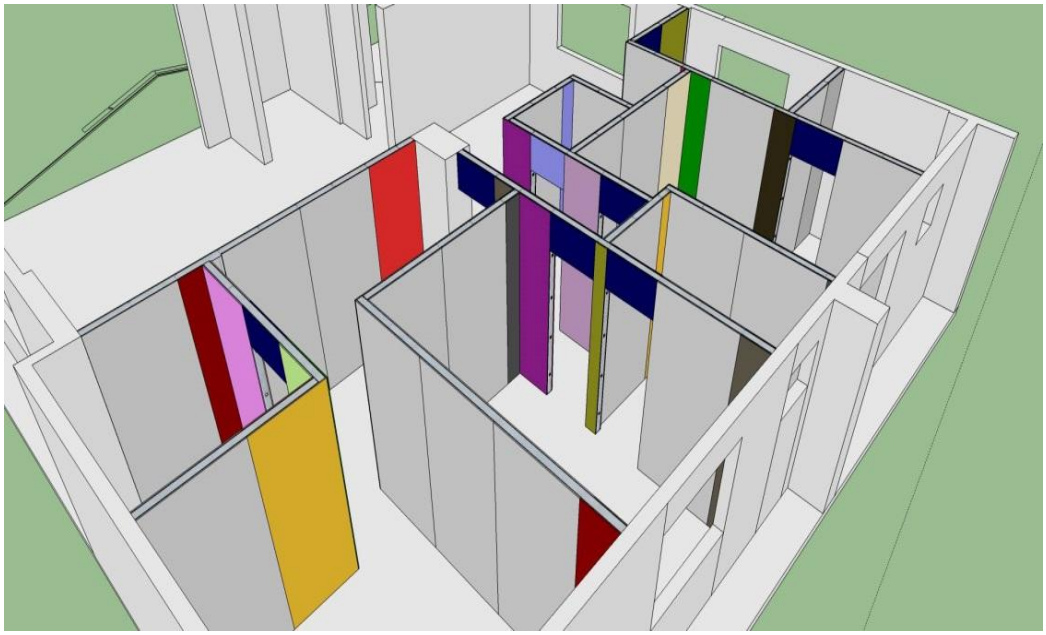

*Fig 4: Plaster layout in the apartment*

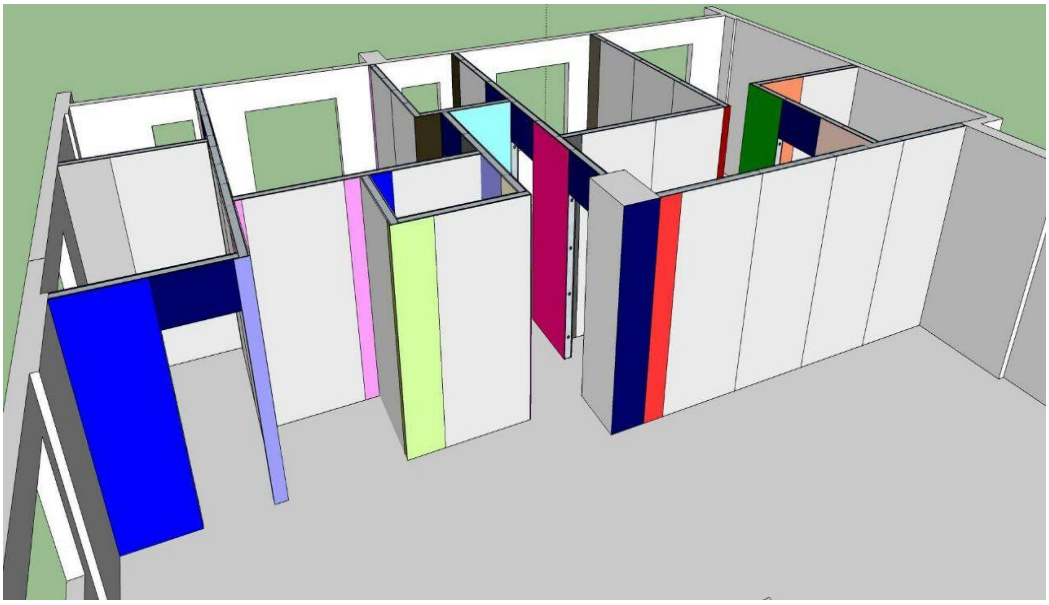

*Fig. 5 - Plaster layout in the apartment*

https://dx.doi.org/10.22161/ijaers.5.1.18 ISSN: 2349-6495(P) | 2456-1908(O)

*Fig. 6: Arrangement of the plaster in the apartment*

*Fig. 7: Arrangement of the plaster in the apartment*

The work is in its implementation phase with estimated completion in 2018. The drywalls are being implemented without a layout design, and the only guidance in the use of the panels is the experience of the executing plasterer. Figure 6 and 7 show the placement of the drywall panels without layout. In the conventional method, the executing company informed that a total of 68 panels are being used, i.e. 220.32 m², for the modeling of the internal walls (data provided by the contractor responsible for the work) per apartment.

Considering the 68 panels (220.32 m²) that the contractor uses per floor, and the theoretical consumption of 207.36 m², the loss in cuts is 12.96 $m^2$ (6.25%) of drywall per floor.

After the end of the execution of the work, the amount of boards used in the conventional work method will be compared with the layout design to check the reduction in consumption of panels with the use of the layout design, which consequently will generate a reduction in waste of this raw material in the work.

*https://dx.doi.org/10.22161/ijaers.5.1.18* *ISSN: 2349-6495(P) | 2456-1908(O)*

## V. RESULTS AND DISCUSSION

Table 2 shows the reductions in losses with the layout of the panels. The drywall layout design used a total of 65 drywall panels (210.60 m²) to modulate the internal walls of the apartment, considering a consumption of 207.36 m², the loss with cuts was of 3.24 m² (1.562%) of drywall per floor.

*Table.2: Reduction indicators using the layout*

| Indicators | Without layout | With layout |
|---|---|---|
| Drywall panels | 68.00 | 65.00 |
| Plaster consumption | 220.32 m² | 210.60m² |
| Losses with cuts (waste) | 12.96m² | 3.24 m² |
| Percentage of losses | 6.25% | 1.562% |
| Percentage of waste reduction | ------ | 75% |

Taking the consumption with the layout method in comparison with the consumption by the executing company into consideration, the layout yielded a reduction in consumption of 4.41%.

This reduction represents a total of 3 panels less per apartment. This number may seem of minor importance, but when added up, for example in a building with 20 apartments, this represents a total reduction of 60 panels. Consequently, the reduction in the amount of plaster panels will cause a considerable reduction in the generation of waste, approximately 162.00 m², or 2.02 m³ of plaster residue. As such, the waste reduction generated by the layout design with the best arrangement and utilization of panels will be positive.

A study conducted by Feijo, França and Caetano (2013) sought to estimate the importance of the layout before placing ceramics and tiles in bathrooms. They showed the layout resulted in economic gains, with a reduction of 10% in the amount spent for the execution of the lining. The same authors emphasize a reduction of 6% in the amount of tiles used, and a 47% reduction in the amount of waste generated. Similar results were obtained by Pimentel (2009).

The absence, or even omission, of data in the literature in all the projects regarding specifications and information about the inherent technology for the implementation of the proposed solutions, in addition to the absence of information allowing for a geometric, technological and productive integration between components and subsystems, demonstrates the importance of developing projects to contribute to sustainability (Novaes, 1998). The layout study also proved to be important for the economic analysis, aiming to reduce costs (Poubel, 2001), which may vary significantly according to the decision taken.

The result of this layout methodology enables gains in competitiveness, either through the financial aspect of waste reduction, or by minimizing the environmental impact caused by the plaster residue. Using this new technique makes it possible to conquer increasingly restricted markets in terms of technical and environmental requirements.

## VI. IDENTIFICATION OF BARRIERS

The layout design is laborious and should be done by professionals in the industry. There is a need to train professionals in the labor market in the development of plaster layout designs.

The lack of qualified professionals for the implementation may hinder the full understanding and execution of the layout method, which is the main barrier in the reduction of waste. Because of the costs of developing a layout design, this type of design is rarely performed in small works, where the consumption of gypsum in the work is small, but in the global scenario this use in small works is significant.

## VII. CONCLUDING REMARKS

The layout of plaster in drywall system projects significantly decreases the employment of panels through their optimal arrangement. The main benefit of the layout is the reduction in waste generated in civil construction. The use of sustainability as an environmentally correct and economically viable option makes the implementation of the layout method extremely relevant in the construction industry.

More studies are needed in order to estimate the exact reduction of plaster that the layout method can generate.

## REFERENCES

[1] ABD - Associação Brasileira De Drywall. (2003). Números do segmento. São Paulo, 2013. Disponível em: <http://www.drywall.org.br/index.php/6/numeros-do-segmento>. Acesso em: 15 maio. 2017.

[2] ABNT - Associação Brasileira De Normas Técnicas. NBR 14716: Chapas de gesso acartonado – Verificação das características geométricas. Rio de Janeiro, 2001.

[3] Baltar CAM, Bastos FFE, Luz AB. (2008) - Rochas & minerais industriais: gipsita. 2. ed. Rio de Janeiro: CETEM/MCT, p.989.

[4] Campbell - Steve Lead by Example Walls and Cieling. (2003). Disponível em:< http://www.wconline.com>. Acesso em: 23 abr. 2017.

[5] Conama - Conselho Nacional do Meio Ambiente. Resolução Nº 43. Altera o art. 3º da Resolução nº 307/ 2002. Brasília, 2011.

[6] Feijo CC, França SLB, Caetano FBF. Análise de técnicas construtivas sustentáveis para indústria da construção civil: Estudo de caso em serviços de edifício residencial. In: Congresso Nacional de Excelência em Gestão, 4, 2013, Rio de Janeiro, Rio de Janeiro. Anais... Congresso Nacional de Excelência em Gestão. Rio de Janeiro, RJ: Inovarse, 2013.

[7] Follner S, Wolter A, Preusser A, Indris S, Silber C, Follner H. (2002). The Settings Behavior of Beta– and Alpha-$CaSO_4$ x 0,5 $H_2O$ as Function of Crystal

*https://dx.doi.org/10.22161/ijaers.5.1.18* *ISSN: 2349-6495(P) | 2456-1908(O)*

Structure and Morphology. Cryst. Res. Technol, 37(10): 10075- 1087.

[8] Melo DCP. (2012). Processo de calcinação da gipsita/resíduo em um forno rotativo contínuo para a produção de gesso beta reciclável. 2012. 177f. Tese (Doutorado em Engenharia Química) - Universidade Federal de Pernambuco, Recife. Brasil.

[9] Munhoz FC, Renocio A. Uso da gipsita na construção civil e adequação para a P+L. In: Encontro Nacional de Engenharia de Produção. 27, 2007, Foz do Iguaçu, Paraná. Anais... Encontro Nacional de Engenharia de Produção, Foz do Iguaçu, 2007.

[10] Novaes CC. Projetos para Produção como Instrumentos da Melhoria da Qualidade do Processo de Projeto de Edificações. Construção 2001. In: Encontro Nacional da Construção. Lisboa. 1, 1998, Lisboa. Anais... Encontro Nacional da Construção. IST: Lisboa - Portugal.

[11] Pimentel SH. Produção Mais Limpa Aplicada à Construção Civil. (2009). 72f. Monografia (Graduação em Engenharia Ambiental) - Universidade de Passo Fundo, Passo Fundo. Rio Grande do Sul – Brasil.

[12] Poubel MFG. Gerenciamento de Custos no Sistema Construtivo de Gesso Acartonado, "Drywall". In: Workshop Brasileiro de. Gestão do Processo de Projeto na Construção de Edifícios. São Paulo, 2, (2001). Anais... Workshop Brasileiro de. Gestão do Processo de Projeto na Construção de Edifícios. WBGPPCE: São Paulo - Brasil.

[13] Sindusgesso. Derivados de Gesso e de Minerais Não-Metálicos do estado de Pernambuco. Disponível em: < www.sindusgesso.org.br>. Acesso em: 15 maio. 2017.

https://dx.doi.org/10.22161/ijaers.5.1.19 ISSN: 2349-6495(P) | 2456-1908(O)

# Analysis of Short Term and Long Term Dependence of Stream Flow Phenomenon in Seonath River Basin, Chhattisgarh

Shashikant Verma, Bhupendra Kumar Dhiwar

M.Tech. Scholar, Water Resources Development & Irrigation Engineering, Department Civil Engineering, NIT Raipur, India

***Abstract—*** *In this paper to investigate long rang phenomena ( Hurst effect) of river flows which characterizes hydrological time series is studied, especially in connection with various climate-related factors, is important to improve stochastic models for long-range phenomena and in order to understand the deterministic and stochastic variability in long-range dependence of stream flow. Long rang dependence represented by the Hurst coefficient H is estimated for 5 mean monthly discharge time series of Chhattisgarh state for a period of 32 years from 1980-2012.long memory analyzed for both monthly and seasonally stream flow time series of the Seonath River Basin at Chhattisgarh State by using Hurst exponent and testing specifically the null hypothesis of short-term memory in the monthly and seasonal time series by (Von Neumann ratio test, Kendall's rank correlation test, Median crossing test, Run above and below the median for general randomness, Turning point test, Rank difference test).*

***Keywords— Hurst Phenomena, Stochastic, Streamflow Processes, Long Memory Time Series.***

## I. INTRODUCTION

The number of time scale studies have been analyzing for the long-term behaviour of streamflow has increase adequately in the accomplished duration with exceptional quality and data availability with increasing interest of influence of climate change and climate-related factors on stream flow processes (Bloschl and Montanari, 2010), [1] the extent and complexity of such a consideration have increased. The necessity of such research lies in the need for incorporate long-range dependence and to developed speculative models, which can be used for illustration in the management of water resources or reservoir action. Another property characterizing time series from a long-range perspective is the long-term dependence (Hurst phenomenon (Hurst, 1951). [2] The phenomena of long-range persistence have a long history and have been authenticated appropriately in hydrology, meteorology and geophysics. Present day studies have led to reawakening and to add analyze long-term persistence in temporal time series of hydrologic data and also to developed applicable methods for estimating and modelling the intensity of long-term persistence in time series, as well as providing the reason for the Hurst phenomena. Based on the consideration of long-term persistence, a stationary process $x_t$ processes long memory if there be present in a real number H ε (0.5, 1), called the Hurst exponent (Montanari et al., 2000).[3] The exponent H, in a hydrological time series, is called the devotion of long-term persistence and it can be numerically denoted by the Hurst coefficient H. when H>0.5 higher the intensity of long-term or long-range persistence in the data and when H <0.5 be identical to short-term negative time persistence, which is almost never encountered in the analysis of hydrological data (Montanari et al., 2000).[3] To test for significant statistically long-term memory on a hydrologic time series, a significant difference between short term and long term persistence must be accomplished (Rao and Bhattacharya,1999).[4] The phenomena of short-term persistence are based on the concept of strong mixing (Rosenblatt,1956) [5] which measure correlation sequentially among two cases distinct by increasing time lags. Against this background, Towards this end Hurst exponent used for ascertain the appearance of long term persistence in data series and testing specifically the null hypothesis of short term Long range dependence also called long memory or long-range persistence is a phenomenon that may arise in the analysis of spatial and time series data usually considered to have long range dependence if the dependence decays more slowly than an exponential decay and Short range dependence also called short memory or short range persistence a process is said to be short range dependence if the dependence among the observations diminishes fast.

The phenomena of short-term dependence are based on the notion of strong mixing (Rosenblatt, 1956). [5] Which measure correlation successively between two events separated by increasing time lags. Against this background, the primary objective of this study is, (1) to investigate the streamflow time series of Seonath River

*https://dx.doi.org/10.22161/ijaers.5.1.19* *ISSN: 2349-6495(P) | 2456-1908(O)*

for monthly and seasonal time scales are characterised by long-term dependence. If it is present in the given series then it can not a significant serial correlation among the observations which are far apart in time. (2) The purpose of Long-range dependence and short-range dependencies are to determine the magnitude and pattern of variations in streamflow during the study period, which will be helpful to predict the behaviour of streamflow in future over the study area. exponent used for detecting the presence of long-term dependence in data series and testing specifically the null hypothesis of short-term dependence in the monthly and seasonal time series by (Von Neumann ratio test, Kendall's rank correlation test, Median crossing test, Run above and below the median, Turning point test, Rank difference test).

## II. STUDY AREA AND DATA QUALITY APPROACHES

The study area is the seonath river basin of Chhattisgarh state, India.It is a major tributary of Mahanadi river which is situated between 20° 16'N to 22° 41'N Latitude and 80° 25'E to 82° 35'E Longitude it consists a large portion of the upper Mahanadi valley and its traverse length of 380 kilometres.The area of the basin is 30560 square kilometres. The Monthly Discharge data of 5 Meteorological stations for whole Seonath River Basin for a period of 32 years i.e. 1980-2012 is collected from Department of state data centre Water Resources, Raipur (Chhattisgarh).To investigate the long term and short term dependence phenomena in the flow series, the average daily flows are aggregated to mean monthly stream flows by summing the average daily flow over the total number of days in the month. thus, for long-term dependence analysis, the seasonality must be removed. To remove the seasonality in the monthly flow series are log-transformed to normalise the data then deseasonalized; the deseasonalized is done as follows.

$$m_{(j,i)} = \frac{x_{(j,i)} * \bar{x}}{S_{(i)}}$$

Where $\bar{x}$, is the monthly mean, $S_{(i)}$ the standard deviation and $x_{(j,i)}$ is the flow data matrix.

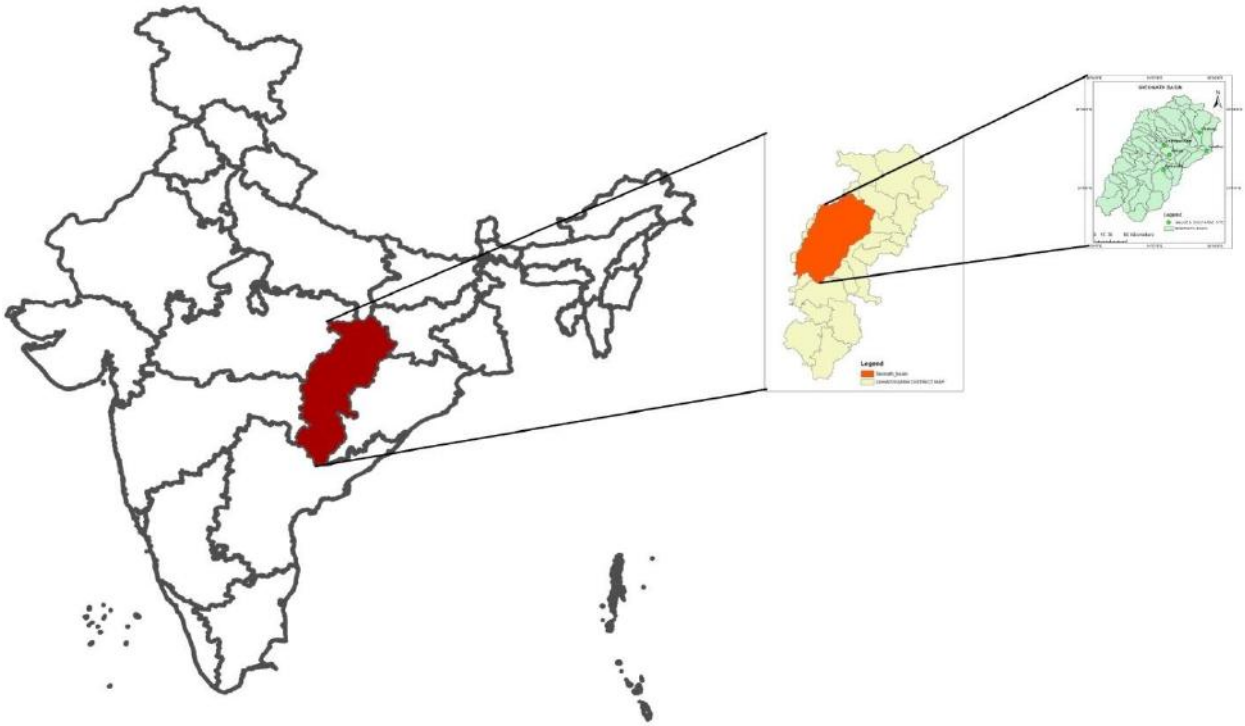

*Fig.2.1: An Index of Seonath River Basin*

### 2.1 Test for independence:

The serial correlation coefficient (SCC) was performed to verify the dependency. It is the correlation between adjacent observations in time series data. According to Box and Jenkins the $lag_1$ serial correlation coefficient, $r_1$ is computed as follows, for 5% significance level, if $r_1 <$ 0.5 then the station is considered as independent, $r_1$ is given as below.

$$\frac{\sum_{i=1}^{n-1}(x_i - \bar{x}) * (x_{i+1} - \bar{x})}{\sum_{i=1}^{n}(x_i - \bar{x})^2}$$

### 2.2 Test for randomness:

Test for randomness is performed to identify whether there is any recognised pattern. If the data is non-random it shows that process then generates the event is following a trend. The data should be random for any time series analysis; the run test is carried out for this purpose, for 5% significance level, if Z > 0.05 then the station is

*https://dx.doi.org/10.22161/ijaers.5.1.19* *ISSN: 2349-6495(P) | 2456-1908(O)*

considered as random. As per test when randomness is more in given time series it means there is more probability to become trendless in such a time series.

$$Z = \frac{R - R_1}{S_r}$$

$$R_1 = 1 + \frac{(2 * A * B)}{n}$$

$$S_r = \sqrt{\frac{2 * A * B\,((2 * A * B\,(-N)}{n^2 * (n-1)}}$$

Where R is observed number of runs, $R_1$ is the expected number of run, n is the number of observation, A is the number of observation above k, B is the number of observations above k, and k is the mean of the observations

**2.3 Test for consistency/Homogeneity:**

Consistency test is performed to identify that the behaviour mechanism that generates a part of time series data is considered with the segment of the time series data. For this purpose, standard normal homogeneity test (SNHT) is done with the help of XLSTAT plug in a package for MS-Excel is used. For 5% significance level, if p > 0.05 then the station is considered as consistent.

*Table. Results of Data Quality Test Results of G&D Station*

| S.NO. | G&D STATION NAME | TEST FOR INDEPENDENCE | TEST FOR RANDOMNESS | TEST FOR HOMOGENEITY |
|---|---|---|---|---|
| | | SCC TEST | RUNS TEST | SNH TEST |
| | | P<0.5 | P>0.05 | P>0.05 |
| 1. | ANDHYAKORE | 0.35 | 0.26 | 0.34 |
| 2. | GHATORA | 0.43 | 0.50 | 0.21 |
| 3. | JONDHRA | 0.49 | 0.1 | 0.125 |
| 4. | PATHARDIH | 0.43 | 0.26 | 0.91 |
| 5. | SIMGA | 0.48 | 0.16 | 0.58 |

## III. METHODOLOGY

### 3.1 METHODS FOR DETECTING LONG TERM DEPENDENCE:

#### 3.1.1 HURST EXPONENT:

Long range dependence is numerically expressed by the Hurst coefficient H (0 - 1) in general holds H = 0.5, the time series is random noise for H < 0.5, the time series is said to be anti-persistence.

Range $(R_n)$ =Max. $\left|\sum (Zi-Z)\right|$ - Min. $\left|\sum (Zi-Z)\right|$

$$R_n = d_n^{+} - d_n^{-}$$

Where, $d_n^{+}$ is maximum positive cumulative deviation and $d_n^{-}$ is minimum negative cumulative deviation.

$$H = \frac{\ln(R_n*)}{\ln(\frac{n}{2})}$$

Where n is the no. of data set where,

$$R_n * = \{\frac{Rn}{\sigma_n}\}$$

Where, $\sigma_n$ is the standard deviation, Long rang dependence can be numerically by the Hurst coefficient this is a coefficient ranging between 0 and 1, where H > 0.5 indicates long-range dependence in the data.

### 3.2 NULL HYPOTHESIS TESTING FOR SHORT TERM DEPENDENCE:

#### 3.2.1 VON NEUMANN RATIO TEST:

The null hypothesis test for short-term dependence is done by using the von Neumann ratio test, (Madansky, 1988).[6] The null hypothesis of no long-term dependence, the following test statistics is computed for both monthly and seasonal streamflow time series. The null hypothesis in this test is that the time series variable is independently and identically distributed (random). The alternate hypothesis is that the series is not random, The von Neumann ratio (N) is the most widely used test for testing a time series for the absence or presence of homogeneity and also identified the presence of short-term dependence and the null hypothesis of no short-term dependence in given time series.

$$NR = \frac{\sum_{t=2}^{n}(x_t - x_{t-1})^2}{\sum_{i=1}^{n}(x_t - \bar{x})^2}$$

Where $x_t$ =hydrologic variable constituting the sequence in time, n = total number of hydrologic records, and $x$ = average of $x_t$ , If data are independent, NR is approximately normally distributed with E (V) = 2 under the null hypothesis, E (NR) = 2. The mean of NR tends to be smaller than 2 for a non-homogeneous series and Var (NR) = $\frac{4 * (n-2)}{(n^2-1)}$ , i.e.

$$Z = \frac{V-2}{[4 * \frac{(n-2)}{(n^2-1)}]^{0.5}}$$

#### 3.2.2 KENDALL'S RANK CORRELATION TEST:

Rank correlation (Kendall, 1948; Abdi, 2007). [7, 8] Can be used to establish whether an apparent trend in a series is significant or not. The number of times p in all pairs of observations $x_i$ , $x_j$ ; j > i that $x_j > x_i$ is determined (i.e., for $i$ = 1, N – 1 how many times $x_j > x_i$ is for $j = i + 1, i + 2$, N).

*https://dx.doi.org/10.22161/ijaers.5.1.19* *ISSN: 2349-6495(P) | 2456-1908(O)*

The test is carried out using the statistic Ƭ (known as Kendall's Ƭ and which varies between ±1) defined as Ƭ = $\frac{4P}{N*(N-1)-1}$ for a random series, E (Ƭ) = 0, and its variance is given as Var (Ƭ) = $\frac{2*(2N+5)}{9N*(N-1)}$ As N increases, $\frac{Ƭ-E(Ƭ)}{\sqrt{Var(Ƭ)}}$ converges to a standard normal distribution. It may also be possible to carry out a test using E (Ƭ) that takes values of –1 and 1, leading to the inference that there is a rising or falling trend. In this test we have to correlate the two adjacent variables in between -1 to 1 and after adding all the variables we get to chances of no trend in series if the value of 'z' lies within the limits ±1.96 at the 5% significance level, the null hypothesis of no trend cannot be rejected.

### 3.2.3 MEDIAN CROSSING TEST:

(Fisz, 1963). [9] *x* is replaced by zero if *x*~ < *x* (median), and X is replaced by one if $x_i > x$. If the original sequence of *x*~ has been generated by a purely random process. In this test we have to compare all variables from a median of the series and after comparing us gets to a number of crossed or not crossed in given time series.

$$m = N\left[\frac{(N-1)}{2}\right], \left[\frac{(N-1)}{4}\right]^{0.5}$$

### 3.2.4 RUN ABOVE OR BELOW THE MEDIAN TEST FOR GENERAL RANDOMNESS:

(Shiau and Condie, 1980). [10] The necessary condition for applying this test is that the observations in the sample are obtained under similar conditions. Null hypothesis (H0) is made that the observations in a time series are independent of the order in the sequence, which is tested by the run test on successive differences. From the sequence of observations $x_t$ (t = 1, 2… n), a sequence of successive differences ($x_{t+1} - x_t$ ) is formed (i.e., each observation has the preceding one subtracted from it). In this test, we have to compare all variables from a median of the series and after comparing us get to a number of run above or run below in given time series. The test-statistic (K) is defined as the number of runs of '+' and '–' signs in the sequence of differences. If $M_s$ represents the total number of runs above and below the median of length s, then for a random process.

$$E(M_s) = \frac{(n+3-s)}{(2^s-1)} \text{ and}$$

$$\frac{\sum_{s=1}^{s'}[M_s - E(M_s)]^2}{E(M_s) \approx x^2 * (s'-1)},$$

where s' is the maximum run length in the sequence.

### 3.2.5 TURNING POINTS TEST:

Let's assume that a turning point occurs in the series $x_t$ (t = 1, 2… n) at any time t (t = 2, 3… n–1) if $x_t$ is larger than each of $x_{t-1}$ and $x_{t+1}$ or $x_t$ is smaller than $x_{t-1}$ and $x_{t+1}$ this situation has four chances of occurrence in six different possibilities of the occurrence of $x_{t-1}$ and $x_{t+1}$, assuming that all three elements have different values. In this test, we have to identify the number of turning points in given time series, when number turning point is more it means more chances to randomness or trendless in the dataset. Accordingly, the chance of having a turning point in a sequence of three values is 4/6 or 2/3, for all the values of' except for t = 1 and t = n. In other words, the expected number of turning points ($\bar{p}$) in the given random series can be expressed as (Kendall and Stuart, 1976). [11].

$$\bar{p} = \frac{2*(n-2)}{3} \text{ for the same}$$

random series, variance is given by (Kendall, 1973)

$$\text{Var}(\bar{p}) = \frac{(16n-29)}{90}$$

The test-statistic is represented by the standard normal variate (z), and is given as:

$$Z = \frac{|p-\bar{p}|}{\sqrt{Var(\bar{p})}} \text{ where p is}$$

observed number a of turning points

It is a very easy to test to apply to a series of randomness observation involves the counting of the number of local maxima and minima, the interval between two turning points is called phase Turning point test reasonable against cyclicity but poor as a test against the trend.

### 3.2.6 RANK DIFFERENCE TEST:

(Meacham, 1968). [12] Flows are replaced by their relative ranks $R_i$ with the lowest being denoted by Rank 1 ($R_i$). The U statistic is evaluated by

$$U = \sum_{i=2}^{n} |R_i - R_{i-1}|$$

For large n,

$$U = \{\frac{(n+1)*(n-1)}{3}, [\frac{(n-2)*(n+1)*(4*n+7)}{90}]^{0.5}\}$$

## IV. RESULTS AND DISCUSSION

The Hurst exponent (K) for different months of the year and seasonal time series is presented in table-1.

*Table.1: Values of Hurst exponent (k) for (G&D Stations)*

| Months | Andhyakore | Ghatora | Jondhra | Pathardih | Simga |
|---|---|---|---|---|---|
| **January** | 0.6574 | 0.6130 | 0.6832 | 0.8838 | 0.8003 |
| **February** | 0.5999 | 0.5868 | 0.5327 | 0.7374 | 0.5760 |
| **March** | 0.7404 | 0.7576 | 0.7901 | 0.8024 | 0.8261 |

*https://dx.doi.org/10.22161/ijaers.5.1.19* *ISSN: 2349-6495(P) | 2456-1908(O)*

| Months | Andhyakore | Ghatora | Jondhra | Pathardih | Simga |
|---|---|---|---|---|---|
| **April** | 0.7670 | 0.8010 | 0.7884 | 0.8251 | 0.8321 |
| **May** | 0.8196 | 0.7276 | 0.8035 | 0.7528 | 0.7945 |
| **June** | 0.6253 | 0.6292 | 0.6371 | 0.6703 | 0.6006 |
| **July** | 0.7103 | 0.6049 | 0.5680 | 0.7234 | 0.6088 |
| **August** | 0.6925 | 0.7240 | 0.5970 | 0.8516 | 0.4956 |
| **September** | 0.6342 | 0.7382 | 0.4819 | 0.7848 | 0.5770 |
| **October** | 0.5541 | 0.6545 | 0.5754 | 0.7557 | 0.5317 |
| **November** | 0.7162 | 0.7102 | 0.6919 | 0.7956 | 0.5977 |
| **December** | 0.6586 | 0.6435 | 0.6243 | 0.8279 | 0.6900 |
| **Annual** | 0.6872 | 0.7343 | 0.5220 | 0.8730 | 0.5280 |
| **Winter** | 0.7256 | 0.7186 | 0.6925 | 0.8473 | 0.7417 |
| **Pre-monsoon** | 0.7812 | 0.7963 | 0.8030 | 0.8043 | 0.8280 |
| **Monsoon** | 0.6907 | 0.6936 | 0.5279 | 0.8720 | 0.5298 |
| **Post-monsoon** | 0.7038 | 0.6890 | 0.6027 | 0.7861 | 0.5198 |

Where the bold value represents no long-term dependence for the given time series and remaining value shows term persistence.

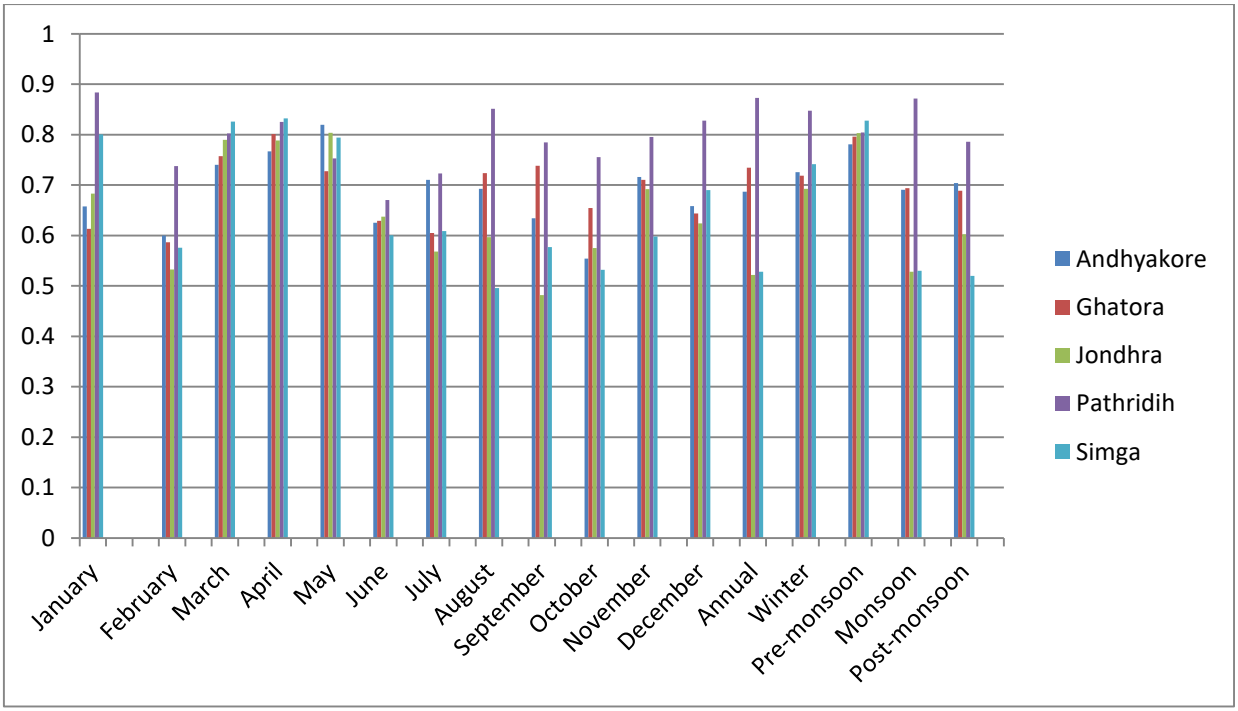


*Fig.2: Hurst Exponent (K) For (G&D Stations)*

*Table.2: Values of Z statistics for short-term dependence by Von Neumann ratio test*

| Months | Andhyakore | Ghatora | Jondhra | Pathridih | Simga |
|---|---|---|---|---|---|
| JANUARY | 0.0650 | 0.0052 | 0.0047 | **8.0933** | 0.0197 |
| FEBUARY | 0.0508 | 0.0320 | 0.0141 | 1.5799 | 0.0451 |
| MARCH | 0.0731 | 0.0981 | 0.0353 | **9.0117** | 0.3008 |
| APRIL | 0.0919 | 0.3380 | 0.3435 | **9.0288** | 0.6840 |
| MAY | 0.1800 | 0.2216 | 0.5737 | **3.9725** | 0.7284 |
| JUNE | 0.0533 | 0.0362 | 0.0680 | 0.0649 | 0.0478 |
| JULY | 0.0095 | 0.0070 | 0.0299 | 0.1708 | 0.0029 |
| AUGEST | 0.1160 | 0.0722 | 0.0348 | 0.2600 | 0.0590 |
| SEPTEMBER | 0.0171 | 0.0869 | 0.1240 | 0.1140 | 0.0241 |
| OCTOBER | 0.1207 | 0.0644 | 0.1114 | 0.0204 | 0.1071 |

*https://dx.doi.org/10.22161/ijaers.5.1.19* *ISSN: 2349-6495(P) | 2456-1908(O)*

| Months | Andhyakore | Ghatora | Jondhra | Pathridih | Simga |
|---|---|---|---|---|---|
| NOVEMBER | 0.0811 | 0.1801 | 0.0427 | 0.0679 | 0.0016 |
| DECEMBER | 0.0937 | 0.0459 | 0.0204 | **3.0213** | 0.0444 |
| ANNUAL | 0.0128 | 0.0704 | 0.1081 | 0.2678 | 0.0404 |
| WINTER | 0.3226 | 0.2549 | 0.1944 | **4.8820** | 0.0783 |
| PRE-MONSOON | 0.1103 | 0.2598 | 0.2335 | **7.5652** | 0.5561 |
| MONSOON | 0.0116 | 0.0701 | 0.1050 | 0.2683 | 0.0282 |
| POST-MONSOON | 0.1613 | 0.0127 | 0.1105 | 0.0368 | 0.1233 |

Where, Table -2 represent The Null hypothesis of no short-term dependence in the series is accepted and thus the given series can be assumed to be random at 10%, 5% and 1% significance level.

*Table.3: Values of Z statistics for short-term dependence by Kendall's Rank Correlation test*

| Months | Andhyakore | Ghatora | Jondhra | Pathridih | Simga |
|---|---|---|---|---|---|
| JANUARY | 1.8811 | 1.2067 | 2.7024* | 0.6969 | 2.8384* |
| FEBRUARY | 1.7514 | 2.6344* | 1.9206 | 0.1190 | **2.5665** |
| MARCH | 3.1784* | 3.3823* | 3.1783* | 2.8384* | 3.8922* |
| APRIL | 3.6649* | 3.7562* | 3.5183 | 3.5183* | 3.5183 |
| MAY | 3.1784* | 3.5523* | 3.5183 | 3.9262* | 3.4503 |
| JUNE | 0.5189 | 1.4787 | 1.3087 | 0.8668 | 1.5807 |
| JULY | 1.5568 | 1.7166 | 0.2210 | 2.7024* | 1.0368 |
| AUGEST | 1.1676 | 1.5462 | 0.5949 | **2.1246** | 0.3909 |
| SEPTEMBER | 0.2595 | 1.0028 | 0.1870 | 3.4503* | 0.3909 |
| OCTOBER | **2.3027** | 1.1388 | 1.2407 | **2.5665** | 0.4929 |
| NOVEMBER | 0.7784 | 0.5949 | 0.5269 | **2.1925** | 0.7648 |
| DECEMBER | **2.1406** | **2.0226** | **2.0566** | 0.0170 | **2.4645** |
| ANNUAL | 0.6811 | 1.6487 | 0.4929 | **2.3285** | 0.4589 |
| WINTER | **1.9784** | 1.4787 | 2.1925* | 0.7648 | **2.4305** |
| PRE-MONSOON | 2.7892* | 3.4843* | 3.5523* | 2.8044* | 3.7562* |
| MONSOON | 0.5838 | 1.9546 | 0.5269 | **2.4305** | 0.2549 |
| POST-MONSOON | 1.1597 | 0.9688 | 1.2067 | **2.2945** | 0.6969 |

Where,

- The Bold value represents null hypothesis of **No short-term dependence** in the series is accepted and thus the given series can be assumed to be having **No trend at 1% significance level.**
- ____ Marks represents null hypothesis of **No short-term dependence** in the series is accepted and thus the given series can be assumed to be having **No trend at 5% and 1% significance level.**
- 1.8811 represent represents null hypothesis of **No short-term dependence** in the series is accepted and thus the given series can be assumed to be having **No trend at 10% significance level.**
- (*) marks represents null hypothesis of **No short-term dependence** in the series is accepted and thus the given series can be assumed to be having **No trend**
- The remaining value represents null hypothesis of **No short-term dependence** in the series is accepted and thus the given series can be assumed to be having **No trend at 10%, 5% and 1% significance level.**

*Table.4: Values of Z statistics for short-term dependence by Median crossing test*

| Months | Andhyakore | Ghatora | Jondhra | Pathridih | Simga |
|---|---|---|---|---|---|
| JANUARY | 1.0954 | 1.0954 | 0.3651 | **3.2863** | 1.0954 |
| FEBUARY | 1.8257 | 1.0954 | 1.8257 | **2.5560** | 1.8257 |
| MARCH | 0.3651 | 0.3651 | 1.0954 | **3.2863** | 2.1908 |
| APRIL | **2.5560** | **2.5560** | 1.4605 | **2.5560** | 1.4605 |
| MAY | 1.8257 | **3.2863** | 1.8257 | **-3.2863** | 2.1908 |

*https://dx.doi.org/10.22161/ijaers.5.1.19* *ISSN: 2349-6495(P) | 2456-1908(O)*

| Months | Andhyakore | Ghatora | Jondhra | Pathridih | Simga |
|---|---|---|---|---|---|
| JUNE | 0.7302 | 1.4605 | 0.7302 | **2.5560** | 1.4605 |
| JULY | 0.000 | 0.7303 | 0.3651 | 1.4605 | 1.0954 |
| AUGEST | 0.7302 | 0.000 | 0.000 | 1.4605 | 0.3651 |
| SEPTEMBER | 0.000 | 0.000 | 0.3651 | **2.1908** | 0.3651 |
| OCTOBER | 1.8257 | 1.4605 | **2.1908** | **2.1908** | -0.3651 |
| NOVEMBER | 1.4605 | 0.7303 | 0.3651 | **2.9211** | 0.3651 |
| DECEMBER | 0.7302 | 0.000 | 0.7303 | **2.5560** | 1.8257 |
| ANNUAL | 0.000 | **2.1908** | 1.8257 | **2.1908** | 0.3651 |
| WINTER | **2.5560** | 1.0954 | 1.0954 | **3.2863** | **2.5560** |
| PRE-MONSOON | 1.0954 | **2.5560** | 1.0954 | **3.2863** | 1.4605 |
| MONSOON | 0.000 | 1.4605 | 0.3651 | 1.4605 | 0.3651 |
| POST-MONSOON | 1.4605 | **2.1908** | **2.5560** | **2.1908** | 0.3651 |

Where,

- The Bold value represents **short-term dependence is observed** in the given series thus the data **cannot be random at 5% significance level.**
- The remaining value represents **No short-term dependence is observed** in the given series thus the data **can be random at 5% significance level.**

*Table.5: Values of Z statistics for short-term dependence by Run above and below the median for general randomness*

| Months | Andhyakore | Ghatora | Jondhra | Pathridih | Simga |
|---|---|---|---|---|---|
| JANUARY | **3.00** | **8.00** | **2.00** | 45.00 | **2.00** |
| FEBUARY | 10.00 | **8.00** | 24.00 | 88.00 | 26.00 |
| MARCH | **3.00** | 15.00 | **7.00** | 178.00 | 19.00 |
| APRIL | **3.00** | 18.00 | 19.00 | 371.00 | **3.00** |
| MAY | **4.00** | 127.00 | 103.00 | 347.00 | 26.00 |
| JUNE | **5.00** | **4.00** | **7.00** | 63.00 | **3.00** |
| JULY | 15.00 | **7.00** | **7.00** | 41.00 | **3.00** |
| AUGEST | **3.00** | **2.00** | **6.00** | 86.00 | **5.00** |
| SEPTEMBER | **2.00** | **2.00** | **3.00** | 88.00 | **1.00** |
| OCTOBER | **5.00** | **3.00** | **3.00** | 85.00 | **3.00** |
| NOVEMBER | **1.00** | **3.00** | 11.00 | 88.00 | **5.00** |
| DECEMBER | **7.00** | **6.00** | **6.00** | 88.00 | **7.00** |
| ANNUAL | **1.00** | **8.00** | **1.00** | 87.00 | **3.00** |
| WINTER | 10.00 | **5.00** | **8.00** | 49.00 | 20.00 |
| PRE-MONSOON | **1.00** | **8.00** | 22.00 | 86.00 | 19.00 |
| MONSOON | 13.00 | **8.00** | **1.00** | 86.00 | **5.00** |
| POST-MONSOON | **2.00** | **6.00** | **3.00** | 93.00 | 10.00 |

Where The Bold value represents “No short-term dependence” in the given series and remaining has No dependence at 5% significance level in the given series.

*Table.6: Values of Z statistics for Randomness by Turning point test*

| Months | Andhyakore | Ghatora | Jondhra | Pathridih | Simga |
|---|---|---|---|---|---|
| JANUARY | 0.7317* | 0.1463* | 0.1463* | **1.9023** | 1.1707* |
| FEBUARY | 0.1463* | **1.9023** | 1.0243* | 3.6583 | 0.7317* |
| MARCH | 1.0243* | **1.9023** | 0.7317* | 4.9753 | 0.2927* |
| APRIL | 1.0243* | 3.6583 | 1.0243* | 4.9753 | 0.2927* |
| MAY | 2.7803 | 3.6583 | 2.3413 | 5.4143 | 0.1463* |

*https://dx.doi.org/10.22161/ijaers.5.1.19* *ISSN: 2349-6495(P) | 2456-1908(O)*

| Months | Andhyakore | Ghatora | Jondhra | Pathridih | Simga |
|---|---|---|---|---|---|
| JUNE | 0.2927* | 0.7317* | 0,2927* | 4.5363 | 0.7317* |
| JULY | 0.5853* | 1.0243* | 1.1707* | **1.9023** | 0.1463* |
| AUGEST | 1.4633* | 0.1463* | 1.1707* | 2.3413 | 1.1707* |
| SEPTEMBER | 1.1707* | 0.1463* | **1.9023** | 3.2193 | 1.4633* |
| OCTOBER | 0.7317* | 2.0487 | 1.1707* | 1.4633* | 1.1707* |
| NOVEMBER | 0.7317* | 0.1463* | 0.7317* | 2.3413 | 0.1463* |
| DECEMBER | 0.7317* | 0.1463* | 0.2927* | 3.6583 | 1.1707* |
| ANNUAL | 4.5363 | 3.6583 | 4.0973 | 5.4143 | 3.6583 |
| WINTER | 2.7803 | 2,3413 | **1.9023** | 5.5363 | 1.4633* |
| PRE-MONSOON | 1.0243* | **1.9023** | 0.7317* | 4.9753 | 0.2927* |
| MONSOON | 1.4633* | 1.6097* | 0.7317* | 2.3413 | 1.1707 |
| POST-MONSOON | 0.7317* | 1.1707* | 1.6097* | 4.9753 | 1.1707 |

Where,

- (*) Marks represents null hypothesis of no short-term dependence in the series is accepted and thus the given series can be assumed to be random at 10%, 5% and 1% significance level.
- The Bold value represents null hypothesis of no short-term dependence in the series is accepted and thus the given series can be assumed to be random at 5% and 1% significance level.
- ____ Sign represents null hypothesis of no short-term dependence in the series is accepted and thus the given series can be assumed to be random at 1% significance level.

*Table.7: Values of Z statistics for short-term dependence by Rank difference test*

| Months | Andhyakore | Ghatora | Jondhra | Pathridih | Simga |
|---|---|---|---|---|---|
| JANUARY | 1.2380 | 1.5835 | 0.8349 | **5.8157** | 1.5259 |
| FEBUARY | 1.9002 | **2.6200** | 0.9789 | **5.8733** | 1.2092 |
| MARCH | **2.2457** | **2.5912** | **2.0154** | 7.4280 | 2.3896 |
| APRIL | **3.0518** | **5.2111** | **2.2169** | 7.7735 | 2.7351 |
| MAY | **3.7140** | **5.0096** | **3.2246** | 7.6008 | 2.6488 |
| JUNE | 0.9213 | 0.1152 | 0.6046 | 4.7793 | 0.4319 |
| JULY | 0.6334 | 0.6622 | 0.3743 | 4.2323 | 0.2303 |
| AUGEST | 1.3532 | 0.4319 | 0.5470 | 4.5490 | 0.2591 |
| SEPTEMBER | 0.5182 | 0.4607 | 0.6046 | 4.8944 | 0.2303 |
| OCTOBER | 0.9789 | 0.8061 | 1.1228 | 3.8004 | 0.7198 |
| NOVEMBER | 0.4607 | 0.6046 | 0.4319 | 4.8657 | 0.0288 |
| DECEMBER | 1.0365 | 0.7774 | 0.5470 | 5.4991 | 1.8138 |
| ANNUAL | 0.5182 | 0.2303 | 1.1516 | 4.5490 | 0.2591 |
| WINTER | **3.742** | **3.2246** | **2.8503** | 6.2476 | 2.8503 |
| PRE-MONSOON | **2.591** | **4.2035** | **2.2457** | 7.2553 | 2.3896 |
| MONSOON | 0.4894 | 0.4607 | 1.2092 | 4.4914 | 0.2879 |
| POST-MONSOON | 0.1152 | 0.4319 | 1.0077 | 3.9443 | 0.8349 |

Where,

- At 5% significance level, the value of standard normal variate is "1.95996" below this level show "No short-term dependence observed" thus given series can be random at 5% significance level.
- The Bold value represents Null hypothesis of no short-term dependence in the given series, at 5% significance level.

## V. CONCLUSION

The main objective of this study was to detect short-term and long-term dependence of streamflow time series. As a first step, Hurst coefficient was estimated at 5 Gauge and Discharge stations of daily river discharge time series for Seonath River Basin, Chhattisgarh State. For Hurst phenomena, the Hurst exponent was greater than 0.5. And this Statistical analysis H is estimated greater than 0.7 in

*https://dx.doi.org/10.22161/ijaers.5.1.19* *ISSN: 2349-6495(P) | 2456-1908(O)*

the majority of different time scales and also observed that the null hypothesis of no dependence at 10%, 5% and 1% significance level for all the estimators. The finding of this study has more important implications for hydrological modelling especially in reservoir operation and water resource management for example, in order to estimate the risk of supply from a reservoir the long-term dependence primary incorporated into the model, this study suggests that to identify the main factors associated with the climate variability and storage that affects the long-term dependence of streamflow at a regional scale. Change in climate could have directly and indirectly affected by the various environmental variables including discharge in many countries of the world. Change in discharge regime directly affects the management of water resources, agriculture, hydrology and ecosystems. Hence it is important to identify the changes in the magnitude of the temporal and spatial behaviour of discharge is imperative for suggesting the suitable strategies for sustainable management of water resources, agriculture, environment and ecosystems.

## REFERENCES


[1] Blöschl, G. and Montanari, A., 2010. Climate change impacts—throwing the dice? *Hydrological Processes*, *24*(3), pp.374-381.

[2] Hurst, H.E., 1951. The long-term storage capacity of reservoirs. *Trans. Amer. Soc. Civil Eng.*, *116*, pp.770-808.

[3] Montanari, A., Rosso, R. and Taqqu, M.S., 2000. A seasonal fractional ARIMA model applied to the Nile River monthly flows at Aswan. *Water Resources Research*, *36*(5), pp.1249-1259.

[4] RAMACHANDRA RAO, A. and BHATTACHARYA, D., 1999. Hypothesis testing for long-term memory in hydrologic series. *Journal of Hydrology*, *216*(3-4), pp.183-196.

[5] Rosenblatt, M., 1956. A central limit theorem and a strong mixing condition. *Proceedings of the National Academy of Sciences*, *42*(1), pp.43-47.

[6] Madansky, A., 1988. Testing for normality. In *Prescriptions for working statisticians* (pp. 14-55). Springer New York.

[7] Kendall, M.G., 1948. Rank correlation methods.

[8] Abdi, H., 2007. The Kendall rank correlation coefficient. *Encyclopedia of Measurement and Statistics. Sage, Thousand Oaks, CA*, pp.508-510.

[9] Fisz, M., 1963. Probability theory and mathematical statistics John Wiley and Sons. *Inc., New York*.

[10] Shiau, S.Y. and Condie, R., 1980. Statistical tests for independence, trend, homogeneity and randomness. Hydrologic Applications Division. *Water Resources Branch, Inland Waters Directorate, Environment Canada, Ottawa, Ont*.

[11] Kendall, M.G. and Stuart, A., 1968. The Advanced Theory of Statistics, Vol. 3, Charles Griffin & Co. *London, 1946Kendall1The Advanced Theory of Statistics1946*.

[12] Meacham, I., 1968. Correlation in sequential data three sample indicators. *Civil Eng. Trans. Inst. Eng. Aust*, *10*, pp.225-228.

[13] Koutsoyiannis, D., 2003. Climate change, the Hurst phenomenon, and hydrological statistics. *Hydrological Sciences Journal*, *48*(1), pp.3-24.

[14] Otache, M.Y., Li, Z. and Bakir, M., 2008. Analysis of long-term dependence phenomenon in Benue River flow process and its hypothesis testing. *Chinese Journal of Oceanology and Limnology*, *26*(3), pp.313-322.

[15] Percival, D.B., 1996. Statistics for Long-Memory Processes. *Journal of the American Statistical Association*, *91*(435), pp.1379-1381.

https://dx.doi.org/10.22161/ijaers.5.1.20 ISSN: 2349-6495(P) | 2456-1908(O)

# Statistical Analysis of Rainfall Event in Seonath River Basin Chhattisgarh

Shashikant Verma, Bhupendra Kumar Dhiwar

M.Tech. Scholar, Water Resources Development & Irrigation Engineering, Department Civil Engineering, NIT Raipur, India

***Abstract***— *To understand the mechanism of potential hydrologic impacts of climate and land use land cover changes. In this study identified to the significant temporal trend was carried out monthly, seasonal timescales. Using the rainfall data of 39 Meteorological stations under entire seonath basin which is subdivided into five weighted stations with the help of by creating Thiessen polygon over Seonath River, Chhattisgarh state of 32 years for a period of 1980-2012. Hydro metrological variables are analysed by using a combined Mann-Kendall/Thiel-Sen slope estimator trend detection approach. The results reveal a significant decreasing trend for the month of January, February, March, and may, September, October and December for all the five gauging stations similarly the month of April, June, July, August and November show the significant increasing trend. For all the five gauging stations excluded month of January in simga gauging station shows having no trend. Whereas the trend in different seasons are follows (1) season of winter and pre-monsoon shows significant decreasing trend for all the five gauging stations and post-monsoon season andhyakore, pathridih and simga gauging stations also represents the decreasing trend and (2) the season of monsoon shows increasing trend for all the five gauging stations and seasons of winter and pre-monsoon of ghatora and simga stations also shows the increasing trend.*

***Keywords— Trend Analysis, Rainfall, Mann-Kendall, Sen Slope, Thiessen polygon.***

## I. INTRODUCTION

Change in climate is a long-term phenomenon and most alarming issues for the entire world, Therefore; quantification of climate changes has become preliminary. Identification of temporal trend of hydro-metrological variables is important to sustainable management and development of water resources in future. Rainfall is one of a most important event of the hydrological cycle.[1] This depends on the changes in the variations of atmospheric concentration of greenhouse gaseous. A number of studies done on rainfall trend analysis in various regions. Most of the paper used non-parametric approaches for detecting trend and few of the paper have used a linear regression test. In this study we have to use non-parametric methods because they are distributed free and mostly used non-parametric method which is recommended for detection of significant monotonic upward and downward trend for different climatologic and hydrologic time scale by World Meteorological Organization (WMO) and Thiel-Sen slope estimator is mostly used for estimating magnitude of linear trend and it has been also most commonly used for detecting the magnitude of linear trend in hydro-meteorological time series.[2]

## II. STUDY AREA AND DATA USED

The study area is the seonath river basin of Chhattisgarh state, India.It is a major tributary of Mahanadi river which is situated between 20° 16'N to 22° 41'N Latitude and 80° 25'E to 82° 35'E Longitude it consists a large portion of the upper Mahanadi valley and its traverse length of 380 kilometres.The area of the basin is 30560 square kilometres. The Monthly precipitation data of 39 Meteorological stations for whole seonath river basin for a period of 32 years i.e. 1980-2012 is collected from Department of state data centre Water Resources, Raipur (Chhattisgarh) this data is then analysed for detecting if the trend is monotonic increasing or decreasing. The latitude, longitude and area (Thiessen polygon) for each station is shown in table Moreover, the location of each station in Seonath river basin map is represented in figure

https://dx.doi.org/10.22161/ijaers.5.1.20 ISSN: 2349-6495(P) | 2456-1908(O)

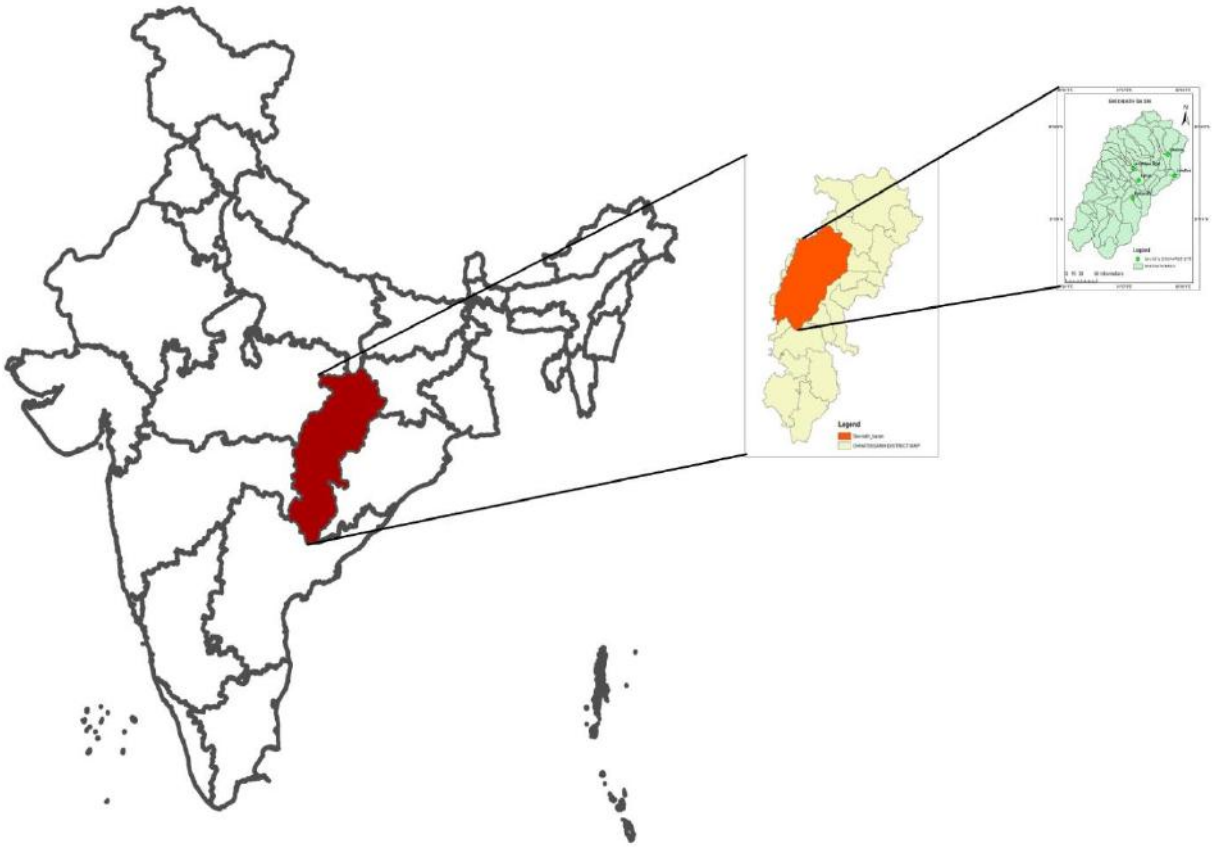

*Fig: Seonath River basin with Gauge & Discharge stations.*

*Table.1: Location and Area (Thiessen Polygon) for Station*

| STATION NAME | LATITUDE | LONGITUDE | AREA ($km^2$) |
|---|---|---|---|
| Ambagarh Chowki | 20.7778 | 80.7486 | 1298.78 |
| Andhyakore CWC | 21.78 | 81.61 | 364.887 |
| Balod | 20.7334 | 81.23334 | 934.391 |
| Bemetara | 21.7291 | 81.5486 | 537.711 |
| Bilaspur | 22.08334 | 82.15 | 1185.89 |
| Bodla | 22.1816 | 81.223334 | 114.63 |
| Chilhaki | 21.7916 | 82.30833 | 1030.25 |
| Chirapani | 22.2083 | 81.1958 | 547.10 |
| Chuikhadan | 21.53334 | 81.01666 | 1167.67 |
| Dhamtari | 20.8219 | 81.55222 | 1158.84 |
| Dongargaon | 20.975 | 80.8625 | 622.855 |
| Dongargarh | 21.1833 | 80.7666 | 976.89 |
| Doundi | 20.4847 | 81.0958 | 789.881 |
| Durg | 21.2166 | 81.28334 | 1574.88 |
| Gandai | 21.667 | 81.1166 | 684.03 |
| Ghonga | 22.30 | 81.9667 | 1562.45 |
| Gondly | 20.75 | 81.1334 | 641.39 |
| Jondhara CWC | 21.72 | 82.34 | 490.28 |
| Kawardha | 22.0166 | 81.2334 | 630.16 |
| Kendiri | 21.10 | 81.7334 | 563.02 |
| Kharkhara | 20.9667 | 81.0334 | 924.55 |
| Khuria | 22.3875 | 81.59889 | 1519.24 |
| Khutaghat | 22.30 | 82.208334 | 1523.80 |
| Kota | 22.2667 | 82.0334 | 382.00 |
| Kotni CWC | 22.130 | 81.240 | 229.80 |
| Madiyan | 21.990 | 83.20 | 386.26 |
| Mungeli | 21.1334 | 80.61667 | 1114.24 |

*https://dx.doi.org/10.22161/ijaers.5.1.20* *ISSN: 2349-6495(P) | 2456-1908(O)*

| STATION NAME | LATITUDE | LONGITUDE | AREA ($km^2$) |
|---|---|---|---|
| Nawagarh | 22.0667 | 81.68334 | 689.73 |
| Newara | 21.9061 | 81.60583 | 1050.78 |
| Pandariya | 21.550 | 81.83334 | 881.23 |
| Patharidih CWC | 22.2166 | 81.41667 | 552.49 |
| Pindrawan | 21.34 | 81.60 | 610.78 |
| Raipur | 21.40 | 81.850 | 394.21 |
| Semartal | 21.25 | 81.6334 | 432.25 |
| Shahspur | 20.97 | 81.87 | 667.41 |
| Simga CWC | 21.90 | 81.11666 | 291.54 |
| Simga WRD | 22.1834 | 82.16667 | 590.47 |
| Sond | 21.6202 | 81.705 | 931.62 |
| Surhi (Palemeta ) | 21.22 | 81.69 | 472.04 |

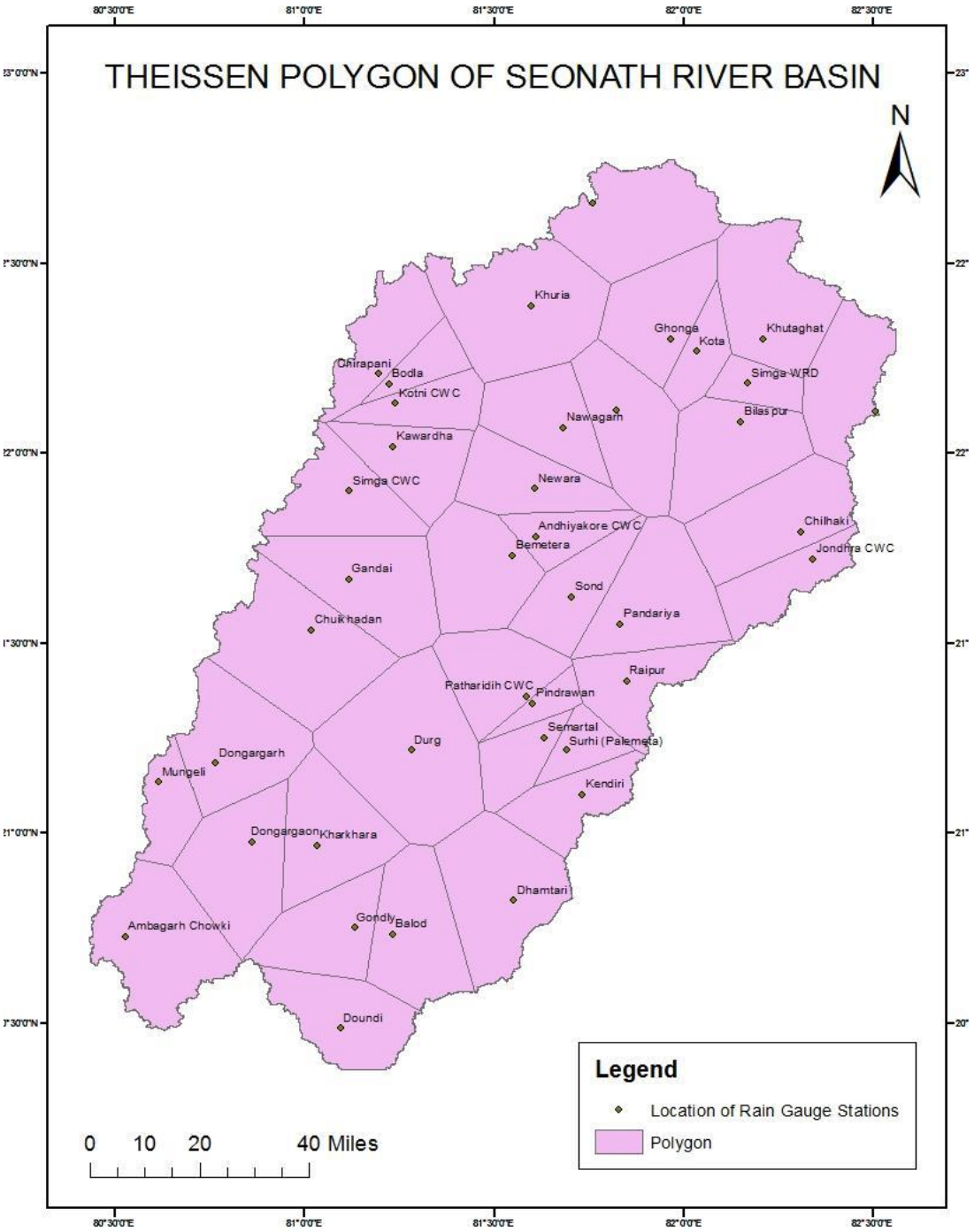

*https://dx.doi.org/10.22161/ijaers.5.1.20* *ISSN: 2349-6495(P) | 2456-1908(O)*

*Fig.1: Location of rainfall station over whole Seonath River basin (Thissen Polygon)*

## III. METHODOLOGY

### 3.1 STUDY OF TIME SERIES

A time series is a combination of statistics, usually collected at a regular interval ( average monthly rainfall, annual rainfall temperature) and it occurs naturally in many application areas ( precipitation, rainfall, temperature).The method of time series analysis pre-date those for general stochastic processes and Markov chains.[3] The objective of time series analysis is to describe and summarise the time series data and assembles to low dimensional model and to predict the future forecast.

### 3.2 TREND ANALYSIS

It is a statistical method which is most commonly used for studying the temporal trend of hydroclimatic timescales. In the present study, trend detection analysis has been done by using non-parametric (Mann-Kendall test and Thiel Sen Slope estimator test).A non-parametric test approach is taken into account against the parametric one because it is distribution-free, robustness against outliers. [4]

## IV. METHODS FOR TREND DETECTION ANALYSIS

### 4.1 Testing significance of trend by MK test

The purpose of the Mann-Kendall (MK) test is to statistically assess if there is a monotonic upward or downward trend of the variable of interest over time series. A monotonic upward (downward) trend means that the variables consistently increase (decreases) through time, but the trend sometimes may or may not be linear. An assumption not required by the MK test, that is the MK test is a nonparametric (distribution-free) test. In MK test statics we have to use Signum function and correlate the variables if X1<X2 =-1, ifX1=X2, =0 and if X1>X2,=1and by adding all this correlation values to detect whether significant increasing or decreasing trend in the given series In MK test statics the sample size should not be less than 4. It is the most widely used for the analysis of detecting a trend in climatologic and hydrologic time scales.[5]

The test is based on statistic S defined as follows:

$$S = \sum_{i=1}^{N-1} \sum_{j=i+1}^{N} sgn(xj - xi)$$

Where N is the number of data point in the given time series, xi and xj are the data values at time scale I and j (j>i) respectively. This test statistics represent a number of positive differences minus negative of differences for considering all the differences. And denoted by,

$$\delta = (xj\text{-}xi)$$

$$\text{sgn}(\delta) = \{1 \quad if\ \delta > 0, 0 \quad if\ \delta = 0, -1 \quad if\ \delta < 0\}$$

For sample (N>4), the distribution of S is assumed to follow the normally distributed with variance and zero mean.

$$\text{Var}(S) = \frac{N(N-1)(2N+5) - \sum_{k=1}^{n} tk(tk-1)(2tk+5)}{18}$$

Where N is the number of tied (the difference between compared values is zero) group and tk is the number of data points in the kth group of tied.

The Z- statistics or standard normal deviate is computed by using the equation:

$$Z = \left\{ \frac{s-1}{\sqrt{var(s)}} \quad if\ S > 0, \quad 0\ if\ S = 0, \quad \frac{s+1}{\sqrt{var(s)}} \quad if\ S < 0 \right\}$$

Here, if the value of $|Z|$ >Z' then the null hypothesis of no trend is rejected at 0.05% of significance level in a two-tailed test. (Trend is significant), in this study, a positive value of Z represents an upward or increasing trend and negative value of Z represents the downward or decreasing trend.[5]

### 4.2 THIEL SEN'S SLOPE ESTIMATOR TEST

Thiel-Sen's slope estimator is useful for estimating the changes in the amount of trend and it has been most commonly used for detecting the magnitude of a linear trend in hydro-meteorological time series. Here, the Slope (Ti) of the entire data group is computed as follows.[6]

$$\mathbf{Ti} = \frac{xj - xk}{j - k} \qquad \text{for i = 1, 2, 3.....N}$$

Where, xj and xk are taken as values of data at time j and k (j>k) respectively.

The median of the sen's slope estimator is represented as,

$$Qi = \left\{ \frac{TN+1}{2}, N\ is\ odd, \quad \frac{1}{2}\left(\frac{TN}{2} + \frac{TN+2}{2}\right), \ N\ is\ even \right\}$$

A positive value of Qi represents the upward trend and a negative value represents a downward trend in the given time series.

## V. RESULT AND DISCUSSION

The Mann-Kendall Statistic (Zmk) for different months and seasons of a year is represented in figure 2. The Zmk values for five gauge & discharge stations are (1) Andhyakore, the (Zmk) values are -1.10,-0.50,-0.60,-0.40,-1.40, 0.20, 1.40, 0.50,-0.40,-1.0,1.90 and -0.50 respectively from January to December the month of January, February, March April, may, September, October and December clearly mention significant decreasing trend in streamflow whereas the month of June, July, August and November shows increasing trend for monthly streamflow for 1980-2012. And Zmk values for seasonal variations for andhyakore stations are -1.10,-1.0, 0.30 and -0.30 respectively for winter, pre-monsoon, monsoon and post-monsoon. The season of winter, pre-monsoon and post-monsoon represent a decreasing trend and monsoon season shows the increasing trend.(2)

*https://dx.doi.org/10.22161/ijaers.5.1.20* *ISSN: 2349-6495(P) | 2456-1908(O)*

Ghatora, the (Zmk) values are -0.90,-1.10,0.90,0.40,1.0,0.40,1.40,2.10,0.40,0.10,0.80and -1.0 respectively from January to December the month of January, February, and December clearly mention significant decreasing trend in streamflow whereas the month of March April, may, June,July, August, September, October and November shows increasing trend for monthly streamflow for 1980-2012. And Zmk values for seasonal variations for ghatora stations are -1.20, 1.60, 1.70 and 0.30 respectively for winter, pre-monsoon, monsoon and post-monsoon. The season of winter represents decreasing trend and pre-monsoon, monsoon and post-monsoon season show the increasing trend. (3) Jondhara, the (Zmk) values are -1.20,-1.0,-0.50,0.80,-0.80,-0.20,1.70,-0.20,0.10,-0.80,1.10 and -0.50 respectively from January to December the month of January, February, March, may, June, August, October and December clearly mention significant decreasing trend in streamflow whereas the month of April, July, September and November shows increasing trend for monthly streamflow for 1980-2012. And Zmk values for seasonal variations for jondhara stations are -0.80, -0.10, 0.30 and 0.10 respectively for winter, pre-monsoon, monsoon and post-monsoon. The season of winter and pre-monsoon represents decreasing trend and monsoon and post-monsoon season shows the increasing trend. (4) Pathridih, the (Zmk) values are -0.70,-0.30,-0.80,1.20,-1.0,-0.60,1.10,-0.70,0.13,-1.0,0.20 and -0.70 respectively from January to December the month of January, February, March, may, June, August, October and December clearly mention significant decreasing trend in streamflow whereas the month of April, July, September and November shows increasing trend for monthly streamflow for 1980-2012. And Zmk values for seasonal variations for pathridih stations are -0.50, -0.30, 0.30 and -0.70 respectively for winter, pre-monsoon, monsoon and post-monsoon. The season of winter and pre-monsoon and post-monsoon represents decreasing trend and monsoon season shows the increasing trend. (5) Simga, the (Zmk) values are 0.00,0.00,-1.20,0.30,-1.30,-0.50,0.90,-1.10,0.20,-0.60,1.10 and -0.30 respectively from January to December the month of March, may, June, August, October and December clearly mention significant decreasing trend in streamflow whereas the month of April, July, September and November shows increasing trend for monthly streamflow for 1980-2012. And the month of January and February shows having no trend similarly the Zmk values for seasonal variations for simga stations are 0.50, -0.50, -0.60 and -0.10 respectively for winter, pre-monsoon, monsoon and post-monsoon. The season pre-monsoon, monsoon and post-monsoon represent decreasing trend and winter season shows the increasing trend.

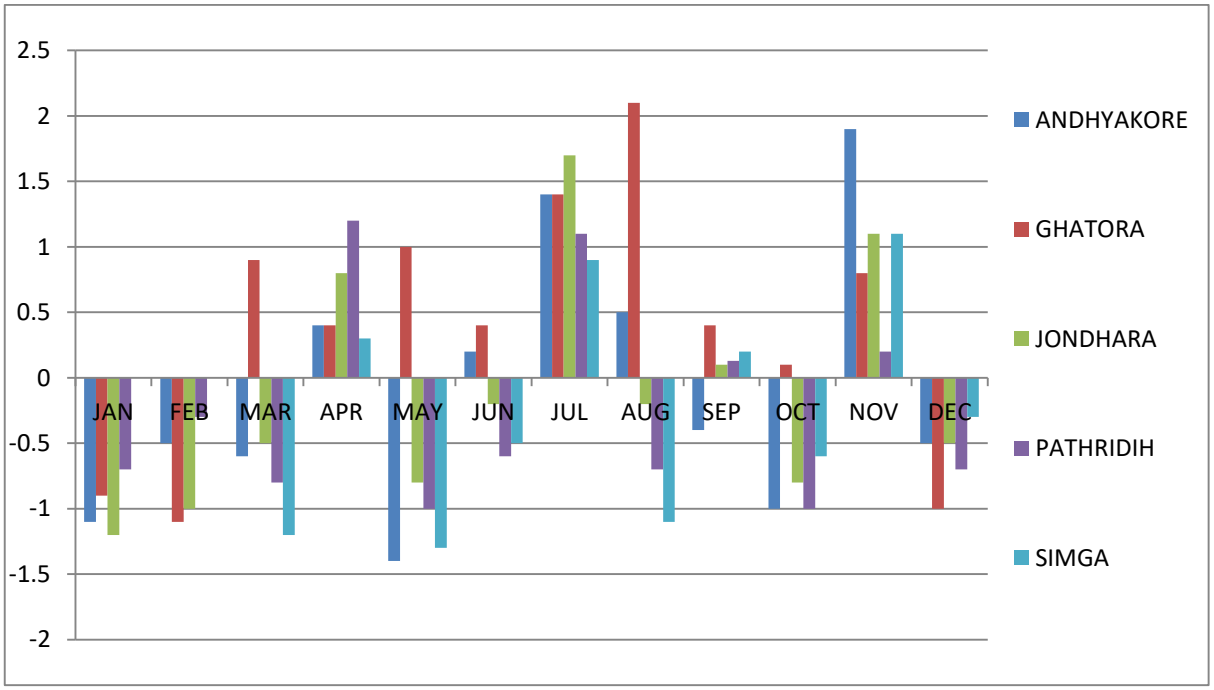


*Fig.2: Mann-Kendall test statistics for five gauging stations for different months of the year from 1980-2012.*

*https://dx.doi.org/10.22161/ijaers.5.1.20* *ISSN: 2349-6495(P) | 2456-1908(O)*

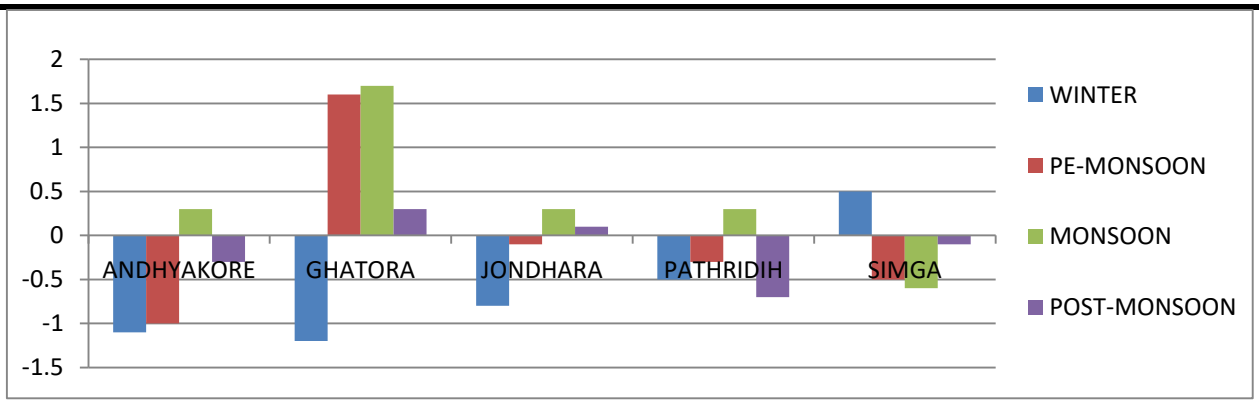


*Fig.3: Mann-Kendall test statistics for five gauging stations for different Seasons of the year from 1980-2012.*

*Table.1: Sen Slope (Qi) values for different months and seasons of year from 1980-2012*

| Effective Rainfall Stations | Andhyakore | Ghatora | Jondhara | Patharidih | Simga |
|---|---|---|---|---|---|
| **JANUARY** | -0.200 | -0.0012 | -0.0123 | -0.430 | 0.00 |
| **FEBUARY** | -0.300 | -0.0013 | -0.0241 | -0.320 | 0.00 |
| **MARCH** | -0.0005 | 0.0014 | -0.0092 | -0.0014 | -0.0025 |
| **APRIL** | 0.0006 | 0.30 | 0.0112 | 0.0028 | 0.0009 |
| **MAY** | -0.0051 | 0.0019 | -0.0151 | -0.0032 | -0.0095 |
| **JUNE** | 0.007 | 0.0226 | -0.048 | -0.0313 | -0.0345 |
| **JULY** | 0.0643 | 0.1048 | 0.3987 | 0.0808 | 0.0529 |
| **AUGEST** | 0.0254 | 0.0929 | -0.0019 | -0.0529 | -0.0947 |
| **SEPTEMBER** | -0.014 | 0.0274 | 0.0068 | 0.0031 | 0.0204 |
| **OCTOBER** | -0.0151 | 0.001 | -0.0595 | -0.0187 | -0.007 |
| **NOVEMBER** | 0.0002 | 0.70 | 0.0062 | 0.10 | 0.90 |
| **DECEMBER** | -0.600 | -0.50 | -0.40 | -0.520 | -0.120 |
| **WINTER** | -0.0119 | -0.0158 | -0.1734 | -0.0048 | 0.0062 |
| **PRE-MONSOON** | -0.0138 | 0.0166 | -0.0108 | -0.0036 | -0.0079 |
| **MONSOON** | 0.0281 | 0.2298 | 0.196 | 0.0309 | -0.0877 |
| **POST-MONSOON** | -0.0052 | 0.0041 | 0.0112 | -0.017 | -0.0024 |

Where the Positive value of Qi represents the increasing or upward trend and a negative value represents a decreasing or downward trend in the given time series.

Sen's slope and corresponding significance values are presented in Table 1. Very similar to the results obtained from Mann-Kendall test, Sen Slope Estimator test values are also negative for the months January, February, March, and may, September, October and December for all the five gauging stations similarly the month of April, June, July, August and November shows the significant increasing trend. For all the five gauging stations excluded month of January in simga gauging station shows having no trend. Whereas the trend in different seasons are follows (1) season of winter and pre-monsoon shows significant decreasing trend for all the five gauging stations and post-monsoon season andhyakore, pathridih and simga gauging stations also represents the decreasing trend and (2) the season of monsoon shows increasing trend for all the five gauging stations and seasons of winter and pre-monsoon of ghatora and simga stations also shows the increasing trend.

*https://dx.doi.org/10.22161/ijaers.5.1.20* *ISSN: 2349-6495(P) | 2456-1908(O)*

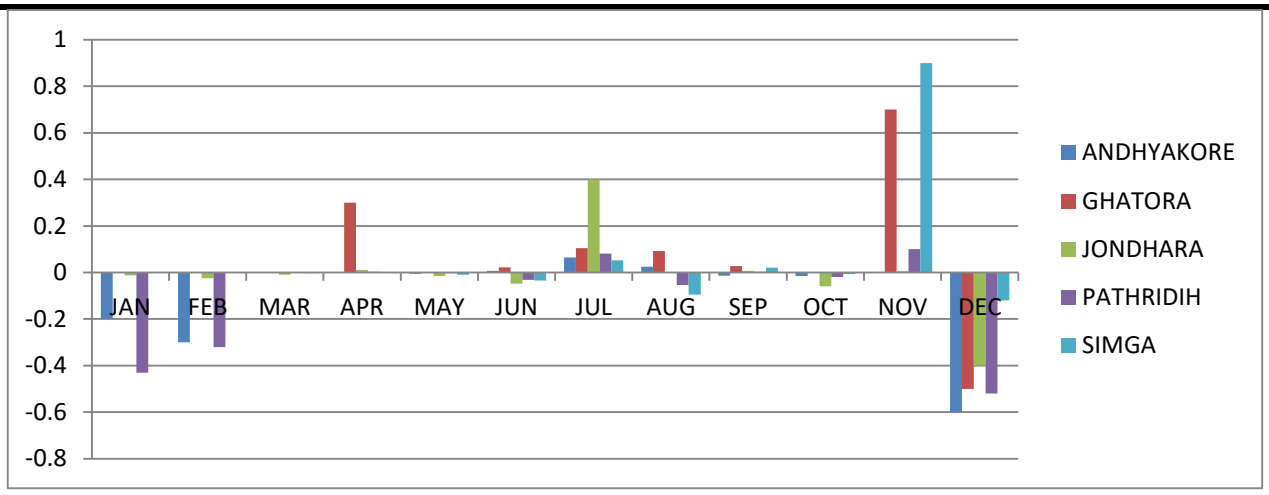


*Fig.4: Sen Slope (Qi) values for different months of year from 1980-2012*

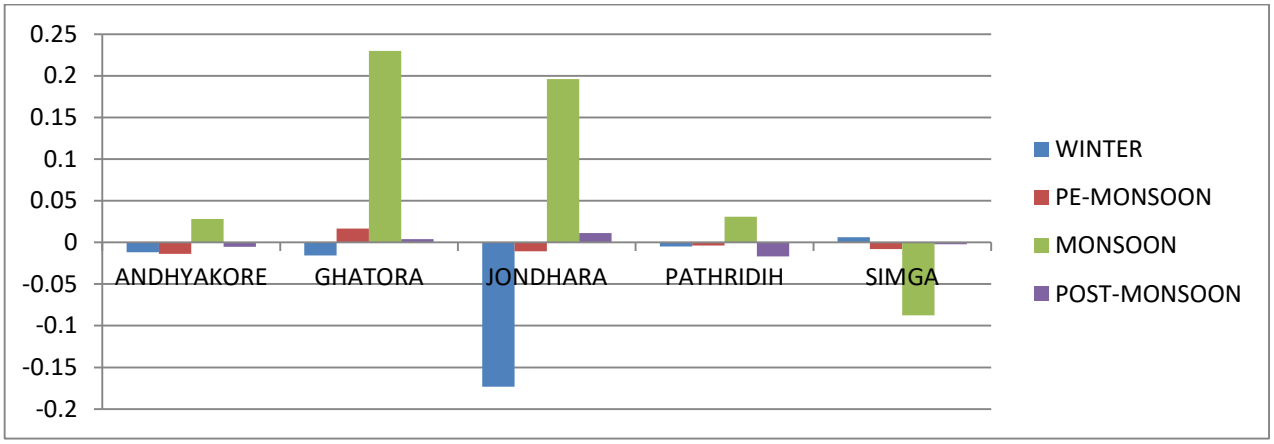


*Fig.5: Sen Slope (Qi) values for different seasons of year from 1980-2012*

## VI. CONCLUSION

Change of climate is very preliminary to cope up with ever-changing conditions. The trend analysis is done for seonath river basin of Chhattisgarh state for monthly rainfall data for the period of 1980-2012 is analysed by using a non-parametric Mann-Kendall and Theil-Sen Slope Estimator test. The results reveal a downward or decreasing trend for most of the months and seasons of a year for the period of 1980-2012 under the analysis. In this study, we noticed that the rainfall events in the whole seonath river basin are continuous decreases. Both from Mann-Kendall's and Sen Slope estimator test. The adverse effect of the observed decreasing trend in rainfall event may be expected for different water-related sectors, primarily rain-fed agriculture and freshwater availability in the region. This study suggests that the knowledge of changes in rainfall pattern and its periodicity estimation could be useful for the hydrologist and management of irrigation planners for more efficient utilisation of water in the region and to make an appropriate decision on cropping pattern.

## REFERENCES

[1] Berryman, D., Bobée, B., Cluis, D. and Haemmerli, J., 1988. Nonparametric tests for trend detection in water quality time series. *JAWRA Journal of the American Water Resources Association*, *24*(3), pp.545-556.

[2] Chakraborty, S., Pandey, R.P., Chaube, U.C. and Mishra, S.K., 2013. Trend and variability analysis of rainfall series at Seonath River Basin, Chhattisgarh (India). *Journal of Applied Sciences and Engineering Research*, *2*(4), pp.425-434.

[3] Hipel, K.W. and McLeod, A.I., 1994. *Time series modelling of water resources and environmental systems* (Vol. 45). Elsevier.

[4] Hirsch, R.M. and Slack, J.R., 1984. A nonparametric trend test for seasonal data with serial dependence. *Water Resources Research*, *20*(6), pp.727-732.

[5] Jain, S.K. and Kumar, V., 2012. Trend analysis of rainfall and temperature data for India. *Current Science*, pp.37-49.

[6] Jaiswal, R.K., Lohani, A.K. and Tiwari, H.L., 2015. Statistical analysis for change detection and trend

*https://dx.doi.org/10.22161/ijaers.5.1.20* *ISSN: 2349-6495(P) | 2456-1908(O)*

assessment in climatological parameters. *Environmental Processes*, *2*(4), pp.729-749.

[7] Longobardi, A. and Villani, P., 2010. Trend analysis of annual and seasonal rainfall time series in the Mediterranean area. *International Journal of Climatology*, *30*(10), pp.1538-1546.

[8] Machiwal, D. and Jha, M.K., 2012. Methods for time series analysis. In *Hydrologic Time Series Analysis: Theory and Practice* (pp. 51-84). Springer Netherlands.

[9] Swain, S., Verma, M. and Verma, M.K., 2015. Statistical trend analysis of monthly rainfall for Raipur District, Chhattisgarh. *Int. J. Adv. Engg. Res. Studies/IV/II/Jan.-March*, *87*, p.89.

[10] Verma, M.K., Verma, M.K. and Swain, S., 2016. Statistical Analysis of Precipitation over Seonath River Basin, Chhattisgarh, India. *International Journal of Applied Engineering Research*, *11*(4), pp.2417-23.

*https://dx.doi.org/10.22161/ijaers.5.1.21* *ISSN: 2349-6495(P) | 2456-1908(O)*

# Statistical analysis of the lithic furniture of the Ifri Ouberrid site in Ain Elleuh in the Moroccan Central Middle Atlas

Rabia Hajila

Institut National des Sciences de l'Archéologie et du Patrimoine, Rabat, Maroc

***Abstract—*** *The archeological potential of the central Medium Atlas is characterized by its richness and its diversity. The lithic furniture discovered in the site of Ifri Ouberrid is very significant and its exploration requires a powerful statistical tool allowing to simultaneously process all the quantities of objects collected in the various abductions. The Principal Component Analysis – A.C.P. is the most favorable and necessary method to fully understand and refine the work of archeologists.*

***Keywords— Archaeological potential, Lithic furniture, Multivarious analysis, Principal Components analysis, Site Ifri Ouberrid.***

## I. INTRODUCTION

The cave of Ifri Ouberrid is located in the municipality of Aïn Elleuh, about 15km as the crow flies at the south of the city of Azrou. It's formed of two caves which pierce a cliff in oolithique limestone. The main cave measures 6m of breadth at the entrance on a height of 2,30m and about 10 meters deep.

Excavations carried out in the main cave have allowed to reveal anthropogenic deposits that extend to a depth of about 1,80 m. Their analysis has identified 7 stratigraphic units that contain two important human's occupations: the first would go back to the early Neolithic and would be dated 6846 ± 56 cal. BP and the second would be of epipaleolithic age and would be located around 8222-8416 cal. BP. These two levels of occupation have delivered important quantities of lithic industry with a clear dominance of debitage products and nuclei attesting to intense debitage on the site itself.

## II. METHOD AND ANALYSIS

The total number of lithic furniture collected in the Ifri Ouberrid site is 4051 pieces. All the archaeological levels have delivered, although in a visibly unequal way, objects in rather significant quantities. The table below gives the distribution of the lithic industry by removal:

| Removal | Shards | Blades | Lamellas | Nucleus | Debris& splinters | Tools | Total |
|---|---|---|---|---|---|---|---|
| 1 | 122 | 16 | 28 | 226 | 583 | 13 | 988 |
| 2 | 136 | 22 | 25 | 111 | 346 | 9 | 649 |
| 3 | 112 | 36 | 34 | 167 | 366 | 8 | 723 |
| 4 | 71 | 35 | 33 | 63 | 160 | 1 | 363 |
| 5 | 101 | 42 | 61 | 43 | 210 | 5 | 462 |
| 6 | 82 | 31 | 31 | 84 | 241 | 5 | 474 |
| 7 | 38 | 31 | 27 | 14 | 139 | 3 | 252 |
| 8 | 14 | 5 | 10 | 2 | 51 | 1 | 83 |
| 9 | 14 | 4 | 0 | 4 | 26 | 0 | 48 |
| 10 | 0 | 0 | 0 | 2 | 7 | 0 | 9 |
| Total | 690 | 222 | 249 | 716 | 2129 | 45 | 4051 |

We know how to analyze each of these six variables separately, either by drawing a graph or by calculating numerical summaries. We also know that we can look at the links between two variables (for example shards and lamellas), either by making a graph of the cloud of dots type, or by calculating their linear correlation coefficient, or by carrying out the regression of one on the other.

However, how to study six variables simultaneously, if only by making a graph ?

The difficulty comes from the fact that the individuals (the removals) are no longer represented in a plane, space of dimension 2, but in a space of dimension 6 (each removal being characterized by the 6 objects detected). The objective of the Principal Component Analysis (A.C.P) is to return to a reduced dimension space by distorting the reality as little as possible. It is therefore necessary to obtain the most relevant summary of the initial data.

*https://dx.doi.org/10.22161/ijaers.5.1.21* *ISSN: 2349-6495(P) | 2456-1908(O)*

We present below some results of the A.C.P. performed with SPSS software on this data. This will help to realize the possibilities of the method. The results have been limited to two decimals, although software programs generally provide much more, but they are rarely useful.

## III. PRELIMINARY RESULTS

The software first provides the average, standard deviation, minimum and maximum of each variable. It is therefore, for the moment, univariate studies.

Basic statistics

| **Variable** | **Average** | **Standard deviation** | **Minimum** | **Maximum** |
|---|---|---|---|---|
| Shards | 69,00 | 49,57 | 0,00 | 136,00 |
| Blades | 22,20 | 15,12 | 0,00 | 42,00 |
| Lamellas | 24,90 | 18,15 | 0,00 | 61,00 |
| Nucleus | 71,60 | 76,82 | 2,00 | 226,00 |
| Debris & splinters | 212,90 | 179,72 | 7,00 | 583,00 |
| Tools | 4,50 | 4,37 | 0,00 | 13,00 |

Let us note the great heterogeneity of the six considered variables: different orders of magnitude for averages, standard deviations, minima and maxima.

The following table is the correlation matrix. It gives the linear correlation coefficients of the variables taken two by two. It is a succession of bivariate analyzes, constituting a first step towards multivariate analysis.

Correlation coefficients

| **Variables** | Shards | Blades | Lamellas | Nucleus | Debris & splinters | Tools |
|---|---|---|---|---|---|---|
| Shards | 1,00 | 0,62 | 0,69* | 0,82** | 0,88** | 0,87** |
| Blades | 0,62 | 1,00 | 0,91** | 0,31 | 0,38 | 0,32 |
| Lamellas | 0,69* | 0,91** | 1,00 | 0,37 | 0,48 | 0,45 |
| Nucleus | 0,82** | 0,31 | 0,37 | 1,00 | 0,96** | 0,92** |
| Debris & splinters | 0,88** | 0,38 | 0,48 | 0,96** | 1,00 | 0,97** |
| Tools | 0,87** | 0,32 | 0,45 | 0,92** | 0,97** | 1,00 |

* The correlation is significant at the 0,05 level (bilateral).

** The correlation is significant at the 0,01 level (bilateral).

Note that all linear correlations are positive, which means that all variables vary, on average, in the same direction. Some correlations are very strong (0,97 and 0,96), other are averages (0,69 and 0,62), others are rather weak (0,32 and 0,31).

Let's continue the examination of the outputs of this analysis by studying the matrix of variances-covariances, matrix of the same nature as that of the correlations. The diagonal of this matrix gives the variances of the six variables considered (it should be noted that at the level of calculations, it is more convenient to manipulate the variance than the standard deviation, for this reason, in many statistical methods, such as the A.C.P, the variance is used to take into account the dispersion of a quantitative variable).

Matrix of variances-covariances

| **Variables** | Shards | Blades | Lamellas | Nucleus | Debris&splinters | Tools |
|---|---|---|---|---|---|---|
| Shards | 2457,33 | 470,11 | 628,33 | 3143,11 | 7885,00 | 190,55 |
| Blades | 470,11 | 228,84 | 251,02 | 361,08 | 1045,68 | 21,44 |
| Lamellas | 628,33 | 251,02 | 329,43 | 517,40 | 1581,10 | 36,05 |
| Nucleus | 3143,11 | 361,08 | 517,40 | 5901,60 | 13374,40 | 310,33 |
| Debris & splinters | 7885,00 | 1045,68 | 1581,10 | 13374,40 | 32302,76 | 769,27 |
| Tools | 190,55 | 21,44 | 36,05 | 310,33 | 769,27 | 19,16 |

The eigenvalues below are those of the variances-covariances matrix.

Eigen values ; explained values

| **Factors** | **Eigenvalues** | **Variance Percentage** | **Cumulated Percentage** |
|---|---|---|---|
| 1 | 4,40 | 73,33 | 73,43 |
| 2 | 1,35 | 22,50 | 95,83 |
| 3 | 0,12 | 2,00 | 97,83 |
| 4 | 0,08 | 1,33 | 99,16 |
| 5 | 0,04 | 0,67 | 99,83 |
| 6 | 0,01 | 0,17 | 100,00 |
| Total | 6,00 | 100,00 | ----- |

Each row of the table above corresponds to a virtual variable (the factors) whose eigenvalue column provides the variance (each eigenvalue represents the variance of the corresponding factor). The percentage of variance column is the percentage variance of each row relative to the total. The cumulative percentage column represents the sum of these percentages.

Let’s add now the variances of the 6 initial variables (diagonal of the variances-covariances matrix):

2457,33 + 228,84 + 329,43 + 5901,60 + 32302,76 + 19,16 = 41239,12

The total dispersion of the abductions considered in dimension 6 is thus equal to 41239,12.

*https://dx.doi.org/10.22161/ijaers.5.1.21* *ISSN: 2349-6495(P) | 2456-1908(O)*

Let's add otherwise the 6 eigenvalues obtained:
4,40 + 1,35 + 0,12 + 0,08 + 0,04 + 0,01 = 6,00
The cloud of points in dimension 6 is not the same and its global dispersion has changed a lot. The first two factors alone account for almost the entire dispersion of the cloud, which allows to neglect the other 4.
As a result, the 2-dimensional charts summarize almost exactly the actual configuration of the data in dimension 6: the goal (relevant summary of the small-scale data) is therefore achieved.

## IV. RESULTS ON THE VARIABLES

The fundamental result concerning the variables is the table of correlations variables factors. It is these correlations that will allow to make sense of the factors and interpret them.

| Factors | F1 | F2 |
|---|---|---|
| Shards | 0,97 | 0,02 |
| Blades | 0,65 | 0,73 |
| Lamellas | 0,73 | 0,65 |
| Nucleus | 0,89 | -0,39 |
| Debris&splinters | 0,94 | -0,31 |
| Tools | 0,92 | -0,35 |

First of all, the two columns of this table allow to realize the graph of the variables given by the following figure. But these two columns also make it possible to give a meaning to the factors and thus to the axes of the graphs.

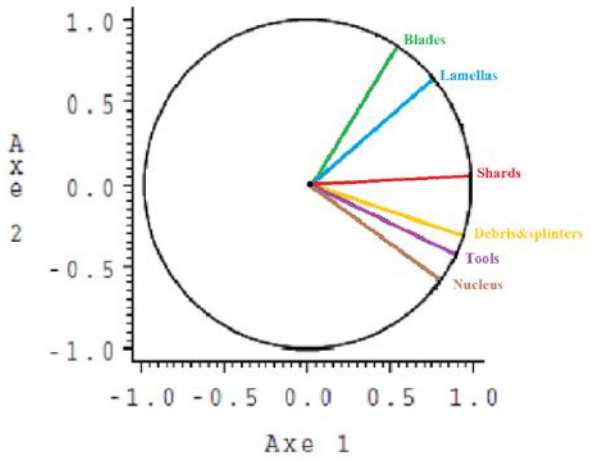


*Fig. 1: Representation of the variables*

Thus, we see that the first factor is correlated positively, and quite strongly, with each of the 6 initial variables: the higher the removal, the greater the quantity of lithic furniture is significant on axis 1; conversely, the deeper it is, the lower the quantity; the axis 1 represents, in some ways, the overall result for all 6 types of objects considered compared to the abductions made.
As regards axis 2, it opposes, on the one hand, shards, blades and lamellas (positive correlations), on the other hand, nucleus, debris and splinters and tools (negative correlations). It is therefore an axis of opposition between these two types of objects. This interpretation can be specified with graphs and tables relating to abductions. We present them below.
Note that the presentation quality of each type of object is relevant. Debris and splinters are represented at 99,10%.

## V. RESULTS ON THE ABDUCTIONS

The table given below gives the results of the A.C.P. on removals.

| Removals | Weight | Factor1 | Factor2 | Average |
|---|---|---|---|---|
| Removal 1 | 0,10 | 220,12 | -18,89 | 164,66 |
| Removal 2 | 0,10 | 126,44 | 12,59 | 108,16 |
| Removal 3 | 0,10 | 133,44 | -8,33 | 120,50 |
| Removal 4 | 0,10 | 53,53 | 8,56 | 60,50 |
| Removal 5 | 0,10 | 66,65 | 27,46 | 77,00 |
| Removal 6 | 0,10 | 84,98 | 6,62 | 79,00 |
| Removal 7 | 0,10 | 45,14 | 15,30 | 42,00 |
| Removal 8 | 0,10 | 17,27 | 6,18 | 13,83 |
| Removal 9 | 0,10 | 9,35 | 3,30 | 8,00 |
| Removal 10 | 0,10 | 2,72 | -0,35 | 1,50 |

It should be noted that each removal represents 1 element out of 10, hence a weight or a weighting of 1/10 = 0,10, which is provided by the first column of the table.
The following 2 columns provide the coordinates of the removals, on the first two axes (the factors) and thus allowed to draw up the abductions graph. The latter makes it possible to specify the meaning of the axes, therefore of the factors.

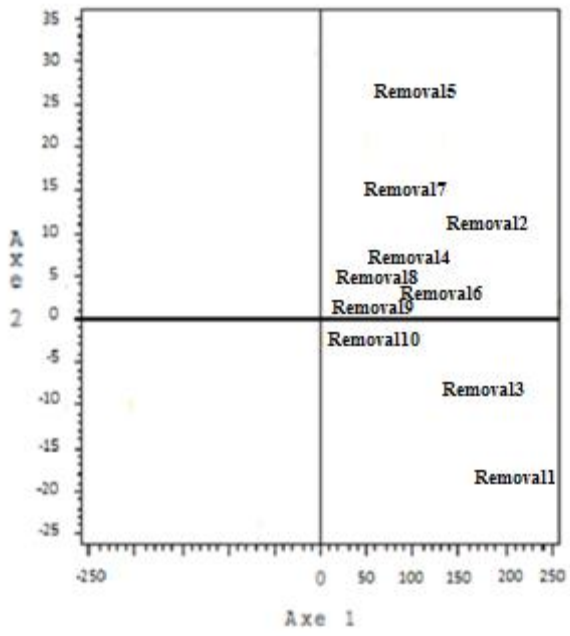


*Fig. 2: Representation of the abductions*

We confirm that as well as the first axis represents the overall result of the removals: if we take their score on axis 1, we obtain the same ranking as if we take their

*https://dx.doi.org/10.22161/ijaers.5.1.21* *ISSN: 2349-6495(P) | 2456-1908(O)*

overall average. Moreover, the highest removal on the graph, the one with the highest coordinate on axis 2, is the removal 5 which the results are the most contrasting in favor of debris and splinters and shards. This is exactly the opposite for removal 1 where 583 debris and splinters were obtained, 226 nucleus and 122 shards, but small quantities of tools, blades and lamellas. It should be noted that the removal 10 has a score close to 0 on the axis 2 because the quantity of objects obtained is very homogeneous for each type of object.

## VI. CONCLUSION

The contributions of the variance removals according to the axes 1 and 2 (remember that we use the variance here to measure the dispersion) are given by the general contributions, ie the dispersion in dimension 6 (it is what is called the inertia of the cloud of abductions, the notion of inertia generalizes that of variance in any dimension, the variance always being relative to a single variable). These contributions are provided in percentages and make it possible to locate the most important removals at each axis (or the cloud in dimension 6). They are generally used to refine the interpretation of the results of the analysis.

The first removal represents nearly 94% of the variance: it is preponderant in the definition of the axis 1, in contrast, the contribution of the removal 10 is almost null. Finally, concerning the quality of the representation, the removal 1 is represented at 100%: its representation is then very good.

## REFERENCES

[1] A. Baccini (2010). “Statistique descriptive multidimensionnelle”. Institut de Mathématiques de Toulouse - UMR CNRS 5219.

[2] A. Mikdad, F. Nekkal, M. Nami, C. Zielhofer et F. Amani (2012). Recherches sur le peuplement humain et l'évolution paléoenvironnementale durant le Pléistocène et l'Holocène au Moyen Atlas central: résultats préliminaires. Bulletin d'archéologie marocaine (ISSN: 0068-4015), dépôt légal: 20/1956, tome 22, p.53-71.

[3] IBM SPSS Statistics 20.

[4] R. Chenorkian (1975). Atlas préhistorique du Maroc, Mémoire de maitrise, Aix.

[5] R. Hajila (2013). “La statistique: La partie cachée du patrimoine culturel. Cours et exercices corrigés”. Tome 1 (ISBN: 978-9954-32-626-8), n° du dépôt légal: 2013 MO 2792.

[6] R. Hajila (2016-2017). “Statistique descriptive multidimensionnelle: L'analyse en composantes principales”, séminaires pour les filières: Histoire et Archéologie de l'Occident Méditerranéen, Muséographie et Archéologie préhistorique, unpublished yet.

[7] R. Hajila (2011-2012). “L'analyse en composantes principales”, séminaires pour la filière: Archéologie préhistorique, unpublished yet.